Holocene environmental changes in the central highlands of Iceland as recorded in soils

Sigurveig Gunnarsdóttir

Faculty of Engineering and Natural Sciences
University of Iceland
2018

Holocene environmental changes in the central highlands of Iceland as recorded in soils

Sigurveig Gunnarsdóttir

60 ECTS thesis submitted in partial fulfillment of a
Magister Scientiarum degree in Geology

MS Committee
Áslaug Geirsdóttir
Þorvaldur Þórðarson

Master's Examiner
Egill Erlendsson

Faculty of Earth Sciences
School of Engineering and Natural Sciences
University of Iceland
Reykjavik, October 2018

Holocene environmental changes in the central highlands of Iceland as recorded in soils
Holocene environmental changes as recorded in soils.
60 ECTS thesis submitted in partial fulfillment of a *Magister Scientiarum* degree in Geology

Faculty of Earth Sciences
School of Engineering and Natural Sciences
University of Iceland
Sturlugata 7
101, Reykjavik
Iceland

Telephone: 525 4000

Bibliographic information:
Sigurveig Gunnarsdóttir, 2018, *Holocene environmental changes in the central highlands of Iceland as recorded in soils*, Master's thesis, Faculty of Earth Sciences, University of Iceland, pp. 166.

Printing: Háskólaprent
Reykjavik, Iceland, October 2018

Abstract

Across the central highlands of Iceland soil sections are accessible in *rofabörð* were they can reach back to the time of initial soil formation after the deglaciation around 11.5 ka. These soil sections have been used to reconstruct tephrochronology and also to study soil erosion in Iceland. The main focus of this project is to study soil sections by Kjölur for the purpose of reconstructing the environmental and climate changes that have occurred during the Holocene with the help of tephrochronology and geochemical researches. Five soil sections were in total measured and samples collected for studying carbon content as well as for the branched glycerol dialkyl glycerol tetraether (brGDGT) paleothermometer to estimate temperature changes for the Holocene. Numerous tephra layers can be found in the soil sections which were identified to their volcanic source and age which made it possible to obtain age models for each section. By identifying the tephra layers it was also possible to correlate between sections and calculate the soil accumulation rate for each section. By interconnecting the results from the identification of tephra layers, calculation of soil accumulation, carbon content and the brGDGT it was possible to reconstruct environmental and climate changes for the area and compare the results to similar studies that have been done on sediment from Hvítárvatn by Langjökull and Arnarvatn Stóra. The main results of studying the soil sections reflect the results from the lake studies and indicate that a gradual cooling has been occurring for the last 10 ka superposed by more stepped changes at 8.2, 6.0, 4.4, 2.7, 1.4 and 0.6 ka when increased soil erosion took place. Soil erosion was most active during the Little Ice Age (LIA 1300-1900 CE) when soil accumulation rate was highest in the sections located furthest to the southwest in the research area. This indicates that strong northerly winds were dominant during that time. Although a brGDGT temperature calibration of Icelandic soils is yet to be developed to accurately quantify Iceland's Holocene summer temperature history, relative temperatures can be estimated from the measurements and appearance of the soil showing the coldest temperatures during the LIA with possible local permafrost conditions in the Kjölur area at that time.

Útdráttur

Víða á hálendi Íslands er að finna rofabörð þar sem opnast hafa snið í jarðveg sem nær allt aftur til upphafstíma jarðvegsmyndunar á nútíma eftir hörfun ísaldarjökla fyrir um 11.5 þús. árum. Jarðvegssnið þessi hafa nýst vel til uppbygginga gjóskulagatímatals og ekki síður til rannsókna á jarðvegsrofi á Íslandi. Megináhersla þessa verkefnis er að rannsaka jarðvegssnið á Kili í þeim tilgangi að draga fram umhverfis- og loftslagsbreytingar sem átt hafa sér stað á nútíma með aðstoð gjóskulagafræðinnar og jarðefnafræðilegra rannsókna. Alls voru fimm snið mæld og fjöldi sýna tekinn til rannsókna á kolefnisinnihaldi, auk rannsókna á hitanæmum bakteríum til áætlunar á hitastigsbreytingum á nútíma. Fjölda gjóskulaga er að finna í jarðvegssniðunum sem greind voru til uppruna og aldurs, þannig að unnt var að setja fram aldursmódel fyrir hvert snið. Með greiningu gjóskulaga var hvort tveggja hægt að tengja á milli mismunandi sniða og reikna út upphleðsluhraða jarðvegs í hverju sniði. Með samtengingu niðurstaðna gjóskulagagreininga, útreikninga á jarðvegssupphleðslu, kolefnisgreininga og greininga á hitanæmum bakteríum var unnt að endurbyggja umhverfis- og loftslagsbreytingar á svæðinu og bera saman við sams konar rannsóknir sem gerðar hafa verið á seti Hvítárvatns við Langjökul og Arnarvatns Stóra. Helstu niðurstöður rannsókna á jarðvegssniðunum endurspegla niðurstöður rannsókna á stöðuvötnunum og benda til stigvaxandi kólnunar síðustu 10 þús. ár. Aukið jarðvegsrof átti sér stað fyrir um 8200, 6000, 4400, 2700, 1400 og 600 árum. Jarðvegsrof var virkast á tímum Litlu ísaldar (1300-1900 CE) þegar mest upphleðsla jarðvegs átti sér stað í þeim opnum sem liggja suðvestast á rannsóknarsvæðinu, sem hugsanlega bendir til sterkrar norðanáttar á tímabilinu. Þó enn sé ekki til íslensk viðmiðunargögn fyrir hitanæmu bakteríurnar má áætla út frá mælingunum og ásýnd jarðvegs, að hitastig var kaldast á Litlu ísöldinni sem bendir til þess að svæðisbundinn sífreri gæti hafa verið til staðar í jarðveginum.

Dedication

To my late grandmother, Sigurveig Þórarinsdóttir, I know she would have loved this project.

Table of Contents

List of Figures

List of Tables

Acknowledgements

I would like to begin by thanking my supervisors, Áslaug Geirsdóttir and Þorvaldur Þórðarson, for their guidance through all the work as well as their encouragement and enthusiasm. I will be forever grateful for the opportunity to work on this project, it has been a valuable learning process.

Secondly, special thanks to David Harning for all his support, enthusiasm in the project and helpful comments as well as overseeing the brGDGT measurements on the soil samples. I would also like to thank Sæmundur Ari Halldórsson for his assistance and guidance in using the magnetic separator, and Guðmundur H. Guðfinnsson for his help with the microprobe analysis. Also, I thank Egill Erlendsson for his help and guidance in burning soil samples for carbon content measurements.

Special and genuine thanks to my father, Gunnar Baldursson, for his valuable help both in the field and through all the work on the thesis. None of this would have been possible without him. I would also like to give special thanks to my mother, Guðrún Reynisdóttir, for her encouragement and inspirational words.

I also thank my best friend, Viðar Birkir Viðarsson, for always being there for me and ready to give me a hug or encouraging words when I needed as well as bringing me chocolate on command.

I also thank my late grandmother, Sigurveig Þórarinsdóttir, who supported me throughout my BSc. study and gave me a warm place to live. Kjölur was one of her favorite places and I know she would have loved this project. My family and friends deserve special thanks as well, for their support and kind words. Last but not least, I would like to thank my cat, Snúður, and all the horses in the herd for their warm snuggles and unconditional love when I most needed it.

1 Introduction

Paleoclimate reconstruction is important in Iceland due to its strategic location relative to changes in both air and ocean surface currents. Iceland lies at the polar oceanic front a boundary between two water masses that highly influence the climate; the cold and relatively fresh East Greenland current (EGC) and the warmer and more saline North Atlantic Current (NAC; see Figure 1). Any changes in the relative strength of these two water masses is reflected in the climate of Iceland and recorded in lake and marine sediments in and around Iceland. Thus, by studying those two archives it is possible to reconstruct paleoclimate at least back 10 ka (e.g. Massé et al., 2008; Geirsdóttir et al., 2009a). Presently, there are rapid climate and environmental changes taking place and it is important to look into the past to get an idea about what to expect in the future. Information on Holocene (the last 11.7 ka) climate fluctuations can provide critical context for understanding the details of current climate change. The central highlands of Iceland is a large study area for Holocene climate as it has been highly affected by climate fluctuations since it became ice free after the last glaciation. The central highlands are also vulnerable and sensitive towards fluctuations in climate as the area has limited vegetation cover and experiences active soil erosion (Arnalds, 2008), thus it responds quickly towards changes occurring in the climate. Lakes in the central highlands, such as Hvítárvatn and Arnarvatn Stóra, have been studied regarding to Holocene climate and provide continuous and well dated records for environmental changes. Soil erosion has been severe across Iceland for centuries. The prevailing argument is that the onset of soil erosion began with the Settlement of Iceland (871 ± 2 CE). However, proxy reconstruction from Haukadalsvatn in western Iceland has led to the conclusion that periods of landscape instability and soil erosion are also likely due to both volcanic activity and cooling climate rather than only grazing of livestock (Geirsdóttir et al., 2009a). The Settlement of Iceland mostly took place around the lowlands rather than the highlands, which emphasizes the importance of studying paleoclimate in the highlands when obtaining information that can differentiate climate driven landscape instability and human impact.

The dominating soil type in Iceland, Andosols, is mostly derived from volcanic material due to active volcanism. The soil lacks cohesion making it fragile to aeolian activity and erosion. Active soil erosion in Iceland has caused the formation of *rofabörð*, which provide easy access to soil sections which contain Holocene tephra layers. The tephra layers play a key role in observing soil sections as they give timing of eruptions which provides a chronology for the soil sections (Arnalds, 2004; Arnalds, 2008; Dugmore et al., 2009). When soil erosion is active, soil organic matter gets diminished with reduced vegetation cover. Thus, soil sections can provide information about periods of significant erosion by measuring the carbon content (Óskarsson et al., 2004). Another measurable factor in soils is a proxy based on the branched glycerol dialkyl glycerol tetraether (brGDGT) which is a paleothermometer that uses microbial communities and the chemical structure of their cell membranes in response to environmental temperature (e.g. Weijers et al., 2007).

The aim of this study is to:

- Develop a story of Holocene landscape evolution using soil profiles along a strike from NE to SW across the central highlands of Kjölur located between Langjökull

and Hofsjökull ice caps (Figure 2). The soil sites were chosen based on their likelihood to record the whole of Holocene with the aim to retrieve information about Holocene landscape responses to climate change. This is done by comparing lithofacies changes detected in the soil sections, sediment accumulation rate and carbon content.

- Use a new method, the brGDGTs temperature estimates to obtain information about Holocene temperature fluctuations in the area.
- Establish the tephra stratigraphy from Holocene volcanic eruptions of known age and thus facilitate accurate age control and direct comparison between all soil sites.
- Conclude whether soil profiles indicate similar climate changes as research has shown in lacustrine sediment. Thus, the environmental parameters contained in the soil archives were analyzed at multi-centennial resolution and compared to existing paleoenvironmental records from the nearby lakes Hvítárvatn and Arnarvatn Stóra to provide insight into the landscape responses to periods of known Holocene climatic change, as well as, the timing of human settlement in Iceland.

2 Geographical and geological background

2.1 Position of Iceland and geology

Iceland is strategically located at the polar oceanic front, which is a boundary between the East Greenland current (EGC) from the Arctic Ocean and the North Atlantic Current (NAC) from the tropical areas in the south (Figure 1). These two currents have different temperatures and salinity, the EGC is relatively cold and fresh while the NAC is warmer and salty. The Irminger current (IC) is a branch of the NAC, which travels along the western and north-western coasts of Iceland where it becomes the North Iceland Irminger Current (NIIC) and the EGC flows along the eastern coast of Greenland from the Arctic Ocean. The East Iceland Current (EIC) is a branch of the cold Arctic current and flows from west to east along the northern coast of Iceland. Any shifts in the balance between these two water masses will influence the position of the polar oceanic front, which in turn affects the climate of Iceland. Studies of lake and marine sediments in and around Iceland show that any changes associated with the strength of these ocean surface currents through time are reflected in the two archives (e.g. Massé et al., 2008; Geirsdóttir et al., 2009a).

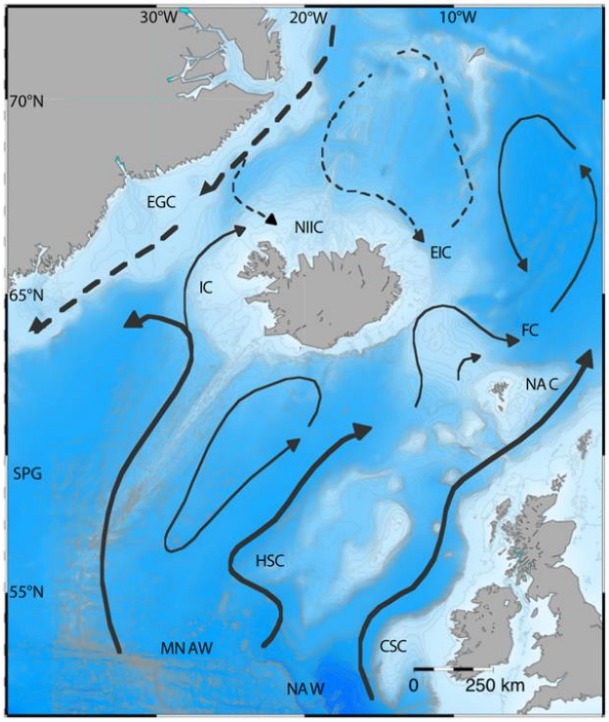

Figure 1. Map showing Iceland's position in the North Atlantic and the ocean currents that influence the island's climate (Geirsdóttir et al., 2013).

Atmospheric and oceanic variability on decadal to centennial time-scales have a strong impact on Iceland's climate; the North Atlantic Oscillation (NAO) being an important example of such a source. The NAO shows decadal-scale variability and displays the fluctuations in the difference of sea level pressure between the Icelandic Low and the Azores high. The strength and direction of westerly winds and storm tracks across the North Atlantic are controlled by the NAO. In its positive phase the NAO causes low-pressure anomalies over Iceland, which in turn produces strong Atlantic westerly winds (Hurrell, 1995). The Atlantic Multi-decadal Oscillation (AMO) is another important process causing multi-decadal variability. This process is a coherent pattern of oscillatory changes in North Atlantic sea surface temperature (SST), with a period of around 60-90 years (e.g. Knudsen et al., 2011). One important factor which affects the Atlantic sea surface temperature and the thermohaline circulation is the North Atlantic meridional overturning circulation (AMOC), which transports warm and salty surface waters to high latitudes causing the waters to cool, sink and return southwards again as deep water (Thornalley et al., 2009).

Iceland is a volcanic island situated on the North Atlantic Ridge and is affected by a spreading plate boundary and a mantle plume. Iceland rises more than 3000 m above the surrounding sea floor. The formation of Iceland is thought to have begun about 24 million years ago although the mantle plume underneath the island has been active for the last 65 million years. The mantle plume formed the 2000 km long North Atlantic Igneous Province which includes Iceland which is the only part that is still active (e.g. Sæmundsson, 1979; Vink, 1984; Saunders et al., 1997; Guðmundsson, 2000; Thordarson & Larsen, 2007). The arrangement of the active volcanism in Iceland results from superposition of the spreading plate boundary over the Iceland mantle plume and also the relative motion of these two structures. The interaction is seen on the surface as discrete 15-50 km wide belts of active faulting and volcanism (e.g. Sæmundsson, 1979; Vink, 1984). The most prominent belt is the axial volcanic zone where active spreading and plate growth follows the plate boundary across Iceland from Reykjanes in the southwest to Öxarfjörður in the north. Tholeiitic magmatism characterizes the axial zone and it is divided into the West (WVZ) and the North (NVZ) Volcanic Zones, these two are connected by the Mid-Iceland Belt (MIB) and linked to the Mid-Atlantic Ridge system by the Reykjanes Volcanic Zone (RVZ) in the south and the Tjörnes Fracture Zone (TFZ) in the north. An axial rift in the making is the East Volcanic Zone (EVZ) which will in the future take over from the West Volcanic Zone (e.g. Thordarson & Höskuldsson, 2008; Figure 2).

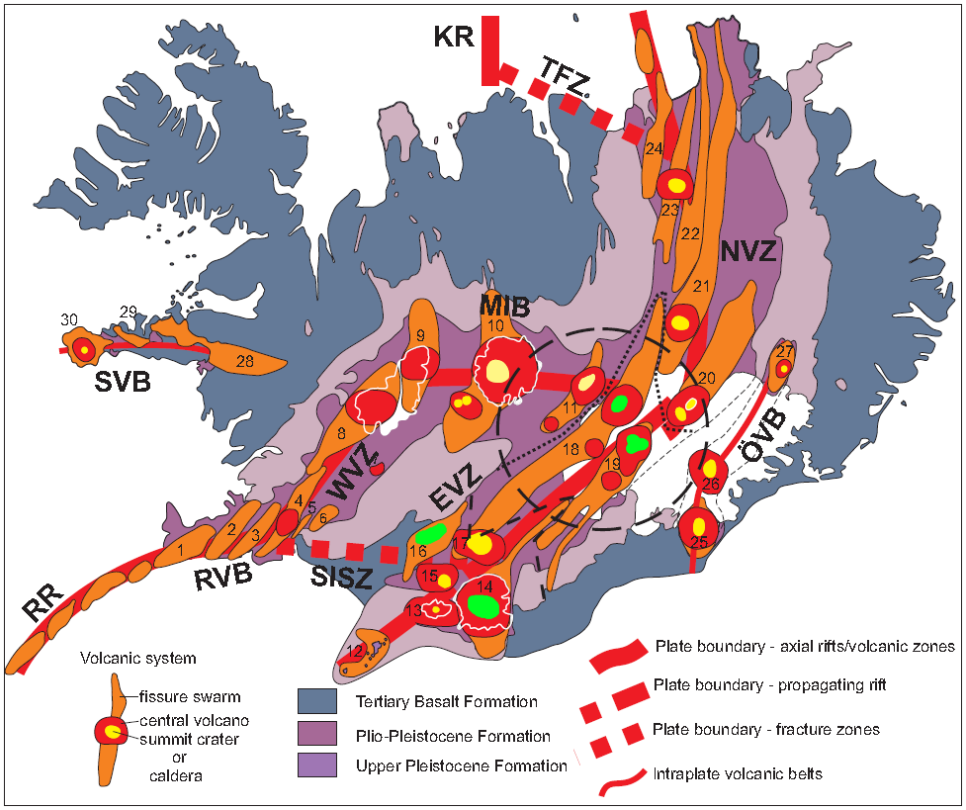

Figure 2. Location and distribution of active volcanic systems as well as volcanic zones and belts found in Iceland. The volcanic systems marked green are the ones expected to have influenced the study area the most, Bárðarbunga-Veiðivötn, Grímsvötn, Hekla and Katla (modified from Thordarson & Höskuldsson, 2008).

2.2 Study area

The landscape of the central highlands of Iceland displays the results from the sculpturing effect of the Icelandic ice sheet (IIS), which developed during the last glacial period, the Weichselian, and reached its maximum extent during the Last Glacial Maximum (LGM) around 20 ka. The IIS was mostly marine-based reaching out onto the shelf of Iceland during the LGM (Hubbard et al., 2006). It started to retreat from the shelf possibly a little after 18.6 ka (Norðdahl & Ingólfsson, 2015). The deglaciation was rapid and the IIS most likely collapsed from its marine-based sector between 15 and 14.7 ka. It is thought that the collapse of the IIS occurred due to rapid sea level rise associated with meltwater pulses into the ocean (Syvitski et al., 1999; Norðdahl & Ingólfsson, 2015). Most of the central highlands became ice free in the early Holocene, or around 10.5 ka (Geirsdóttir et al., 2009a; Larsen et al., 2012; Gunnarson, 2017; Harning et al., 2018a).

The Holocene is the present interglacial period, which started around 11.5 ka, at a time when summer insolation reached a maximum and since then has been steadily declining (Berger & Loutre, 1991). The Northern Hemisphere shows influences from this decrease in summer insolation on millennial timescales, but on decadal to centennial timescales the Holocene climate shows more fluctuating climate, varying between warmer and colder, more humid and more arid states (Wanner et al., 2011). The northernmost North Atlantic indicates

complex changes in atmospheric and ocean surface currents occurring through the Holocene (e.g. Alley & Ágústsdóttir, 2005; Geirsdóttir et al., 2013). With maximum summer insolation the Holocene Thermal Maximum (HTM) occurred around 11 ka, although the warm conditions did not start until a couple of thousand years later in the North Atlantic due to the lingering effect of the meltwater from the disintegrating Laurentide Ice Sheet (LIS). Thus, the HTM conditions did not occur in Iceland until between 8 and 6 ka (Kaufmann et al., 2004; Geirsdóttir et al., 2009b). This cooling caused spatiotemporal variabilities through the HTM (Renssen et al., 2009; Renssen et al., 2012). The smooth linear decline of the Northern Hemisphere summer insolation resulted in a change in the distribution of total solar irradiance especially after ca 5 ka. The Earth's climate responded to these changes with non-linear responses, such as glacier nucleation and advances which marked the beginning of the Neoglacial. The Neoglacial spans the mid-to-late Holocene, reaching its maximum with the Little Ice Age (LIA) between 0.6 and 0.1 ka (Wanner et al., 2008). During the LIA most of Iceland's glaciers advanced and reached their Holocene maximum extent (e.g. Geirsdóttir et al., 2009b; Larsen et al., 2013; Harning et al., 2016). Severe soil erosion during the LIA is evident in the central highlands based on studies of both Hvítárvatn and Haukadalsvatn lake sediments indicating reduced summer temperatures and windy conditions (Geirsdóttir et al., 2009a; Larsen et al., 2011). A widespread area has still yet to recover from the active aeolian processes during the LIA. Due to the large impact of this cooling on the highlands of Iceland it is an important area to study late Holocene climate in Iceland (e.g. Geirsdóttir et al., 2009b).

The study area is within Kjölur the highland between Langjökull and Hofsjökull (Figure 3). The soil sites were chosen based on their possibility to cover the whole of Holocene in order to retrieve information about Holocene environmental change. The area is a part of the Western Volcanic Zone (WVZ), thus the bedrock consists mostly of basalt lava flows from early Holocene and subglacial volcanic material, such as pillow lavas and hyaloclastite, from late Pleistocene, covered by fluvial sediments (Sinton et al., 2005). In the vicinity of Langjökull is a sandy desert. The majority of this desert area is found southward from the glacier and often experiences intense aeolian activity. The dominating dry wind direction for this area is from the north and northeast, resulting in material being transported to the south and southwest towards the sandy desert (Gísladóttir et al., 2005; Arnalds, 2010). The Hveravellir weather station is located approximately 30 km northeast from Hvítárvatn at 500 m a.s.l. The average annual temperature from that station for the years 1966-2003 is -0,87°C (Veðurstofa Íslands, 2018). The location of this weather station is quite useful since temperature estimates will be presented in the current study.

The locations and paleoclimate records available for Hvítárvatn (Larsen et al., 2011; Larsen et al., 2012) and Arnarvatn Stóra (Gunnarson, 2017) make the two lakes ideal for comparison to the results from the soil sites by Kjölur. The study area is highly influenced by the glacier Langjökull and the proglacial lake Hvítárvatn. Hvítárvatn is situated 422 m a.s.l., it spans an area of 28,9 km^2, a maximum depth of 83 m and is located adjacent to the eastern margin of Langjökull. Langjökull has two outlet glaciers, Suðurjökull and Norðurjökull, both of which are major sediment sources for the lake. The outlet glaciers are warm-based and both advanced into Hvítárvatn during the LIA, but have since then retreated leaving behind moraines marking their maximum extent (Larsen et al., 2011), which can be seen in the lake with bathymetric data and multibeam studies (Geirsdóttir et al., 2008). Suðurjökull retreated from the lake around 60 years ago, while Norðurjökull retreated from the lake in 2009 (Larsen et al., 2011).

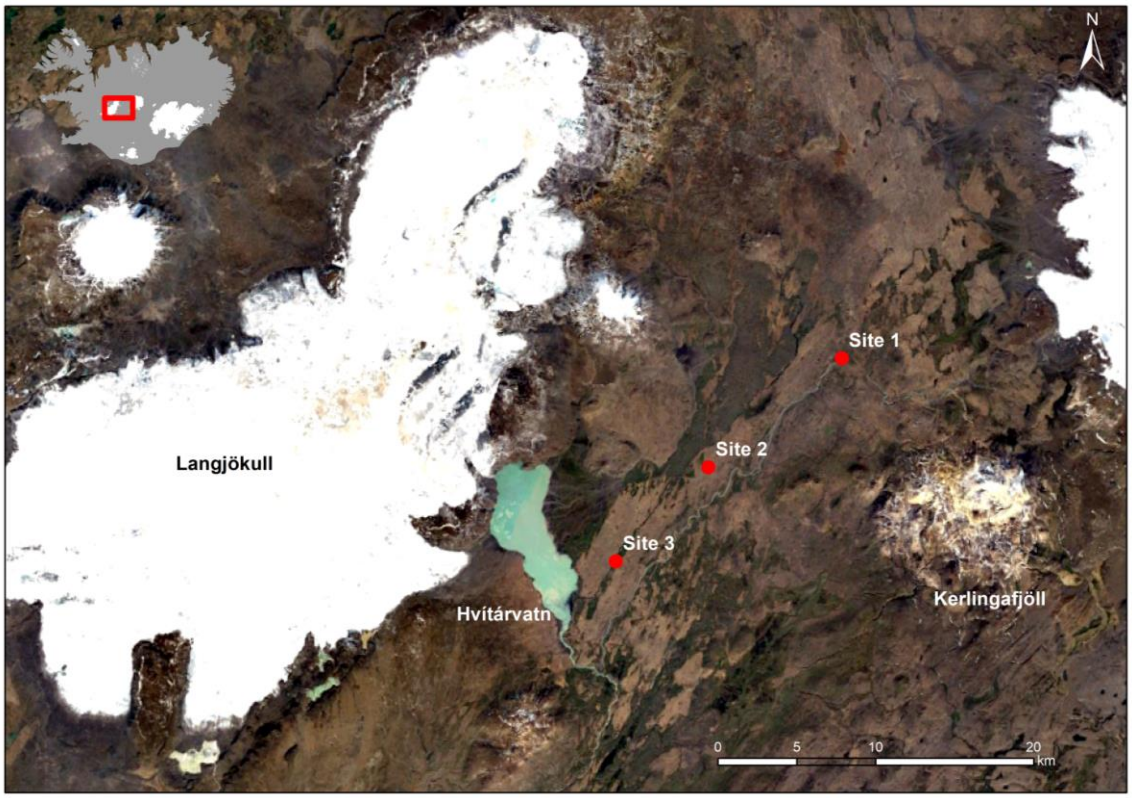

Figure 3. Aerial photograph of the study area (Google Earth) showing the location of the three soil sites chosen for measurements.

Arnarvatn Stóra is also located in the central highlands at 476 m a.s.l. and is a shallow bedrock-controlled lake in Arnarvatnsheiði, about 18 km NW of the northern lobe of Langjökull. The maximum depth of the lake is 3 m and the total area is 4 km^2. Arnarvatn Stóra does not receive water directly from Langjökull as it has inlets connected to other smaller lakes to the east and south. One core has been recovered from Arnarvatn Stóra, taken from the deepest part of the eastern basin of the lake and is 8 m long (Gunnarson, 2017).

Numerous sediment cores have been obtained from Hvítárvatn sediments providing valuable data for multi-proxy reconstruction of Holocene climate in Iceland. The records are well dated with high resolution for environmental changes and glacier activity. The Hvítárvatn record shows that the climate changes during the Holocene were non-linear and stepwise (Larsen et al., 2012). Haukadalsvatn, a lake in northwest Iceland has also provided a high-resolution climate reconstruction for the Holocene (Geirsdóttir et al., 2009a; Geirsdóttir et al., 2013). Both records show a great increase in soil erosion for the past 2 ka, as well as following a large explosive eruption through the last 10 ka. Thus, it is of great interest to compare the records of climate and landscape stability in the central highlands of Iceland using lake and soil stratigraphic archives. Paleoclimate reconstruction from Arnarvatn Stóra correlates well with Hvítárvatn record and provides a regional climate signal for the central highlands (Gunnarson, 2017).

Hvítárvatn was formed before 10.5 ka, indicated by sedimentological and seismostratigraphic studies (Geirsdóttir et al., 2009b; Larsen et al., 2013). The presence of the 10 ka Grímsvötn tephra series in cores from the post-glacial sediment fill in the lake,

confirms that the IIS had retreated from Hvítárvatn prior to 10.3 ka (e.g. Jóhannsdóttir, 2007; Larsen et al., 2012). The same tephra layer is found in the bottom parts of the core from Arnarvatn Stóra (Gunnarson, 2017). In the hillslopes on the north and west side of Hvítárvatn are multiple paleo-shorelines, which reach up to 200 m higher than the present lake level. These shorelines formed during the retreat of the IIS from the region, marking multiple stages of an ice-dammed lake and subsequent jökulhlaup activities (Tómasson, 1993). Although, after 10.3 ka there is no evidence for significant lake level changes (Larsen et al., 2012).

2.3 Soil around Kjölur

Due to active volcanic activity in Iceland, the Icelandic soils differ from most other soils of Europe. There are three dominating types of soils in Iceland, the main one is Andosols which is black or dark brown soil formed from volcanic material and is covered by vegetation. The second type is Vitrosols, which contains less than 1% organic carbon and is found in desert areas, and the third one is Histosols, dominated by organic material and located in some wetland areas. Andosols is the dominant soil type in Iceland, which is also the largest area of Andosols in Europe. Andosols cover about 78.000 km^2 or 86% of Icelandic soils, which is equal to >5% of all Andosols in the world. Andosols are not that common in other areas in Europe, but are found in active volcanic areas of the world (Arnalds, 2004; Arnalds, 2008).

Soil erosion is an active process, particularly in the highlands of Iceland, as the Icelandic soil types lack cohesion making them more vulnerable to erosion processes (Arnalds, 2008). At present the wind is the dominant process eroding the soil, especially cold and dry north-easterly winds and it is thought that this has been the case throughout the past 2 ka. Soil becomes most vulnerable to aeolian erosion and transport when vegetation cover is reduced and wind velocities are high, which is most likely to occur after a series of unusually cold and dry summer. After vegetation cover becomes reduced, the soil erosion can continue even during warmer summers (Arnalds, 2000; Geirsdóttir et al., 2009a). Almost 41.000 km^2 or about 40% of Iceland is affected by severe soil erosion, which has created a variety of landforms. Deserts are the largest areas of severe soil erosion, with sandy surfaces covering nearly 22.000 km^2. Another erosional form is *rofabörð*, vegetated islands of eroded soil and separate areas stripped of soil from surviving areas of soil and vegetation. *Rofabörð* cover about 3600 km^2 (Arnalds et al., 2001; Dugmore et al., 2009). Organic matter in soil, such as carbon content, is an important factor when dealing with soil and soil erosion. Andosols and Histosols store a great amount of carbon and thus are characterized as non-degraded when they contain high levels of organic carbon but when soil erosion is severe, large vegetated areas become barren and reduced in carbon content (Arnalds, 2004; Óskarsson et al., 2004).

Tephra layers preserved in the landscape and soil sections document the eruption history of explosive volcanism and the volcanoes or volcanic systems that produced them. Individual eruptions are preserved with the tephra layers and they form time marker horizons that span across large areas. The tephra record may cover the last 9000-10000 years in Icelandic terrestrial soils, depending on the timing of deglaciation and sea level changes. The record in lacustrine sediments may reach into the Lateglacial and the extent is much further back in time in marine sediments. Explosive volcanic eruptions are a sizable part of Holocene volcanism in Iceland. During the Holocene the East Volcanic Zone (EVZ) was most active regarding explosive eruptions, thus producing the majority of tephra layers found in the highlands (Larsen & Eiríksson, 2008). Due to active erosion in the central highlands soil

sections containing tephra layers are exposed in *rofabörð*, enabling both dating the soil accumulation and events of erosional activity (e.g. Dugmore et al., 2009).

Based on a soil map (Figure 4) from Arnalds & Grétarsson (2001) the soils by Kjölur can be divided into three main soil types, Brown and Gleyic Andosols, and Vitrisols. Gleyic Andosols are wetland soils with organic carbon <12% in surface horizons, these soils are found in wetland areas in the central highlands where rapid aeolian deposition occurs. Brown Andosols have the same carbon content as Gleyic Andosols, and are freely drained Andosols found in Iceland, both dark basaltic and light colored rhyolitic tephra layers can easily be identified within those profiles. The soil surface of Vitrisols usually have limited plant cover, around 5-10%, and often have a stone pavement resulting from frost heaving of coarse fragments. Due to Iceland's moist climatic conditions and temperatures (Boreal and Sub-Arctic climate), the Icelandic Vitrisols are unusual because these climatic conditions would elsewhere sustain vegetation growth. Vitrisols contain <1% organic carbon and are sandy and shallow, they develop from aeolian deposits. If vegetation is able to stabilize at the surface, the Vitrisols soils can develop characteristic Brown Andosols (Arnalds, 2004).

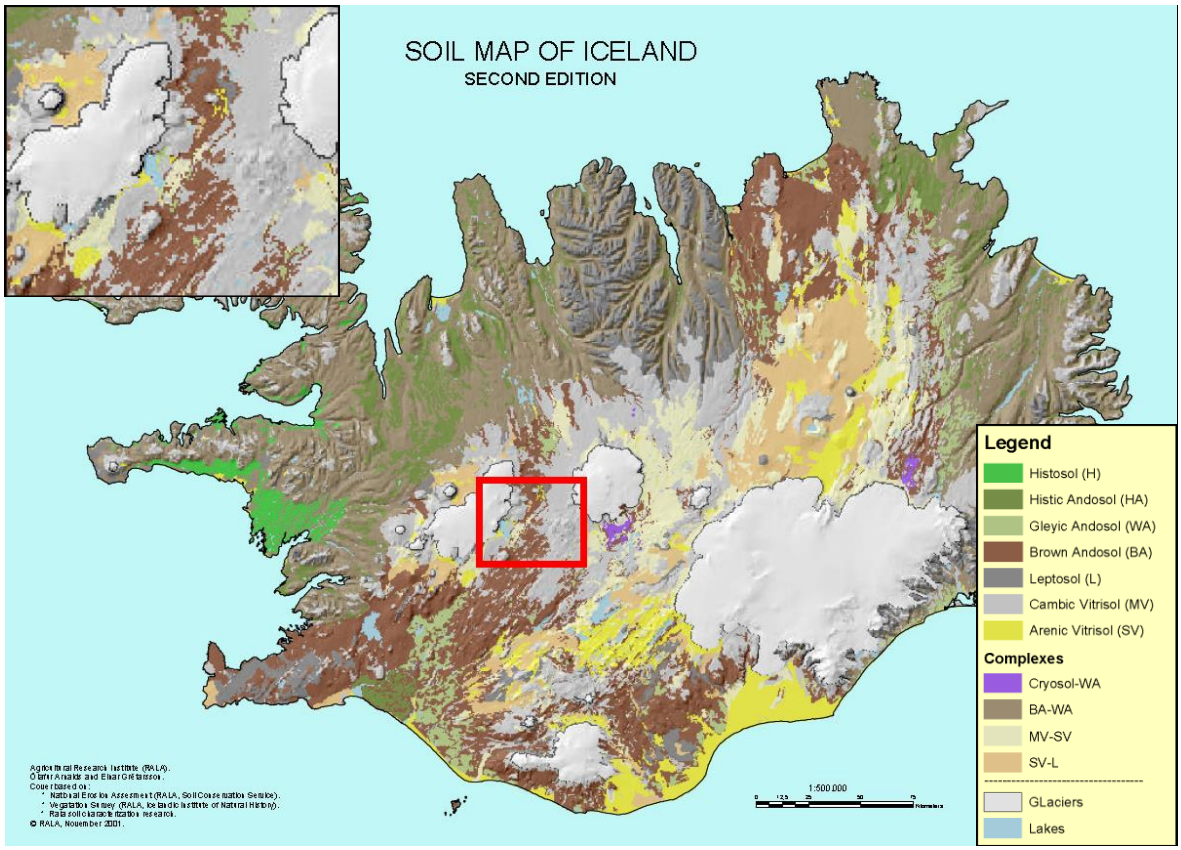

Figure 4. A soil map showing the dominating soil types in Iceland (modified from Arnalds & Grétarsson, 2001). The research area is marked with red and in the upper left corner is a zoomed in image of the area. The brown color represents Brown Andosol, the gray color is Vitrosol. There might also be some indication of Gleyic Andosol.

The dominating soil type within the Kjölur area are Andosols, made up of aeolian sand and tephra, and are found in small vegetated areas or *rofabörð*, often found near stream channels. Andosols lack cohesion and thus are very vulnerable to erosion by wind or water. Soil erosion is very active in the highlands and due to that fact, *rofabörð* in the area contain soil

profiles that include continuous records of mid-to-late Holocene age interbedded by tephra layers, indicating that the soil has been developing steadily (Arnalds, 2004; Geirsdóttir et al., 2009a; Larsen et al., 2011).

Since the soil lacks cohesion and soil erosion is an active process in the highlands of Iceland, the soil there is continuously modified by aeolian processes, as well as frequent tephra deposition events and freeze-thaw cycles due to the sub-arctic climate. Even though the climate is moist in much of the country, one of the unique characteristics of Icelandic soil environments is the existence of extensive deserts, such as the area around Langjökull. Resulting from the active aeolian processes there is a steady flux of aeolian materials deposited to the surface of preexisting soils. The majority of the Icelandic highlands are made up of sandy deserts, which makes them a primary source for aeolian materials (Arnalds et al., 2001; Arnalds, 2008). The highlands were covered by glacier/ice sheet during the last glaciation that sculptured the landscape. During the deglaciation and particularly during the HTM (between 9 and 6 ka), soil and vegetation started to form and develop (e.g. Larsen et al., 2012). Thus there is no soil older than of Holocene age found in the central highlands.

2.3.1 brGDGT measurements in soil

The development of proxies such as the lipid-based paleothermometer branched glycerol dialkyl glycerol tetraether (brGDGT) is possible due to the reason that microbial communities adjust the chemical structure of their cell membranes in response to environmental temperature. By calibrating surface sediment a strong empirical relationship between the relative distribution of brGDGTs and temperature, is obtained. As long as the organic material is not thermally mature, this temperature proxy can be used in marine, lacustrine and paleosol sequences (Tierney, 2012). This paleothermometer is rather newly developed and is providing new and exciting possibilities to estimate quantitatively past temperatures. This is an important factor for paleoclimate reconstructions.

2.4 Tephra layers found in the area

Tephra stratigraphy has been studied in Hvítárvatn and Arnarvatn Stóra (Jóhannsdóttir, 2007; Larsen et al., 2011; Gunnarson, 2017) providing an insight in what tephra layers can possibly be found by Kjölur. The oldest tephra expected to be found in the soil sections is the Saksunarvatn tephra (10.3 ka) which is a part of the 10 ka Grímsvötn tephra series and has been found in both lakes. Then there are three silicic tephra layers from Hekla present in Hvítárvatn and Arnarvatn Stóra, all of them being important tephra marker layers, they are ~ 7 ka H5, ~ 4.2 ka H4 and ~ 3 ka H3 (Larsen & Thorarinsson, 1977; Dugmore et al., 1995; Jóhannsdóttir, 2007; Gunnarson, 2017). The Settlement layer (871 ± 2 CE; e.g. Grönvold et al., 1995) is another important tephra marker layer and is originated from the Bárðarbunga-Veiðivötn volcanic system. This layer is generally seen above a black tephra layer from Katla (1.2 ka) referred to here as Katla prehistoric. Both of these tephra layers are found in Hvítárvatn, however the Settlement layer is only present in Arnarvatn Stóra. Hekla 1104 is present in both lakes and Hekla 1300 is present in Hvítárvatn. Bárðarbunga-Veiðivötn 1477 is a tephra layer which was identified in both lakes as well as Katla 1721, that is the youngest tephra found in Arnarvatn Stóra. The youngest tephra layer found in Hvítárvatn is Hekla 1766 (Larsen et al., 2011; Gunnarson, 2017; Figure 5). Tephra dispersal maps also indicate that tephra layers that are present in Hvítárvatn should be in the soil at Kjölur (Figures 6 and 7).

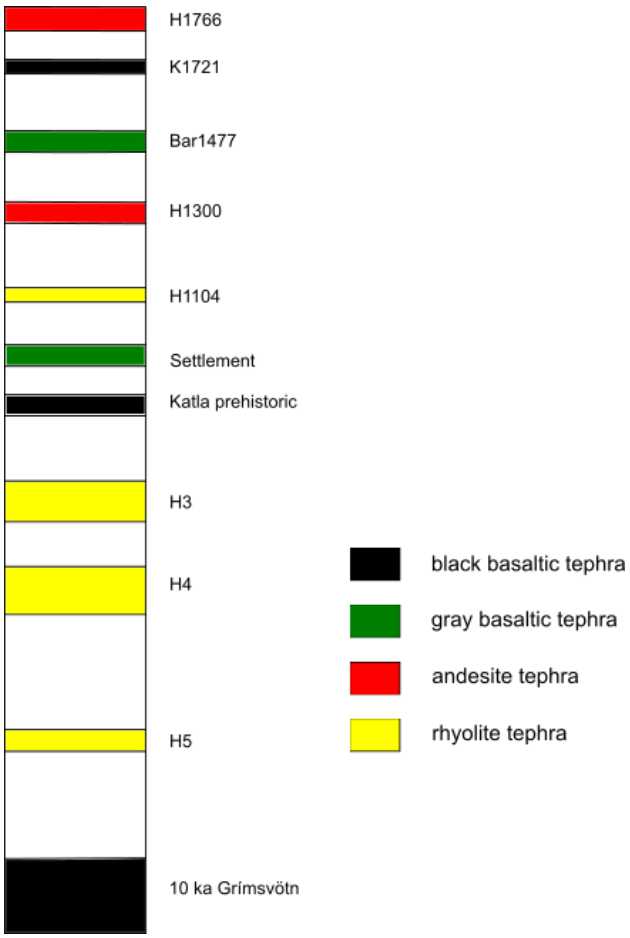

Figure 5. Schematic stratigraphic column displaying the most common tephra layers present in the area. All of these tephra layers are found in Hvítárvatn.

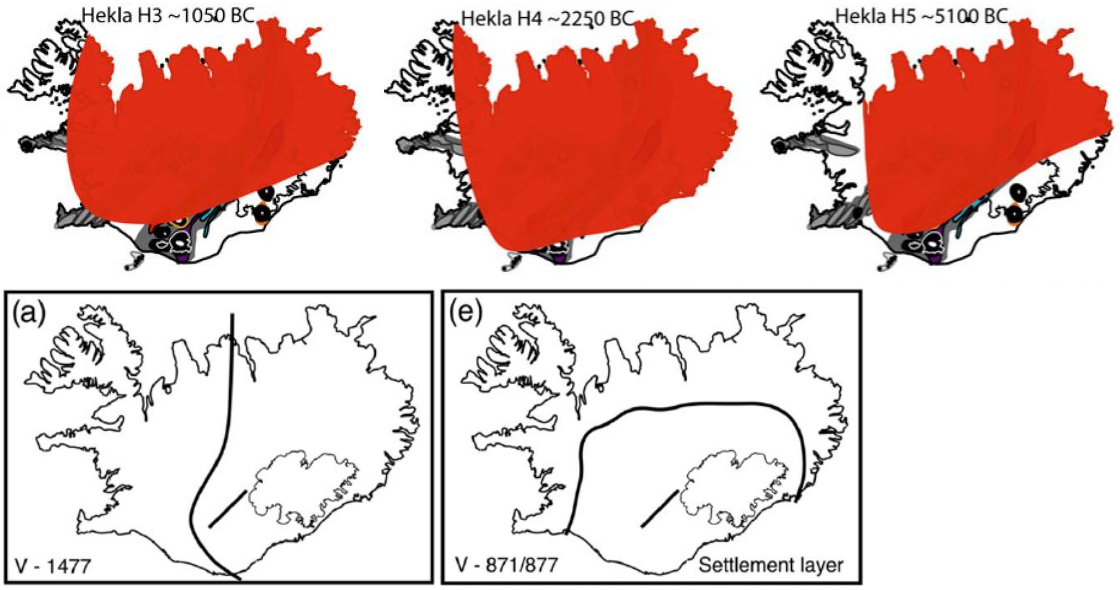

Figure 6. Examples of tephra dispersal maps for known tephra marker layers expected to be found by Kjölur. The upper three images show H3, H4 and H5 (Óladóttir et al., 2011). The two images below display dispersal of two tephra layers from Bárðarbunga-Veiðivötn volcanic system, 1477 and the Settlement layer (Larsen et al., 2002).

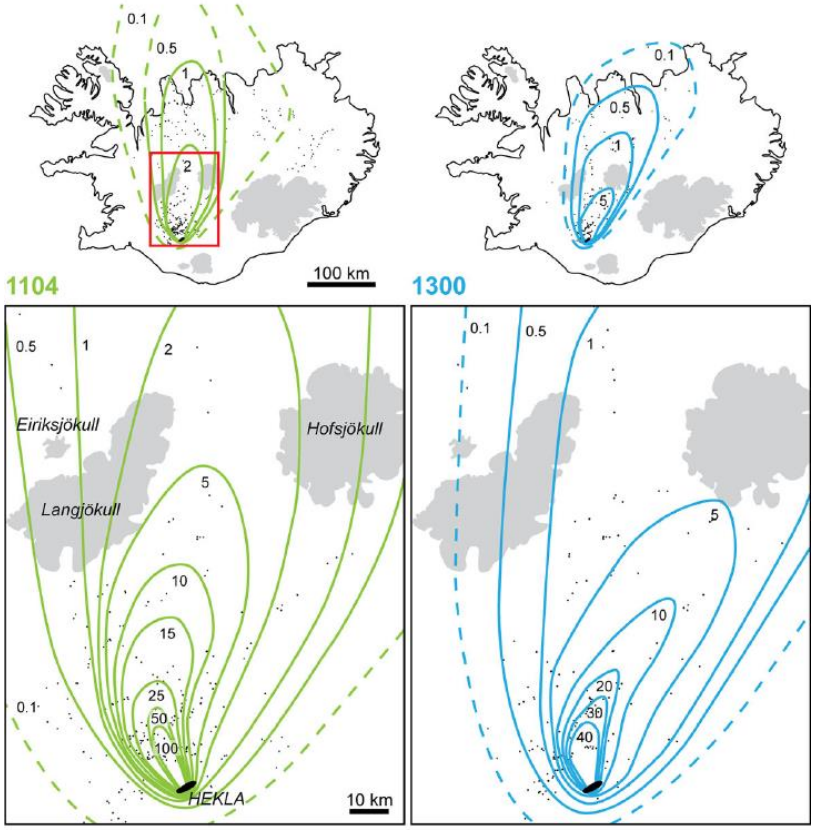

Figure 7. Tephra dispersal maps showing two Hekla tephras, 1104 and 1300, with zoomed in images that focus on the research area (Janebo et al., 2016).

3 Methods

3.1 Field work and sampling

Sampling and measurements in the field were completed in summer 2017. Three soil sites were chosen with two profiles measured in the first two sites, thus five profiles measured in total and samples collected from all of them. Each profile was measured and described in detail, they were also divided into layers based on appearance and color. When describing the material in the soil, the Wentworth scale is used to estimate grain size (e.g. Nichols, 2009) and for the tephra layers the pyroclastic grain size terminology is used (White & Houghton, 2006). Both bulk soil samples and tephra samples were collected. The soil samples were collected at every few centimeters in 2x2 cm plastic boxes and marked with a letter J, the tephra samples were put in plastic bags and marked with G. Also, when possible, a plastic u-tube was pushed up against the section to obtain a continuous sample reaching from top to bottom of the section, those samples were marked with the letter S.

During the observation and description of the soil profiles in the field, a difference in appearance of the profiles could be seen. Large parts of some profiles were dominated by medium to coarse grained sand mixed in with rounded tephra grains. These parts were determined to be reworked and redeposited and gave the soil a dark gray color mixed with light colored tephra grains originating from thick primary rhyolite tephra layers that were present in profiles in the area. This conclusion was confirmed when the tephra samples examined further in the laboratory for angularity/roundness under binocular microscope. Rounded grains in a tephra sample indicates that the grains have been abraded during aeolian transport thus been subjected to reworking and redeposition (e.g. Gudmundsdóttir et al., 2011).

3.2 Age model development

3.2.1 Sample preparation

First step in preparation for microprobe analysis, the tephra samples were dried and sieved. The size range used for the sieving was between 125 and 500 µm. Grains from 250-500 µm were collected and put in an ultrasonic bath to get rid of any finer grains covering the bigger ones. After the bath they were dried and then the samples were viewed in a binocular microscope to determine which samples would be suitable for the electron microprobe. Some samples collected as tephra were in fact not primary tephra layers but redeposited material. To obtain the best age model possible it is important to differentiate between primary tephra layers and the ones that are reworked and redeposited.

Some of the samples were put through a magnetic separator to separate out crystalline rock fragments. When the tephra samples were ready to be analyzed they were put into five probe plugs, with seven tephra samples in each plug. Thus in total 35 tephra samples were seleted for chemical analysis. To be sure that the correct grains were analyzed in the microprobe,

the probe plugs and each sample were photographed under microscope, which in turn were used as a map to mark each point taken for each tephra sample in the microprobe.

3.2.2 Microprobe analysis

The tephra samples were analyzed in a Jeol JXA-8230 SuperProbe Electron Probe Microanalyzer (EPMA) at the University of Iceland, which provides accurate quantitative chemical analysis of elements from a very small volume of solid inorganic material. With the EPMA it is possible to analyze areas down to 1 µm in diameter in a sample. The EPMA directs a powerful X-ray onto the sample and the beam stimulates the electron shells (K, L, M) in the atom, each element reflects a certain frequency of the X-ray. The device measures this frequency and thus also measures the amount of all elements found in the sample. Each chemical analysis usually takes a few minutes. The EPMA also has an optical microscope, used to locate the area within the sample, which is ideal for chemical analysis (e.g. Reed, 2005).

The basaltic tephra was analyzed first and a standard basaltic glass (A99) was analyzed before and after the tephra samples, to verify the precision and the accuracy of the microprobe setup used in this study. For the silicic tephra samples a standard silicic glass (ATHO) was analyzed beforehand as well as afterwards. The EPMA is setup differently for analyzing basaltic and silicic glass, due to possible loss of sodium when using a basaltic setup for silicic glass. For basaltic and intermediate glass the voltage of the beam was 15 kV and the current was 10 nA. For silicic glass the voltage was also 15 kV, but the current 5 nA. The diameter of the beam was 5-10 µm, depending on the size of the glass in the samples, as well as the width of glass bubble walls, and the amount of microliths. In each sample 10-15 points were obtained for chemical analysis.

3.2.3 Tephra identification

Tephrochronology is very important in research in Iceland and in Quaternary studies, as it gives information about explosive eruption history as well as providing time markers. Volcanism was very active during the last deglaciation subsequent to the retreat of the IIS (e.g. Larsen & Eiríksson, 2008). The Icelandic Holocene tephrochronology is well established and eases the identification of tephra layers present in the soil sites. The identification is very important as reaching a conclusion towards the eruption ages also provides age points for the age models.

By calculating average and standard deviation for the microprobe results for each tephra, it was possible to identify points in the chemical analysis that did not belong in the results, such as minerals and non-primary volcanic glass grains. The source identification of the tephra layers was done by using a setup of geochemical discrimination plots prepared by T. Thordarson using available chemical data on Icelandic tephra layers from all of the active volcanic systems (Thorvaldur Thordarson, unpublished data 2018). When applicable, knowing the source volcanic system of a particular layer enables use of the chemical composition in conjunction with stratigraphic position to match the layer in question with known and previously age dated tephra layers (e.g. Grönvold et al., 1995; Thordarson et al., 1998; Larsen et al., 2002; Óladóttir et al., 2008; Óladóttir et al., 2011). To be able to use the geochemical discrimination plots, the sum of Na_2O and K_2O was calculated for each tephra sample, as well as the magnesium number and the proportion between titanium and iron. The first graph estimates if the tephra is basaltic or silicic, depending on the results the plots

go in different directions displaying known lines for volcanic systems that produce either basaltic or silicic tephra. Differentiation between alkalic or tholeiitic tephra, is determined by using the lines provided by Kuno (1966) and, MacDonald and Katsura (1964). Figure 8 shows an example of how the geochemical discrimination plots are used for the tephra identification, by displaying two well-known tephra layers, the plots used for the analyzed tephra samples are shown in Appendix A.2.

Some tephra samples reveal more than one dominating rock type, the reason for that might be because of redeposition of tephra grains into a primary tephra layer or two primary tephra layers lying together due to short time between eruptions. The pictures obtained from the probe plugs are used to be able to distinguish which grains are primary by looking at the texture and angularity of the grains. Using the pictures it is possible to identify if the grains have fragile corners that would break if the grains would be transported, indicating that those grains are most likely primary. If grains are rounded that indicates that they have undergone transport and have been redeposited. Explosive volcanism has been a common eruption type throughout the Holocene, thus a lot of the same volcanic systems have produced many tephra layers found in soil sections. Also, the chemical characteristics of these volcanic systems has remained fairly stable during the Holocene, which causes difficulty in distinguishing between different tephra layers from the same volcanic system by using major element chemistry alone. Due to this fact, the stratigraphic position of the tephra layers becomes very important. The position of the tephra layer in relation to other tephra layers can then be used as a characteristic (Larsen & Eiríksson, 2008). Thus, in the final steps of tephra identification it is important to look at the stratigraphy for each section while looking at published chemical analysis data. When potential volcanic sources were established for the tephra layers after using the geochemical discrimination plots to conclude their rock types, the stratigraphy of the soil profiles was used and comparison were made between the tephras found in the soil sections and the Hvítárvatn and Arnarvatn Stóra sediments, thus reaching a conclusion regarding the ages of the tephra layers. By looking at tephra dispersal maps (e.g. Larsen et al., 2002; Óladóttir et al., 2011; Janebo et al., 2016) (Figures 6 and 7) it is clear that the tephra deposited in Hvítárvatn should also be deposited in Kjölur.

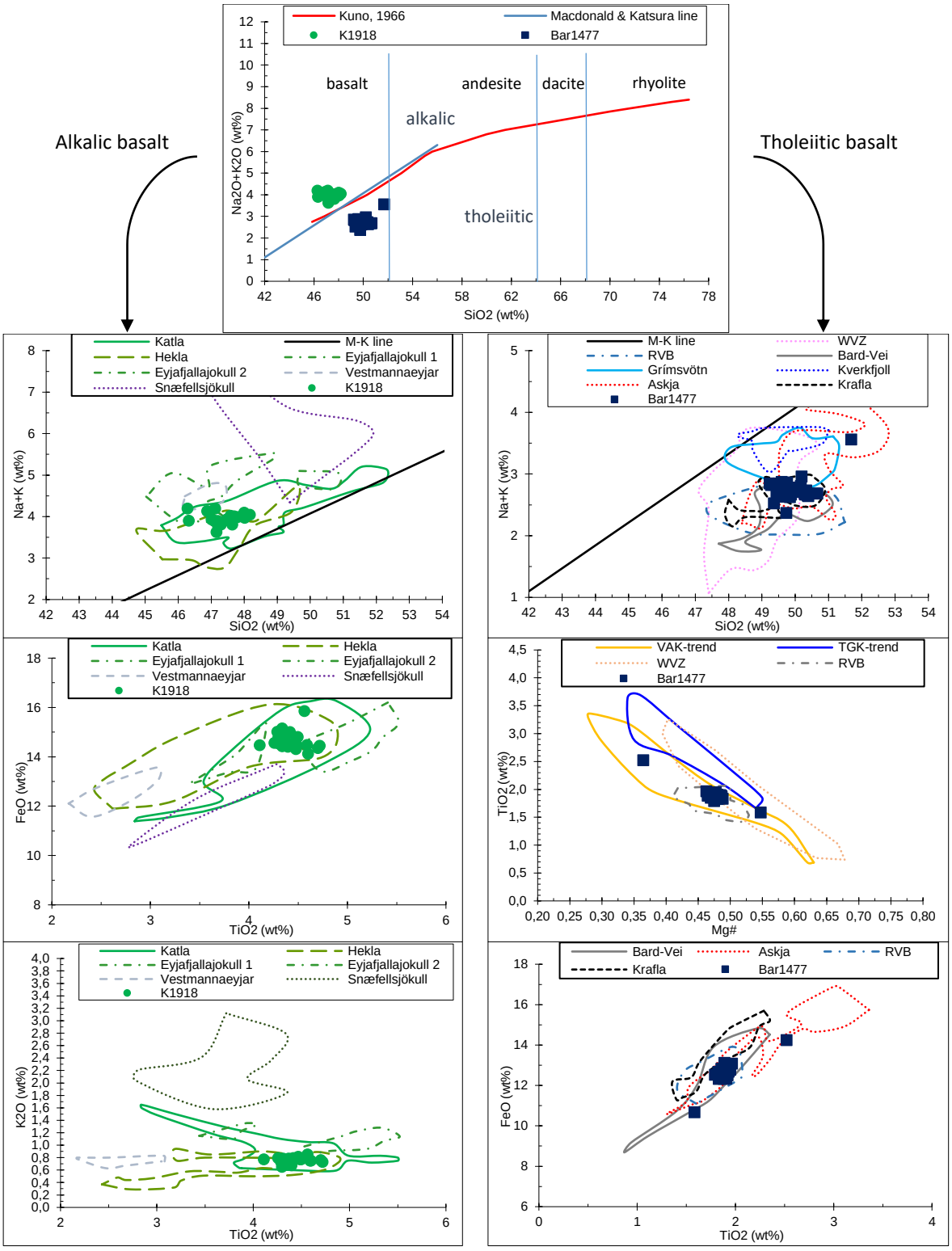

Figure 8. Example of geochemical discrimination plots and how they are used for different rock types. The top graph is the initial graph plot used to distingish between rock types using the lines provided by Kuno (1966) and MacDonald and Katsura (1964). The plots on the left side show an example of an alkalic basalt sample, Katla 1918 (Óladóttir et al., 2008; Thorvaldur Thordarson, unpublished data 2018). On the right side is an example of a tholeiitic basalt sample, Bárðarbunga-Veiðivötn 1477 (Larsen et al., 2002; Thorvaldur Thordarson, unpublished data 2018).

3.2.4 Age model

Age-depth models are necessary when estimating the evolution of climate proxies through time. Subsequent to the identification of the main tephra layers found in each soil profile the *Clam 2.2* software was used to reconstruct tephra-based age models with linear interpolation. The software uses calibrated ages (BP) and to obtain a reliable age model the software needs a minimum of four dating points (Blaauw, 2010). Five age models were created, one for every section measured. The *Clam* software was not used on profile 2.2 as it only contains three data points, not enough to create accurate age-depth model for the profile. Instead a simple linear interpolation was used to create a tentative age model for that profile.

3.3 Loss on ignition

A common and widely used method to estimate organic matter and carbonate content in sediments is sequential loss on ignition (LOI). For this research the soil samples were only measured for organic matter or rather carbon content. The soil samples chosen for the measurement were 29 in total and first they were all weighted, then dried for a day at 50°C. After the samples were dried they were weighted again before they were heated overnight at 105°C in ceramic crucibles, to get rid of any remaining water in the samples. Then finally the soil samples were heated at 550°C for four hours to remove organic matter, which gets oxidized to CO_2 and ash at that temperature. After each heating step the samples were allowed to cool completely without taking in any moisture and then weighted. The LOI of organic matter is then calculated using the equation below, where the LOI_{550} represents LOI at 550°C as a percentage, DW_{105} is the dry weight of the samples before being heated to 550°C and DW_{550} is the dry weight of the samples after the final heating step at 550°C, both of the dry weight values are in grams. Then the weight loss is proportional to the amount of organic carbon contained in each sample (Heiri et al., 2001).

$$LOI_{550} = \left(\frac{DW_{105} - DW_{550}}{DW_{105}}\right) \times 100$$

Soils that contain high levels of organic carbon have extensive vegetation and are characterized as non-degraded. On the other hand, soils that contain low organic carbon have experienced severe erosion, resulting in extensive barren areas (Óskarsson et al., 2004). With this in mind the organic carbon content can also provide information about climate evolution, since erosion is more active during cooler climate when wind strength is increased. Geirsdóttir et al. (2009a) identified higher values of terrestrial organic matter in Haukadalsvatn sediments during cold intervals of the LIA reflecting unstable catchment and increasing aeolian activity. Thus, the organic matter that gets eroded away from the soil gets transported to nearby lakes. The organic carbon concentration in types of Andosols ranges from 17% in Histic Andosols to 3,3% in Brown Andosols. By observing vertical distribution of organic carbon between non-degraded soil and areas effected by erosion, a large difference can be observed. Also, the organic carbon content for non-degraded soil does not vary much with depth. The formation of soil horizons with less carbon content occurred at a time with intense soil erosion and mainly contain aeolian material (Óskarsson et al., 2004).

3.4 brGDGT

In lake and coastal marine sediments, soil and peat branched glycerol dialkyl glycerol tetraethers (brGDGTs) are abundant lipids. They are derived from bacteria carrying 4-6 methyls attached to the linear C_{28} alkyl chains and by internal cyclization, up to two cyclopentanyl moieties are formed (De Jonge et al., 2013). The brGDGTs have over the last decade become very useful and an important part of organic geochemistry and paleoclimate research, because their distribution correlates with soil pH and mean annual air temperature. The use of this proxy has been increasingly applied to coastal marine and lake sediments, and also loess and paleosols to obtain data regarding past terrestrial temperatures (e.g. Weijers et al., 2007; Naafs et al., 2017). When temperature decreases the number of methyls increases and when soil pH gets higher the degree of cyclization increases (e.g. Weijers et al., 2007; De Jonge et al., 2013).

At the University of Colorado Boulder, 13 soil samples weighing 1-4 g, were ground and homogenized using an agate mortar and pestle, then freeze-dried. Total lipids were extracted using a Dionex accelerated solvent extractor (ASE 200) with dichloromethane:methanol (9:1, v/v) at 100°C. Portions of the total lipid extracts were filtered in 99:1 hexane:isopropanol (99:1, v/v) using a 0.45 µm PTFE syringe filter. Before the analysis a C_{46} brGDGT internal standard was added to all filtered. Isoprenoid brGDGTs were identified and quantified through high performance liquid chromatography – mass spectrometry (HPLC-MS) following the methods of Hopmans et al. (2016) on a Thermo Scientific Ultimate 3000 HPLC interphased to a Q Exactive Focus Orbitrap-Quadrupole MS. Scanning was performed on full scan (FS) mode. Following recent improvements in the chromatographic separation of 5-methyl and 6-methyl isomers (De Jonge et al., 2013), the MBT'$_{5ME}$ index was adopted (De Jonge et al., 2014), thus these indices were converted to quantitative mean annual air temperature (MAT) using the refined global soil calibration (Naafs et al., 2017):

$$MBT'_{5ME} = \frac{(Ia + Ib + Ic)}{(Ia + Ib + Ic + IIa + IIb + IIc + IIIa)}$$

$$MAAT'_{soil} = 39.09 \times MBT'_{5ME} - 14.50$$

4 Results

4.1 Soil profiles

The sites lie along a transect from NE to SW across Kjölur between Kerlingafjöll and Hvítárvatn (Table 1) and are described from site 1 (Fossrófulækur) to site 3 (Hvítárvatn) (Figure 3). Detailed description of each profile is presented in Appendix A.1 and images of the soil profiles are shown in Figures 9 and 10.

Table 1. GPS coordinates for all three soil sites.

Site	Coordinates
1	N 64°42.832’ W019°25.925’
2	N 64°39.085’ W019°36.465’
3	N 64°35.857’ W019°43.748’

4.1.1 Site 1, profile 1

Site 1 is located within a little creek called Fossrófulækur, by the road to Kerlingafjöll at 562 m a.s.l. The soil cut where the profile was described and measured is oriented roughly NE-SW. The first profile (1.1) at this site is 238 cm thick, although the 170 cm at the bottom were measured and described. The section is divided into 16 layers based on appearance and color (Figure 11). The measured part of this profile contains three tephra layers and the organic material has a brown color. There are some rock fragments present through the profile found in the organic material.

4.1.2 Site 1, profile 2

Profile 1.2 at site 1 is located a few meters NE from the first soil profile. The total thickness of this section is 327 cm and it is divided into 24 layers (Figure 11). Profile 1.2 contains 13 tephra layers and similar appearance of organic material as for profile 1.1. The organic material does contain some rock fragments, although some parts are quite homogeneous.

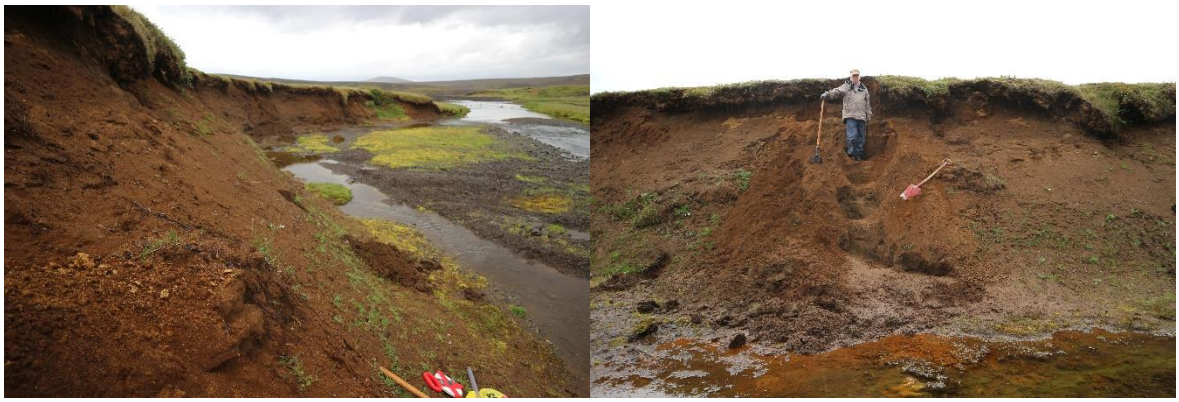

Figure 9. To the left is the SW end of sit 1 and to the right is profile 2 at site 1.

4.1.3 Site 2, profile 1

Site 2 is located SE from Baldheiði, which is located slightly NE from Hvítárvatn (Figure 2). This site is 495 m a.s.l. The first profile (2.1) at this site is in total 326 cm thick and is divided into 19 layers (Figure 12). There are 7 tephra layers present in profile 2.1 and the organic material is characterized by coarser grainsize compared to the profiles in site 1. This profile also contains some redeposited material as was described in chapter 4.1.

4.1.4 Site 2, profile 2

The second profile (2.2) at site 2 is located on the other side of a dried riverbed, a few kilometers NW from profile 1 at this site. This profile is divided into 23 layers and has a total thickness of 305,5 cm (Figure 12). This profile only contains three tephra layers and is dominated by coarse grained organic material and redeposited material. Due to the redeposited material, the brown color of the organic material becomes darker and contaminated by non-primary tephra grains.

4.1.5 Site 3, profile 1

Site 3 with profile 1 is located a few kilometers east from Hvítárvatn by the Hvítárvatn delta. It is situated at 453 m a.s.l. This profile is divided into 32 layers and is in total 395 cm thick (Figure 13). Seven tephra layers are found in this profile and the dominating material is similar to profile 2.2, coarse grained organic material and redeposited material.

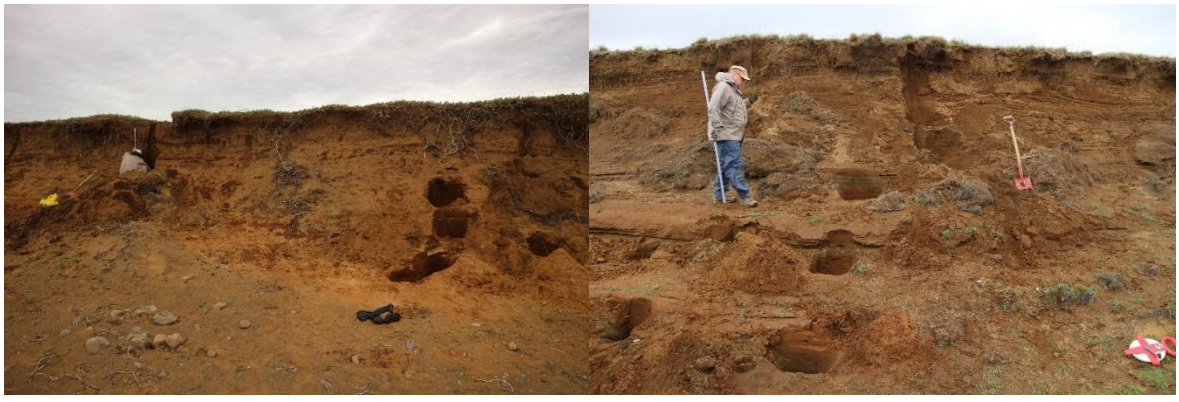

Figure 10. Soil profile 1 at site 2 to the left and soil profile at site 3 to the right.

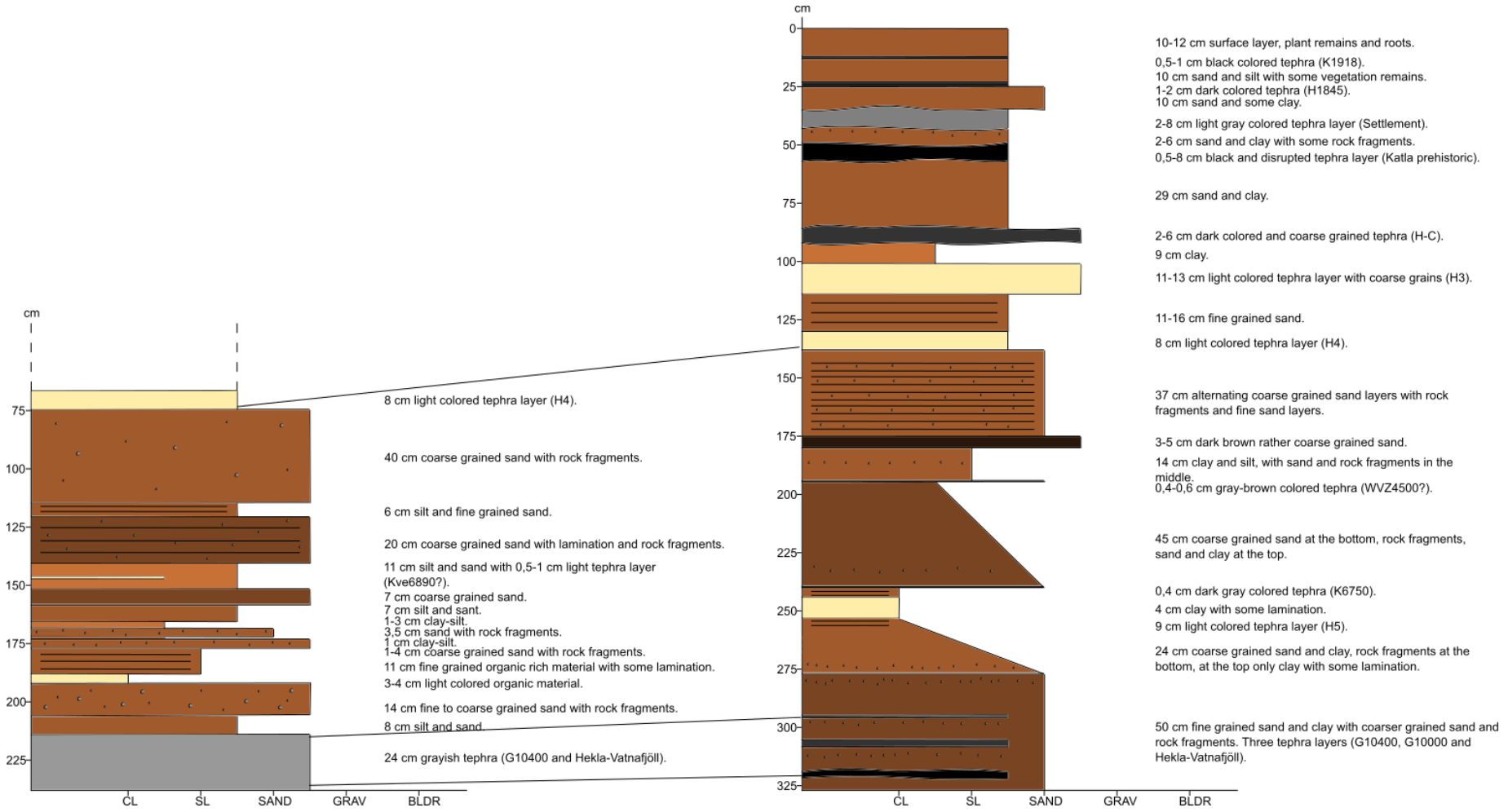

Figure 11. Stratigraphic columns for site 1, profile 1 is displayed on the left and profile 2 on the right. The grain size of each layer is displayed by the width and the depth is shown in centimeters on the vertical line. The tephra layers present in both profiles are marked with their identification in brackets which will be discussed further in chapter 5.2.

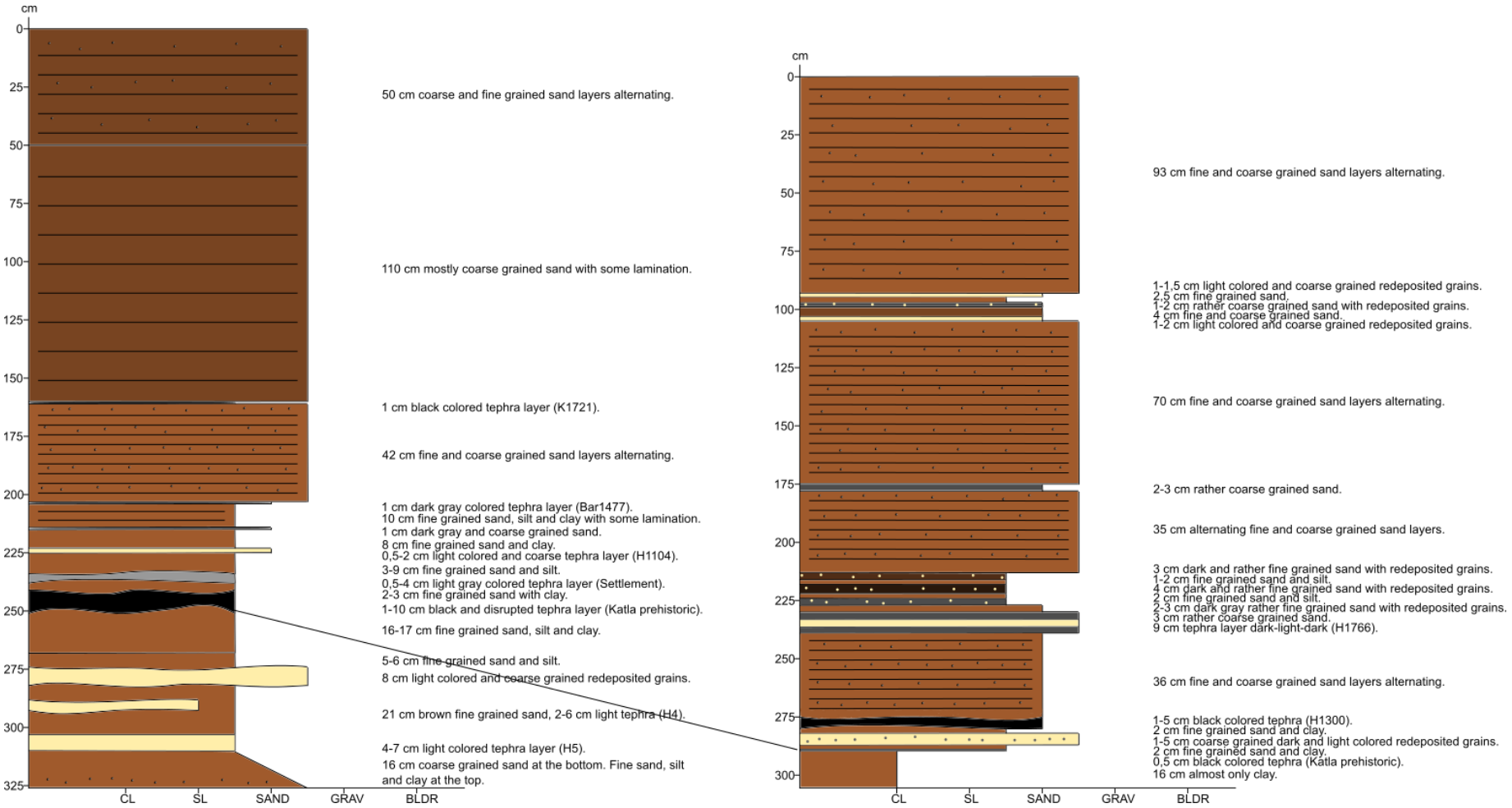

Figure 12. Stratigraphic columns for site 2, profile 1 is shown on the left side and profile 2 on the right. The grain size is displayed on the vertical line, more width a layer has means larger grain size. The horizontal line displays the depth of the profiles, shown in centimeters. By each tephra layer present in the profiles is their identification in brackets, this will be further discussed in chapter 5.2.

Figure 13. Stratigraphic column showing how profile 3 is devided into layers. The horizontal line displays the grain size and the vertical line shows the depth of the profile in centimeters. The identification of the tephra layers present in this profile is indicated in brackets, but will be discussed further in chapter 5.2.

4.2 Tephrochronology

The tephra samples which were analyzed and identified were in total 35. The results from the chemical analysis and identification is shown in Table 2. The data is reported in weight percentage (wt%, uncorrected) and FeO* is a representative for both Fe(II) (FeO) and Fe(III) (Fe_2O_3) oxides. The average for each major component is listed in the table for every tephra sample and also the standard deviation in italic. The ages for the tephra layers (TL) are reported in calibrated years BP and all are marked with age references used to help with the identification. Many tephra layers were present in more than one soil profile which made it easier to correlate between the profiles and identify tephra layers in between common known tephras.

4.2.1 Site 1, profile 1

TL 238-214 cm: Grayish and coarse sand grained. Chemical analysis matches partly to the Grímsvötn volcanic system and also to Hekla. The Grímsvötn part was identified as Grímsvötn 10.4 ka (G10400) which is the oldest part of the 10 ka Grímsvötn tephra series and the Hekla part identified as Hekla-Vatnafjöll with an age of 9.100 years BP, which is often present above the 10 ka Grímsvötn tephra series (Figure 14; Jóhannsdóttir, 2007; Thorvaldur Thordarson, unpublished data 2018).

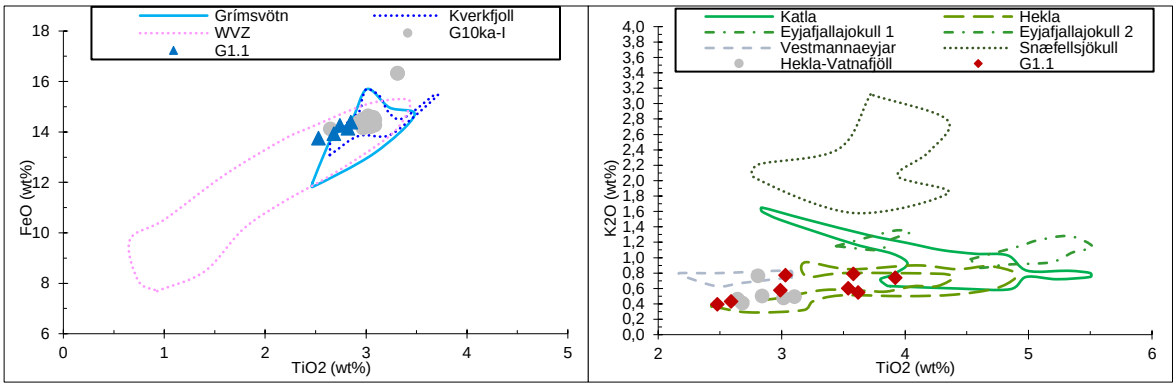

Figure 14. Examples of graphs used to identify G10400, shown on the left, and Hekla-Vatnafjöll, shown on the right with comparison data from Thorvaldur Thordarson (unpublished data 2018). The rest of the graphs are shown in Appendix A.2.

TL 146-145 cm: Light colored and fine sand grained. Based on chemical analysis and the geochemical discrimination plots this tephra was originated from Kverkfjöll. This tephra was hard to identify due to few grains ideal for chemical analysis in the sample. Although, based on calculated SAR age the tephra was given an estimated age of 6890 years BP. The assigned age is supported by data from Óladóttir et al. (2011) (Figure 15).

TL 74,5-66,5 cm: Light colored and very fine sand grained. The geochemical discrimination plots revealed that the chemical analysis for this tephra matches the Hekla volcano. By observing the stratigraphy and using comparison data the tephra was identified as H4 (Figure 15; Jóhannsdóttir, 2007; Thorvaldur Thordarson, unpublished data 2018).

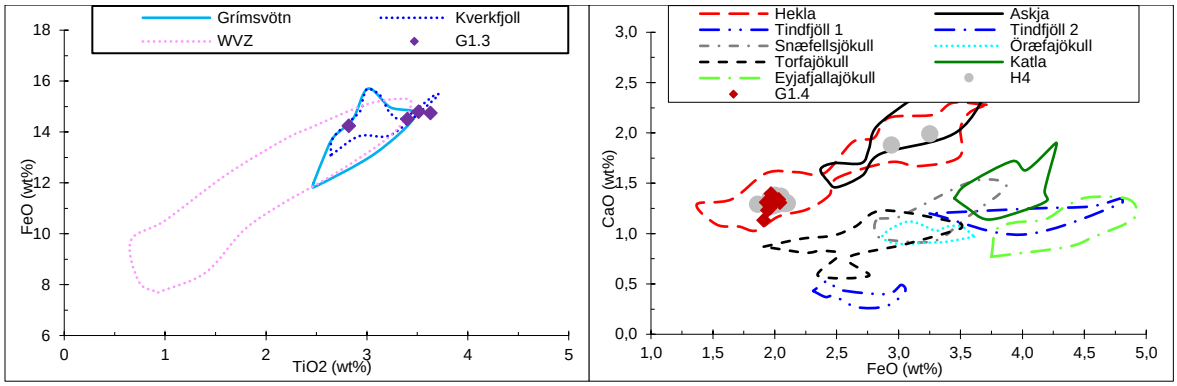

Figure 15. The left graph shows how the volcano origin was identified for sample G1.3, from Kverkfjöll. No comparison data was available for that tephra. The right graph shows how the H4 tephra was identified with comparison data from Thorvaldur Thordarson (unpublished data 2018). The rest of the plots for these samples are found in Appendix A.2.

4.2.2 Site 1, profile 2

TL 325-322 cm: Black and rather coarse to fine sand grained. The chemical analysis for this tephra matches the Grímsvötn volcanic system and was identified to be a part of the 10 ka Grímsvötn tephra series. By using comparison data, observing the stratigraphy and correlating to profile 1.1, the tephra was estimated to have an age of 10.4 ka (G10400) (Figure 16; Jóhannsdóttir, 2007; Thorvaldur Thordarson, unpublished data 2018).

TL 317-314 cm: Gray colored and rather coarse to fine sand grained. Based on chemical analysis and geochemical discrimination plots this tephra was also identified to be a part of the 10 ka Grímsvötn tephra series. Comparison data and stratigraphy estimated that the tephra has an age of 10 ka (G10000) (Figure 16; Jóhannsdóttir, 2007; Thorvaldur Thordarson, unpublished data 2018).

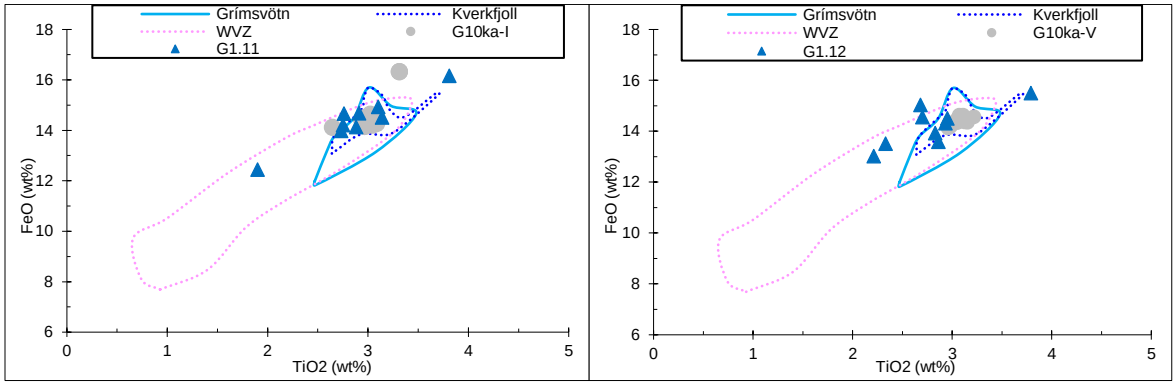

Figure 16. Comparison data from Thorvaldur Thordarson (unpublished data, 2018) and an example of a geochemical discrimination plot used to identify samples G1.11 (G10400) and G1.12 (G10000), more graphs are displayed in Appendix A.2.

TL 300-299 cm: Gray but not very visible and rather coarse sand grained. The chemical analysis for this tephra matches the Hekla volcano and was identified as Hekla-Vatnafjöll 9.1 ka by using comparison data, stratigraphy and correlation to profile 1.1 (Figure 17; Thorvaldur Thordarson, unpublished data 2018).

TL 253-244 cm: Light colored, the bottom 2-3 cm contain coarse sand grains while the upper 6-7 cm have finer sand grains. Due to this difference in appearance, two samples were collected from the tephra and analyzed. Chemical analysis and geochemical discrimination plots revealed this tephra to originate from Hekla. The stratigraphy and comparison data made it possible to identify the tephra with an eruption age, thus this tephra was identified as H5 (Figure 17; Jóhannsdóttir, 2007; Thorvaldur Thordarson, unpublished data 2018).

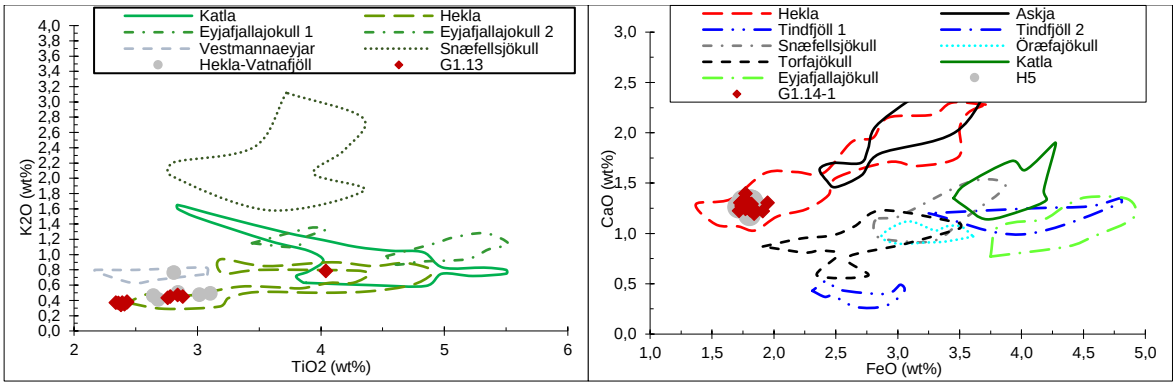

Figure 17. To the left is an example of how Hekla-Vatnafjöll was identified, using a geochemical discrimination plot and comparison data. To the right is an example from one out of two samples from the H5 tephra. Comparison data from Thorvaldur Thordarson (unpublished data 2018). The rest of the plots are shown in Appendix A.2.

TL 240-239,6 cm: Dark gray color and coarse sand grains. This tephra originates from Katla as was observed using the chemical analysis and geochemical discrimination plots. The eruption age was estimated to be 6750 years BP, based on comparison data (Figure 18; Thorvaldur Thordarson, unpublished data 2018).

TL 194,6-194 cm: Brown-gray color and rather coarse sand grained. Identifying this tephra layer was quite difficult due to the lack of grains in the sample to analyze. Although, the chemical analysis and geochemical discrimination plots did reveal that the tephra originated from the WVZ. Not many tephra layers are known from the WVZ but comparing to published chemical and stratigraphical data by Sinton et al. (2005) gives an estimated eruption age of 4.5 ka (Figure 18).

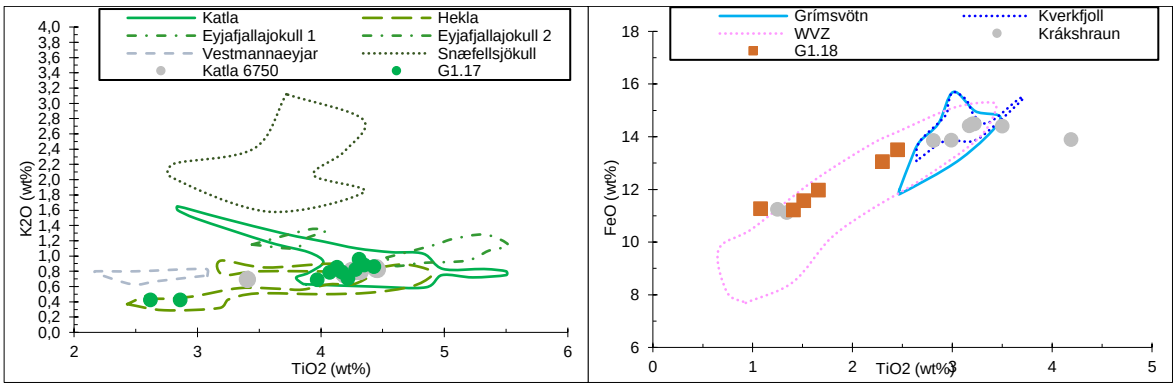

Figure 18. The left graph is an example of how Katla 6750 was identified with comparison data (Thorvaldur Thordarson, unpublished data 2018). The graph to the right that was used to reveal the origin of the WVZ tephra and comparison data from Sinton et al. (2005). The rest of the graphs are listed in Appendix A.2.

TL 114-101 cm: Light colored and coarse grained, grains are around 1 mm in size. This tephra originates from Hekla and using stratigraphy and comparison data was identified as H3 (Figure 19; Jóhannsdóttir, 2007; Thorvaldur Thordarson, unpublished data 2018).

TL 92-86 cm: Dark color and coarse grained, grain size is 2-3 mm. This tephra also matches chemical data from Hekla and was revealed to be the 2.9 ka H-C tephra by using comparison data and stratigraphy (Figure 19; Thorvaldur Thordarson, unpublished data 2018).

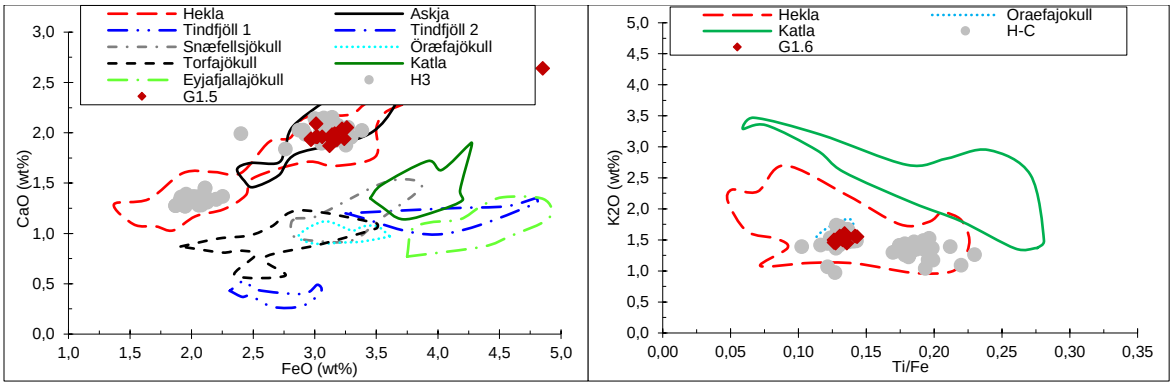

Figure 19. H3, to the left, and H-C, to the right, shown in geochemical discrimination plots and comparison data used for identification (Thorvaldur Thordarson, unpublished data 2018). More plots are found in Appendix A.2.

TL 57-49 cm: Black colored and rather fine grained, this tephra is disrupted due to cryoturbation. The volcanic origin of this tephra is Katla as the chemical analysis matches to what has been observed from Katla. Using comparison data and stratigraphy the tephra was identified to be Katla prehistoric with an age of 1.150 years BP (Figure 20; Thorvaldur Thordarson, unpublished data 2018).

TL 43-35 cm: Light gray colored and rather fine grained, cryoturbation has also effected this tephra causing it to have variable thickness. The chemical analysis from this tephra matches to the Bárðarbunga-Veiðivötn volcanic system and the tephra was identified to by the Settlement layer (1.079 years BP) based on stratigraphy and comparison data (Figure 20; Grönvold et al., 1995; Larsen et al., 2002).

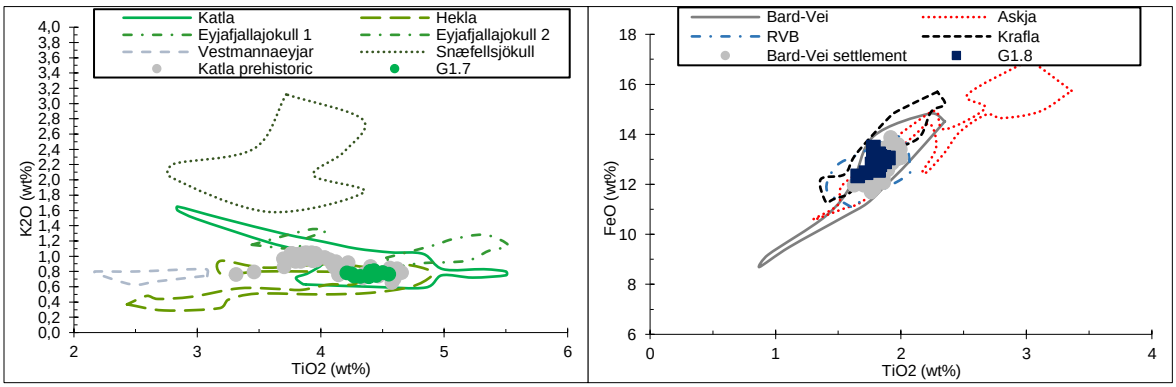

Figure 20. To the left is an example of a plot used to identify Katla prehistoric. The plot to the right was used to identify the Settlement layer. Both plots have comparison data from Thorvaldur Thordarson (unpublished data 2018). Additional data is shown in Appendix A.2.

TL 25-23 cm: Dark gray or black colored with rather fine sand grainsize. This tephra layer originates from the Hekla volcano as was confirmed by the chemical analysis and geochemical discrimination plots. The stratigraphy and comparison data helped in reaching the conclusion that this tephra is Hekla 1845 (Figure 21; Thordarson et al., 1998; Guðnason, 2017).

TL 13-12 cm: Black colored and rather fine grained. Observing the chemical analysis and using the geochemical discrimination plots, it was revealed that this tephra matches the Katla volcano. Identifying the eruption age was done by using stratigraphy and comparison data, which concluded that this tephra is Katla 1918 (Figure 21; Óladóttir et al., 2008).

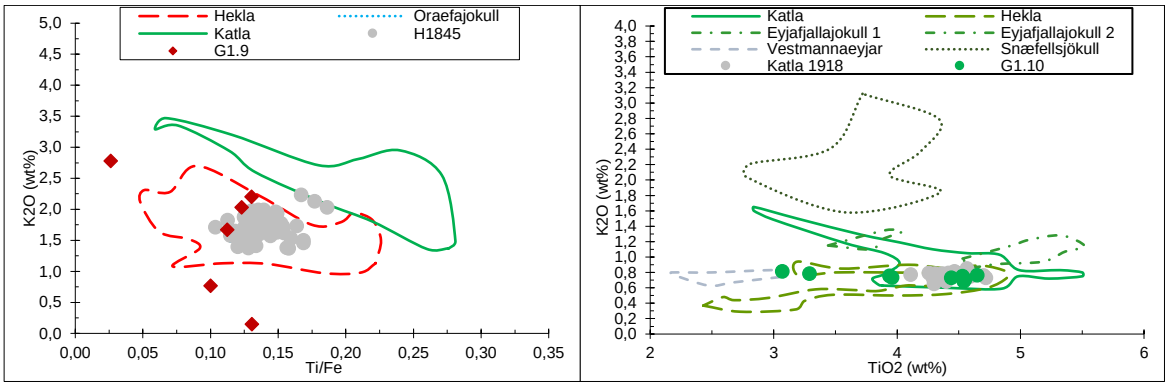

Figure 21. Sample G1.9 is shown on the graph to the left which was identified as Hekla 1845 based on the plots and comparison data (Thordarson et al., 1998; Guðnason, 2017). To the right is an example of a graph used to identify Katla 1918 and comparison data from Óladóttir et al. (2008) and from Thorvaldur Thordarson (unpublished data 2018). The rest of the graphs are listed in Appendix A.2.

4.2.3 Site 2, profile 1

TL 310-303 cm: Light colored and rather fine sand grains. Chemical analysis matches with the Hekla volcano and this tephra was identified to be H5 by using comparison data (Figure 22; Jóhannsdóttir, 2007; Thorvaldur Thordarson, unpublished data 2018).

TL 292-286 cm: Light colored and disrupted with a fine and coarse grained part. Due to difference in appearance two samples were collected from this tephra and both analyzed. This tephra also matches the Hekla volcano and was identified as H4 based on comparison data and stratigraphy (Figure 22; Jóhannsdóttir, 2007; Thorvaldur Thordarson, unpublished data 2018).

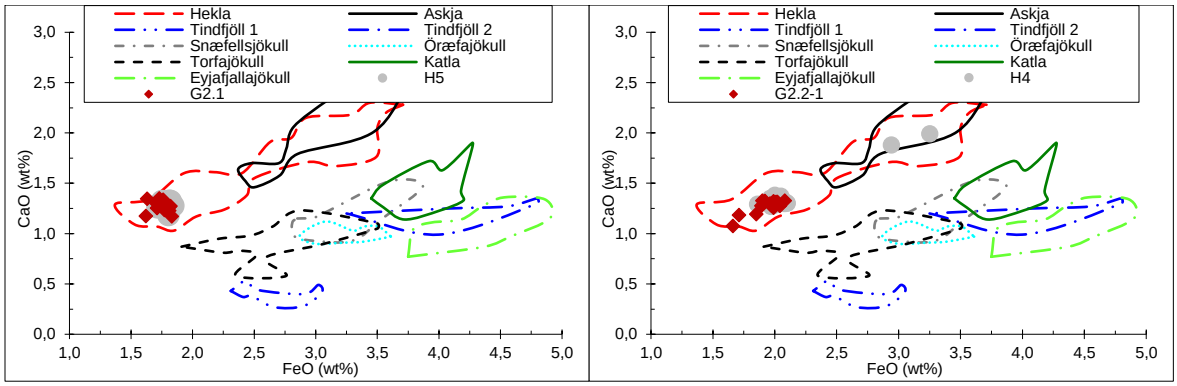

Figure 22. Examples of graphs used to identify H5 and one out of two H4 samples as well as comparison data (Thorvaldur Thordarson, unpublished data 2018). The rest of the graphs are displayed in Appendix A.2.

TL 251-241 cm: Black color with a variable thickness due to cryoturbation, grains are rather fine sand. The origin volcano was determined to be Katla based on chemical analysis and by observing the stratigraphy and comparison data the tephra was identified to be Katla prehistoric (Figure 23; Thorvaldur Thordarson, unpublished data 2018).

TL 238-234 cm: Gray color and rather fine sand grains. The layer has a variable thickness and shows sign of cryoturbation. The chemical analysis for this tephra concludes that the origin volcanic system is Bárðarbunga-Veiðivötn. The stratigraphy and comparison data identified the tephra as the Settlement layer (Figure 23; Grönvold et al., 1995; Larsen et al., 2002).

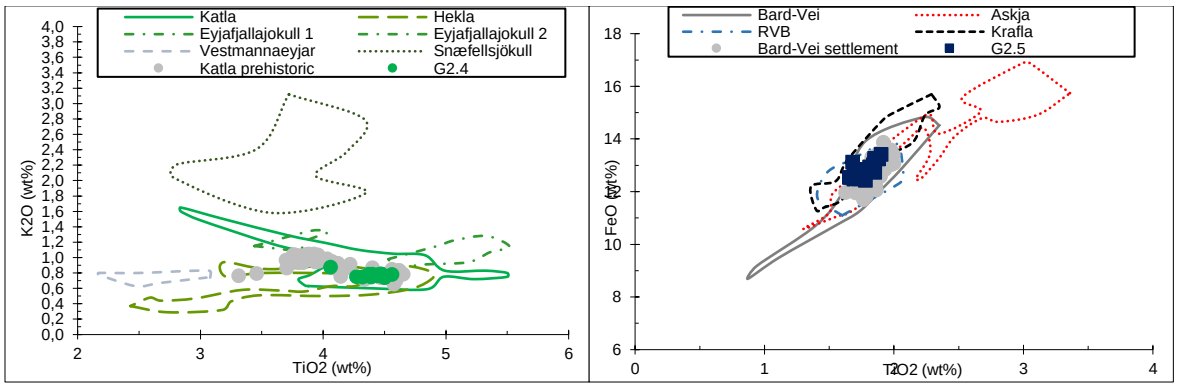

Figure 23. Example of a plot used for sample G2.4 is shown to the left, which was identified as Katla prehistoric. To the right is an example of a graph used to identify sample G2.5 as the Settlement layer. Both examples contain comparison data used for each sample (Thorvaldur Thordarson, unpublished data 2018). Displayed in Appendix A.2 are the rest of the graphs used.

TL 225-223 cm: Light colored and coarse sand grains. Hekla is the origin volcano for this tephra based on the chemical analysis and geochemical discrimination plots. The eruption age was found based on stratigraphy and comparison data, this tephra is Hekla 1104 (Figure 24; Larsen et al., 1999).

TL 204-203 cm: Dark gray color and rather coarse sand grains. This tephra is originated from the Bárðarbunga-Veiðivötn volcanic system and based on the stratigraphy and

comparison data was identified as Bárðarbunga-Veiðivötn 1477 (Figure 24; Larsen et al., 2002).

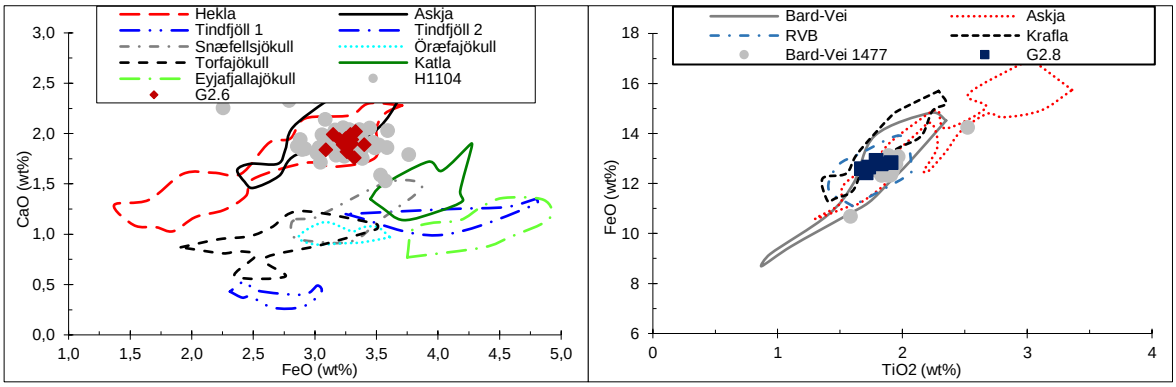

Figure 24. Hekla 1104 is displayed in a plot to the left which was used to identify it. Graph to the right shows how sample G2.8 was identified as Bárðarbunga-Veiðivötn 1477. Both tephras were identified based on comparison data from Thorvaldur Thordarson (unpublished data 2018). More graphs are listed in Appendix A.2.

TL 161-160 cm: Black colored and rather fine sand grains. Chemical analysis revealed that this tephra is from Katla volcano. The identity of the tephra is Katla 1721 based on stratigraphy and comparison data (Figure 25; Thorvaldur Thordarson, unpublished data 2018).

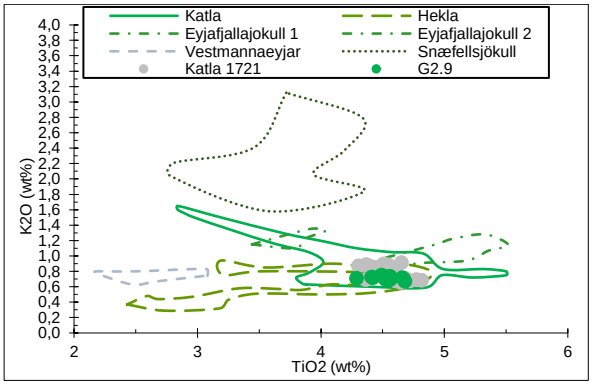

Figure 25. Example of how Katla 1721 was identified using a geochemical discrimination plot and comparison data (Thorvaldur Thordarson, unpublished data 2018). Appendix A.2 contains the rest of the plots used.

4.2.4 Site 2, profile 2

TL 289,5-289 cm: Black color and rather fine sand grains. Based on the chemical analysis and geochemical discrimination plots the origin volcano was determined to be Katla. Comparison data helped in reaching a final conclusion about the identity of the tephra, which was concluded to be Katla prehistoric (Figure 26; Thorvaldur Thordarson, unpublished data 2018).

TL 280-275 cm: Very dark color and coarse sand grains. Chemical analysis matches with the Hekla volcano and based on stratigraphy and comparison data the tephra was identified as Hekla 1300 (Figure 26; Larsen et al., 2002).

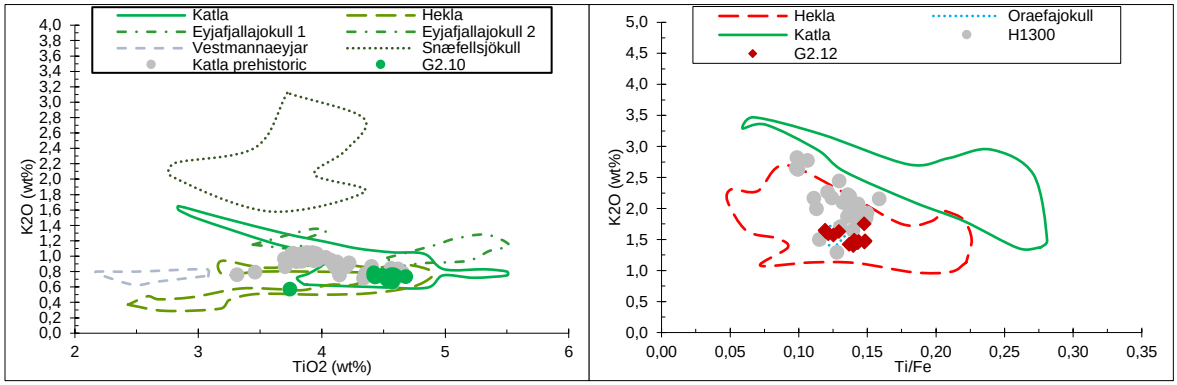

Figure 26. To the left is a graph used for Katla prehistoric and to the right an example of a graph used to identify it as Hekla 1300. Both graphs contain comparison data from Thorvaldur Thordarson (unpublished data 2018). Appendix A.2 contains the rest of the graphs used.

TL 239-230 cm: Coarse sand grained, at the bottom the layer is dark colored, in the middle it is light colored and at the top it is dark colored again. The coarsest grains are in the light colored middle part. Chemical analysis revealed that this tephra is also from Hekla and was identified to the Hekla 1766, based on comparison data and stratigraphy (Figure 27; Janebo, 2016).

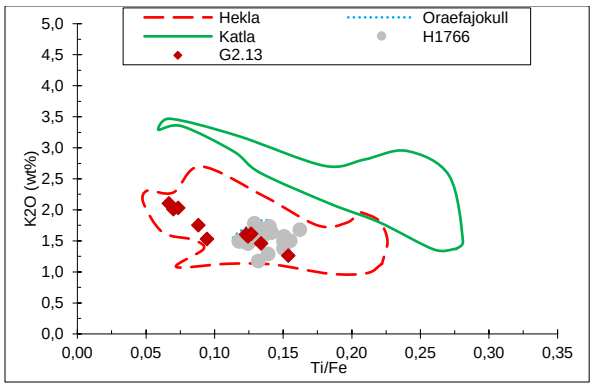

Figure 27. Example of a geochemical discrimination plot used to identify Hekla 1766 and comparison data (Thorvaldur Thordarson, unpublished data 2018). The rest of the plots are shown in Appendix A.2.

4.2.5 Site 3, profile 1

TL 386-384 cm: Black color and rather fine sand grained. Katla was determined to be the origin volcano for this tephra based on the chemical analysis and geochemical discrimination plots. Using comparison data the tephra was identified to be Katla prehistoric (Figure 28; Thorvaldur Thordarson, unpublished data 2018).

TL 374-364 cm: Gray colored, the bottom is a mix of coarse and fine sand grains, then finer grains. Above that the layer contains coarser sand grains. Two samples were collected from this tephra due to the changes in appearance, both were analyzed. The results from the chemical analysis revealed that this tephra originated from the Bárðarbunga-Veiðivötn volcanic system. Based on stratigraphy and comparison data this tephra was identified to be the Settlement layer (Figure 28; Grönvold et al., 1995; Larsen et al., 2002).

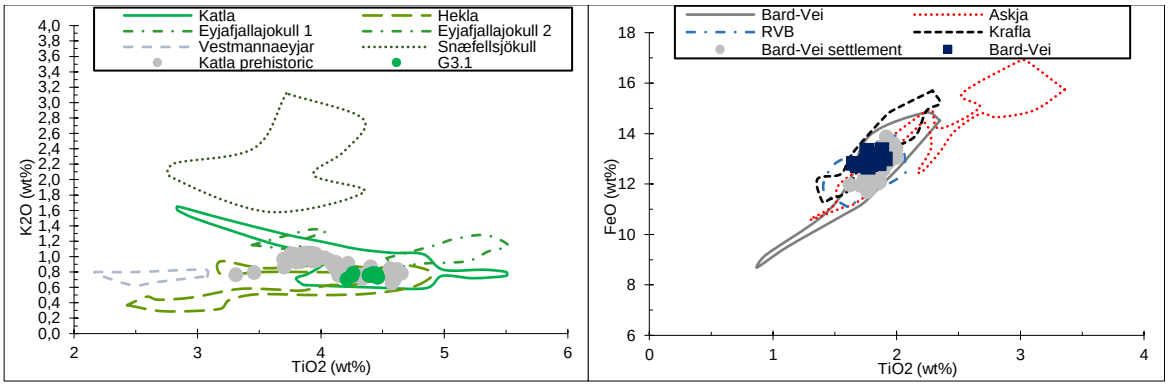

Figure 28. Sample G.31 is displayed on the left which was identified as Katla prehistoric. The Settlement layer is to the right and an example of a plot used to identify one out of two samples from that tephra. Both examples contain comparison data from Thorvaldur Thordarson (unpublished data 2018). The rest of the plots used are displayed in Appendix A.2.

TL 341-339 cm: Dark gray color and the grain size is rather coarse to fine sand, with a bit larger grains in between. The chemical analysis matches to the Hekla volcano and by using the stratigraphy and comparison data the tephra was identified to be Hekla 1300 (Figure 29; Larsen et al., 2002).

TL 272-271,5 cm: Black colored and rather fine sand grains. This part is also quite mixed with organic rich material. Based on the chemical analysis and geochemical discrimination plots it was determined that this tephra originated from Katla. Comparison data and stratigraphy revealed that the tephra is Katla 1721 (Figure 29; Thorvaldur Thordarson, unpublished data 2018).

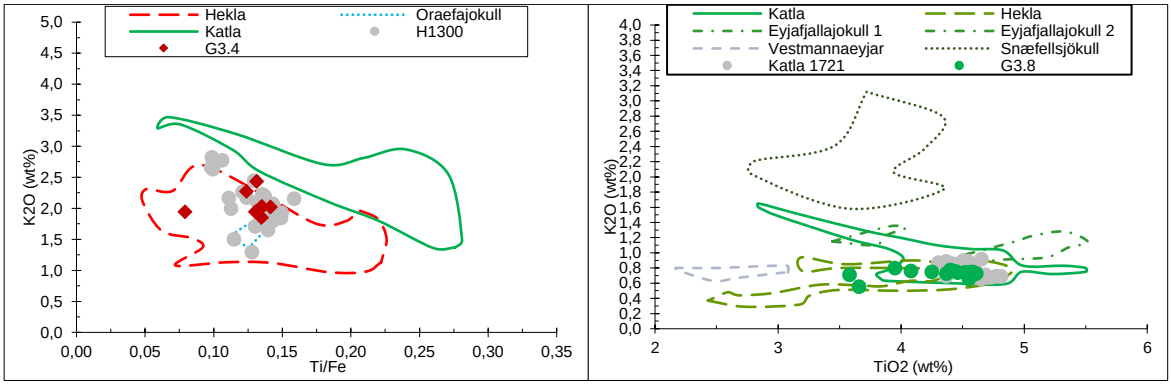

Figure 29. On the left is a graph used to identify Hekla 1300. To the right is an example of for Katla 1721. Both tephras were identified with comparison data from Thorvaldur Thordarson (unpublished data 2018). More plots are displayed in Appendix A.2.

TL 256-255 cm: Black color and coarse sand grains. Hekla was concluded to be the origin volcano based on the chemical analysis and geochemical discrimination plots. The identity of the tephra was determined based on comparison data and stratigraphy, the tephra was identified to be Hekla 1766 (Figure 30; Janebo, 2016).

TL 48-46 cm: Dark gray color and rather fine sand grains. This layer is mixed with light colored redeposited grains. This tephra was also concluded to originate from Hekla and determined to be Hekla 1845 based on stratigraphy and comparison data (Figure 30; Thordarson et al., 1998; Guðnason, 2017).

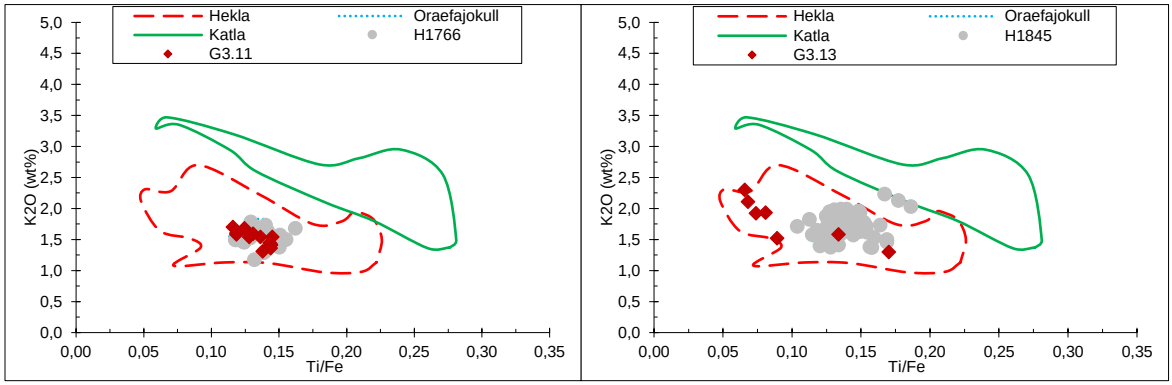

Figure 30. Example of a graph used to identify Hekla 1766 is displayed on the left with comparison data (Thorvaldur Thordarson, unpublished data 2018). Sample G3.13 displayed on the right in a graph used to identify it as Hekla 1845 and comparison data used (Thordarson et al., 1998; Guðnason, 2017). The rest of the graphs are shown in Appendix A.2.

TL 33-32 cm: Black colored with fine to coarse sand grains. Light colored redeposited grains are found at the bottom boundary. The chemical analysis matches with the Katla volcano and by using the stratigraphy and comparison data the tephra was identified as Katla 1918 (Figure 31; Óladóttir et al., 2008).

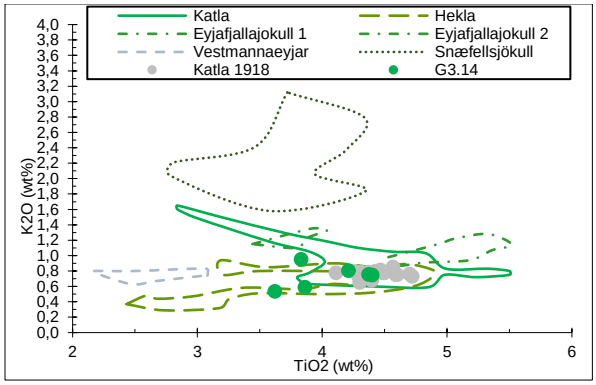

Figure 31. Katla 1918 and an example of a geochemical discrimination plot used for the tephra and comparison data (Óladóttir et al., 2008; Thorvaldur Thordarson, unpublished data 2018). More plots are displayed in Appendix A.2.

4.2.6 Tephra

The measured part of profile 1.1 contains four tephra layers (G10400, Hekla-Vatnafjöll, Kve6890 and H4), although H3 was also present and used to obtain an age model for this profile. Profile 1.2 contains the most tephra layers with 12 layers (G10400, G10000, Hekla-Vatnafjöll, H5, K6750, WVZ4500, H3, H-C, Katla prehistoric, Settlement, H1845, K1918) chemically analyzed and one additional (H4) used for the age model, since that layer was described in the field but not samples due to easy correlation to profile 1.1.

Profile 2.1 contains 7 tephra layers (H5, H4, Katla prehistoric, Settlement, H1104, Bar1477, K1721), all of them were analyzed and used to obtain the tephra derived age model for the profile. Only three tephra layers were found in profile 2.2 (Katla prehistoric, H1300 and H1766). Profile 3 contains 7 tephra layers (Katla prehistoric, Settlement, H1300, K1721, H1766, H1845 and K1918).

The oldest tephra layers found are from the 10 ka Grímsvötn series with an oldest age of 10.400 years BP (Thorvaldur Thordarson, unpublished data 2018) and containing the so-called Saksunarvatn tephra, which has been dated 10.300 years BP in the Faroe Islands where it was first found (Mangerud et al., 1986). Recent studies show that the 10 ka Grímsvötn series contains at least seven tephra layers with an age range between 10.400 and 9.900 years BP (Jennings et al., 2014; Thordarson, 2014). Another tephra layer identified as part of the 10 ka Grímsvötn series was found in the soil sections, estimated to have an age of 10.000 years BP (Thorvaldur Thordarson, unpublished data 2018). Above the tephras from the 10 ka Grímsvötn series, is a basaltic Hekla layer which is often found with this series. The basaltic Hekla tephra has an age of about 9.100 years BP (Thorvaldur Thordarson, unpublished data 2018; Harning et al., 2018a). The rest of the sections contain tephra layers spanning the Holocene showing among them the important tephra marker layers H5, H4, H3, Katla prehistoric and the Settlement layer (Table 2).

By using the geochemical discrimination plots, the different rock types of the tephras were easily recognized as well as their volcanic source. All of the geochemical discrimination plots used to determine the origin of the tephra layers are displayed in Appendix A.2. After estimating the volcanic source for each tephra it was possible to identify their age by using the stratigraphy of the soil sites and compare to other geochemical data. The graphs in Appendix A.2 also show comparison samples used to identify the age of each tephra layer. Most of the comparison samples are from the lacustrine sediment core obtained from Hvítárvatn (Thorvaldur Thordarson, unpublished data 2018). The comparison samples help with reaching a final conclusion about the age of the tephra layers, since it is estimated that tephra layers found in Hvítárvatn should be present in the soil sections. A few other sources for comparison samples were used when a tephra layer did not correlate to Hvítárvatn, those sources were Thordarson et al. (1998), Sinton et al. (2005), Óladóttir et al. (2011), Guðnason (2017) and Thorvaldur Thordarson (unpublished data 2018).

Four major volcanic systems produced the tephra layers found in the soil profiles, they are Hekla, Katla, Bárðarbunga-Veiðivötn and Grímsvötn. Additionally, one tephra layer is present from Kverkfjöll and one from the WVZ. The four dominating volcanic systems all belong to the East Volcanic Zone (EVZ), where the great majority of explosive Holocene eruptions took place. The reason for that is partly due to its numerous central volcanoes and partly because parts of the volcanic zone is currently covered by ice caps which during eruptions results in explosive volcanism due to water-magma interaction. All four volcanic

systems produce basaltic tephra that is found in the soil sections, and all of them except Hekla, are major producers of basaltic tephra through the Holocene with Grímsvötn having the highest eruption frequency (Larsen & Eiríksson, 2008). The only silicic tephra layers found in the soil profiles are from Hekla, which is the major producer of silicic tephra in Iceland. Hekla has produced some large tephra layers during the Holocene such as H3 and H4, which both are important marker tephras, and caused vegetation in the central highlands to be temporary destroyed in large areas (Larsen & Eiríksson, 2008).

The microprobe used to analyse major element composition in the tephra samples, requiers different setups for analysing basaltic and silicic glass. If silicic glass is analysed using the setup for basaltic glass, the silicic sample looses a part of its sodium content. This problem is displayed in some of the intermediate and silicic tephra samples when comparing them to geochemical data from Hvítárvatn sediment cores (Thorvaldur Thordarson, unpublished data 2018), graphs can be seen in Appendix A.2. This loss of sodium is seen when using plots for sodium content, but when using plots for other major elements, the tephra sample for this study and a tephra sample from Hvítárvatn compare well together and thus makes it possible to identify the age of the tephra correctly.

Table 2. Geochemical results for tephra layers found in the five soil sections. The tephras are sorted by age, the youngest being at the top.

Volcanic source	Sample name	Section	Depth	n	Age BP	Age reference	SiO_2	TiO_2	Al_2O_3	FeO	MnO	MgO	CaO	Na_2O	K_2O	P_2O_5	Total
Katla 1918	G3.14	3	42	6	32	Óladóttir et al., 2008	47,59	4,05	13,22	14,31	0,22	5,23	9,98	2,92	0,73	0,46	98,72
							0,89	*0,32*	*0,49*	*0,35*	*0,01*	*0,58*	*0,81*	*0,18*	*0,15*	*0,05*	*0,35*
Katla 1918	G1.10	1.2	12	7	32	Óladóttir et al., 2008	47,19	4,37	13,02	15,03	0,23	4,97	9,62	3,01	0,73	0,61	98,78
							0,25	*0,30*	*0,21*	*0,29*	*0,02*	*0,14*	*0,11*	*0,06*	*0,03*	*0,11*	*0,74*
Hekla 1845	G3.13	3	56		105	Thordarson et al., 1998;											
Alkalic basalt				4		Guðnason, 2017	47,29	4,17	13,34	14,46	0,23	5,09	9,97	2,88	0,72	0,49	98,63
							0,62	*0,44*	*0,34*	*0,42*	*0,01*	*0,55*	*0,81*	*0,15*	*0,13*	*0,09*	*0,03*
Tholeiitic				3			60,07	1,34	15,06	9,97	0,28	1,90	5,33	2,75	1,47	0,65	98,80
andesite							*4,46*	*0,65*	*1,08*	*2,16*	*0,06*	*0,99*	*1,07*	*0,17*	*0,15*	*0,46*	*0,66*
Dacite				4			67,35	0,46	15,18	6,30	0,20	0,46	3,37	2,52	2,07	0,10	98,01
							1,80	*0,08*	*0,35*	*0,84*	*0,03*	*0,12*	*0,30*	*0,15*	*0,18*	*0,04*	*0,45*
Hekla 1845	G1.9	1.2	23		105	Thordarson et al., 1998;											
Alkalic basalt				4		Guðnason, 2017	46,58	3,44	14,35	14,54	0,22	5,99	11,41	2,65	0,49	0,34	99,99
							0,49	*1,17*	*2,38*	*2,29*	*0,04*	*1,59*	*0,66*	*0,18*	*0,25*	*0,11*	*0,67*
Tholeiitic				4			58,57	0,70	20,56	6,05	0,16	0,87	7,54	3,79	1,15	0,28	99,67
andesite							*3,86*	*0,53*	*7,61*	*4,39*	*0,12*	*0,74*	*4,06*	*0,81*	*0,85*	*0,26*	*2,21*
Dacite				2			65,95	0,56	16,53	5,02	0,17	0,53	4,23	3,69	2,49	0,33	99,49
							1,00	*0,73*	*4,04*	*4,62*	*0,15*	*0,57*	*0,39*	*1,22*	*0,41*	*0,46*	*0,53*
Hekla 1766	G3.11	3	255	13	184	Janebo, 2016	59,93	1,28	15,64	9,58	0,26	1,78	5,31	2,90	1,52	0,55	98,74
							1,32	*0,15*	*0,08*	*0,44*	*0,02*	*0,27*	*0,31*	*0,17*	*0,12*	*0,10*	*0,37*
Hekla 1766	G2.13	2.2	230	7	184	Janebo, 2016	62,87	0,94	15,23	8,48	0,25	1,34	4,61	2,81	1,69	0,40	98,62
							4,15	*0,44*	*0,37*	*2,00*	*0,04*	*0,76*	*1,08*	*0,39*	*0,28*	*0,24*	*0,73*
Katla 1721	G3.8	3	272	15	229	Thorarinsson, 1975	47,05	4,30	12,98	14,71	0,24	5,01	9,67	2,99	0,73	0,61	98,29
							0,34	*0,33*	*0,23*	*0,29*	*0,02*	*0,25*	*0,38*	*0,09*	*0,06*	*0,11*	*0,44*
Katla 1721	G2.9	2.1	160	12	229	Thorarinsson, 1975	47,12	4,53	12,76	14,83	0,23	4,98	9,55	2,93	0,71	0,65	98,29
							0,85	*0,12*	*0,15*	*0,35*	*0,01*	*0,12*	*0,15*	*0,17*	*0,02*	*0,04*	*1,42*
Bárðarbunga-Veiðivötn	G2.8	2.1	203	6	473	Larsen et al., 2002	49,55	1,77	13,87	12,70	0,21	6,67	11,38	2,39	0,22	0,17	98,94
1477							*0,16*	*0,09*	*0,22*	*0,18*	*0,01*	*0,24*	*0,29*	*0,07*	*0,03*	*0,02*	*0,41*
Grímsvötn				5	*615*		49,29	2,74	13,14	14,48	0,24	5,51	9,89	2,64	0,41	0,32	98,65
1335?							*0,21*	*0,23*	*0,47*	*0,83*	*0,02*	*0,60*	*0,65*	*0,20*	*0,04*	*0,03*	*0,32*
Hekla 1300	G3.4	3	339	8	650	Larsen et al., 2002	64,00	1,17	13,94	9,10	0,25	1,07	4,04	3,13	2,06	0,50	99,25
							2,23	*0,30*	*0,66*	*1,36*	*0,03*	*0,32*	*0,44*	*0,46*	*0,19*	*0,17*	*0,63*

Volcanic source	Sample name	Section	Depth	n	Age BP	Age reference	SiO_2	TiO_2	Al_2O_3	FeO	MnO	MgO	CaO	Na_2O	K_2O	P_2O_5	Total
Hekla 1300	G2.12	2.2	275	15	650	Larsen et al., 2002	59,68	1,35	15,49	9,91	0,27	1,95	5,46	3,13	1,53	0,57	99,33
							0,98	*0,15*	*0,17*	*0,42*	*0,02*	*0,29*	*0,33*	*0,25*	*0,10*	*0,11*	*0,44*
Hekla 1104	G2.6	2.1	223	15	846	Larsen et al., 1999	72,28	0,22	14,26	3,26	0,11	0,11	1,91	3,43	2,66	0,02	98,27
							0,34	*0,03*	*0,23*	*0,07*	*0,02*	*0,01*	*0,07*	*0,50*	*0,06*	*0,03*	*0,66*
Settlement	G3.2-2	3	364	11	1.079	Grönvold et al., 1995;	49,74	1,77	13,86	12,80	0,23	6,45	11,25	2,36	0,22	0,15	98,83
						Larsen et al., 2002	*0,13*	*0,06*	*0,12*	*0,21*	*0,01*	*0,14*	*0,23*	*0,04*	*0,01*	*0,03*	*0,38*
Settlement	G3.2-1	3	368	15	1.079	Grönvold et al., 1995;	49,80	1,80	13,87	12,94	0,23	6,35	11,31	2,36	0,23	0,17	99,05
						Larsen et al., 2002	*0,28*	*0,07*	*0,11*	*0,22*	*0,02*	*0,10*	*0,14*	*0,09*	*0,01*	*0,02*	*0,42*
Settlement	G2.5	2.1	234	15	1.079	Grönvold et al., 1995;	49,61	1,79	13,86	12,90	0,23	6,54	11,45	2,37	0,22	0,17	99,13
						Larsen et al., 2002	*0,21*	*0,08*	*0,17*	*0,32*	*0,02*	*0,14*	*0,25*	*0,06*	*0,01*	*0,02*	*0,32*
Settlement	G1.8	1.2	35	15	1.079	Grönvold et al., 1995;	49,71	1,80	13,92	12,92	0,22	6,47	11,33	2,39	0,22	0,17	99,15
						Larsen et al., 2002	*0,30*	*0,06*	*0,17*	*0,30*	*0,01*	*0,14*	*0,17*	*0,05*	*0,01*	*0,02*	*0,48*
Katla prehistoric	G3.1	3	384	13	1.150	Thorvaldur Thordarson,	47,22	4,39	13,09	14,90	0,24	4,92	9,55	3,00	0,75	0,54	98,61
						unpublished data 2018	*0,27*	*0,09*	*0,13*	*0,17*	*0,01*	*0,08*	*0,10*	*0,09*	*0,02*	*0,03*	*0,47*
Katla prehistoric	G2.10	2.2	289	13	1.150	Thorvaldur Thordarson,	47,06	4,48	12,92	14,97	0,24	5,00	9,51	3,02	0,72	0,63	98,55
						unpublished data 2018	*0,36*	*0,24*	*0,45*	*0,25*	*0,02*	*0,18*	*0,15*	*0,10*	*0,05*	*0,07*	*0,42*
Katla prehistoric	G2.4	2.1	241	15	1.150	Thorvaldur Thordarson,	47,23	4,40	13,02	14,97	0,23	4,87	9,54	3,01	0,77	0,54	98,60
						unpublished data 2018	*0,30*	*0,12*	*0,16*	*0,31*	*0,01*	*0,10*	*0,15*	*0,10*	*0,03*	*0,03*	*0,63*
Katla prehistoric	G1.7	1.2	49	13	1.150	Thorvaldur Thordarson,	47,59	4,39	13,11	14,94	0,24	4,92	9,58	2,89	0,77	0,55	98,97
						unpublished data 2018	*0,48*	*0,10*	*0,13*	*0,21*	*0,02*	*0,06*	*0,14*	*0,12*	*0,03*	*0,04*	*0,57*
Hekla H-C	G1.6	1.2	86	10	2.869	Thorvaldur Thordarson,	61,76	1,05	15,68	7,90	0,20	1,55	4,77	3,80	1,52	0,38	98,61
						unpublished data 2018	*0,79*	*0,04*	*0,24*	*0,16*	*0,02*	*0,04*	*0,16*	*0,09*	*0,05*	*0,04*	*1,10*
Hekla H3	G1.5	1.2	101	15	3.000	Jóhannsdóttir, 2007;	72,08	0,21	14,43	3,22	0,09	0,13	2,01	3,50	2,44	0,02	98,14
						Dugmore et al., 1995	*0,97*	*0,04*	*0,21*	*0,46*	*0,02*	*0,03*	*0,18*	*0,47*	*0,10*	*0,02*	*0,92*
Hekla H4	G2.2-2	2.1	293	14	4.260	Jóhannsdóttir, 2007;	74,06	0,11	13,20	1,99	0,08	0,02	1,31	3,57	2,78	0,01	97,14
						Dugmore et al., 1995	*1,26*	*0,04*	*0,24*	*0,08*	*0,02*	*0,02*	*0,05*	*0,38*	*0,07*	*0,01*	*1,40*
Hekla H4	G2.2-1	2.1	297	14	4.260	Jóhannsdóttir, 2007;	74,37	0,10	13,21	1,93	0,08	0,02	1,27	3,62	2,78	0,00	97,38
						Dugmore et al., 1995	*0,79*	*0,02*	*0,23*	*0,12*	*0,02*	*0,01*	*0,07*	*0,45*	*0,08*	*0,00*	*0,84*
Hekla H4	G1.4	1.1	98	14	4.260	Jóhannsdóttir, 2007;	73,61	0,11	13,10	1,97	0,08	0,01	1,30	3,45	2,76	0,02	96,40
						Dugmore et al., 1995	*1,04*	*0,03*	*0,23*	*0,03*	*0,02*	*0,01*	*0,06*	*0,50*	*0,06*	*0,02*	*1,61*
WVZ	G1.18	1.2	194	6	*4.500*	Sinton et al., 2005	48,52	1,73	14,51	12,10	0,20	7,29	12,05	2,18	0,21	0,15	98,95
							0,53	*0,53*	*0,58*	*0,96*	*0,02*	*0,57*	*0,69*	*0,14*	*0,11*	*0,08*	*0,36*
Hekla?				6			48,45	3,32	13,20	14,99	0,26	4,71	9,54	2,97	0,68	0,50	98,61
							2,08	*0,54*	*0,47*	*0,74*	*0,04*	*0,77*	*1,17*	*0,22*	*0,11*	*0,19*	*0,56*

Volcanic source	Sample name	Section	Depth	n	Age BP	Age reference	SiO_2	TiO_2	Al_2O_3	FeO	MnO	MgO	CaO	Na_2O	K_2O	P_2O_5	Total
Katla	G1.17	1.2	240	11	6.750	Thorvaldur Thordarson, unpublished data 2018	47,30	3,95	13,58	14,71	0,23	5,21	9,93	2,87	0,74	0,43	98,94
							0,72	*0,61*	*0,93*	*0,86*	*0,02*	*0,86*	*0,36*	*0,26*	*0,18*	*0,10*	*0,72*
Hekla H5	G2.1	2.1	303	15	7.000	Jóhannsdóttir, 2007; Larsen & Thorarinsson, 1977	75,62	0,09	12,92	1,75	0,07	0,03	1,27	3,39	2,73	0,01	97,90
							0,75	*0,03*	*0,17*	*0,07*	*0,02*	*0,01*	*0,05*	*0,38*	*0,08*	*0,02*	*0,93*
Hekla H5	G1.14-2	1.2	244	15	7.000	Jóhannsdóttir, 2007; Larsen & Thorarinsson, 1977	75,95	0,11	13,15	1,77	0,07	0,03	1,29	3,46	2,71	0,02	98,56
							0,65	*0,03*	*0,22*	*0,08*	*0,02*	*0,01*	*0,09*	*0,42*	*0,10*	*0,02*	*0,84*
Hekla H5	G1.14-1	1.2	248	15	7.000	Jóhannsdóttir, 2007; Larsen & Thorarinsson, 1977	75,70	0,09	12,93	1,80	0,07	0,04	1,27	3,85	2,74	0,01	98,50
							0,57	*0,02*	*0,18*	*0,07*	*0,02*	*0,01*	*0,05*	*0,29*	*0,06*	*0,01*	*0,91*
Kverkfjöll	G1.3	1.1	147	4	*6.890*	Óladóttir et al., 2011	49,35	3,34	13,06	14,57	0,25	4,98	9,17	2,74	0,64	0,46	98,57
							0,53	*0,36*	*0,32*	*0,25*	*0,02*	*0,39*	*0,44*	*0,32*	*0,13*	*0,09*	*0,47*
Hekla-Vatnafjöll	G1.13	1.2	303	12	9.100	Thorvaldur Thordarson, unpublished data 2018	46,25	2,67	15,04	12,75	0,19	7,08	11,27	2,44	0,43	0,26	98,38
							0,28	*0,48*	*0,56*	*1,14*	*0,01*	*0,85*	*0,82*	*0,26*	*0,12*	*0,06*	*0,48*
10 ka Grímsvötn series	G1.12	1.2	317	7	10.000	Jóhannsdóttir, 2007	49,02	2,96	13,16	14,49	0,25	5,38	9,68	2,70	0,45	0,32	98,41
							0,78	*0,38*	*0,63*	*0,64*	*0,02*	*0,42*	*0,40*	*0,16*	*0,02*	*0,05*	*0,41*
10 ka Grímsvötn series	G1.11	1.2	322	9	10.400	Jóhannsdóttir, 2007	48,97	2,89	13,18	14,41	0,25	5,57	9,87	2,62	0,44	0,33	98,53
							0,35	*0,50*	*0,67*	*0,98*	*0,01*	*0,74*	*0,61*	*0,11*	*0,07*	*0,06*	*0,48*
10 ka Grímsvötn series	G1.1	1.1	214	5	10.400	Jóhannsdóttir, 2007	48,64	2,72	13,31	14,10	0,24	5,69	10,00	2,69	0,44	0,30	98,14
							0,32	*0,13*	*0,10*	*0,26*	*0,01*	*0,12*	*0,20*	*0,16*	*0,04*	*0,04*	*0,32*
Hekla-Vatnafjöll				8	9.100		46,85	3,22	13,75	14,41	0,23	5,69	10,22	2,89	0,61	0,49	98,34
							1,05	*0,52*	*1,29*	*1,18*	*0,05*	*1,12*	*0,86*	*0,25*	*0,15*	*0,27*	*0,42*

4.2.7 Age model

Identification of the tephra layers in each soil profile made it possible to come up with tephra derived age model for each profile. Each age model was generated in the *Clam 2.2* software package using a linear interpolation (Blaauw, 2010) resulting in estimated ages for every centimeter in the section (Figures 32, 33 and 34). The advantage of using the *Clam* software is that it gives a maximum age uncertainty (95% confidence of 1000 iterations, Blaauw, 2010). However, as mentioned in sub-chapter 3.2.4 the software needs a minimum of four data points (Blaauw, 2010) in order to obtain a reliable age model. Hence, the age model made for profile 2.2 at Baldheiði was constructed by using a simple linear interpolation between the three data points available (Figure 33). By observing the incline of the line in each age model it is possible to get information about soil accumulation rate (SAR). If the line is more horizontal then the SAR is low, but if the line is more vertical it indicates an increase in SAR. The age models for profiles 1.1 and 1.2 span the longest times since they contain Grímsvötn tephras from the 10 ka Grímsvötn series, thus spanning around 10 ka. Profile 2.1 spans 7.0 ka, while profiles 2.2 and 3 span a bit more than 1.0 ka.

The age model made for profile 1.1 at Fossrófulækur (Figure 32) is based on five tephra layers (G10400, Hekla-Vatnafjöll, Kve6890, H4 and H3). The model suggests near linear accumulation with the greatest change in SAR between H4 (4.2 ka) and H3 (3.0 ka), which are also among the thickest tephra layers present in the profile. Profile 1.2, also at Fossrófulækur (Figure 32), is constricted by 13 tephra layers (G10400, G10000, Hekla-Vatnafjöll, H5, K6750, WVZ4500, H4, H3, H-C, Katla prehistoric, Settlement, H1845 and K1918) and spans the longest time interval. Slight increase in SAR is detected after 8.0 ka and until just after 7.0 ka. The highest rate of soil accumulation took place between 4.5 and 4.0 ka, which corresponds to similar increase in profile 1.1. The final rise in soil accumulation took place after or around 0.5 ka. As profiles 1.1 and 1.2 are located at the same site they can be easily correlated. Although section 1.2 gives more information and, according to the *Clam* age model, has less age inaccuracy due to higher number of known tephra layers. Some tephra layers found in profile 1.2 could not be found in profile 1.1, and since profile 1.1 was not measured to the surface the model does not give accurate information about the last 3.0 ka.

The age model for profile 2.1 at Baldheiði is shown in Figure 33. There are 7 tephra layers (H5, H4, Katla prehistoric, Settlement, H1104, Bar1477 and K1721) that constrain the model. Soil accumulation is generally slow but increasing between 7.0 to 2.0 ka, accelerating after 1.0 ka. Profile 2.2 (Katla prehistoric, H1300 and H1766) shows slowly increasing rates from 1.0 ka which become very rapid after 0.2 to 0 ka. Profile 3 at Hvítárvatn (Figure 34) is constrained by 7 tephra layers (Katla prehistoric, Settlement, H1300, K1721, H1766, H1845 and K1918) and displays a similar trend to profile 2.2, with increasing SAR to around 0.3 ka, thereafter the rate becomes very fast until 0.1 ka when it decreases slightly again.

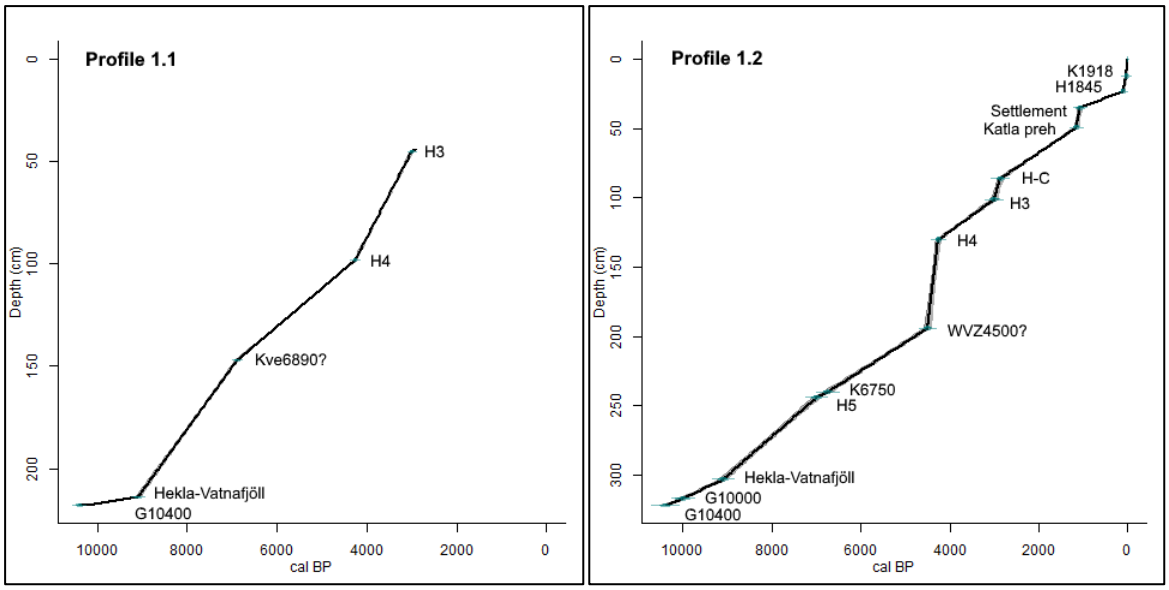

Figure 32. Clam age models for profiles 1.1 and 1.2, all present tephra layers are marked for both profiles.

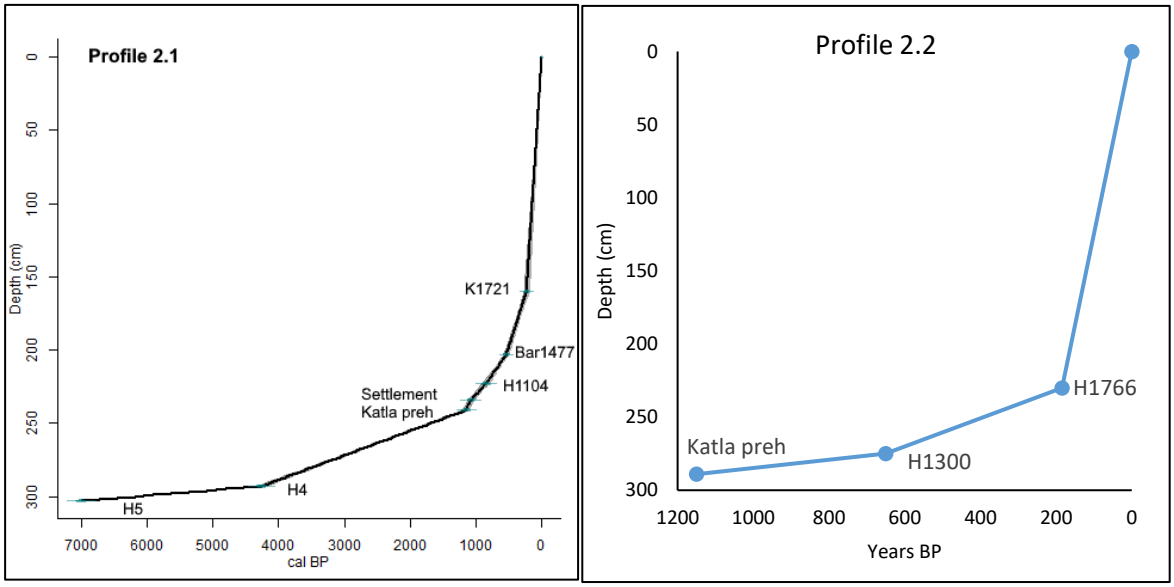

Figure 33. To the left is the Clam age model for profile 2.1 and to the right is the simple linear interpolation age model for profile 2.2. The tephra layers that were used for the age models are marked for both profiles.

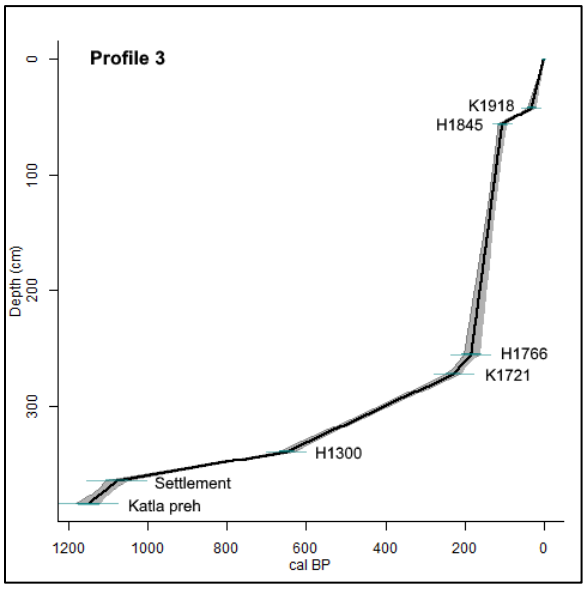

Figure 34. The Clam age model for profile 3. The seven tephra layers used to obtain the age model are marked.

Based on the ages and depths of the tephra layers it was possible to calculate SAR for each profile, thus obtaining further information about SAR based on the age models. By calculating SAR based on tephra layers a linear interpolation is obtained which assumes continuous soil accumulation. Accumulation in soil sections is not continuous since soil undergoes erosion, thus the calculated SAR does not give actual values but rather show how relative accumulation is changing, rising or declining. The figures showing calculated SAR are displayed with simple age-depth graphs for each profile and a table indicating the tephra layers in the profile and accumulation rate (cm/year) for the period between each tephra layer. Even though SAR changes can be observed with the age models, calculated SAR and the simple age-depth graphs do indicate more precise changes.

For profile 1.1 (Figure 35) two distinct increases in SAR values are detected. The first increase occurs between Hekla-Vatnafjöll and Kve6890, starting around 9.0 ka. The second increase occurs between H4 and H3, from ~ 4.3 ka to 3.0 ka. Profile 1.2 shows the greatest changes in SAR (Figure 36), as indicated by the age model. The first increase in SAR is observed between Hekla-Vatnafjöll and H5 tephra layers or between ~ 9.1 to 7.0 ka. The second rise in accumulation is sharp, seen between 4.5 (WVZ4500) and 4.3 ka (H4). A short term increase occurs between 3.0 (H3) and 2.9 ka (H-C), and again between Katla prehistoric and the Settlement layer, around 1.1 ka. The final SAR increase indicated by profile 1.2 is seen around H1845 and K1918, this increase extends to 0 ka.

Profile 2.1 shows slow SAR between 7.0 and 4.3 ka whereas after that SAR starts to rise (Figure 37). Between Katla prehistoric and the Settlement layer is an increase in accumulation, followed by slower rate until around 0.5 ka when SAR rises sharply after the Bar1477 tephra layer and towards K1721. Accumulation increases still towards 0 ka. SAR for profile 2.2 (Figure 38) shows steady and slowly rising rates towards 0.2 ka, H1766. After that SAR rises fast towards 0 ka. As observed in the age models, profiles 2.2 and 3 show similar trends. Profile 3 (Figure 39) also indicates steady and slowly rising rates towards 0.2 ka. Around 0.2 ka the SAR starts to rise and reaches maximum rates at 0.1 ka, H1845. Then

there is a sharp lowering between H1845 and K1918 tephra layers, and rise again towards 0 ka.

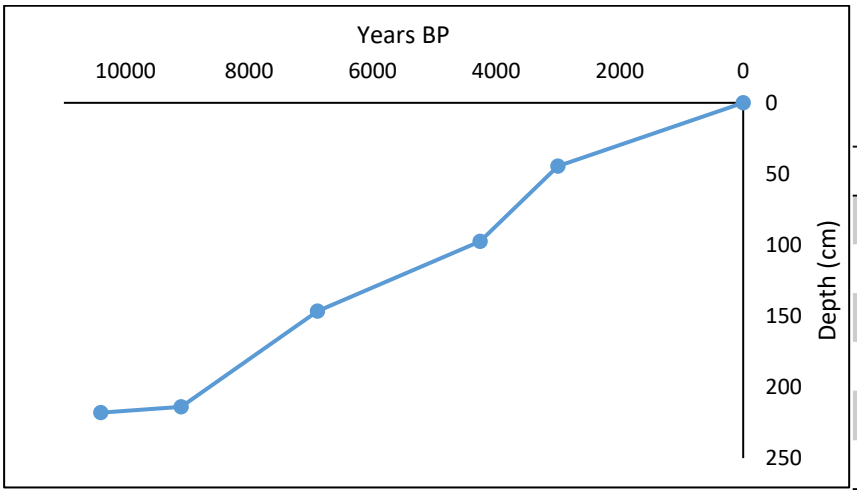

Tephra	cm/year
Surface	0,014833
H3	0,042063
H4	0,021673
Kve6890	0,030995
Hekla	0,003077
G10400	

Figure 35. A simple age-depth graph for profile 1.1 and a table indicating tephra layers and calculated accumulation rates.

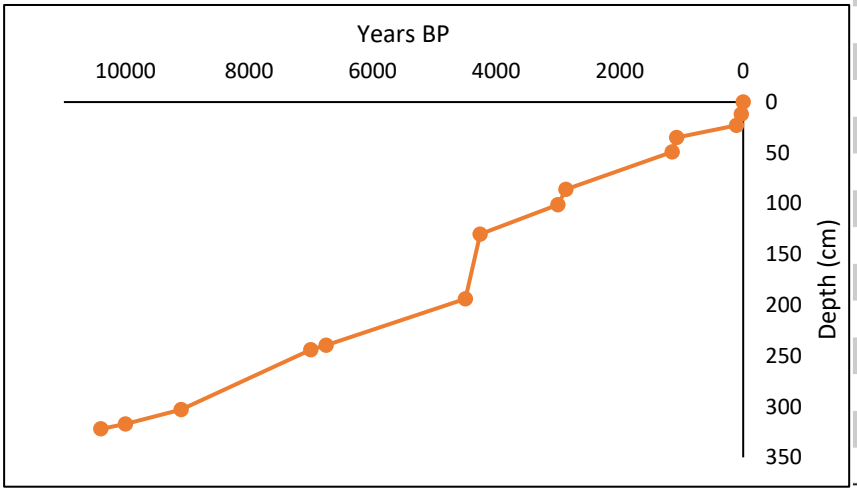

Tephra	cm/year
Surface	0,375
K1918	0,164384
H1845	0,014374
Settlement	0,309859
Katla preh	0,026178
H-C	0,160305
H3	0,033333
H4	0,3
WVZ4500	0,020533
K6750	0,0192
H5	0,032381
Hekla	0,015556
G10000	0,0125
G10400	

Figure 36. Age-depth graph for profile 1.2 indicating changes in accumulation rates. The table to the right lists the tephra layers from the profile and calculated SAR.

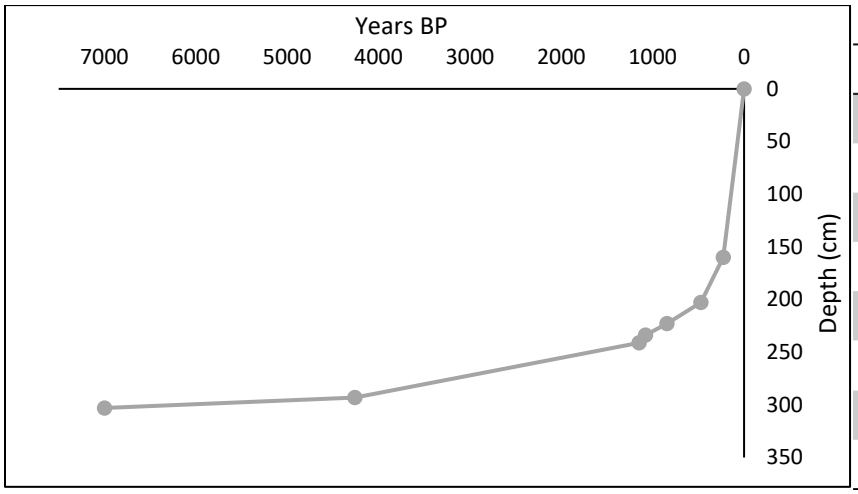

Tephra	cm/year
Surface	0,69869
K1721	0,180328
Bar1477	0,0563
H1104	0,055794
Settlement	0,15493
Katla preh	0,019936
H4	0,005839
H5	

Figure 37. Graph showing the simple age-depth trend for profile 2.1 and to the right is a table indicating the tephra layers and calculated accumulation rates.

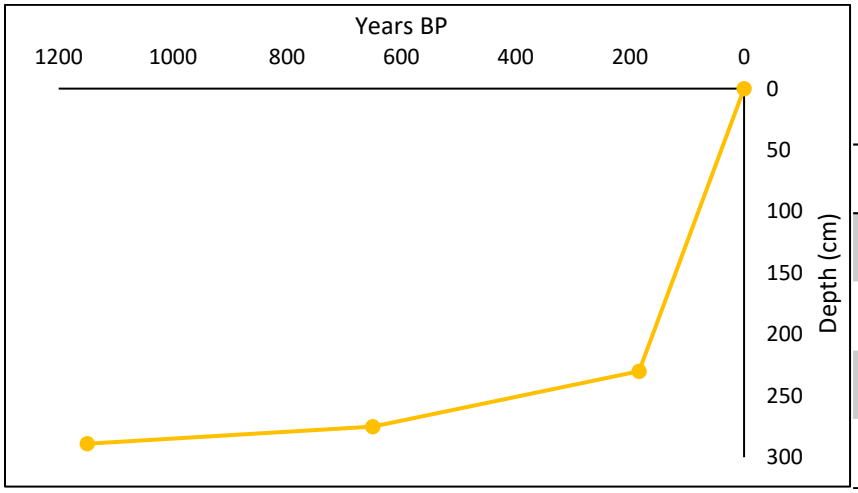

Tephra	cm/year
Surface	1,25
H1766	0,11588
H1300	0,038
Katla preh	

Figure 38. SAR development for profile 2.2 as indicated by the age-depth graph. Tephra layers and calculated accumulation rates are displayed in the table to the right.

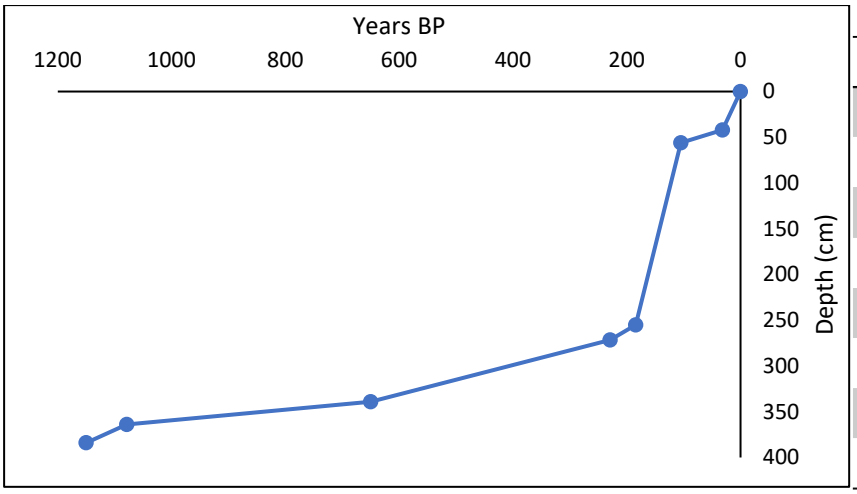

Tephra	cm/year
Surface	1,3125
K1918	0,205479
H1845	2,544304
H1766	0,388889
K1721	0,16152
H1300	0,062937
Settlement	0,422535
Katla preh	

Figure 39. Age-depth graph for profile 3 and a table showing the present tephra layers in the profile and calculated SAR.

4.2.8 Correlation of soil sections based on tephra stratigraphy

Site 1 at Fossrófulækur contains tephra layers from the 10 ka Grímsvötn series and thus, covers most of the Holocene. Profile 1.2 includes in total 13 tephra layers that were identified based on both visual inspection and microprobe analysis. Site 2, profile 2.1 at Baldheiði is dated back 7.0 ka based on the identification of H5 at the bottom. Whereas profiles 2.2 and 3 only go back ca. 1.2 ka. These two sites (2 and 3) show very high SAR during historical times (after the Settlement tephra) in contrast to profiles 1.1 and 1.2 at Fossrófulækur (Figures 40 and 41).

The H3 tephra is present near the top of profile 1.1, above the H4 tephra, although that section was only measured in detail up to H4. The soil profiles containing the oldest tephra layers are from the soil site located in the northeast part of the research area (profiles 1.1 and 1.2). Soil sections located further southwest do not contain as old tephra layers but show higher sediment accumulation in the upper part.

The oldest tephra layers identified in this study are from the 10 ka Grímsvötn series and probably mark the beginning of soil formation in the area. Those tephra layers correlate profiles 1.1 and 1.2 together as well as the H4 and H3 tephras (Figure 41). Correlation of sites 1 and 2 is based on H5 and H4. Katla prehistoric and the Settlement layer are likewise present in both profiles. Profile 2.2 correlates to profiles 1.2 and 2.1 with the presence of the Katla prehistoric tephra layer. Correlation of profile 2.2 and profile 3 is based on H1300 and H1766. Profile 3 additionally correlates to profiles 1.2 and 2.1, based on the Settlement layer. Katla prehistoric is found in profiles 1.2, 2.1, 2.2 and 3 and is used to correlate these profiles. In addition, profiles 3 and 2.1 correlate with K1721. The youngest tephra layers present in the soil profiles are found in profiles 1.2 and 3, H1845 and K1918.

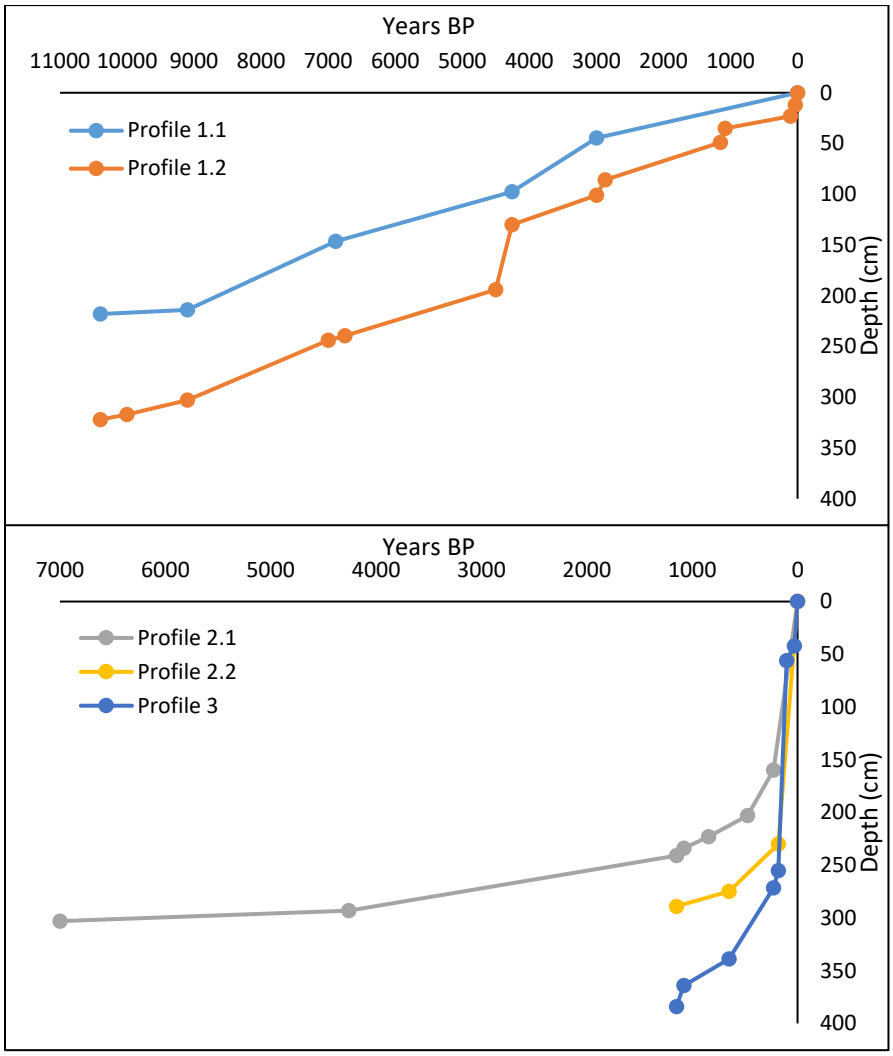

Figure 40. Simple age-depth graph showing all profiles. Profiles 1.1 and 1.2 are displayed on the upper graph as they span the longest time. Profiles 2.1, 2.2 and 3 are displayed on the lower graph to make the changes during the last 1.2 ka more visible.

Most of the tephra layers found in the soil sites are present in lacustrine cores from Hvítárvatn. However, there were also some tephra layers present in the soil sections that were not found in the lake, such as Katla 1918 and Hekla 1845 the youngest tephra layers which are found in soil profiles 1.2 and 3. One explanation for this may be that during this time Langjökull was much affected by the two outlet glaciers that reached the lake basin during the LIA cooling (Larsen et al., 2011), resulting in unstable conditions not favorable for grains to settle and accumulate at the bottom. To be able to identify the eruption age for these youngest tephra layers geochemical data from Thordarson et al. (1998), Óladóttir et al. (2008), Guðnason (2017) and Thorvaldur Thordarson (unpublished data 2018) were used (Appendix A.2). Two other tephra layers were found in the soil sections that are not present in Hvítárvatn. The first layer is tephra from Kverkfjöll (profile 1.1), which has an estimated age of 6.890 years BP based on calculated SAR age and Óladóttir et al. (2011). The second layer is tephra from WVZ (profile 1.2) with an estimated age of 4.500 years BP based on Sinton et al. (2005). Little data is available about these two tephra layers, since they have not been found in many places and their age might thus have some error, although, tephra of

similar age and affinities to the tephra from the WVZ was found in Gedduvatn sediment in the Vestfirðir peninsula (Harning et al., 2018a). The age-depth model for profile 1.2 shows an almost vertical line between WVZ (4.5 ka) and H4 (4.2 ka) which might suggest that the WVZ tephra has a different eruption age (Figure 32).

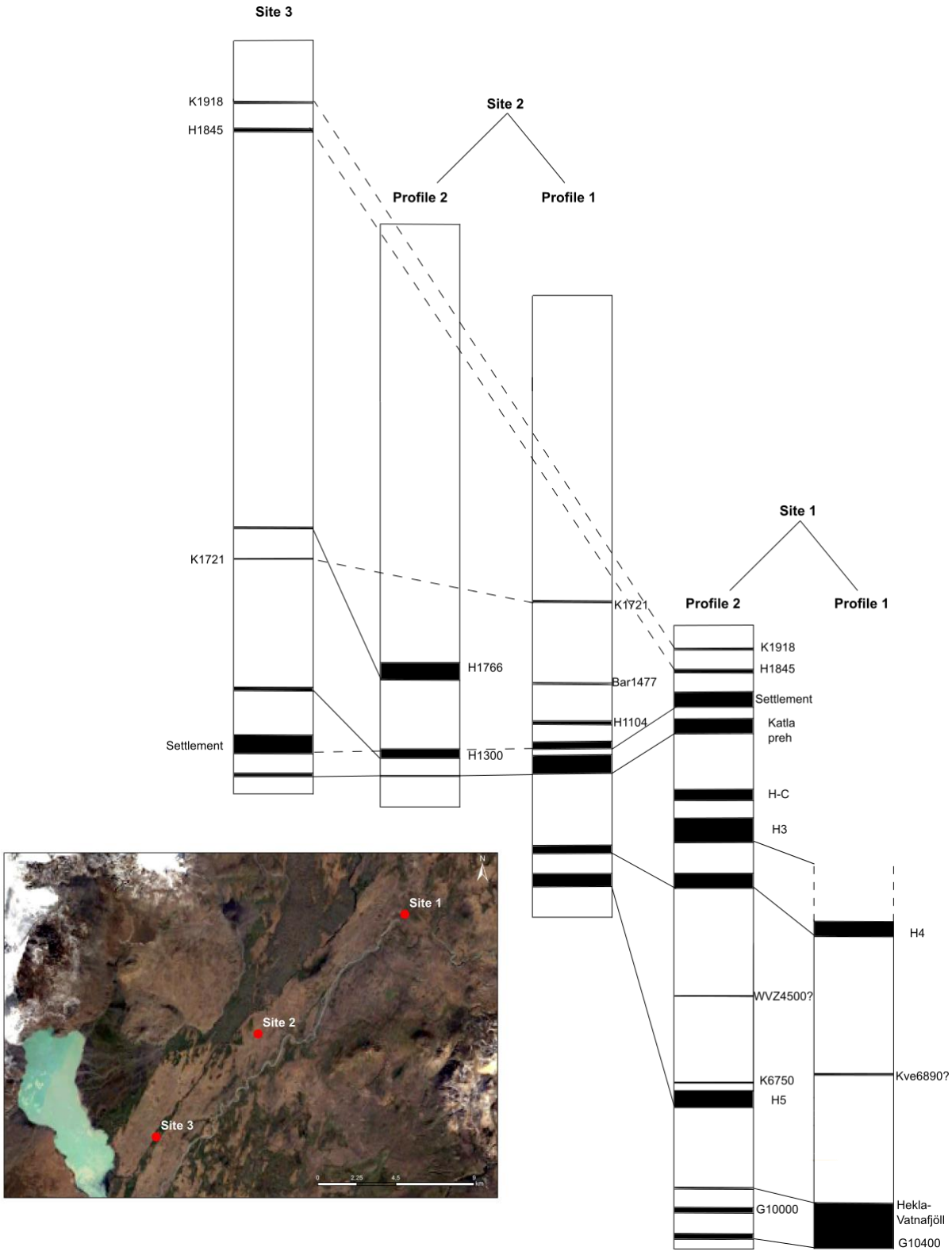

Figure 41. Tephra layers found in each soil section and their connections. On the far right is profile 1.1, then profiles 1.2, 2.1 2.2 and finally on the far left is profile 3. In the bottom left corner is also a zoomed in aerial photograph (Google Earth) of the research area showing the locations of the soil sites.

4.3 Loss on ignition

All samples measured for LOI are from profile 1.2. Results from the LOI shows fluctuations in the percentage of carbon through the Holocene at a multi-centennial scale, although with an increasing first order trend (Figure 42). The LOI results show considerable fluctuations although less fluctuations in the early- to mid-Holocene compared to the late Holocene (after 5.0 ka). The low values of carbon occur at 9.6, 8.0, 5.9, 4.4, 2.8 and 1.4 ka, while the highest values occur at 9.2, 6.8, 5.1, 3.7, 2.5 and 0.7 ka. The minimum carbon proportion of 4% occurs around 9.6 ka. The most abrupt change occurs between 4.5 and 3.7 ka when carbon content drops from 12 to 4% and back to 17% when it reaches the highest percentage through the Holocene. After 0.7 ka the amount of carbon increases towards 0 ka, reaching 15%.

Carbon content in lakes and soil is commonly used to identify periods of landscape instability, which often can be related to climate variations. Since the soil found in the research area are typical Andosols lacking cohesion it is vulnerable to erosion, particularly erosion due to aeolian activity. During intervals of active soil erosion, terrestrial material is transported to nearby lakes, thus an increase in carbon content in lake sediments can indicate landscape instability (e.g. Geirsdóttir et al., 2009a). Comparing the results from this study with carbon content in sediments from Hvítárvatn gives information on the mobility of soils in the Kjölur area.

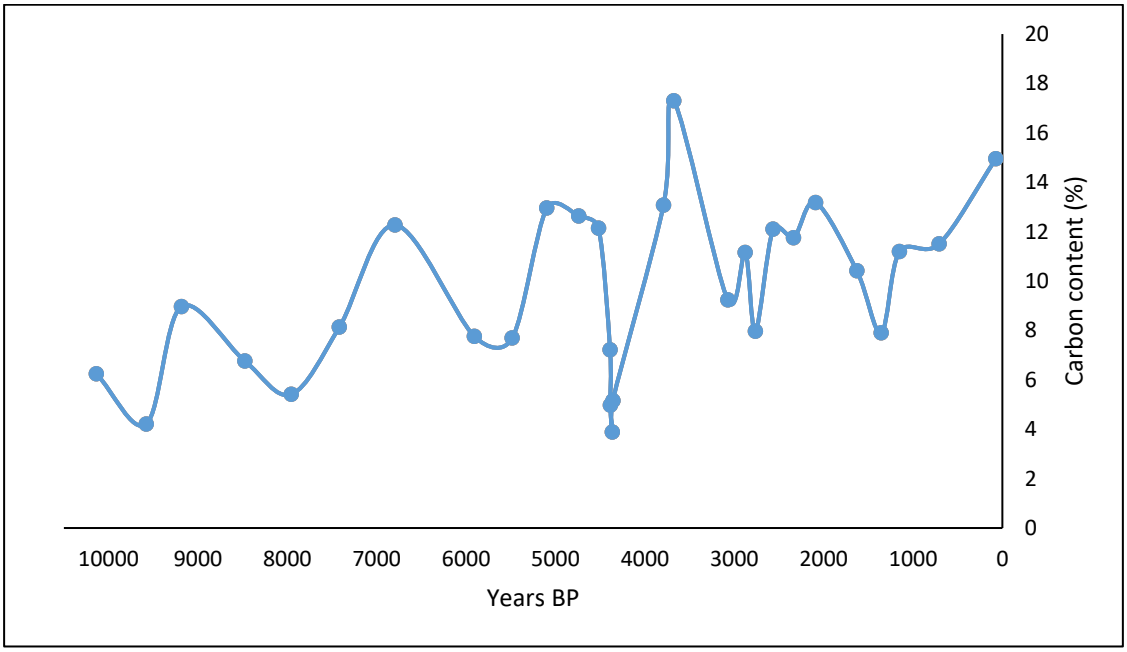

Figure 42. Results from LOI measurements, where the carbon content development through the Holocene of the soil in profile 1.2 is displayed.

4.4 brGDGT temperature estimates

Samples for brGDGT temperature estimates were obtained from the two profiles 1.1 and 1.2 at site 1. These have been correlated based on tephra layers (G10400, H4 and H3). The sampling took place before the tephra-based age model was made for the two profiles, which explains the lack of data between 8.0 ka and 4.2 ka. The results from the measurements are connected based on the tephra correlation and shown as one continuous line (Figure 43).

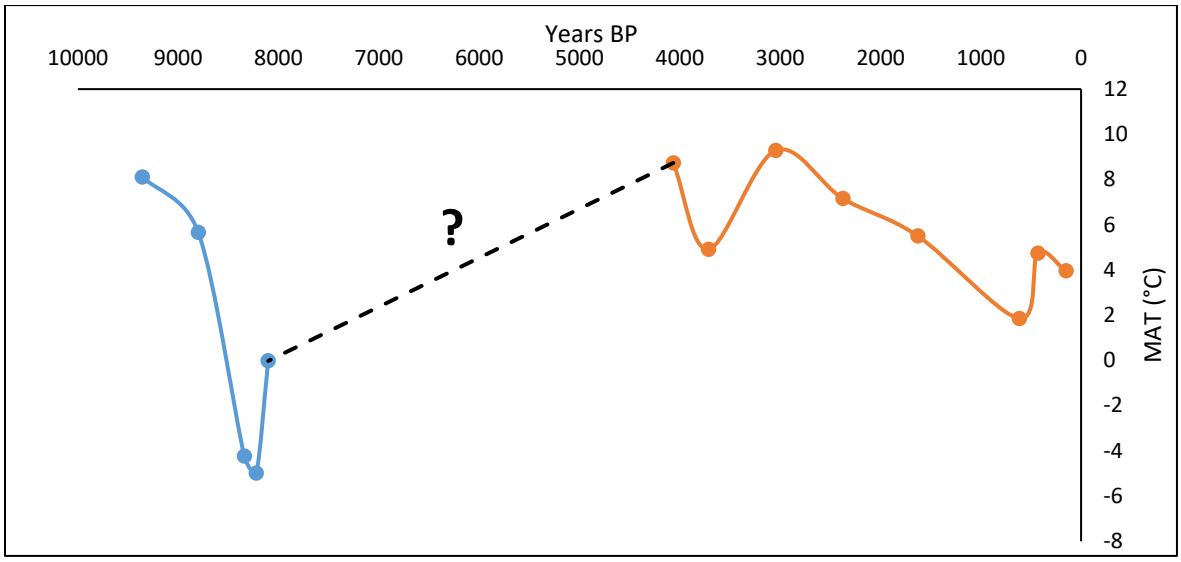

Figure 43. The raw results from the brGDGT measurements. The blue line are samples from profile 1.1 and the orange line from profile 1.2. The black dashed line shows were the two profiles are connected together.

Similar average distributions of brGDGTs in Fossrófulækur compared to the global soil dataset (De Jong et al., 2014, Figure 44) confirms that the extraction and analysis of the Icelandic soils was successful and that the brGDGT distributions can be converted to temperature using different calibrations.

The results for the brGDGT measurements are displayed in Figure 45 where five different calibrations have been used. The calibrations are from three different research papers, Peterse et al. (2012), De Jonge et al. (2014) and Naafs et al. (2017). All the calibrations show a similar trend through the measurements. The main difference between the calibrations is regarding the amplitude of the temperature decreases. The first estimated major temperature decrease occurs around 8.2 ka, the lowest and coldest calibration displays the largest drop and then it gets less severe with the warmer calibrations. A similar observation can be seen with the second temperature decrease which is displayed around 3.7 ka, although this decrease mostly disappears with the topmost calibration. The temperature change estimated around 0.6 ka, is displayed as a temperature increase by all calibrations except one, the calibration MAT-mr (De Jonge et al., 2014) shows this temperature change as a decrease at the end of the plot.

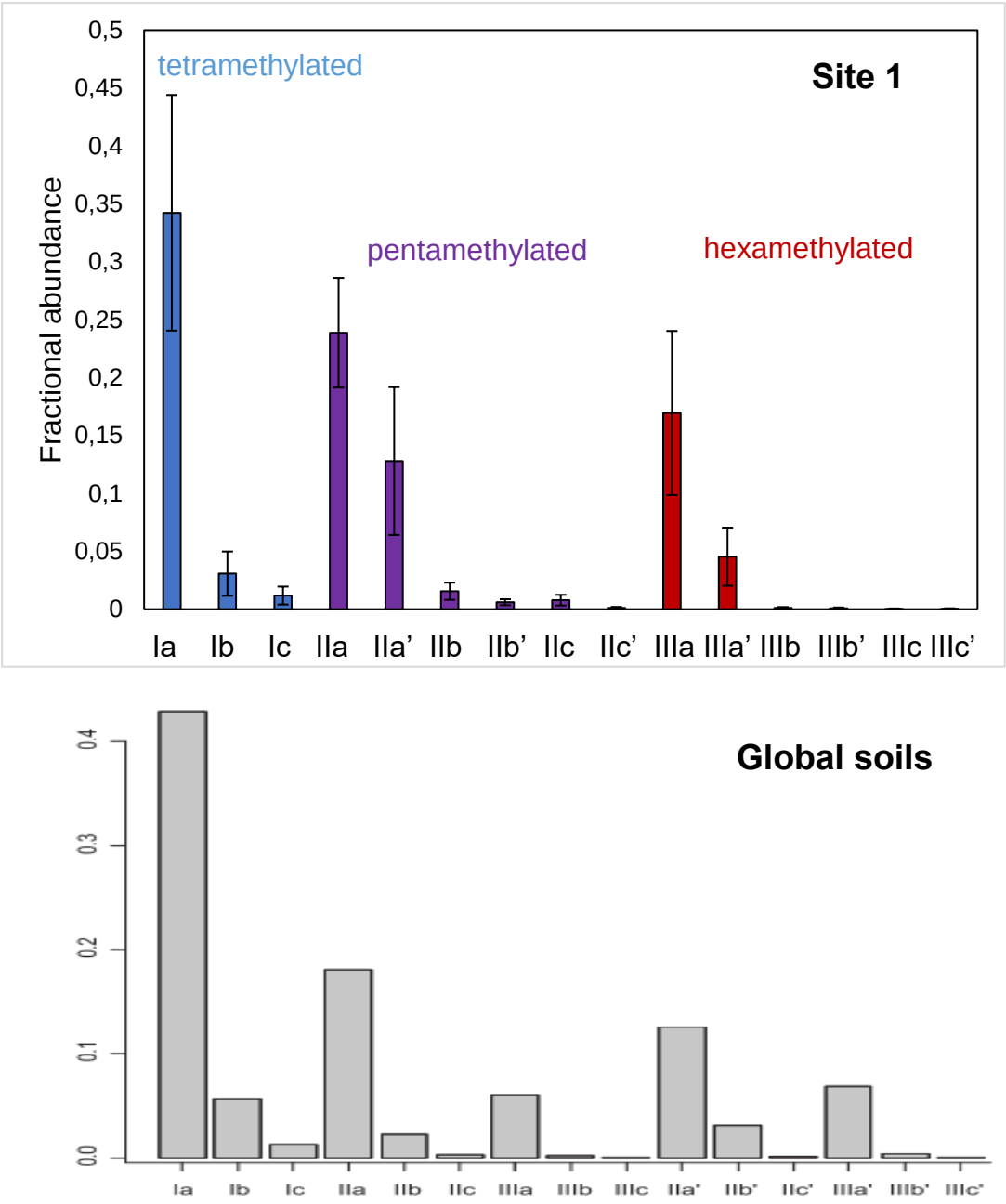

Figure 44. The upper graph displays the brGDGT groups present in the soil samples from site 1 used in the brGDGT measurements. The lower graph shows the brGDGT groups found in the global soil dataset (De Jonge et al., 2014). By looking at these two graphs together, it can be observed that the extraction and analysis of the soil from site 1 worked and the data is usable.

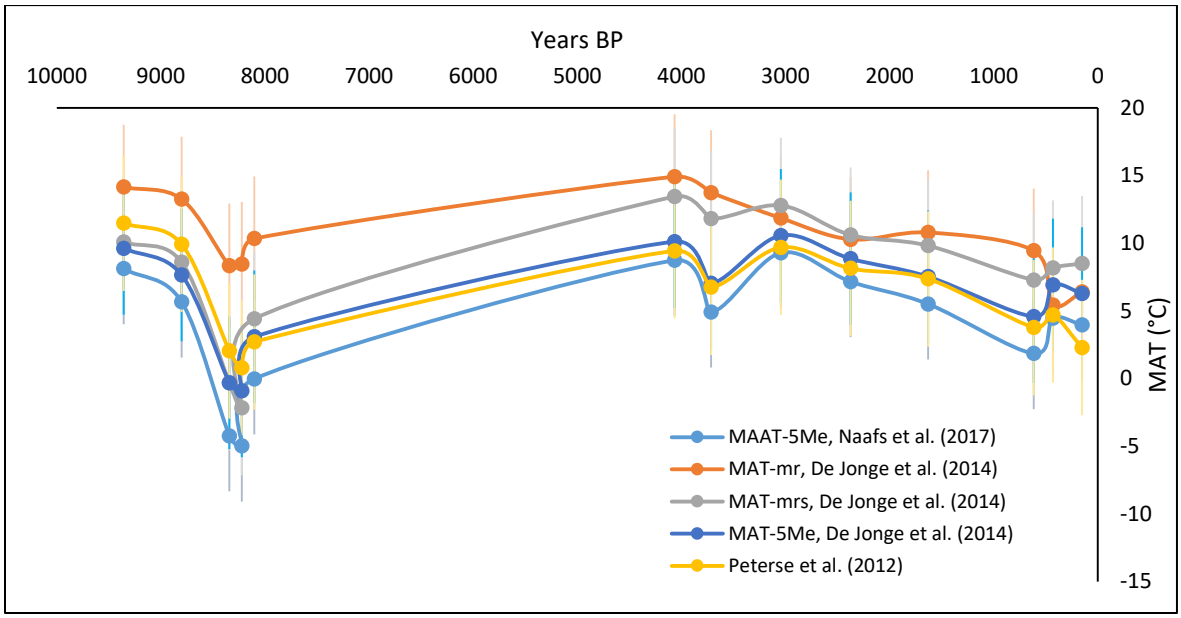

Figure 45. The results from the brGDGT measurements shown with five different calibrations.

5 Interpretation

5.1 Soil accumulation rate

Most of the proxies used were sampled from the thickest soil profiles, 1.1 and 1.2 at site 1 encompassing the last ca. 10 ka. Thirteen tephra layers constrain the age model for profile 1.2 which also gives a rough indication of soil accumulation rate. This can be compared to both the results from the LOI regarding carbon content, and the brGDGT results to help reconstruct a record of environmental change and landscape stability/instability.

Lithofacies analysis of the soil profiles indicate clear grain size variations between sites with coarser sand size grains at sites 2 and 3 compared to site 1, suggesting the impact of aeolian activity in the area and changes in wind strength during the time of soil deposition and development. Weak winds have the capacity to only carry fine particles of fine sand and clay size, whereas stronger winds can transport larger particles of coarse grained sand and up to pebbles (e.g. Jackson et al., 2005). The wind strength can in turn be related to changing climate and landscape stability suggesting stronger winds in cooler and drier climate associated with more active erosion, while the parts of the soil sections which contain fine grains and more brown color (higher organic content) than gray, indicate warmer and more stable climate with calm wind and little or no erosion (Figure 46). This change in appearance, from smaller grain size and brown organic rich material to coarser grain size and gray color, in the soil sections is mostly seen during the last 0.6 ka.

Soil accumulation rates based on the tephra-based age models show in general higher accumulation subsequent to large volcanic eruptions and production of thick tephra layers such as at 4.2 ka (H4), 3.0 ka (H3), 1.1 ka (Settlement). However, changes in accumulation also occur at other times such as around 8.2 ka (site 1) and during the last 0.7 ka (Figure 40). The soil profiles indicate five periods of landscape instability based on a rise in SAR; between 9.0 and 7.0 ka, around 4.5 ka, 3.0 ka, 1.2 ka and after 0.6 ka. The timing and amplitude varies between profiles. Profiles 1.1 and 1.2 indicate the oldest SAR rises, although all five increases can be observed from profile 1.2 as it contains the most tephra layers. The final and most severe SAR increase occurs after 0.6 ka and can be observed in more detail in profiles 2.1, 2.2 and 3.

Visual inspection of the material in each soil profile (see detailed description of each profile in Appendix A.1) reveals considerable amount of redeposited material mostly found in profiles 2.1, 2.2 and 3, while little or no redeposited material is found in profiles 1.1 and 1.2. The redeposited material is seen as gray coarse sand or light colored rounded tephra grains, most likely derived from thick Hekla rhyolite tephra layers such as H4 or H3 (Figure 46). The area east of Langjökull and Hvítárvatn is a sandy desert, affected by very active aeolian activity. The aeolian material is mostly distributed to the south or southwest (Arnalds, 2010; Gísladóttir et al., 2005). The observed differences in thickness of soil sections and accumulation rates from northeast to southwest suggests that redeposited material found in the sections located in the southwest, may be due to aeolian activity and strong, dry northerly winds. Hence, during cooler times such as the LIA when the northerly winds were strong,

transportation of material may have occurred from the northeast to the southwest resulting in the higher SAR in the southwest located sections.

Figure 46. Picture to the left is from profile 2.1 showing soil that does not contain redeposited material. The soil has a brown color and rather fine grain size. The picture to the right is from profile 3 where the soil contained a lot of redeposited material. The material has a dark gray color and coarse grain size, in between the gray grains are lighter colored grains which are most likely originated from the H4 or H3 tephra layers.

5.2 LOI versus SAR

When SAR rises it indicates colder climate and more soil erosion, causing more material being transported with aeolian processes and accumulating faster (e.g. Geirsdóttir et al., 2009b). The LOI shows high peaks when organic matter is high in the soil, indicating warmer or more stable climate and more vegetation cover. When the LOI decreases it indicates that with less organic matter there is more soil erosion and less vegetation cover (Óskarson et al., 2004), while in lake environments, more organic carbon means more terrestrial matter, indicating more erosion and less vegetation cover (Geirsdóttir et al., 2009b). Therefore, when looking at SAR and LOI together, an indication to cooler climate would be displayed as high SAR and low LOI, and vise versa for warmer climate. Cooler climate results in increasing SAR due to more active aeolian transport associated with stronger wind, which results in reduced vegetation cover and then LOI values lower. When climate is warm, erosion and aeolian transport are diminished allowing vegetation cover to strengthen. The LOI results also display an increasing first order trend. That trend is understandable since older soil has been undergoing more erosion and decaying, thus loosing its carbon content for a longer time than the younger soil located closer to the surface. But the relative changes between increasing and decreasing carbon content does give an indication to climate fluctuations.

The LOI soil samples were all collected from profile 1.2, thus it is ideal to compare those results to the SAR observed from the age model for profile 1.2 (Figure 47). The LOI results do indicate more fluctuations compared to the SAR, yet it is possible to correlate changes between these two proxies. The first rise in SAR is observed around 9.0 ka, the LOI responds to this cooling with a change in carbon content going from 9% carbon at 9.2 ka and down to 5,4% at 8.0 ka. The second observed rise in SAR occurs around 4.5 ka and is seen as almost a vertical line indicating very rapid accumulation. Thus, this increase might be exaggerated due to misidentified tephra layers. This increase is seen between H4 and WVZ4500 and the WVZ tephra was difficult to identify and might have another eruption age. At this time the

LOI results display the largest decline with only 4% organic matter around 4.4 ka. However, shortly after or around 3.7 ka, the LOI reaches its highest peak with 17% carbon content. This peak found at 3.7 ka does not correlate with the temperatures expected during this time (see Larsen et al., 2012), which warns against using the LOI directly as a temperature measure. One explanation is that this peak is associated with the H4 tephra deposition around 4.26 ka and subsequent sharp cooling identified in biogenic silica record of Hvítárvatn sediments resulting in accelerated soil erosion (e.g. Larsen et al., 2012) which however also ended quite sharply around 3.9 ka in Hvíatárvatn indicating more environmental stability. The third rise in SAR is shown at 3.0 ka, then the LOI takes a somewhat long dive again from 17% to 9% carbon content. Again, this can be associated with the deposition of the H3 tephra. The LOI reaches 13% carbon around 2.1 ka and then decreases down to 8% around 1.4 ka, the fourth rise in SAR occurs around 1.2 ka. Comparing the locations of tephra layers in section 1.2 to the LOI measurements, some connection between a decrease in LOI and an occurrance of a tephra layer is apparent indicating that an accumulation of a tephra has negative effects on soil cover. Although, the thickness of a tephra layer is important in this case.

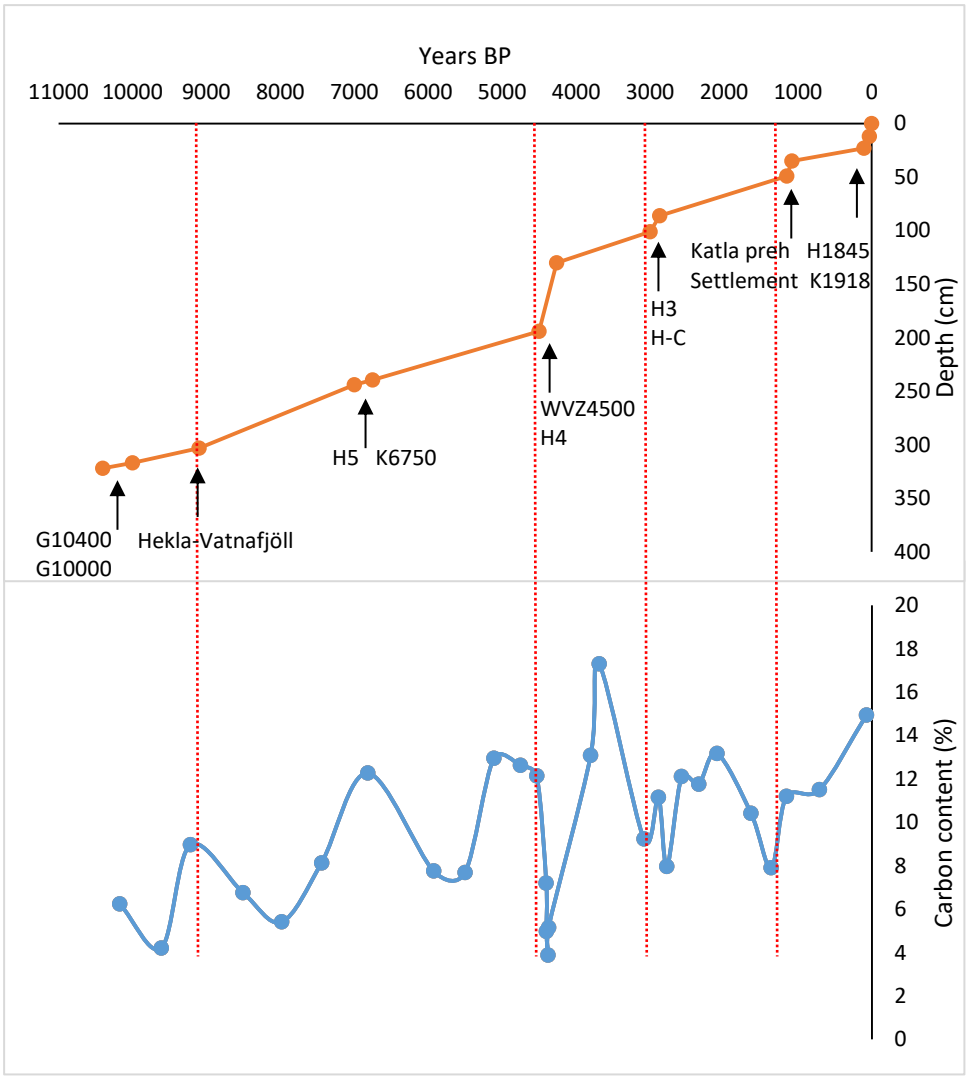

Figure 47. The upper graph shows the simple age-depth model for profile 1.2 and the locations of the tephra layers in that pofile. The lower graph is the LOI results and the red lines indicate times were SAR rises and LOI declines, indicating cooler climate.

5.3 LOI, SAR and brGDGTs

Five different calibrations were used for the brGDGT measurements. The trends for the measurements are shown as one continuous line to make it easier to follow each calibration, although the samples used for the brGDGT measurements were obtained from two soil profiles at the same site, profiles 1.1 and 1.2. The soil samples were chosen before any major tephra identification had been made, thus the measurements do not span the entire Holocene but rather display two parts of it. The measurements show the early Holocene and then the last 4.1 ka years. Due to this the HTM is missing from the plot, when the highest temperatures are assumed and most stable for the Holocene. However, based on comparison with Hvítárvatn and Arnarvatn Stóra records, an idea of what the trend for this interval might look like is shown with a hatched line in Figures 48 and 49 (Larsen et al., 2012; Gunnarson, 2017). The calibration from Petersen et al. (2012) does not separate 5 and 6-methyl isomers, and 6-methyl has been shown to not correlate with temperature (Naafs et al., 2017). The

trends from MAT-mrs and MAT-5ME (De Jonge et al., 2014) and also from the revised global calibrations from Naafs et al. (2017) reconstruct negative MAT occurring around 8.2 ka or early Holocene, which is highly unlikely. By comparing the different calibrations it is suggested to use the MAT-mr calibration (De Jonge et al., 2014) for the brGDGT measurements. The MAT-mr calibration produced the most likely temperature because all MAT estimates are positive and the lowest temperature is recorded during the latest Holocene, which is consistent with other Icelandic paleoclimate reconstruction (e.g. Larsen et al., 2011; Larsen et al., 2012). Hence the brGDGT results are displayed in the graph in Figure 48, with the MAT-mr calibration and 4,6°C error bars. The graph also shows how the measurements lack estimated temperatures for the mid-Holocene. Even though the relative changes in MAT with this calibration do appear to follow the general trend in the nearby qualitative lake proxy records (Hvítárvatn and Arnarvatn Stóra) (Larsen et al., 2012; Gunnarson, 2017), the absolute MAT values appear unrealistic since the annual average temperature for the years 1966-2003 from Hveravellir weather station is -0,87°C (Veðurstofa Íslands, 2018). Also, modeling experiments show that the demise of Langjökull and Drangajökull during the HTM required summer temperatures to rise ca. 3°C above the late 20th Century average at this time (Flowers et al., 2008; Anderson et al., 2018). Similarly, numerical simulations show the maximum expansion of both Langjökull and Drangajökull during the LIA ca. 200 years ago requiring temperature lowering of ca. 1°C below the late 20th Century average (Anderson et al., 2018). The reason for this overestimation of temperature is because the calibration uses a global dataset, resulting in higher MAT than which occurred in Iceland at that time. These MAT estimates would likely be improved with the development of a local Icelandic soil calibration.

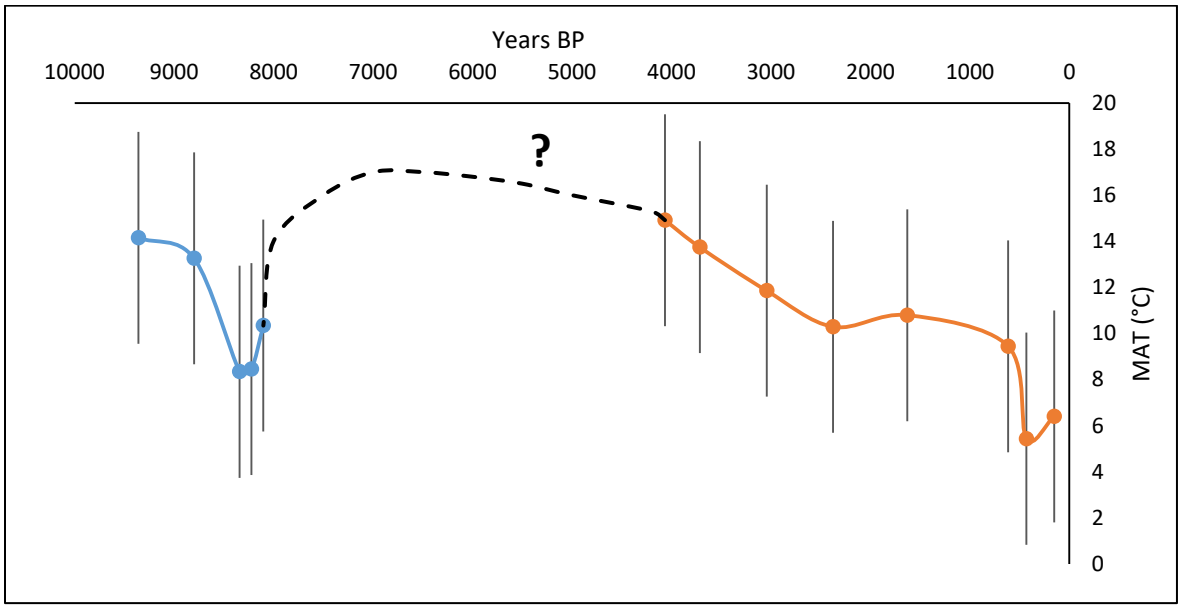

Figure 48. brGDGT measurements showing MAT development for early and late Holocene. Calibration used for the measurements is from De Jonge et al. (2014). Error bars of 4,6°C are seen by every estimated MAT.

The distribution and lack of brGDGT samples does not allow interpretation based on temperature estimates on the period between 8.0 and 4.0 ka. The first part of the brGDGT estimates temperatures between 9.4 and 8.1 ka. MAT is displayed as relatively high in the beginning of the trend and then around 8.8 ka temperatures start to lower, this is in phase

with qualitative temperature estimates based on Arnarvatn Stóra and Hvítárvatn (Larsen et al., 2012; Gunnarson, 2017). Temperature estimates reach lowest values around 8.2 ka and at 8.1 ka start to rise again. The minimum temperature around 8.2 ka corresponds well with SAR for profiles 1.1 and 1.2 as they show rise in accumulation after 9.1 ka, and also the LOI results, with a minimum carbon content occurring around 8.0 ka with 5,4% carbon. Thus, associated with the temperature decline was increased wind strength and soil erosion. This cooling is likely connected to the freshening of the North Atlantic following outburst floods as the LIS was melting (Alley & Ágústsdóttir, 2005). The 8.2 ka cooling event is widespread and is seen in both Hvítárvatn and Arnarvatn Stóra. Both lakes show an increase in SAR and indicate landscape instability during this time (Larsen et al., 2012; Gunnarson, 2017).

From around 7.0 to 5.0 ka is when accumulation rates are displayed as rather even and stable (profiles 1.1, 1.2 and 2.1), correlating to the HTM conditions. That also correlates with what is observed in the lakes, with warm conditions (after the 8.2 ka cold event) reached around 7.0 ka. The lakes indicate landscape stability with low SAR and little terrestrial input during this interval (Larsen et al., 2012; Gunnarson, 2017). SAR for profile 1.2 shows a sharp rise at 4.5 ka which correlates with a sharp decrease in LOI. As mentioned before, information on the brGDGT is lacking for this period. The onset of the Neoglaciation is indicated by the nucleation of Langjökull between 5.5 and 5.0 ka and seen as increasing landscape instability in Hvítárvatn and Arnarvatn Stóra sediments. During this time summers became progressively cooler and a reduction in lake primary productivity followed in both lakes (Larsen et al., 2012; Gunnarson, 2017).

The drop at ca. 4.3 ka in carbon content probably reflects disruption of the vegetation due to the deposition of the H4 tephra with relatively fast recovery around 3.7 ka, thus not necessarily reflecting temperature increase. The brGDGT estimated MAT after 4.0 ka indicates declining temperatures until ca. 2.3 ka similar to what is seen in both Hvítárvatn and Arnarvatn Stóra proxy data, when stable conditions with even slightly warmer summer temperatures are reached until ca. 1.6 ka (Larsen et al., 2012; Gunnarson, 2017). After that the brGDGT MAT starts to decline again until abrupt summer cooling around 0.6 ka (ca. 1275 CE) takes place, culminating around 0.4 ka, or around the time the LIA cooling was intensified with increasing summer temperatures accompanied with cryospheric expansion (Miller et al., 2012). The LIA cooling is also reflected in the increasing SAR in profiles 2.1, 2.2 and 3. These results correlate well with the lake records (Larsen et al., 2011; Gunnarson, 2017) and what is reported from other sites in Iceland for this time period. However, it is more difficult to interpret the results from the LOI measurements, which show an increase in carbon content during what would be considered the coldest time of the studied interval. A likely explanation for this increase in carbon content of the soil might be related to the ground being frozen for a large part of the year at this time. The continuous frozen ground would then prevent the mobilization of vegetation and soils, resulting in organic material being locked into the soils and kept frozen, causing no degradation and thus the LOI do not display a decline in carbon content (Harning et al., 2016; Florian et al., 2015). What also supports this hypothesis is that the SAR for profile 1.2, which contains the LOI soil samples, does not display much effect from the LIA, indicating that there was little or no movement of material at this time. Although, this continuous frozen ground is only indicated for site 1 where profiles 1.1 and 1.2 are located. The other sites show a large increase in SAR following the LIA cooling, indicating very active soil erosion and transport of aeolian material.

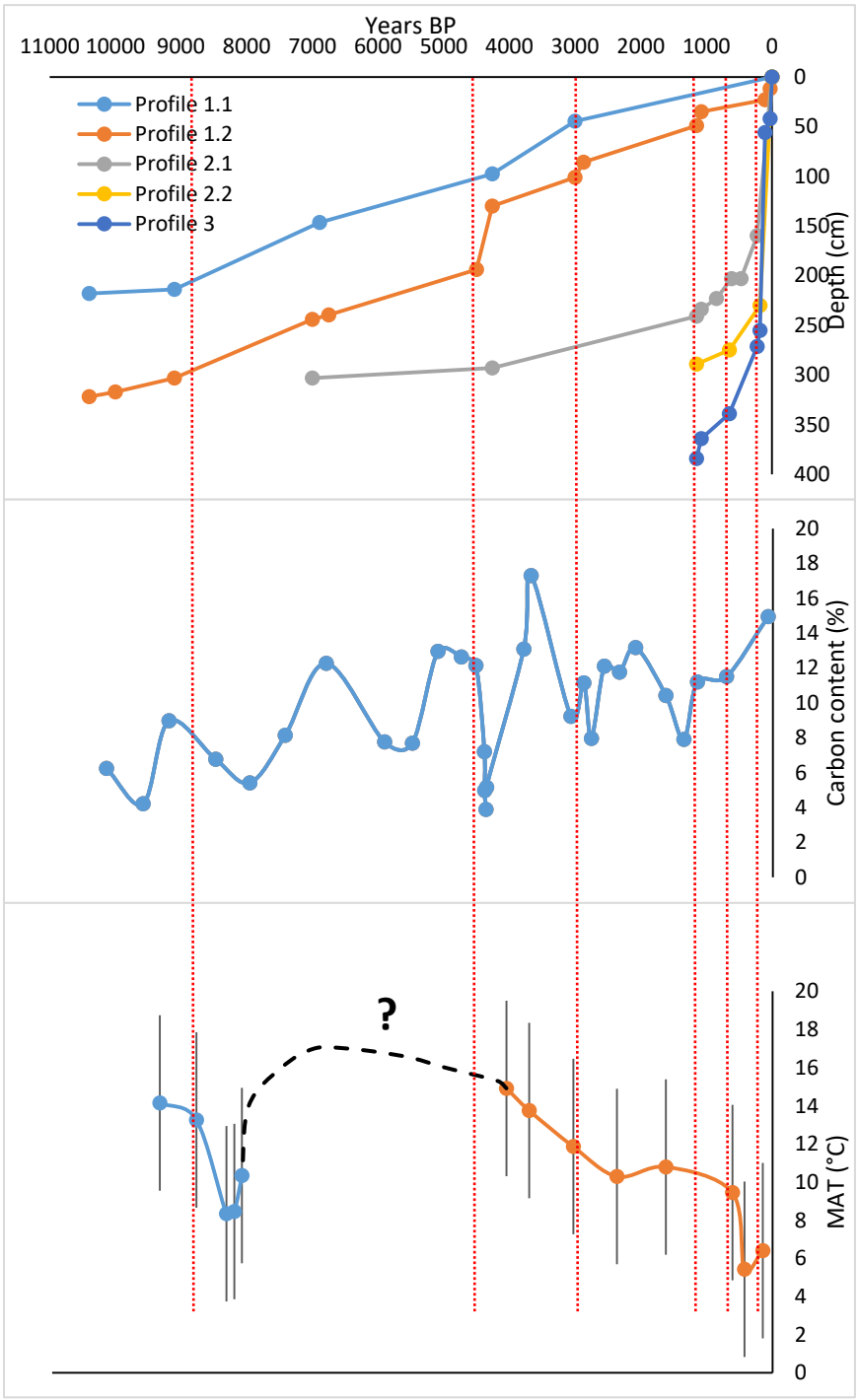

Figure 49. Comparison of all three proxies. The top graph shows all of the age-depth trends for the profiles. The middle graph is the LOI results and the bottom graph is the brGDGT temperature estimates based on the calibration from De Jonge et al. (2014). Additional black dashed line is shown on the brGDGT trend, giving an idea of what the mid-Holocene might look like with these results. The red lines indicate climate fluctuations that can be observed from the proxies.

6 Discussion – The central highlands of Iceland through the Holocene

In this chapter the environmental evolution of the central highlands through the Holocene as seen through the soil sections will be reviewed. The changes observed will be compared to reconstructions from Hvítárvatn and Arnarvatn Stóra. The finding of the 10 ka Grímsvötn tephra series (10.4 ka) in lacustrine sediment cores obtained from lakes in the central highlands show that the area was ice free at that time (Jóhannsdóttir, 2007; Geirsdóttir et al., 2009a; Larsen et al., 2012; Gunnarson, 2017; Harning et al., 2018a). North Atlantic warmth during early to mid-Holocene is indicated by Holocene lacustrine records from Iceland, such as have been obtained from Hvítárvatn and Arnarvatn Stóra (Larsen et al., 2012; Gunnarson, 2017). At present the sediment flux into Hvítárvatn is dominated by Langjökull's outlet glaciers and the changes observed in the sediment give information about the development of the glacier. The sediment from the late Holocene is characterized by varve layers, which cannot be seen in the sediment from early Holocene. The interval between 9.5 and 5.5 ka in Hvítárvatn is dominated by benthic diatoms which infers that Langjökull disappeared or that the glacial erosion products were insignificant at that time (Geirsdóttir et al., 2009b), although with an exception of a possible short lived reformation of the ice cap between 8.7 and 8.0 ka. Ice-cap model simulations of Langjökull (Flowers et al., 2007) give the results that if summer temperatures were at least 3°C higher than the 1961-1990 average, it would result in Langjökull disappearing. This implies that there were largely ice-free conditions across Iceland during early to mid-Holocene (Geirsdóttir et al., 2009b). With that in mind, it is possible to expect the soil sites to indicate the warmest and most landscape stability for the Holocene, during the HTM. After the HTM conditions were terminated climate started to cool with increasing landscape instability and the appearance of the first varves in Hvítárvatn, marking the start of the Neoglaciation around 5.5 ka (Larsen et al., 2012). The Neoglacial cooling trend is observed in both Hvítárvatn and Arnarvatn Stóra, reaching the highest erosion rates and landscape instability during the LIA between 1275-1900 CE (Larsen et al., 2011; Larsen et al., 2012; Gunnarson, 2017).

6.1 Landscape evolution of the central highlands

The landscape development of the research area has been highly influenced by fluctuations in climate since the central highlands became ice free in the beginning of the Holocene. Temperature fluctuations and changes in wind strength are seen affecting soil development through the Holocene. By comparing the results from this study to the climate reconstruction from the proglacial lake Hvítárvatn, which is situated just a few kilometers west from the soil sites, and Arnarvatn Stóra, it helps to underline the interpretations for the climate evolution in the central highlands of Iceland through the Holocene. These two lakes were chosen for comparison due to their location being near to the research area and their Holocene environmental history is well described. The broad overview of the results indicate that the soil sections show responses to the three largest temperature declines during the Holocene, the 8.2 ka event, the 4.5 to 4.0 ka decline and the last ca. 0.6 ka (LIA). Figure 50 shows a comparison between the temperature record derived from the soil sections as well as BSi and C:N records from Hvítárvatn and Arnarvatn Stóra (Larsen et al., 2012;

Gunnarson, 2017) and also composite relative temperature changes for the Holocene based on proxies from Hvítárvatn and Haukadalsvatn (Geirsdóttir et al., 2013). The biogenic silica (BSi) record from the lake sediment has previously been shown to reflect summer temperature as it is a measure of diatom primary productivity, thus an increase in BSi corresponds to warmer climate (Geirsdóttir et al., 2009a; Larsen et al., 2012). The ratio between carbon and nitrogen (C:N) gives information about how much terrestrial material is being transported into a lake with aeolian and fluvial activity (Larsen et al., 2012). The axis for C:N is shown in reverse to display rising lines as warmer and more stable climate. By comparing these records obtained from lake sediment, it underlines that the brGDGT temperature estimates display a trend that is seen in Iceland for the Holocene climate. All of these trends show a decline around 8.2 ka and then rising temperatures reaching the HTM, the comparison plots give an idea of what the conditions were during the HTM, when climate was the warmest. Then after the start of the Neoglaciation there is a cooling trend, which culminates during the LIA.

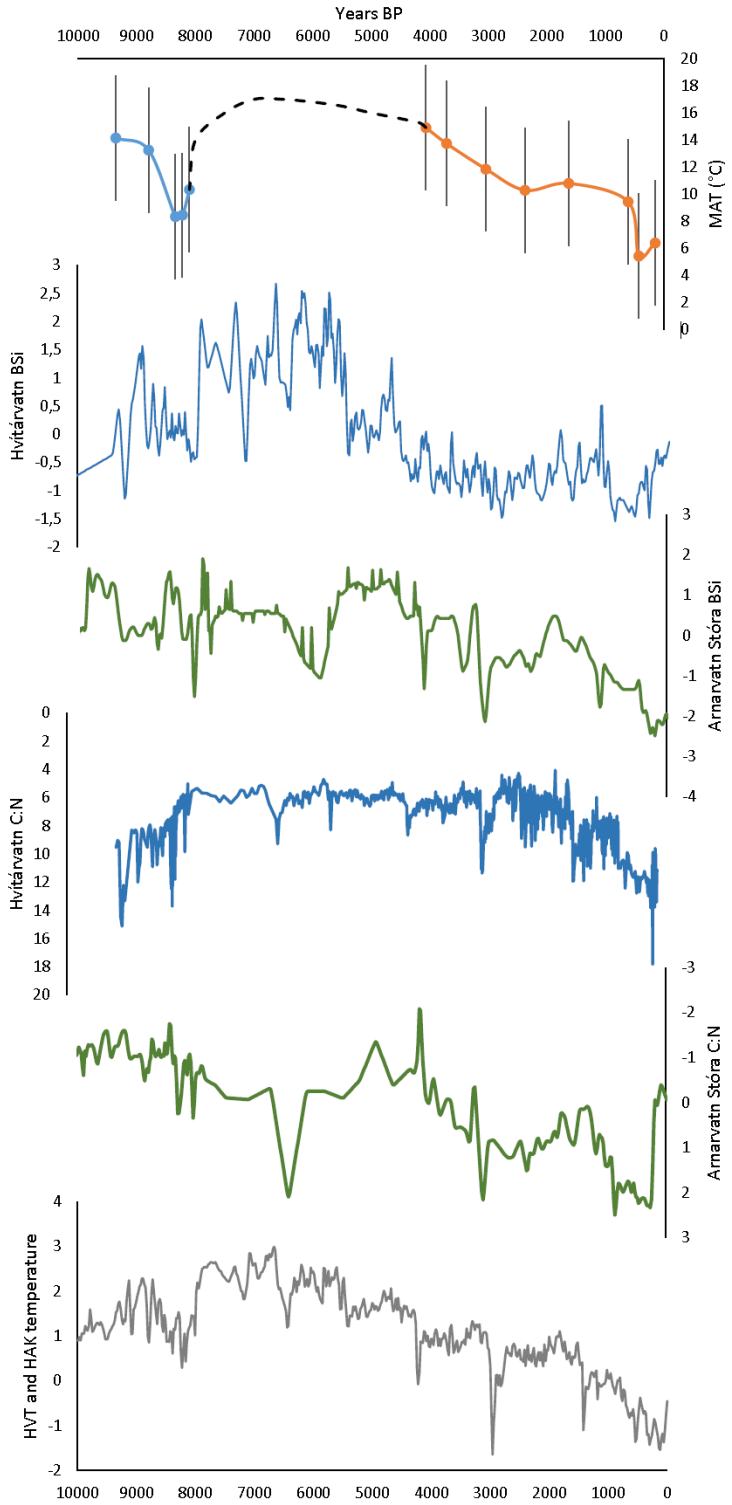

Figure 50. The top graph shows the brGDGT temperature estimates with the calibration from De Jonge et al. (2014). The second graph is the BSi from Hvítárvatn (Larsen et al., 2012) and the third graph contains the BSi from Arnarvatn Stóra (Gunnarson, 2017). The fourth and fifth graphs display C:N for Hvítárvatn and Arnarvatn Stóra (Larsen et al., 2012; Gunnarson, 2017). The bottom graph shows composite relative temperature changes for the Holocene from Hvítárvatn and Haukadalsvatn (Geirsdóttir et al., 2013).

6.1.1 10.3 to 8.7 ka

Information about climate and landscape for the beginning of the Holocene is indicated by SAR at site 1, profiles 1.1 and 1.2, as well as the brGDGT and LOI measurements. The data indicate quite stable conditions with low SAR around 10 ka. The LOI plot shows a drop in carbon content around 9.6 ka which declines down to 4% carbon in the soil, indicating that the soil might have still been unstable at that time and thus more vulnerable to erosion or cool summers. The brGDGT indicate warm conditions at 9.4 ka with relatively high MAT, but these warm conditions did not seem to last long as by 8.8 ka MAT is beginning to decrease and then takes a sharp decline.

These results correlate well with climate reconstruction from Hvítárvatn. For this time interval the lake indicates unstable, freshly deglaciated landscape which is reaching equilibrium with the local climate. There was no glacier where Langjökull is at present, at this time of highest Northern Hemisphere summer insolation. The lake catchment is reaching increased stabilization from 10.2 to 9.0 ka and the lake primary productivity is increasing following warm summers. The proxies from the lake indicate a distinct warm interval from 9.0 to 8.7 ka (Larsen et al., 2012) during which there was an increased influence from the NIIC on the North Iceland Shelf (Castañeda et al., 2004). This warm interval is also recorded in the brGDGT results with MAT estimated as relatively high compared to the rest of the plot. Also, elevated C:N which is derived from terrestrial soil, indicates that some regional soil material was being transported into the lake during this interval as the soil was starting to develop after deglaciation (Larsen et al., 2012). This again correlates well with the results as the LOI plot displays that some soil erosion was taking place. Aeolian activity is also indicated in Arnarvatn Stóra with elevated sediment accumulation and also seen in cores from the North Iceland Shelf. This again, indicates that the soil forming after deglaciation was vulnerable to high wind speeds and that might have delayed a continuous vegetation cover to be formed after deglaciation even though climate was starting to warm (Gunnarson, 2017; Castañeda et al., 2004).

6.1.2 8.7 to 8.0 ka

A cooling event after 8.8 ka is indicated by the brGDGT, LOI and SAR for profiles 1.1 and 1.2. The MAT based on the brGDGT during this interval reached the lowest values at 8.2 ka. The soil erosion that had been decreasing with the start of the Holocene enhanced during this interval, with carbon content in the soil dropping from 9% at 9.2 ka and down to 5% at 8.0 ka. With stronger wind and increasing soil erosion, SAR increased as well showing increased rates between 9.0 and 7.0 ka. The early Holocene warmth was interrupted in the highlands of Iceland due to this cold event that occurred at 8.2 ka. The distinct cold climate identified in the North Atlantic area has been related to the melting of the LIS that caused outburst floods into the North Atlantic disrupting the thermohaline circulation (Alley & Ágústsdóttir, 2005).

The 8.2 ka cold event has been identified in Hvítárvatn and Arnarvatn Stóra as well as in other lake studies in Iceland (Larsen et al., 2012; Geirsdóttir et al., 2013; Gunnarson, 2017; Eddudóttir et al., 2018; Harning et al., 2018b). In the lakes this cold event is indicated with two rapid shifts to cooler conditions occurring at 8.5 and 8.2 ka (Larsen et al., 2012; Gunnarson, 2017). Primary productivity in Hvítárvatn decreased and proxies point towards rapid increases in water turbitidy. Also C:N become relatively high for this interval, suggesting that contribution of soil into the lake increased, following more active aeolian

activity (Larsen et al., 2012). In Vestfirðir a multi-centennial cooling occurred between 8.7 and 7.9 ka with peak cooling at 8.2 ka, correlating to this widespread cooling event. The cooling is indicated by a gradual reduction in algal productivity and increase in soil erosion (Harning et al., 2018b).

The effects from this cooling event ceased after 8.0 ka when the carbon content in the soil started to increase and the brGDGT show a rise in temperature starting around 8.1 ka. This correlates well with Hvítárvatn as the cooling conditions following this cooling event lasted until 7.9 ka in the lake (Larsen et al., 2012).

6.1.3 8.0 to 5.0 ka

Around 7.0 ka, profiles 1.1, 1.2 and 2.1 seem to have recovered from the 8.2 ka cool event and display warmer and more stable conditions with slow SAR. Landscape and vegetation also became stable as soil erosion slowed down or stopped, with LOI reaching a peak of 12% carbon at 6.8 ka. After 6.8 ka LOI shows a carbon decrease towards 6.0 ka, indicating that some cooling might have occurred, although this cooling is not indicated by any other component. The SAR trend for profile 1.2 indicates that the HTM warm conditions were terminated around 4.5 ka, when rates increased very rapidly, responding to an increase in aeolian activity. The LOI display a change from warm to cooler climate around 5.0 ka, when carbon content starts to decrease and reaches its maximum low at 4.4 ka.

Climate started to ameliorate after the 8.2 ka event and the HTM conditions became more prevailing following the Northern Hemisphere summer insolation. Warmer conditions are indicated earlier at Hvítárvatn compared to the soil sections, with peak summer warmth reached by 7.9 ka. Sedimentation rates dropped during this interval as well as terrestrial material, indicating less erosion and transport of material into the lake (Larsen et al., 2012).

The brief cooling indicated by the LOI between 6.8 and 6.0 ka is also seen in Hvítárvatn, Arnarvatn Stóra and in other Icelandic lake records (Larsen et al., 2012; Gunnarson, 2017; Harning et al., 2018a). This cooling may likely be linked to the impact of four fissure vent eruptions from Katla and Bárðarbunga-Veiðivötn volcanic systems between 6.8 and 6.5 ka, causing increased sulfur loading in the atmosphere (Thordarson et al., 2003). The HTM warm conditions lasted until 5.5 ka as indicated by the proxies from Hvítárvatn (Larsen et al., 2012).

6.1.4 5.0 to 1.5 ka

Around 4.4 ka aeolian processes were active as indicated by a fast drop in LOI reaching 4% carbon content. With stronger wind and active soil erosion SAR increased rapidly around 4.5 ka as shown in profile 1.2. Because of lack of brGDGT data between 8.0 and 4.0 ka it is difficult to see any indication of a cooling at this time. However, the trend from 4.1 and 1.5 ka indicates a steady decline in MAT similar to what is indicated by both LOI and SAR.

The second half of the Holocene is characterized by a decline in temperature following the Northern Hemisphere summer insolation decline. The Hvítárvatn record indicates that the Neoglaciation began after 5.0 ka with the nucleation of Langjökull. During this time glaciers advanced and landscape became unstable (Larsen et al., 2012). The lake records reflect reduced productivity and increased terrestrial input, as winds became stronger, resulting in active soil erosion and transport of material. A second cooling step around 4.3 ka near

coinciding with the production of H4 is apparent in the soil sections, more apparent than the initial cooling seen in Hvítárvatn between 5.5 and 5.0 ka. This step is marked by a large increase in sedimentation rate in the soil sections and the first appearance of varves in Hvítárvatn, signifying a great increase in glacier size (Larsen et al., 2012). This cooling around 4.5 and 4.2 ka is also apparent in Arnarvatn Stóra and other lake records in Iceland (Geirsdóttir et al., 2013; Gunnarson, 2017; Harning et al., 2018b).

There is a close similarity between the soil sections and the lake records indicating the onset of the Neoglaciation after ca. 5.0 ka. However, because of lower resolution sampling of proxy data throughout the soil sections the stepped changes seen in the lake records are not clearly identified in the soils. The brGDGT based MAT shows steady temperature decrease until ca. 2.3 ka. During this time Langjökull advanced following the accumulation of the H3 tephra (Larsen et al., 2011). The H3 tephra is approximately 12 km^3 and is thought to be the most severe eruption from Hekla during the Holocene (Larsen & Thorarinsson, 1977). The cooler and/or more unstable conditions following the accumulation of the tephra caused abrasion and increased soil erosion (Larsen et al., 2011). The cooling lasted for more than 100 years and during that time the North Atlantic Deep Water formation was reduced (Oppo et al., 2003), there was an increase in ice rafted debris (Bond et al., 2001), ocean currents shifted (Knudsen & Eiríksson, 2002) and sea surface temperature was low (Eiríksson et al., 2000; Castañeda et al., 2004). The MAT, the LOI and the SAR show that conditions seem to have recovered and stabilized temporarily between 2.3 and 1.5 ka coinciding with limited glacier activity in Hvítárvatn (Larsen et al., 2011). The same can be observed from the carbon content in the soils which reached the lowest values around 2.8 ka but started to rise again after that, indicating that soil erosion decreased.

6.1.5 1.5 to 0 ka

The SAR trend for both profiles shows a small peak starting around 1.2 ka and then rates lower after 1.0 ka reaching more stable rates. The LOI plot shows a decrease in carbon content which correlates to a cooling often known as the Dark Ages Cold Period (DACP), with a carbon content drop from 13% around 2.0 ka and down to 8% around 1.4 ka. After the drop at 1.4 ka the carbon content starts to increase and reaches 11% at 1.1 ka, which correlates to the time the Medieval Warm Period (MWP) occurs.

The effects of cooling during the LIA are indicated in all the results except for the LOI. However, profiles 1.1 and 1.2 do not display the LIA as well as the other profiles, possibly due to the dominating dry wind direction from the northeast towards southwest. The consequence of this dominating dry wind direction is that during colder climate, when wind strength is increased, transported grains will accumulate further southwest of the area rather than in the northeastern part. This is clearly indicated in the studied soil sites, as profiles 2.1, 2.2 and 3 contain a great amount of redeposited material that occurs mostly around the time of the LIA cooling. The SAR graphs for these sections match these interpretations, as they all show a large increase for the onset of the LIA or when the cooling intensified. Even though profile 1.2 does not reflect the cooling of the LIA as well as profiles 2.1, 2.2 and 3, it does show an increase in SAR around 0.3 ka which is a time when the cooling was intensified (Larsen et al., 2012; Miller et al., 2012). Profiles 2.1, 2.2 and 3 all display the onset of the LIA around 0.6 ka. The brGDGT estimated temperatures show the coldest MAT during the LIA at 0.43 ka, when the temperature decline associated with the start of the Neoglaciation reaches its maximum low. As is indicated by the SAR and the brGDGT estimates, the research area was highly influenced by the LIA cooling. The cooling might

also have resulted in a permafrost in the soil (Florian et al., 2015), especially in the area were profiles 1.1 and 1.2 are located. This inferred permafrost may explain the apparent increase in carbon content in the soil occurring during the LIA cooling. If permafrost did form in the soil then organic material would not undergo transportation and thus result in increased carbon content as opposed to decreased carbon content. The lack of transportation is supported by the SAR for profile 1.2, as it only shows an increase after 0.3 ka.

After 1.5 ka glaciers in Iceland such as Langjökull advanced as climate became colder with the start of the DACP. This cold event was short lived and ended around 1.0 ka, after that the MWP took over with warmer and calmer climate (Larsen et al., 2011). Langjökull advanced at 1.4 ka and 0.7 ka which coincide with the timing of the DACP and the LIA. These advances are separated by the MWP with 0.3 ka years of milder conditions. The onset of the LIA is indicated in the lake by a large increase in varve thickness and C:N, indicating more soil erosion, occurring at 0.65 ka. Langjökull advanced in two phases after the onset of the LIA, reaching out into the lake by 0.19 ka (1760 AD) and then reaching its Holocene maximum extent around 0.05 ka (1900 AD) (Larsen et al., 2012). The LIA marks the largest glacier advances during the last 8.0 ka and is an extreme example of a superposed century-scale cold summer anomaly. The origin of the LIA has long been debated since natural forcings are either weak or as for the case of volcanism, short lived. Recently the cold temperatures of the LIA have been explained by four large sulfur rich explosive eruptions occurring within a short interval, resulting in an abrupt summer cooling during a time when hemispheric summer insolation was at a minimum. This resulted in a strong positive feedback which led to sea-ice expansion and possible disruption of sea surface currents in the North Atlantic bringing warmth to the higher latitudes. Thus the cooling was self-sustained for centuries after the volcanic aerosols were removed from the atmosphere (Miller et al., 2012).

The soil erosion seen in late Holocene has often been linked to the settlement of Iceland which occurred around 1.0 ka. However, as the results from this study show the soil erosion began before the acknowledged settlement with relatively stable conditions few centuries after the onset of the settlement. Soil erosion becomes most severe during the LIA (e.g. Geirsdóttir et al., 2009b). The effects from the LIA cooling are seen in a number of records across Iceland with severe impact on the central highlands, an area dominated by soil types that lack cohesion (Arnalds, 2008).

7 Conclusion

The five soil profiles chosen for this project contain information on fluctuating climate during the Holocene and how climate fluctuations influenced the landscape evolution in the central highlands of Iceland. By observing the stratigraphy in the sections and tephra layers, it was possible to obtain age models for the research area, which provided information on SAR. Identification of the tephra layers preserved in the soil sections facilitated comparisons of proxy records such as the LOI and brGDGTs and similar records from Hvítárvatn and Arnarvatn Stóra. This study shows that it is necessary to look at all five soil profiles together to be able to observe and evaluate the main climate fluctuations that occurred through the Holocene. By comparing all the components a complete picture of the Holocene climate and landscape evolution for the research area is achieved.

The brGDGT is a new and very useful tool for paleotemperature reconstruction. The temperature estimates from the brGDGT measurements provide important results that help to reach a final conclusion regarding climate and landscape evolution for the research area through the Holocene. However, the brGDGT measurements for this study lack sample points to reach through the entire Holocene and although they are able to give information on relative temperature changes they provide an overestimation of temperature for the central highlands. The overestimated MAT values are due to the applied calibration set, which uses a global dataset and only reinforces the need for a regional dataset for Iceland to provide more accurate temperature values. Even though the brGDGT MAT values are overestimated they do give a temperature trend similar to what is seen in Hvítárvatn, Haukadalsvatn and Arnarvatn Stóra, for the Holocene. By comparing the brGDGT results to these lakes it is clear that the estimates are usable and that they give the temperature trend seen in similar Holocene records across Iceland.

The soil sections and the components used to reconstruct Holocene climate for the research area indicate three major temperature declines which are detected by almost all components, they are the 8.2 ka event, the cooling around 4.2 ka and the LIA. All three declines are indicated by the SAR trends and the LOI results, but only the oldest and youngest temperature declines are indicated by the brGDGT estimates due to the lack of measurements between 8.0 and 4.0 ka. When all soil record and components are compared and correlated additional three cooling events are identified, at ca. 6.0, 2.7 and around 1.4 ka. These cooling events are indicated as either increases in SAR, decreases in LOI or a decline in brGDGT estimated MAT. All of these cooling events correlate well with what is seen in climate reconstruction for Holocene from Hvítárvatn, as well as other areas in Iceland.

The cooling which influenced the research area the most is the LIA which had an onset around 0.6 ka. During this cooling Iceland's glaciers reached their Holocene maximum extent and severe soil erosion occurred. The soil erosion is well displayed in the Kjölur area with a dominating dry wind direction going from the northeast and to southwest. Thus, soil sections located further southwest in the area are dominated by redeposited material during the time of the LIA. The redeposited material is seen as coarse sand and tephra grains from thick rhyolite tephras, such as H3 and H4. There is also an indication of regional permafrost condition in soil during this cold event which caused organic material to stay in place rather

than erode away. This is concluded from the LOI measurements as they display an increase in carbon during the LIA, rather than a decrease like is observed for other cooling events. The brGDGT based MAT also display the LIA as the coldest time during the Holocene, supporting the conclusion that there might have been a regional permafrost in a part of the area. All records indicate that the LIA marks the coldest times of the Holocene.

8 Further work

A few things might be valuable to look into in the future regarding this research to obtain greater and more coherent results:

- More brGDGT measurements are needed from the soil sites in the area, to be able to estimate the temperature trend throughout the entire Holocene, rather than just the early and late Holocene. Another aspect concerning the brGDGT is to obtain an Icelandic calibration dataset for soil in Iceland to be able to get more accurate temperature estimates for the past. The brGDGT could become very useful in paleoclimate reconstruction in Iceland.
- More geochemical analysis is needed for the tephra layers found in the soil sites, as some tephra layers were quite hard to identify due to lack of grains present in the samples to analyze. This would provide better age control for the area as well as enhance the knowledge of explosive volcanism record for the central highlands.
- Measure and sample more soil sections at higher resolution than in this study around the Kjölur area, to acquire more precise timing on cooling events and soil erosion that have affected the area.
- Higher resolution sampling for both LOI and brGDGT measurements, which would add important information about timing of severe soil erosion as well as to see if the interpretation that regional permafrost formed in the soil during the LIA is valid.

References

Alley, R.B. & Ágústsdóttir, A.M. (2005). The 8k event: cause and consequences of a major Holocene abrupt climate change. *Quaternary Science Reviews, 24*, 1123-1149.

Anderson, L.S., Flowers, G.E., Jarosch, A.H., Aðalgeirsdóttir, G., Geirsdóttir, Á., Miller, G.H., Harning, D.J., Thorsteinsson, T., Magnússon, E. & Pálsson, F. (2018). Holocene glacier and climate variations in Vestfirðir, Iceland, from the modeling of Drangajökull ice cap. *Quaternary Scienve Reviews, 190*, 39-56.

Arnalds, Ó. (2000). The Icelandic "rofabard" soil erosion features. *Earth Surface Processes and Landforms, 25*, 17-28.

Arnalds, Ó. (2004). Volcanic soils of Iceland. *Catena, 56*, 3-20.

Arnalds, Ó. (2008). Soils of Iceland. *Jökull, 58*, 409-421.

Arnalds, Ó. (2010). Dust sources and deposition of aeolian materials in Iceland. *Icelandic Agricultural Sciences, 23*, 3-21.

Arnalds, Ó., Gísladóttir, F.O. & Sigurjónsson, H. (2001). Sandy deserts of Iceland: an overview. *Journal of Arid Environments, 47*, 359-371.

Arnalds, Ó. & Grétarsson, E. (2001). *Soil map of Iceland.* 1:500.000 (2. edition). Agricultural Research Institute.

Axford, Y., Miller, G.H., Geirsdóttir, Á. & Langdon, P.G. (2007). Holocene temperature history of northern Iceland inferred from subfossil midges. *Quaternary Science Reviews, 26*, 3344-3358.

Blaauw, M. (2010). Methods and code for 'classical' age-modelling of radiocarbon sequences. *Quaternary Geochronology, 5*, 512-518.

Bond, G., Kromer, B., Beer, J., Muscheler, R., Evans, M.N., Showers, W., Hoffmann, S., Lotti-Bond, R., Hajdas, I. & Bonani, G. (2001). Persistent solar influence on north Atlantic climate during the Holocene. *Science, 294*, 2130-2136.

Berger, A. & Loutre, M.F. (1991). Insolation values for the climate of the last 10 million years. *Quaternary Science Reviews, 10*, 297-317.

Castañeda, I.S., Smith, L.M., Kristjánsdóttir, G.B. & Andrews, J.T. Temporal changes in Holocene $\delta^{18}O$ records from the northwest and central North Iceland Shelf. *Journal of Quaternary Science, 19*(4), 321-334.

De Jonge, C., Hopmans, E.C., Stadnitskaia, A., Rijpstra, W.I.C., Hofland, R., Tegelaar, E. & Sinninghe Damsté, J.S. (2013). Identification of novel penta- and hexamethylated

branched glycerol dialkyl glycerol tetraethers in peat using HPLC-MS^2, GC-MS and GC-SMB-MS. *Organic Geochemistry, 54*, 78-82.

De Jonge, C., Hopmans, E.C., Zell, C.I., Kim, J., Schouten, S. & Sinninghe Damsté, J.S. (2014). Occurrence and abundance of 6-methyl branched glycerol dialkyl glycerol tetraethers in soils: Implications for palaeoclimate reconstruction. *Geochimica et Cosmochimica Acta, 141*, 97-112.

Dugmore, A.J., Cook, G.T., Shore, J.S., Newton, A.J., Edwards, K.J. & Larsen, G. (1995). Radiocarbon dating tephra layers in Britain and Iceland. *Radiocarbon, 37*(2), 379-388.

Dugmore, A.J., Gísladóttir, G., Simpson, I.A. & Anthony Newton. (2009). Conceptual Models of 1200 years of Icelandic Soil Erosion Reconstructed Using Tephrochronology. *Journal of the North Atlantic, 2*, 1-18.

Eddudóttir, S.D., Erlendsson, E. & Gísladóttir, G. (2018). An Icelandic terrestrial record of North Atlantic cooling c. 8800-8100. *Quaternary Science Reviews, 197*, 246-256.

Eiríksson, J., Knudsen, K.L., Hafliðason, H. & Henriksen, P. (2000). Late-glacial and Holocene palaeoceanography of the North Icelandic shelf. *Journal of Quaternary Science, 15*, 23-42.

Florian, C.R., Miller, G.H., Fogel, M.L. Wolfe, A.P., Vinebrooke, R.D. & Geirsdóttir, Á. (2015). Algal pigments in Arctic lake sediments record biogeochemical changes due to Holocene climate variability and anthropogenic change. *Journal of Paleolimnology, 54*, 53-69.

Flowers, G.E., Björnsson, H., Geirsdóttir, Á., Miller, G.H. & Clarke, G.K.C. (2007). Glacier fluctuation and inferred climatology of Langjökull ice cap through the Little Ice Age. *Quaternary Science Reviews, 26*, 2337-2353.

Flowers, G.E., Björnsson, H., Geirsdóttir, Á., Miller, G.H., Black, J.L. et al. (2008). Holocene climate conditions and glacier variations in central Iceland from physical modelling and empirical evidence. *Quaternary Science Reviews, 27*, 797-813.

Geirsdóttir, Á., Miller, G.H., Axford, Y. & Ólafsdóttir, S. (2009b). Holocene and latest Pleistocene climate and glacier fluctuations in Iceland. *Quaternary Science Reviews, 28*, 2107-2118.

Geirsdóttir, Á., Miller, G.H., Larsen, D.J. & Ólafsdóttir, S. (2013). Abrupt Holocene climate transitions in the northern North Atlantic region recorded by synchronized lacustrine records in Iceland. *Quaternary Science Reviews, 70*, 48-62.

Geirsdóttir, Á., Miller, G.H., Wattrus, N.J., Björnsson, H. & Thors, K. (2008). Stabilization of glaciers terminating in closed water bodies: Evidence and broader implications. *Geophysical Research Letters, 35*, L17502, doi:10.1029/2008GL034432.

Geirsdóttir, Á., Miller, G.H., Thordarson, T. & Ólafsdóttir, K.B. (2009a). A 2000 year record of climate variations reconstructed from Haukadalsvatn, West Iceland. *Journal of Paleolimnology, 41*, 95-115.

Gísladóttir, F.Ó., Arnalds, Ó. & Gísladóttir, G. (2005). The effect of landscape and retreating glaciers on wind erosion in south Iceland. *Land Degradation & Development, 16*, 177-187.

Grönvold, K., Óskarsson, N., Johnsen, S.J., Clausen, H.B., Hammer, C.U., Bond, G. & Bard, E. (1995). Ash layers from Iceland in the Greenland GRIP ice core correlated with oceanic and land sediments. *Earth and Planetary Science Letters, 135*, 149-155.

Gudmundsdóttir, E.R., Eiríksson, J. & Larsen, G. (2011). Identification and definition of primary and reworked tephra in Late glacial and Holocene marine shelf sediments off North Iceland. *Journal of Quaternary Science, 26*(6), 589-602.

Gudmundsson, A. (2000). Dynamics of volcanic systems in Iceland: example of tectonism and volcanism at juxtaposed hot spot and mid-ocean ridge systems. *Annual Reviews Earth Planet Science, 28*, 107-140.

Guðnason, J. (2017). *Magma fragmentation and tephra dispersal in explosive eruptions: the 1991 and 1845 Hekla eruptions.* Ph.D. thesis. University of Iceland, Reykjavík.

Gunnarson, S. (2017). *Holocene climate and landscape evolution in the west central highlands, Iceland*. M.S. thesis. University of Iceland, Reykjavík.

Harning, D.J., Geirsdóttir, Á., Miller, G.H. & Anderson, L. (2016) Episodic expansion of Drangajökull, Vestifirðir, Iceland, over the last 3 ka culminating in its maximum dimension during the Little Ice Age. *Quaternary Science Reviews, 152*, 118-131.

Harning, D.J., Geirsdóttir, Á. & Miller, G.H. (2018b). Punctuated Holocene climate of Vestfirðir, Iceland, linked to internal/external variables and oceanographic conditions. *Quaternary Science Reviews, 189*, 31-42.

Harning, D.J., Thordarson, Th., Geirsdóttir, Á., Zalzal, K. & Miller, G.H. (2018a). Provenance, stratigraphy and chronology of Holocene tephra from Vestfirðir, Iceland. *Quaternary Geochronology, 46*, 59-76.

Heiri, O., Lotter, A.F. & Lemcke, G. (2001). Loss on ignition as a method for estimating organic and carbonate content in sediments: reproducibility and comparability of results. *Journal of Paleolimnology, 25*, 101-110.

Hopmans, E.C., Schouten, S. & Sinninghe Damsté, J.S. (2016). The effect of improved chromatography on GDGT-based palaeoproxies. *Organic Geochemistry, 93*, 1-6.

Hubbard, A., Sugden, D., Dugmore, A., Norðdahl, H. & Pétursson, H. (2006). A modelling insight into the Icelandic Last Glacial Maximum ice sheet. *Quaternary Science Reviews, 25*, 2283-2296.

Hurrell, J.W. (1995). Decadal trends in the North Atlantic Oscillation: Regional temperatures and precipitation. *Science, 269*, 676-679.

Jackson, M.G., Oskarsson, N., McManus, J.F., Oppo, D.W., Grönvold, K., Hart, S.R. & Sachs, J.P. (2005). Holocene loess deposition in Iceland: Evidence for millennial-scale atmosphere-ocean coupling in the North Atlantic. *Geology*, *33*(6), 509-512.

Janebo, M.H., Thordarson, T., Haughton, B.F., Bonadonna, C., Larsen, G. & Carey, R.J. (2016). Dispersal of key subplinian-Plinian tephras from Hekla volcano, Iceland: implications for eruption source parameters. *Bulletin of Volcanology*, *78*(66), doi:10.1007/s00445-016-1059-7.

Jennings, A.E., Thordarson, T., Zalzal, K., Stoner, J., Hayward, C., Geirsdóttir, Á. & Miller, G.H. (2014). Holocene tephra from Iceland and Alaska in SE Greenland shelf sediments. In: Austin, W.E.N., Abbott, P.M., Davies, S.M., Pearce, N.J.G. & Wastegård, S. (Eds.), *Marine Tephrochronology*, vol. 398 Geological Society, London, Special Publications.

Jóhannsdóttir, G.E. (2007). *Mid Holocene to late glacial tephrochronology in West Iceland as revealed in three lacustrine environments*. M.S. thesis. University of Iceland, Reykjavík.

Kaufman, D.S., Ager, T.A., Anderson, N.J., Anderson, P.M., Andrews, J.T., Bartlein, P.J., Brubaker, L.B., Coats, L.L., Cqynar, L.C., Duvall, M.L., Dyke, A.S., Edwards, M.E., Eisner, W.R., Gajewski, K., Geirsdóttir, Á., Hu, F.S., Jennings, A.E., Kaplan, M.R., Kerwin, M.W., Lozhkin, A.V., MacDonald, G.M., Miller, G.H., Mock, C.J., Oswald, W.W., Otto-Bliesner, B.L., Porinchu, D.F., Rühland, K., Smol, J.P., Steig, E.J. & Wolfe, B.B. (2004) Holocene thermal maximum in the western Arctic (0-180°W). *Quaternary Science Reviews, 23*, 529-560.

Knudsen, K.L. & Eiríksson, J. (2002). Application of tephrochronology to the timing and correlation of palaeoceanographic events recorded in Holocene and Late Glacial shelf sediments off North Iceland. *Marine Geology, 191*, 165-188.

Knudsen, M.F., Seidenkrantz, M.S., Jacobsen, B.H. & Kuijpers, A. (2011). Tracking the Atlantic Multidecadal Oscillation through the last 8000 years. *Nature Communications, 2*(178), doi:10.1038/ncomms1186.

Kuno, H. (1966). Lateral variation of basalt magma type across continental margins and island arcs. *Bulletin Volcanologique, 29*, 195-222.

Larsen, D.J., Miller, G.H., Geirsdóttir, Á. & Thordarson, T. (2011). A 3000-year varved record of glacier activity and climate change from the proglacial lake Hvítárvatn, Iceland. *Quaternary Science Reviews, 30*, 2715-2731.

Larsen, D.J., Miller, G.H., Geirsdóttir, Á. & Ólafsdóttir, S. (2012). Non-linear Holocene climate evolution in the North Atlantic: a high-resolution, multi-proxy record of glacier activity and environmental change from Hvítárvatn, central Iceland. *Quaternary Science Reviews, 39*, 14-25.

Larsen, D.J., Miller, G.H. & Geirsdóttir, Á. (2013). Asynchronous Little Ice Age glacier fluctuations in Iceland and European Alps linked to shifts in subpolar North Atlantic circulation. *Earth and Planetary Science Letters, 380*, 52-59.

Larsen, G., Dugmore, A. & Newton, A. (1999). Geochemistry of historical-age silicic tephras in Iceland. *The Holocene, 9*(4), 463-471.

Larsen, G. & Eiríksson, J. (2008). Holocene tephra archives and tephrochronology in Iceland – a brief overview. *Jökull, 58*, 229-250.

Larsen, G., Eiríksson, J., Knudsen, K.L. & Heinemeier, J. (2002). Correlation of late Holocene terrestrial and marine tephra markers, north Iceland: implications for reservoir age changes. *Polar Research, 21*(2), 283-290.

Larsen, G. & Thorarinsson, S. (1977). H4 and other acid Hekla layers. *Jökull, 27*, 29-46.

MacDonald, G.A. & Katsura, T. (1964). Chemical composition of Hawaiian lavas. *Journal of Petrology, 5*, 82-133.

Mangerud, J., Furnes, H. & Jóhansen, J. (1986). A 9000 year ash bed on the Faroe Islands. *Quaternary Research, 26*, 262-265.

Miller, G.H., Geirsdóttir, Á., Zhong, Y., Larsen, D.J., Otto-Bliesner, B.L., Holland, M.M., Bailey, D.A., Refsnider, K.A., Lehman, S.J., Southon, J.R., Anderson, C., Björnsson, H. & Thordarson, T. (2012). Abrupt onset of the Little Ice Age triggered by volcanism and sustained by sea-ice/ocean feedbacks. *Geophysical Research Letters, 39*, L02708, doi:10.1029/2011GL050168.

Massé, G., Rowland, S.J., Sicre, M., Jacob, J., Jansen, E. & Belt, S.T. (2008). Abrupt climate changes for Iceland during the last millennium: Evidence from high resolution sea ice reconstructions. *Earth and Planetary Science Letters, 269*, 565-569.

Naafs, B.D.A., Gallego-Sala, A.V., Inglis, G.N. & Pancost, R.D. (2017). Refining the global branched glycerol dialkyl glycerol tetraether (brGDGT) soil temperature calibration. *Organic Geochemistry, 106*, 48-56.

Nichols, G. (2009). *Sedimentology and Stratigraphy*. Chichester: Wiley-Blackwell.

Norðdahl, H. & Ingólfsson, Ó. (2015). Collapse of the Icelandic ice sheet controlled by sea-level rise? *Arktos: The Journal of Arctic Geosciences*, doi:10.1007/s41063-015-0020-x.

Oppo, D.W., McManus, J.F., & Cullen, J.L. (2003). Palaeo-oceanography: deepwater variability in the Holocene epoch. *Nature, 422*, 277-278.

Óladóttir, B.A., Larsen, G. & Sigmarsson, O. (2011). Holocene volcanic activity at Grímsvötn, Bárdarbunga and Kverkfjöll subglacial centres beneath Vatnajökull, Iceland. *Bulletin of Volcanology*, doi:10.1007/s00445-011-0461-4.

Óladóttir, B.A., Sigmarsson, O., Larsen, G. & Thordarson, T. (2008). Katla volcano, Iceland: magma composition, dynamics and eruption frequency as recorded by Holocene tephra layers. *Bulletin of Volcanology, 70*, 475-493.

Óskarsson, H., Arnalds, Ó., Gudmundsson, J. & Gudbergsson, G. (2004). Organic carbon in Icelandic Andosols: geographical variation and impact of erosion. *Catena, 56*, 225-238.

Peterse, F., van der Meer, J., Schouten, S., Weijers, J.W.H., Fierer, N., Jackson, R.B., Kim, J. & Sinninghe Damsté, J.S. (2012). Revised calibration of the MBT CBT paleotemperature proxy based on branced tetraether membrane lipids in surface soils. *Geochimica et Cosmochimica Acta, 96*, 215-229.

Reed, S.J.B. (2005). *Electron Microprobe Analysis and Scanning Electron Microscopy in Geology*. United Kingdom: Cambridge University Press.

Renssen, H., Seppä, H., Crosta, X., Goosse, H. & Roche, D.M. (2012). Global characterization of the Holocene Thermal Maximum. *Quaternary Science Reviews, 48*, 7-19.

Renssen, H., Seppä, H., Heiri, O., Roche, D.M., Goosse, H. & Fichefet, T. (2009). The spatial and temporal complexity of the Holocene thermal maximum. *Nature Geoscience, 2*, doi:10.1038/NGEO513.

Saunders, A.D., Fitton, J.G., Kerr, A.C., Norry, M.J. & Kent, R.W. (1997). The North Atlantic Igneous Province. In: Mahoney, J.J. & Coffin, M.F. (Eds.), *Large Igneous Provinces: Continental, Oceanic, and Planetary Flood Volcanism*. Geophysical Monograph Series, Washington, DC, pp. 45-93.

Sinton, J., Grönvold, K. & Sæmundsson, K. (2005). Postglacial eruptive history of the Western Volcanic Zone, Iceland. *Geochemistry, Geophysics, Geosystems, 6*(12), Q12009, doi:10.1029/2005GC001021.

Syvitsky, J.P., Jenning, A.E. & Andrews, J.T. (1999). High-resolution seismic evidence for multiple glaciation across the southwest Iceland shelf. *Arctic and Alpine Research, 31*(1), 50-57.

Sæmundsson, K. (1979). Outline of the geology of Iceland. *Jökull, 29*, 7-28.

Thorarinsson, S. (1975). *Katla og annáll Kötlugosa*. Reykjavík: Ferðafélag Íslands.

Thordarson, T. (2014). The widespread ~10ka Saksunarvatn tephra is not a product single eruption. In: AGU Fall Meeting Abstracts.

Thordarson, T. & Höskuldsson, Á. (2008). Postglacial volcanism in Iceland. *Jökull, 58*, 197-228.

Thordarson, T. & Larsen, G. (2007). Volcanism in Iceland in historical time: Volcano types, eruption styles and eruptive history. *Journal of Geodynamics, 43*, 118-152.

Thordarson, T. & Self, S. (1998). The Roza Member, Columbia River Basalt Group: A gigantic pahoehoe lava flow field formed by endogenous processes? *Journal of Geophysical Research, 103*(B11), 27411-27445.

Thordarson, T., Self, S., Miller, D.J., Larsen, G. & Vilmundardóttir, E.G. (2003). Sulphur release from flood lava eruptions in the Veiðivötn, Grímsvötn and Katla volcanic systems, Iceland. In: Oppenheimer, C., Pyle, D.M. & Barclay, J. (Eds.), *Volcanic Degassing*, vol. 213. Geological Society, London, pp. 103-121. Special Publications.

Thornalley, D.J.R., Elderfield, H. & McCave, N. (2009). Holocene oscillations in temperature and salinity of the surface subpolar North Atlantic. *Nature, 457*, 711-714.

Tierney, J.E. (2012). GDGT thermometry: lipid tools for reconstructing paleotemperatures. In: Ivany, L.C. & Huber, B.T. (Eds.), *Reconstructing Earth's Deep-Time Climate – The State of the Art in 2012, Paleontological Society Short Course*, vol. 18. The Paleontological Society Papers, pp. 115-131.

Tómasson, H. (1993). Jökulstífluð vötn á Kili og hamfarahlaup í Hvítá í Árnessýslu. *Náttúrufæðingurinn, 62*, 77-98.

Vink, G.E. (1984). A hotspot model for Iceland and the Vøring Plateau. *Journal of Geophysical Research, 89*, 9949-9959.

Wanner, H., Beer, J., Bütikofer, J., Crowley, T.J., Cubasch, U., Flückiger, J., Goosse, H., Grosjean, M., Joos, F., Kaplan, J.O., Küttel, M., Müller, S.A., Prentice, I.C., Solomina, O., Stocker, T.F., Tarasov, P., Wagner, M. & Widmann, M. (2008). Mid- to Late Holocene climate change: an overview. *Quaternary Science Reviews, 27*, 1791-1828.

Wanner, H., Solomina, O., Grosjean, M., Ritz, S.P. & Jetel, M. (2011). Structure and origin of Holocene cold events. *Quaternary Science Reviews, 30*, 3109-3123.

Weijers, J.W.H., Schouten, S., van der Donker, J.C., Hopmans, E.C. & Sinninghe Damsté, J.S. (2007). Environmental controls on bacterial tetraether membrane lipid distribution in soils. *Geochimica et Cosmochimica Acta, 71*, 703-713.

White, J.D.L. & Houghton, B.F. (2006). Primary volaniclastic rocks. *Geology, 34*(8), 677-680.

A.1 Description of soil profiles

A.1.1 Site 1, profile 1

238-214 cm: Tephra layer, grayish with some deformed structures.

214-206 cm: Brown sand and silt, showing some lamination.

206-192 cm: Fine to coarse grained sand with coarser material and rock fragments 1 mm to 2 cm in size.

192-188 cm: Very fine grained silt and clay, light colored organic material.

188-177 cm: Rather fine grained silt with some lamination.

177-173 cm: Variable thickness (1-4 cm), coarse sand and rock fragment around 0,5 cm in size.

173-172 cm: Brown clay and silt.

172-168,5 cm: Brown sand with 1 mm sized rock fragments.

168,5-165,5 cm: Variable thickness (1-3 cm), clay and silt with light brown color.

165,5-158,5 cm: Brown silt and sand.

158,5-151,5 cm: Coarse grained sand with darker brown color.

151,5-140,5 cm: Light brown colored silt and sand, and a 0,5-1 cm thick light and fine grained tephra layer in the middle part.

140,5-120,5 cm: Coarse to rather coarse grained sand with dark brown color, showing some lamination and rock fragments around 1 mm in size. At the upper boundary is a 1-2 cm thick silt lens.

120,5-114,5 cm: Silt and fine grained sand with light brown to brown color and some lamination.

114,5-74,5 cm: Mostly coarse grained sand with some finer grained sand and rock fragments in between, in the uppermost part is some clay.

74,5-66,5 cm: Tephra layer, light colored and very fine grained. The boundaries are disrupted so the layer is contaminated at the bottom and top boundaries.

A1.2 Site 1, profile 2

327-277 cm: Brown and dark brown color, clay and fine grained sand with coarser sand in between. This part does not really show laminations but rather some irregular changes through it. At the upper boundary is a 12 cm thick sand lens with rock fragments. At the bottom boundary is a 1-3 cm thick black disrupted tephra layer. Around 5 cm above is a 1-3 cm thick gray tephra layer, which is also disrupted and shows signs of cryoturbation. Above the second tephra layer is another gray tephra layer 14 cm higher in the soil, which is 0,3-1 cm and not as clear.

277-253 cm: Coarse grained sand and clay with some rock fragments at the bottom boundary, above the sand and clay mixture is mostly clay. The clay part has some laminations. This part has a brownish color with some darker brown color in between.

253-244 cm: Tephra layer with a light color. The bottom 2-3 cm contain fine grained sand and silt while the upper 6-7 cm have fine grained silt.

244-240 cm: The same material as in the organic rich layer below the light colored tephra layer, a clay mix with some lamination.

240-239,6 cm: Tephra layer with a dark gray color.

239,6-194,6 cm: The bottom consists of coarse grained sand with a dark brown color and some rock fragments. Above the color changes to brown with a mix of sand and clay showing some lamination, in between are some darker brown silt lenses.

194,6-194 cm: Tephra layer with a brown-gray color and rather coarse grained sand.

194-180 cm: The bottom consists mostly of clay, above that is a 3 cm thick sand lens with coarse grained sand and rock fragments around 1 cm in size. At the top is a mix of silt and clay.

180-175 cm: Coarse grained sand with a dark brown or black color.

175-138 cm: Brown colored coarse grained sand and fine grained silty clay layers alternating mixed with some rock fragments around 0,5 cm in size. The fine layers are around 1 cm thick and the coarse layers are 1-7 cm thick.

138-130 cm: Tephra layer with a light color and fined grained sand.

130-114 cm: Organic rich fine grained sand of variable thickness (11-16 cm) with some laminations.

114-101 cm: Tephra layer of variable thickness (11-13 cm), with a light color and coarse grained. The grains are around 1 mm in size.

101-92 cm: A mix of clay and silt with a light brown color.

92-86 cm: Tephra layer of variable thickness (2-6 cm), with a dark color and coarse grained. The grain size is 2-3 mm. The layer is disrupted and affected by cryoturbation.

86-57 cm: Dark brown colored layer of a mix of clay and sand.

57-49 cm: Tephra layer of variable thickness (0,5-8 cm), black colored and very disrupted due to cryoturbation.

49-43 cm: Variable thickness (2-6 cm), this part is similar to the organic rich material below the tephra layer. With a mix of clay and sand with a thin line of rock fragments, 0,3-0,5 cm in size.

43-35 cm: Tephra layer of variable thickness (2-8 cm), with a light gray color and affected by cryoturbation.

35-25 cm: Sand and clay, brown color and some darker brown in between.

25-23 cm: Tephra (1-2 cm) dark gray or black colored with rather fine grained sand.

23-13 cm: Brown colored silt and sand. In the upper part are some plant remains.

13-12 cm: Tephra layer (0,5-1 cm) black colored.

12-0 cm: (10-12 cm) This is mostly plant remains and roots and is the surface layer of this section.

A1.3 Site 2, profile 1

326-310 cm: The bottom 3-4 cm is made up of coarse grained sand and rock fragments with a dark brown color. The upper 12-13 cm has a brown color and consist of fine grained sand, silt and some clay.

310-303 cm: Tephra layer of variable thickness (4-7 cm), with a light color and fine grained sand.

303-282 cm: This part consists of fine grained sand and has color changes through it, at the bottom the color is dark brown, brown in the middle part and dark brown at the upper boundary. The upper part also contains a 2-6 cm thick light colored tephra layer. The tephra layer is disrupted and has a fine grained sand part and coarse grained sand part.

282-274 cm: A mixture of light colored and coarse grained redeposited sand are mixed with this part, it is also disrupted and has a variable thickness.

274-268 cm: Fine grained sand and silt, with a brown color and some darker color in between. This part has some light colored redeposited grains from the part below.

268-251 cm: Fine grained sand, silt and some clay. The color is brown and this part has little to no color change through it.

251-241 cm: (1-10 cm) Tephra layer with a black color and a variable thickness due to cryoturbation.

241-238 cm: Fine grained sand and some clay, this part is similar to the organic rich material below the black colored tephra layer.

238-234 cm: (0,5-4 cm) Tephra layer with a gray color. The layer has a variable thickness and shows sign of cryoturbation.

234-225 cm: Fine grained sand and silt of variable thickness (3-9 cm), with no color changes or structures.

225-223 cm: Tephra layer (0,5-2 cm) with a light color and coarse grained sand.

223-215 cm: Fine grained sand and clay with a brown color.

215-214 cm: Dark gray colored and rather coarse grained sand.

214-204 cm: Fine grained sand, silt and some clay. This part shows faint laminations, with dark and light brown layers alternating.

204-203 cm: Tephra layer with a dark gray color and rather coarse grained sand.

203-161 cm: Fine and coarse grained sand layers alternating. This part is coarser than the organic rich matter below the dark gray colored tephra layer.

161-160 cm: Tephra layer with a black color and rather fine grained sand.

160-50 cm: Mostly coarse grained sand though with some laminations, brown and dark brown layers alternating. Fine grained sand and some redeposited grains are found at the bottom boundary of the layer.

50-0 cm: Coarse and fine grained sand layers alternating, although the coarser layers are thicker and the fine layers are thinner and fewer.

A1.4 Site 2, profile 2

305,5-289,5 cm: Mostly clay with a brown color.

289,5-289 cm: Tephra layer with a black color and rather fine grained sand.

289-287 cm: Brown colored fine grained sand and clay.

287-282 cm: Variable thickness (1-5 cm), coarse dark and light colored redeposited grains.

282-280 cm: Fine grained sand and clay, similar to the organic rich material below the redeposited grains.

280-275 cm: (1-5 cm) Tephra layer with a very dark color and coarse grained sand. The layer is disrupted and has a variable thickness.

275-239 cm: The bottom boundary of this part consists of fine grained sand and clay, above that are alternating layers with coarser grained sand with dark and light colored grains, and finer grained sand. The coarser layers are thicker than the finer.

239-230 cm: Tephra layer with coarse grained sand. At the bottom the layer is dark colored, in the middle it is light colored and at the top it is dark colored again. The coarsest grains are in the light colored middle part.

230-227 cm: Rather coarse grained sand and some fine grained sand, this part also contains redeposited grains which are coarser grained.

227-224 cm: Dark gray fine grained sand with lighter colored coarser grained redeposited sand.

224-222 cm: Fine grained sand and silt with a brown color.

222-218 cm: Rather fine grained sand with a dark color, this part also contains coarser redeposited grains with a lighter color.

218-216 cm: Brown colored fine grained sand, silt and some clay.

216-213 cm: Fine grained sand with a dark color and some lighter colored redeposited grains.

213-178 cm: At the bottom boundary is a 3 cm thick sand layer. Above that are alternating coarse and fine grained layers, showing some laminations. The fine grained layers are made up of fine grained sand with some clay. The coarser layers have a darker color and often have small rock fragments around 0,2 cm in size.

178-175 cm: This part is not very visible but is made up of rather coarse grained sand with a gray color.

175-105 cm: This part shows laminations where coarse and fine grained sand/silt layers are alternating. The coarser layers are darker in color and mostly made up of coarse grained sand and small rock fragments. The finer layers contain fine grained sand and some silt. The coarser layers are thicker than the finer layers.

105-103 cm: Redeposited grains with a light color and coarse.

103-99 cm: Dark brown coarse and fine grained sand.

99-97 cm: Coarse grained sand with a dark color. This part also contains some lighter colored redeposited grains.

97-94,5 cm: Fine grained sand, this part is not as coarse as the organic rich material below.

94,5-93 cm: Light colored and coarse grained redeposited sand.

93-0 cm: Coarse and fine layers containing sand, showing laminations. The layers are rather thin, around 0.5 cm, but do seem to get thicker upwards.

A1.5 Site 3, profile 1

395-386 cm: Mostly clay with a little bit of silt and fine grained sand.

386-384 cm: Tephra layer with a black color and fine grained sand.

384-374 cm: Rather homogeneous brown colored fine grained sand and clay.

374-364 cm: Tephra layer with a gray color. The layer shows some changes in grain size. At the bottom there is a mix of coarse and fine grained sand, then finer grained sand. Above that the layer has coarser grained sand.

364-351 cm: At the bottom boundary this part contains brown fine grained sand and some clay. The layer has more clay above and shows some change in color.

351-349 cm: Light colored and coarse grained redeposited material.

349-341 cm: Fine grained sand and clay, similar to the soil below the redeposited material. This part also contains some light colored redeposited grains.

341-339 cm: Tephra layer with a dark gray color and the grain size is rather coarse to fine grained sand, with a bit larger grains.

339-320 cm: This part shows some laminations. At the bottom boundary the layer contains fine grained sand and clay, above that is coarse grained sand with some bigger redeposited grains. The coarser part of the layer has a darker brown color compared to the finer part. Fine sand and clay appear again at the upper boundary of the layer.

320-310 cm: Organic rich layer with a number of light colored redeposited coarse grained sand. The bottom 2 cm is the redeposited grains, the next 3 cm is organic rich fine grained sand and some clay. The redeposited grains are found within the organic rich part of this layer. Then the redeposited grains and organic rich material alternate up to the upper boundary, where the light colored material is 2,5 cm thick.

310-307 cm: Laminations shown with alternating brown and dark brown colors. The layer is made up of fine grained sand with some silt and clay.

307-294 cm: Coarse grained redeposited sand dominates this part. The bottom part is 7 cm thick with a light color, the middle part is dark with a thickness of 2 cm, and the upper part is 4 cm thick with a light color.

294-278 cm: The majority of this layer is made up of clay and fine grained sand. There is some lamination with thin coarse layers.

278-276 cm: Sand with a brown color which contains 1 mm sized light colored redeposited grains.

276-272 cm: Brown colored fine grained sand and some clay which also contains 1 mm sized redeposited grains, this part has a larger content of redeposited grains compared to the part below.

272-271,5 cm: Tephra layer with a black color and rather fine grained sand. This part is also quite mixed with organic rich material.

271,5-266,5 cm: Fine grained sand and clay with 1 mm sized light colored redeposited grains. The color of this part is brown, with a bit lighter brown color towards the upper boundary.

266,5-265 cm: Sand layer with a gray-brown color and rather fine grained sand. The layer also has some light colored redeposited grains.

265-263 cm: Brown colored fine grained sand, silt and some clay.

263-260 cm: Coarse grained sand of a light brown color, it also consists of some redeposited material.

260-256 cm: Fine grained sand and clay, with a brown color and a slightly lighter color at the upper boundary.

256-255 cm: Tephra layer with a black color and coarse grained sand.

255-253 cm: Fine grained sand and clay, this part also contains ca. 1 mm sized redeposited grains with a light color. The upper boundary is a bit irregular.

253-252 cm: Sand with a gray-brown color and coarser redeposited light colored grains.

252-230 cm: The bottom 2 cm contain fine grained sand and silt. The next 17 cm above are made up of dark colored coarse grained sand with thin light colored layers. Above that is a 1 cm thick brown and rather fine grained sand with some redeposited grains. The top 3 cm is a sand layer containing fine to rather coarse grained sand, that part also has some 1 mm sized redeposited grains with a light color.

230-210 cm: Brown oranic rich layers and coarse dark sand layers alternate throughout this part. The organic rich layers are made up of fine sand with some light redeposited grains. The sand layers also have redeposited grains and are thicker compared to the organic richer layers.

210-170 cm: Dominantly coarse grained sand layers with light colored redeposited grains. Alternating with the sand layers are thinner organic rich layers containing fine to rather coarse sand.

170-48 cm: Dark and light colored coarse grained sand layers, and organic rich layers containing fine grained sand and some clay. Light colored redeposited grains can be found in most of the layers. The upper 74 cm are dominated by the sand layers. The sand layers are reduced, especially the light colored layers.

48-46 cm: Tephra layer with a dark gray color and rather fine grained sand. This layer is mixed with light colored redeposited grains.

46-33 cm: Fine grained sand with some redeposited light colored grains. The layer is brown with thinner laminae of both darker and light colored sand layers.

33-32 cm: Black colored tephra with fine to coarse grained sand. Light colored tephra grains are found at the bottom boundary.

32-0 cm: Fine grained sand with some larger redeposited grains. The color is brown with occasional thin darker layers. The upper boundary is very loose with roots and plant remains.

A.2 Plots and tephra geochemical data

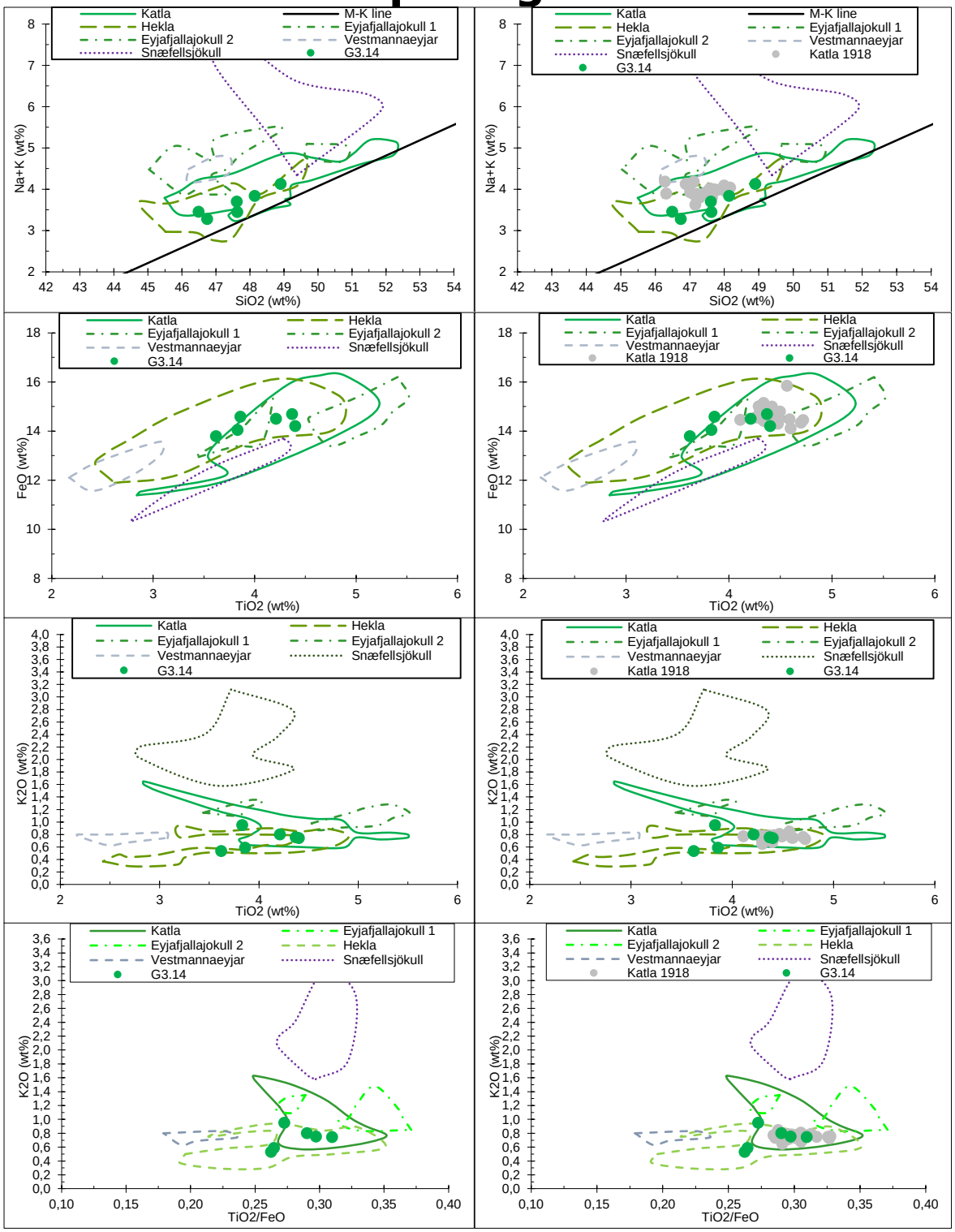

Figure 51. Geochemical discrimination plots for alkalic basalt sample G3.14, which was identified as Katla 1918. The graphs on the right side contain comparison data from Óladóttir et al. (2008) and Thorvaldur Thordarson (unpublished data 2018).

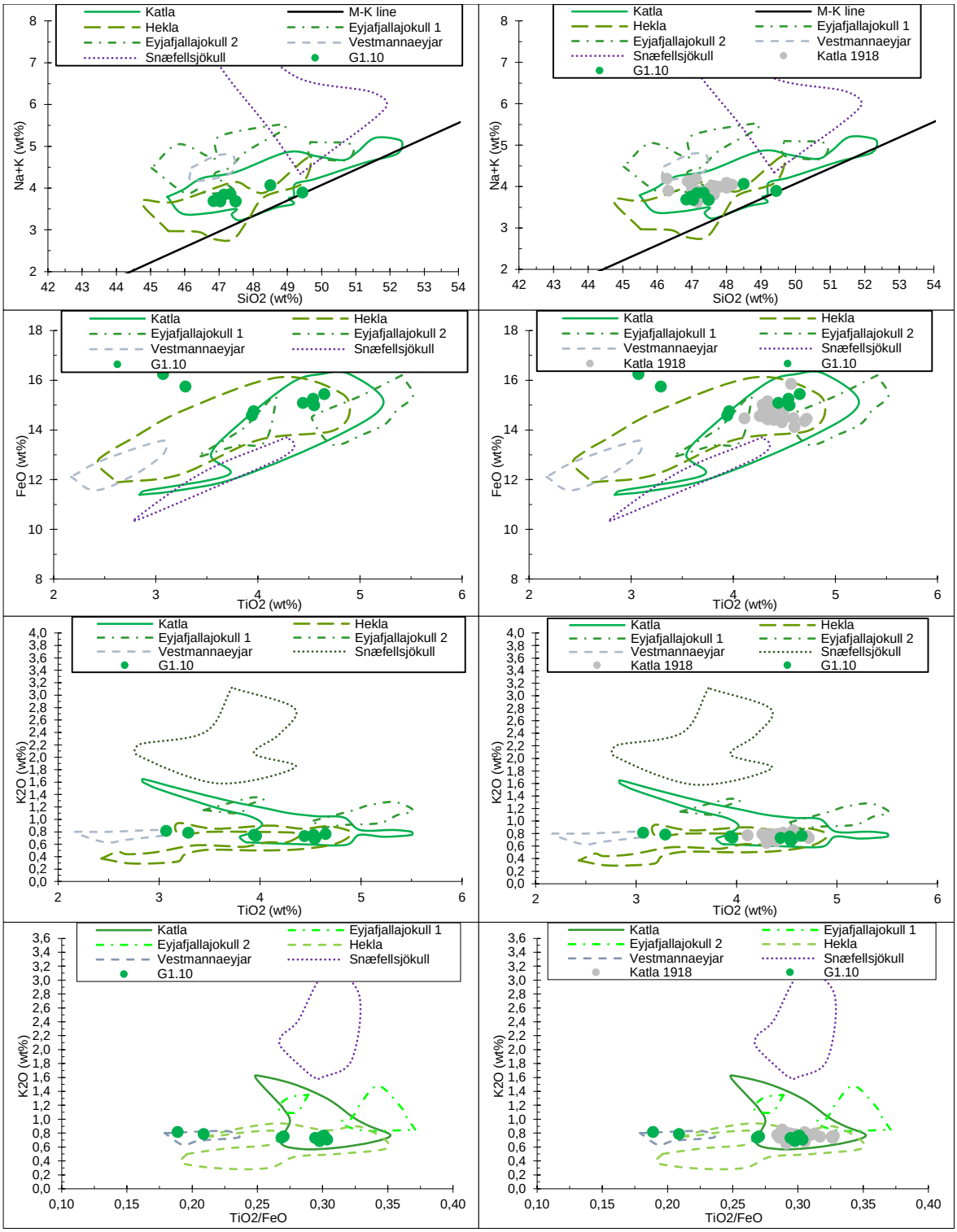

Figure 52. Geochemical discrimination plots used for sample G1.10, which is alkalic basalt and was identified as Katla 1918 using comparison data from Óladóttir et al. (2008) and Thorvaldur Thordarson (unpublished data 2018) shown in graphs on the right side.

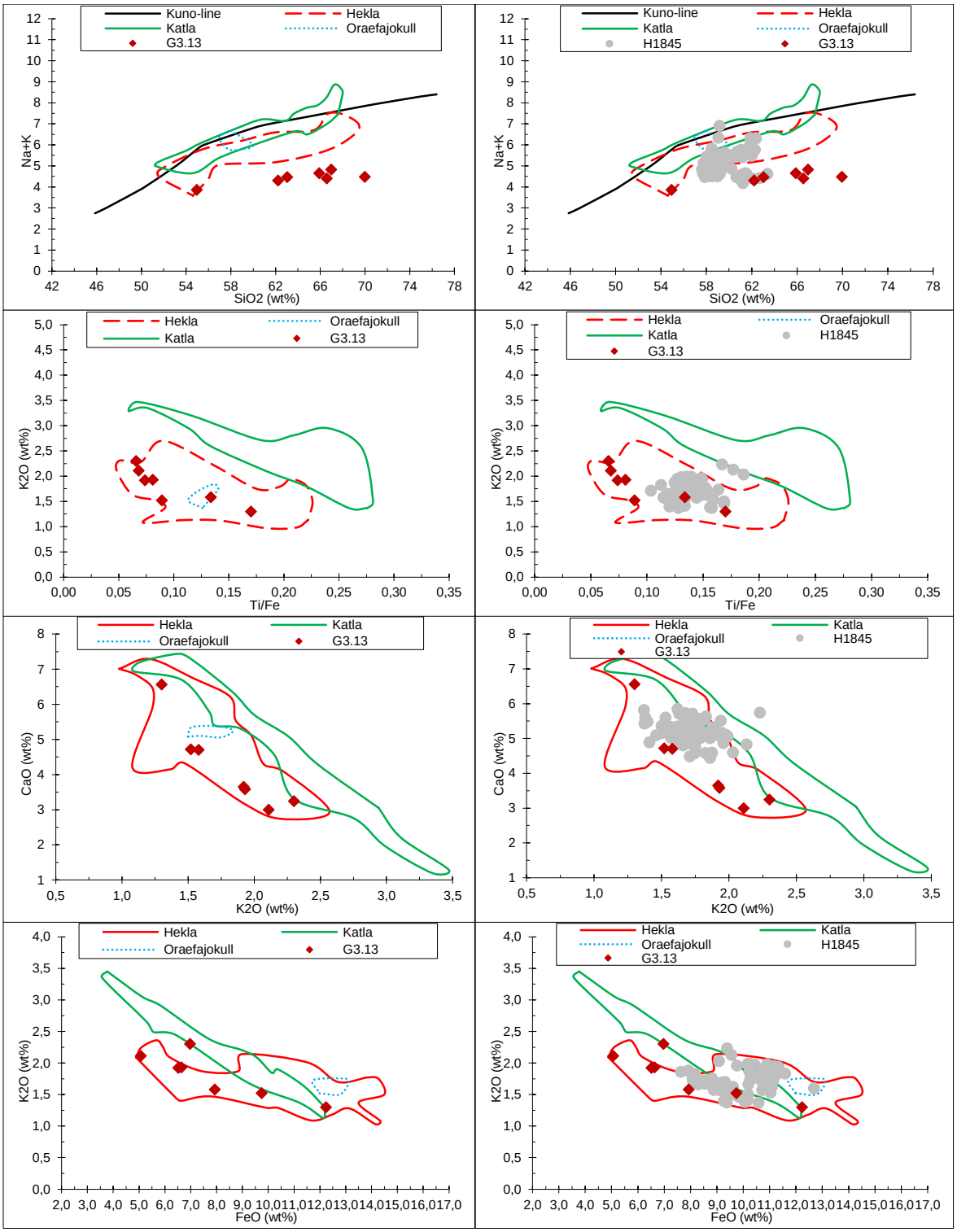

Figure 53. Geochemical discrimination plots used for the andesite part of sample G3.13. This sample was identified as Hekla 1845 using comparison data from Thordarson et al. (1998) and Guðnason (2017), shown on the right side.

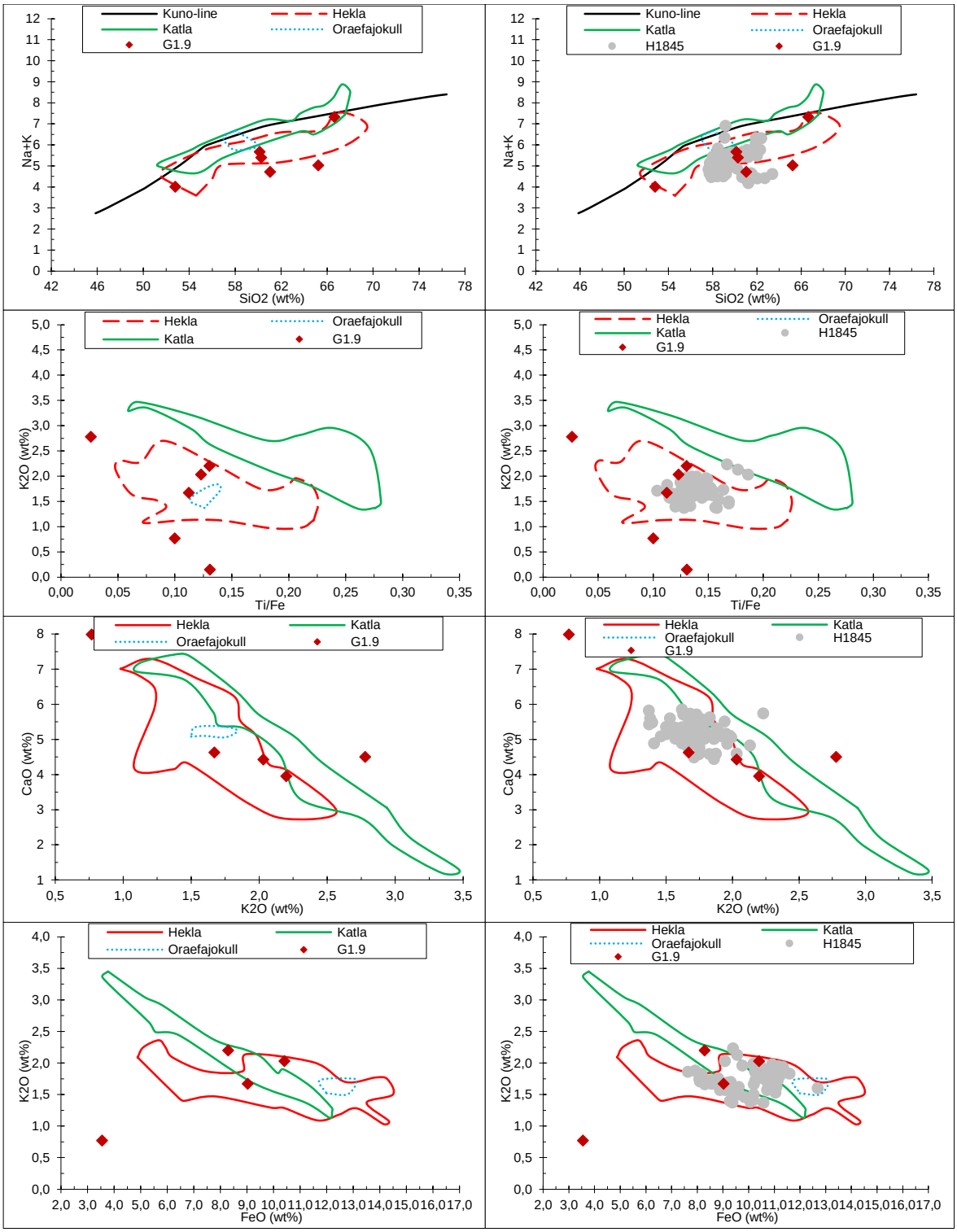

Figure 54. Sample G1.9 shown in the geochemical discrimination plots used to identify the andesite part of the sample. The sample was identified as Hekla 1845, by using comparison data from Thordarson et al. (1998) and Guðnason (2017) displayed in the graphs on the right side.

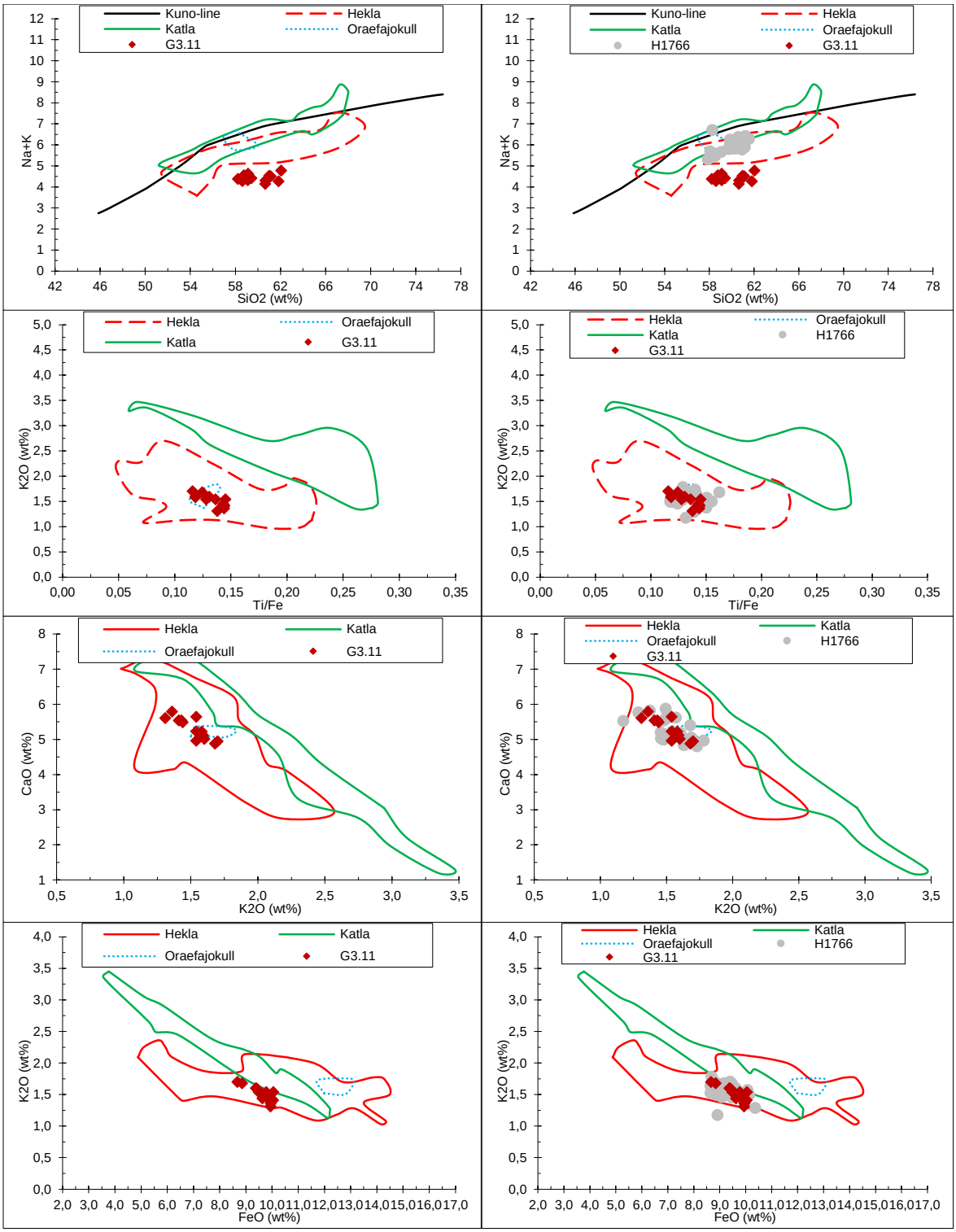

Figure 55. Geochemical discrimination plots for the andesite sample G3.11. By using comparison data from Hvítárvatn (Thorvaldur Thordarson, unpublished data 2018), this sample was identified as Hekla 1766.

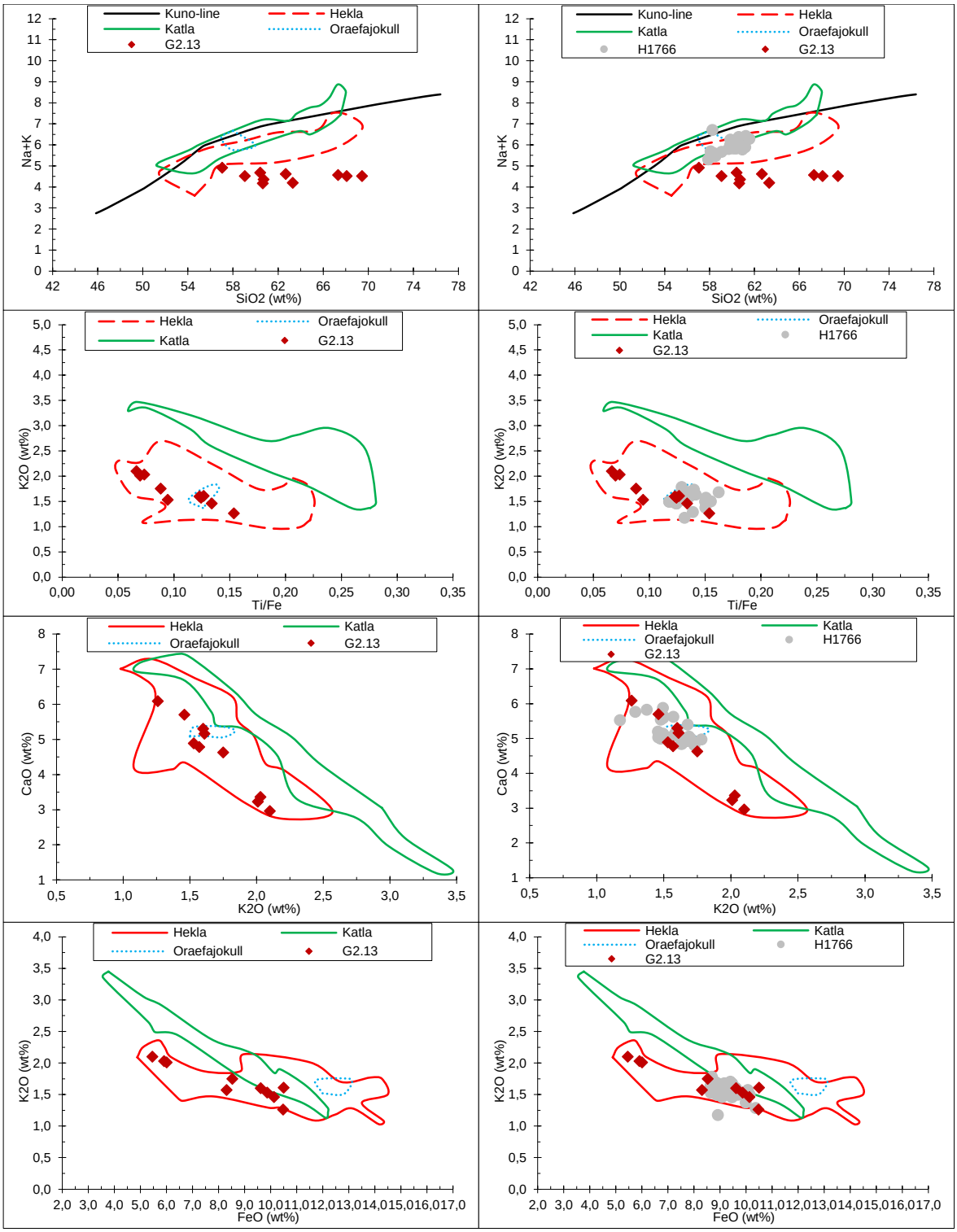

Figure 56. Sample G2.13 shown in geochemical discrimination plots, which was identified as Hekla 1766 by using comparison data from Hvítárvatn (Thorvaldur Thordarson, unpublished data 2018).

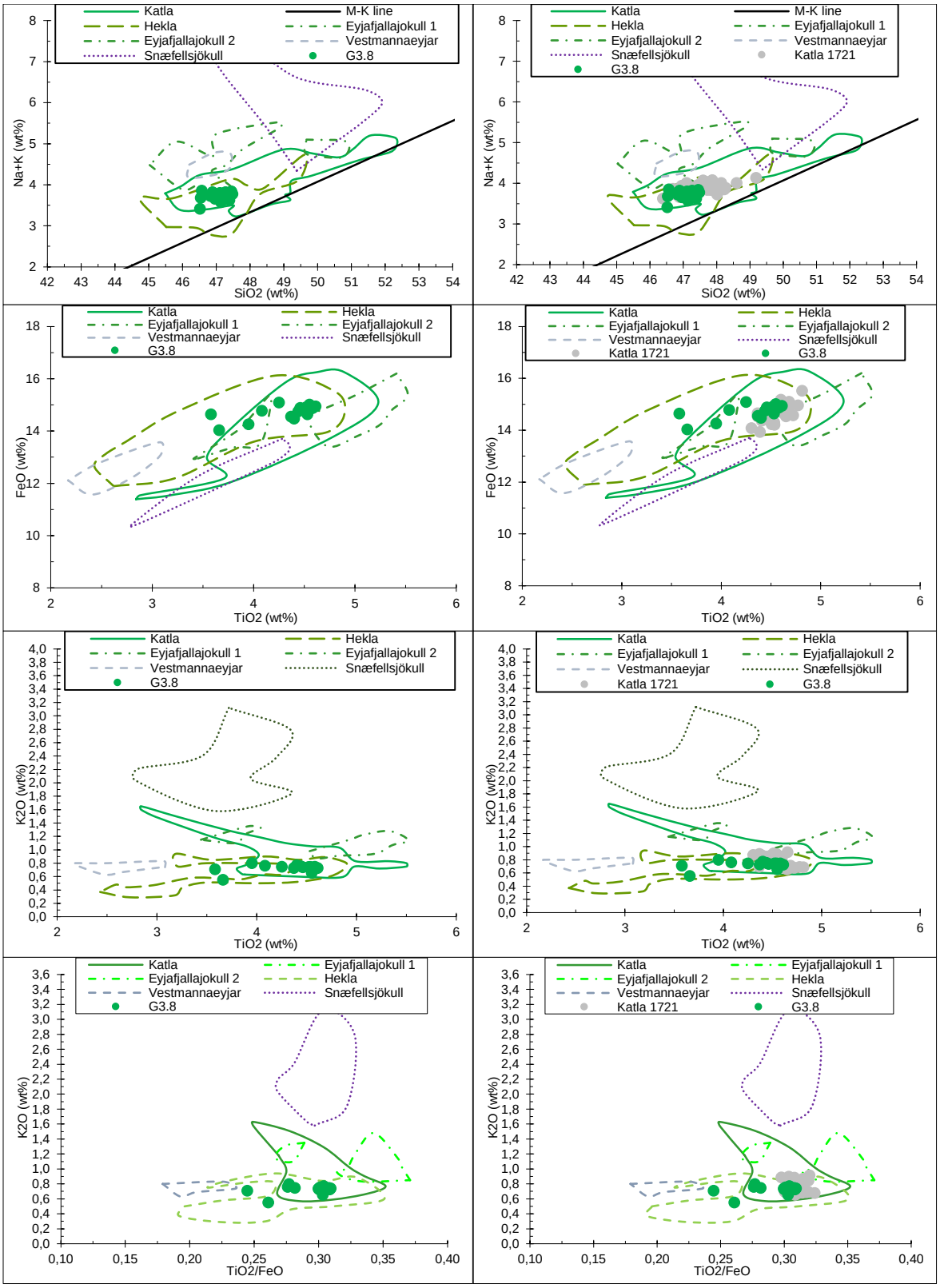

Figure 57. Alkalic basalt sample G3.8 and the geochemical discrimination plots used to identify this tephra as Katla 1721. Comparison data from Hvítárvatn is displayed in the plots on the right side (Thorvaldur Thordarson, unpublished data 2018).

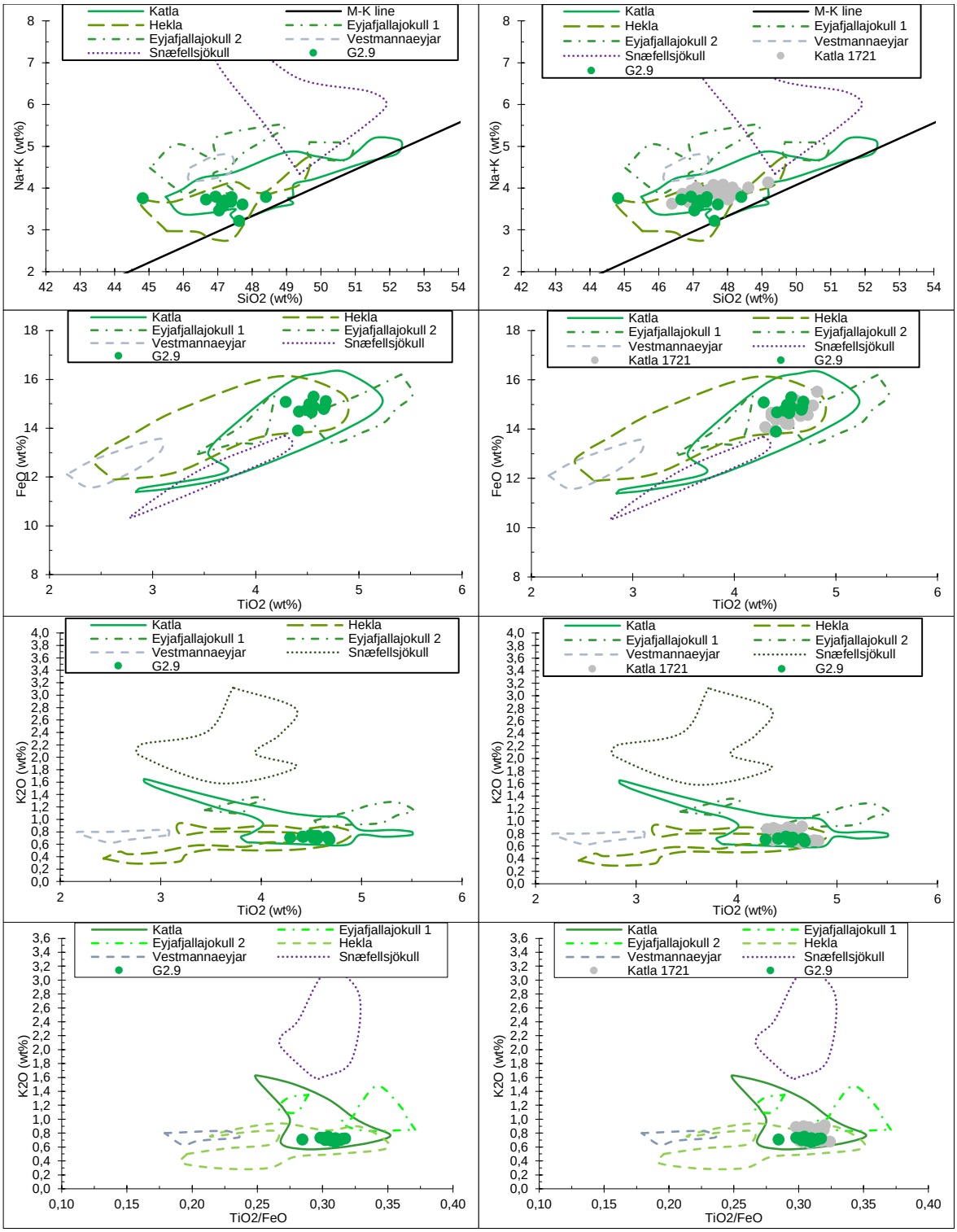

Figure 58. Sample G2.9 which was identified as Katla 1721 with the geochemical discrimination plots. Comparison data from Hvítárvatn is displayed in the plots on the right side (Thorvaldur Thordarson, unpublished data 2018).

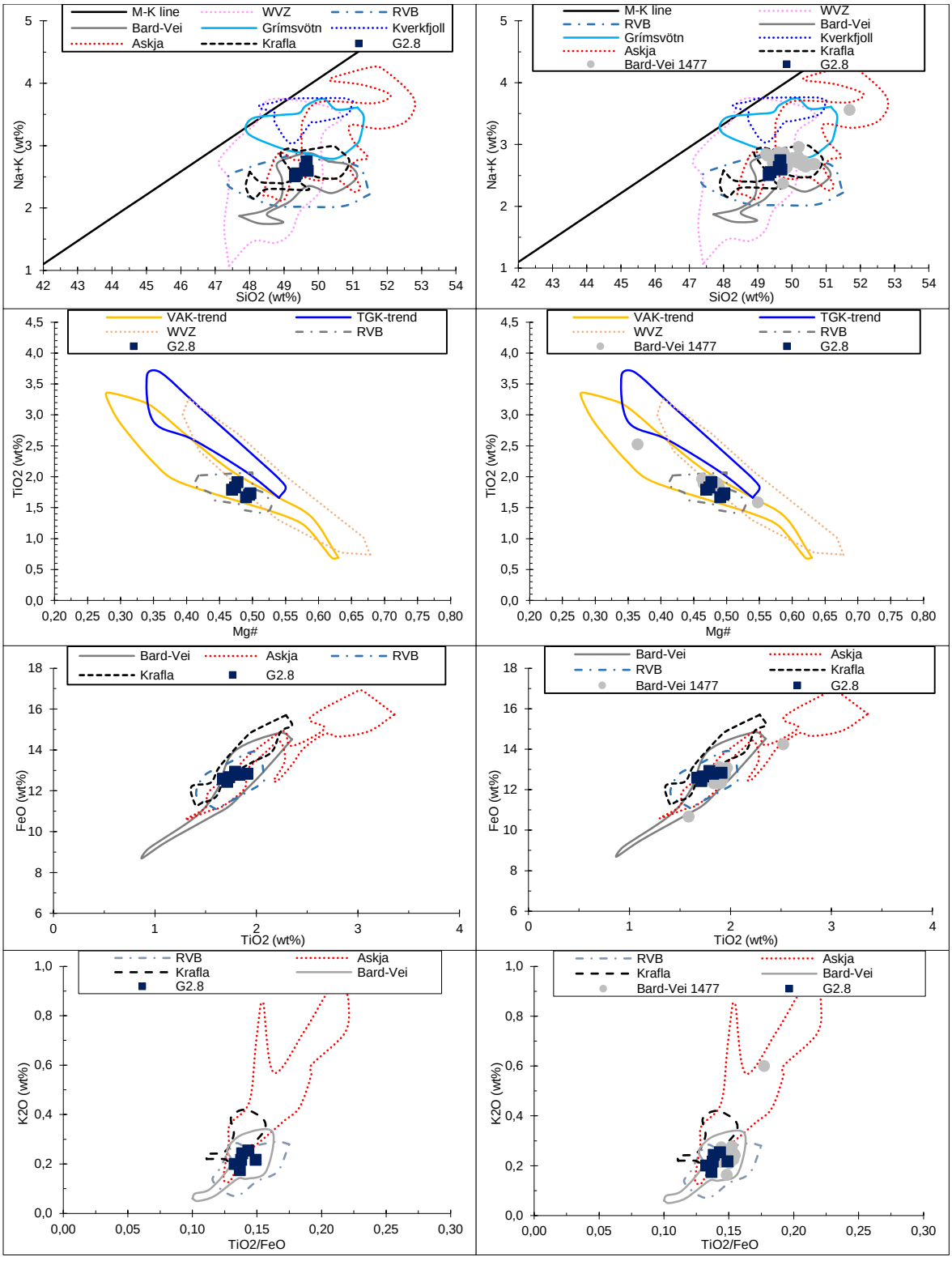

Figure 59. Tholeiitic basalt sample G2.8 and the geochemical discrimination plots used to identify it. By using the comparison data from Hvítárvatn (Thorvaldur Thordarson, unpublished data 2018) the tephra was identified as Bárðarbunga-Veiðivötn 1477.

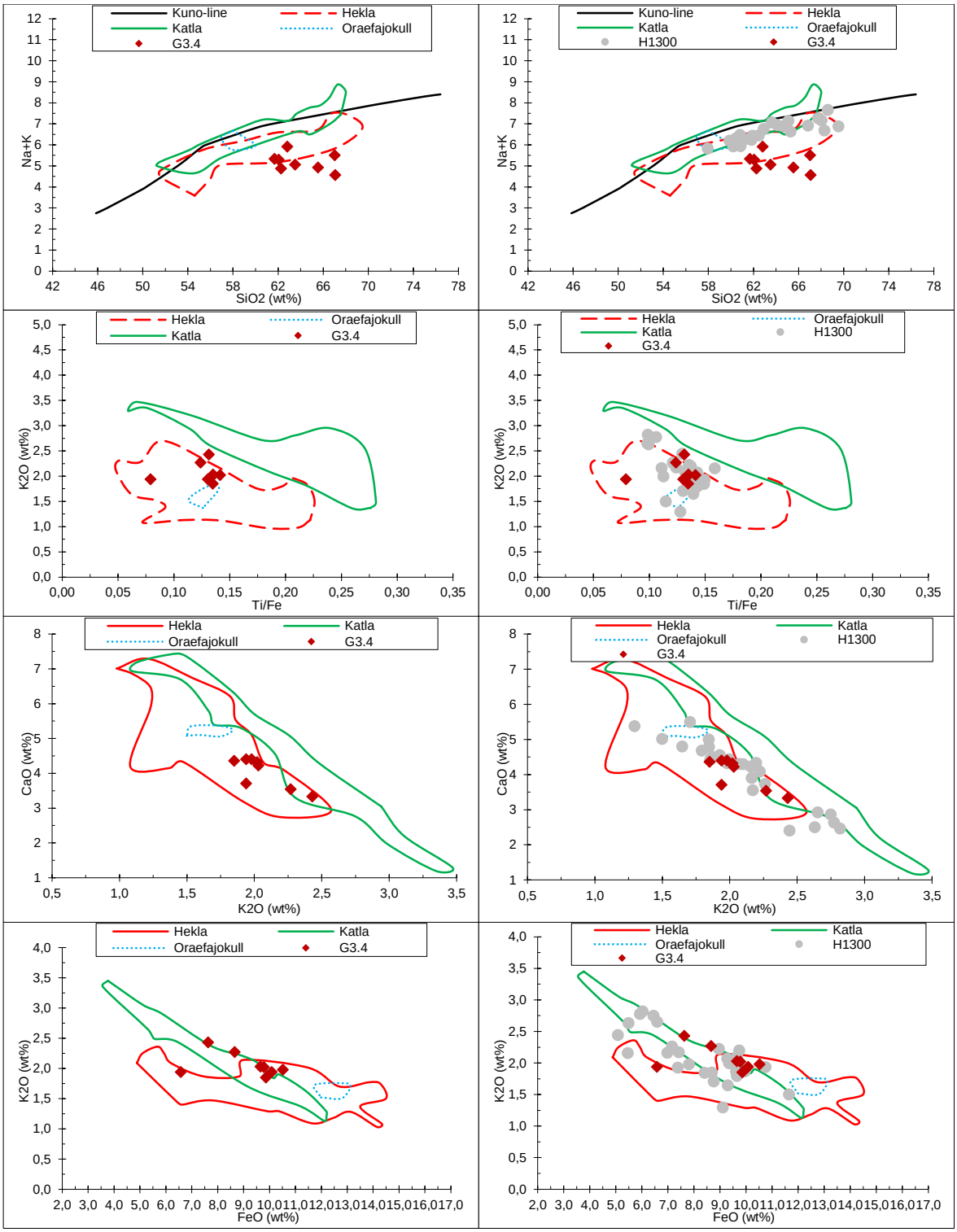

Figure 60. Sample G3.4 and the geochemical discrimination plots used to identify the tephra. Correlating to Hvítávatn, plots shown on the right (Thorvaldur Thordarson, unpublished data 2018), helped determine that this sample is Hekla 1300.

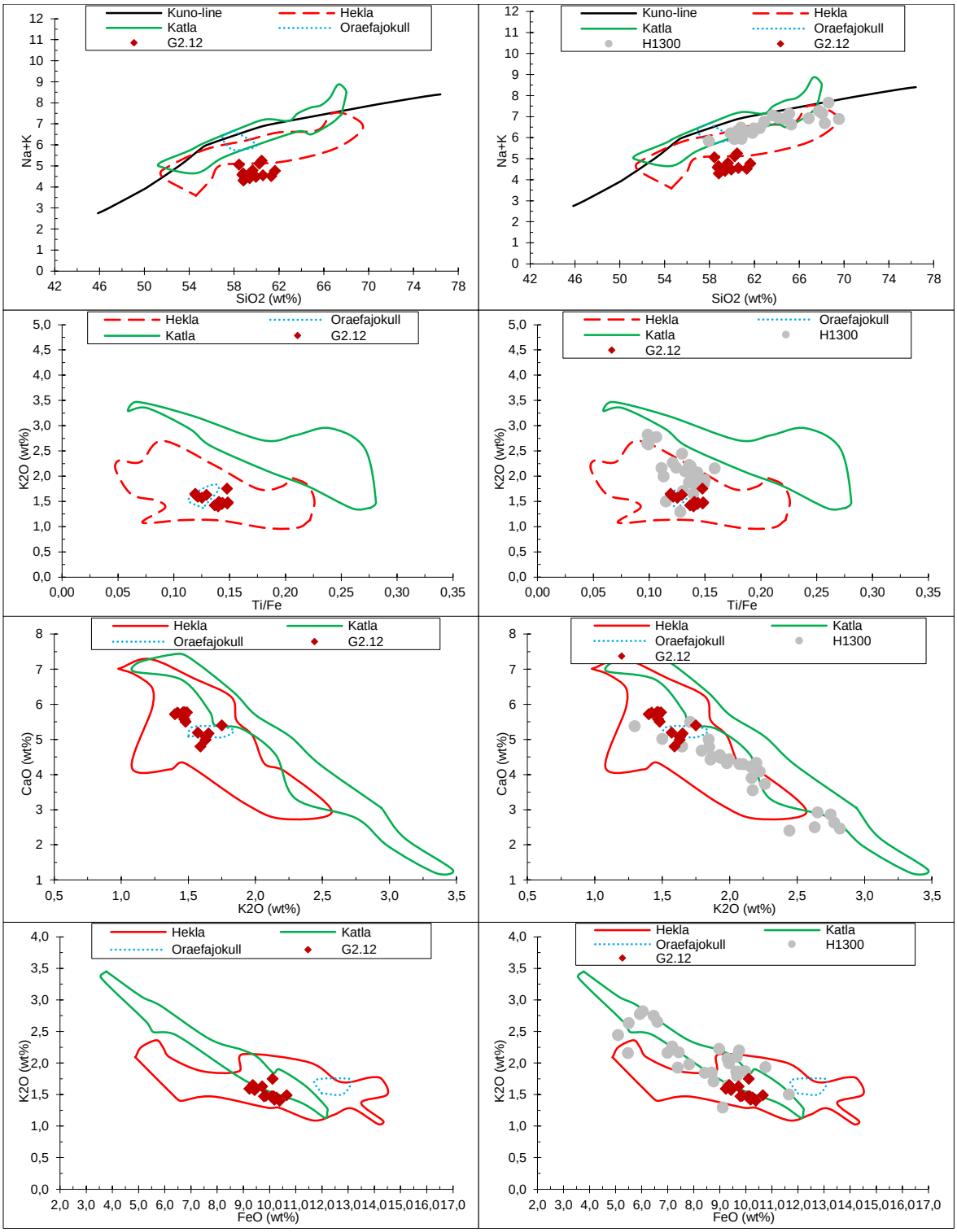

Figure 61. Geochemical discrimination plots used for the intermediate sample G2.12. By comparing to data from Hvítárvatn this tephra was identified as Hekla 1300 (Thorvaldur Thordarson, unpublished data 2018).

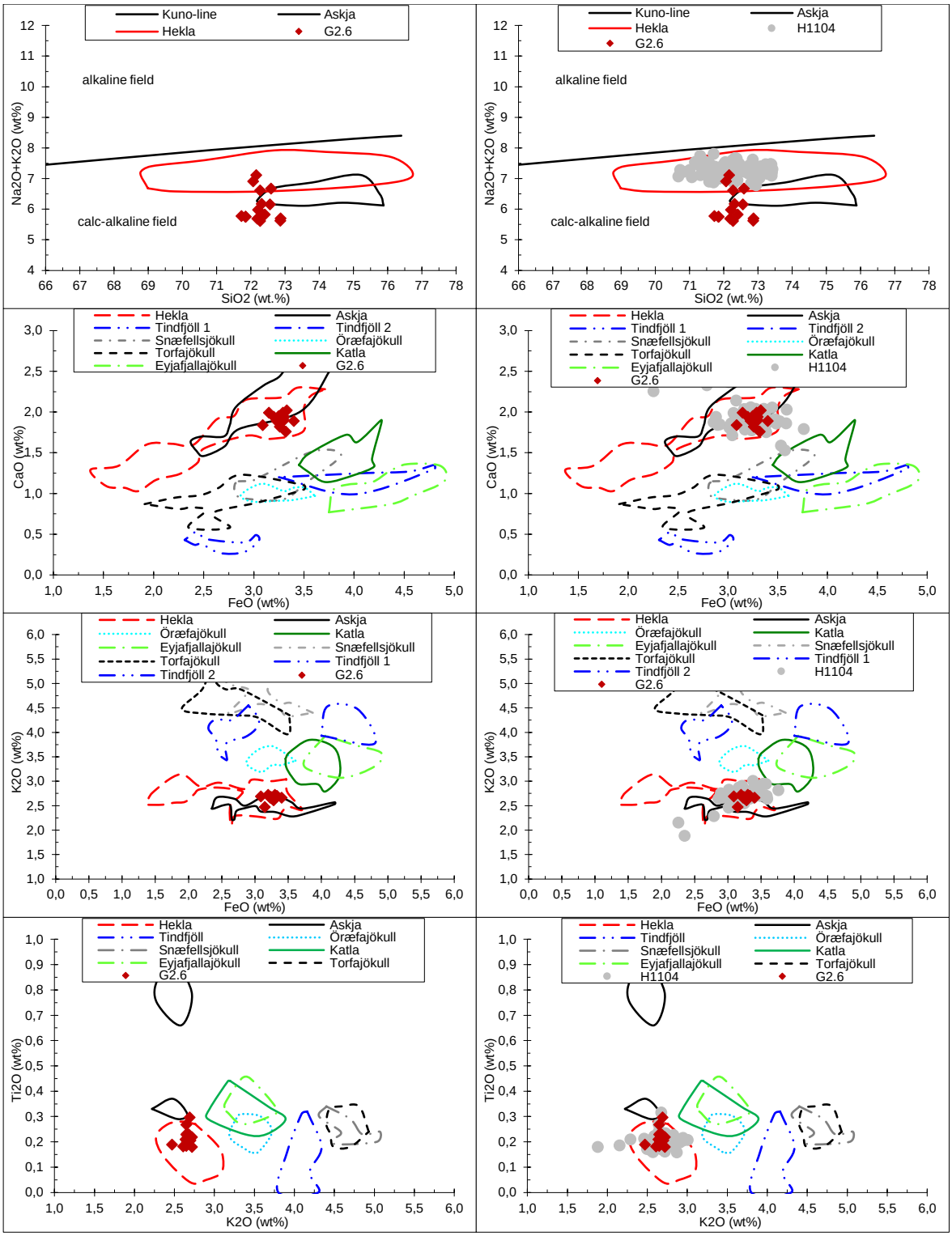

Figure 62. Rhyolite sample G2.6 shown in geochemical discrimination plots that were used to determine its origin. Using comparison data from Hvítárvatn the tephra was identified as Hekla 1104 (Thorvaldur Thordarson, unpulished data 2018).

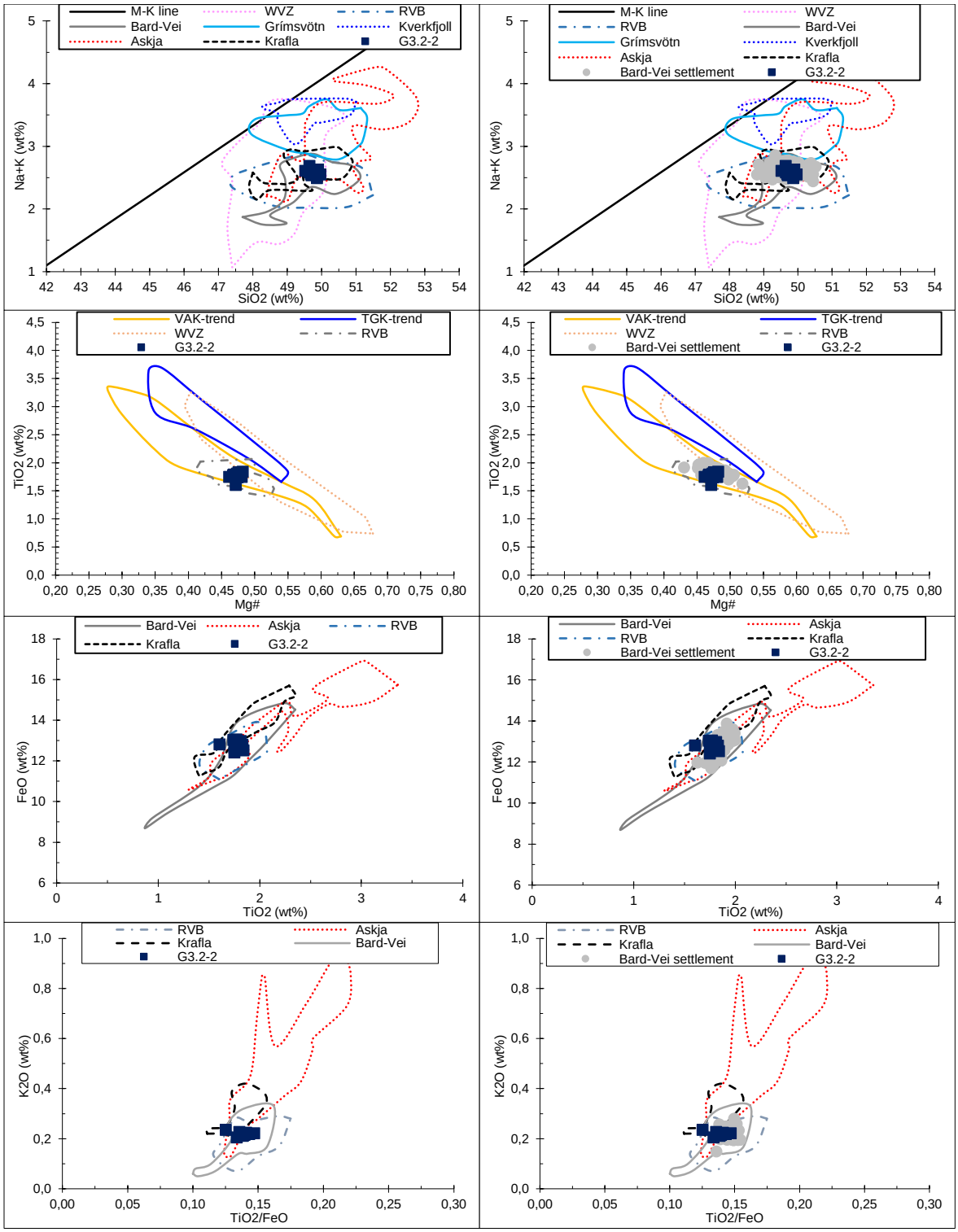

Figure 63. Geochemical discrimination plots used for sample G3.2-2. The plots on the right side contain comparison data from Hvítárvatn which helped to identify the tephra as the Settlement layer from the Bárðarbunga-Veiðivötn system (Thorvaldur Thordarson, unpublished data 2018).

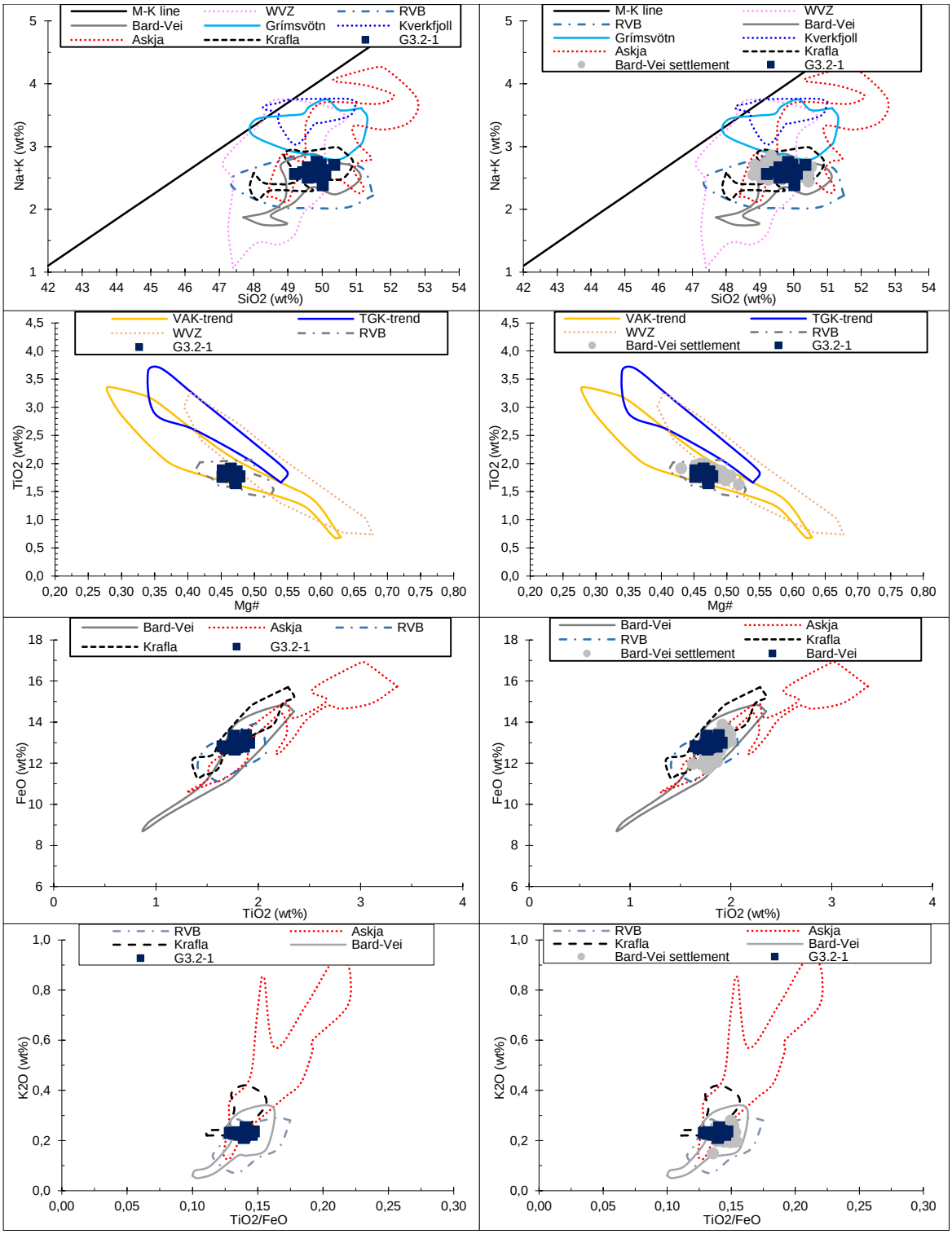

Figure 64. Tholeiitic basalt sample G3.2-1 which was identified as the Settlement layer from the Bárðarbunga-Veiðivötn system, using comparison data from Hvítárvatn shown on the plots on the right side (Thorvaldur Thordarson, unpublished data 2018).

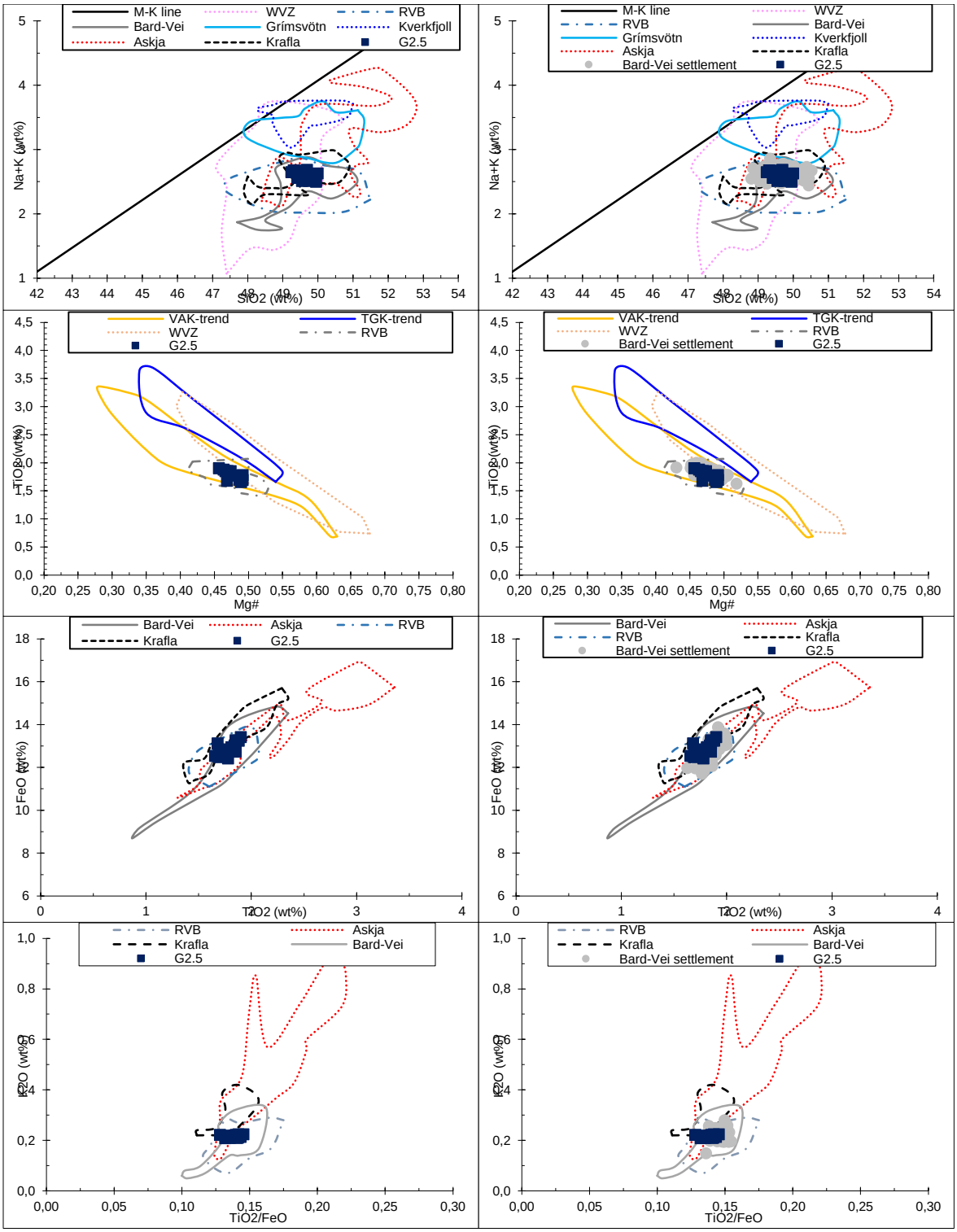

Figure 65. Geochemical discrimination plots used for sample G2.5. The plots on the right contain comparison data from Hvítárvatn (Thorvaldur Thordarson, unpublished data 2018) that helped identify this tephra as the Settlement layer from the Bárðarbunga-Veiðivötn system.

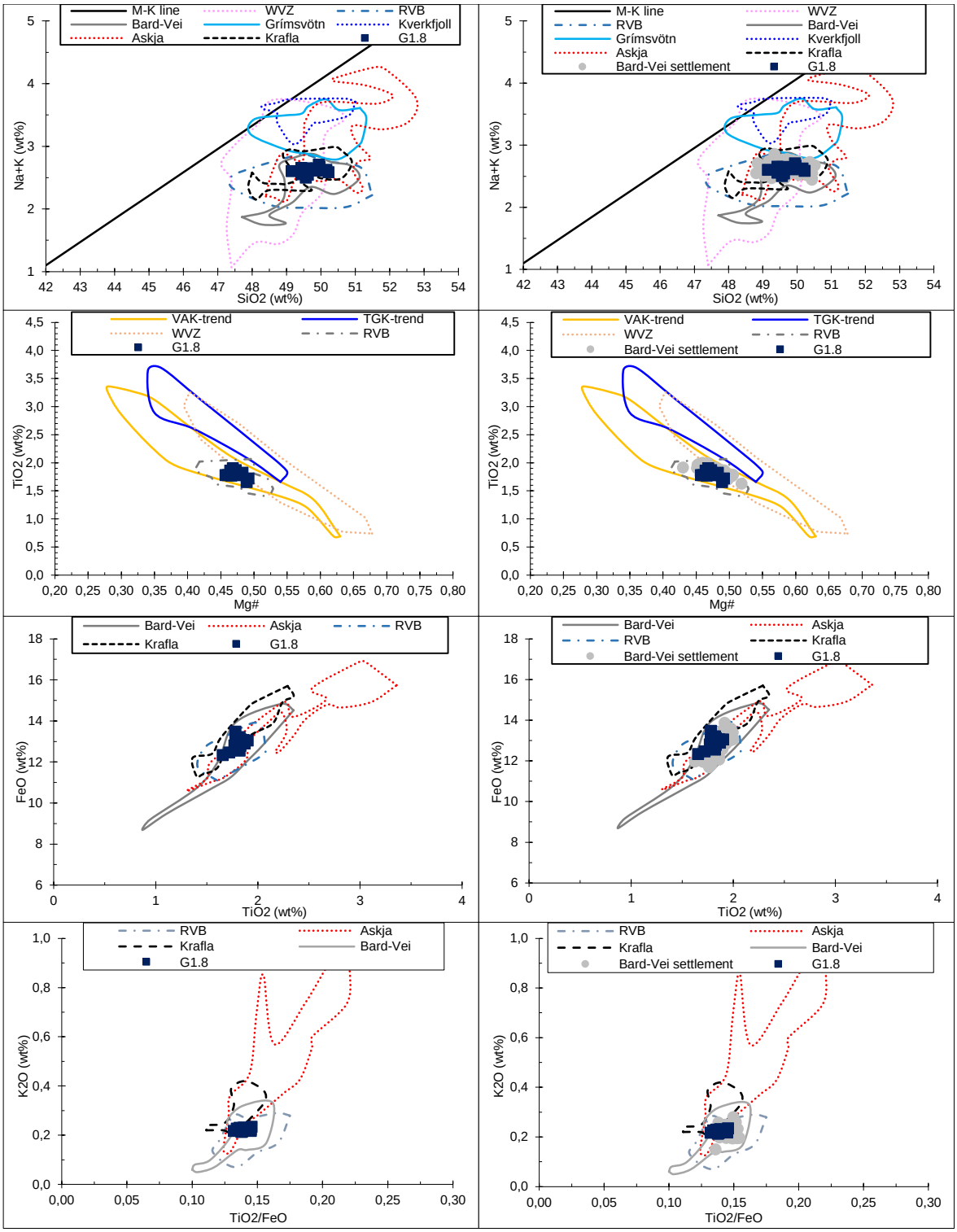

Figure 66. Tholeiitic basalt sample G1.8 and the geochemical discrimination plots used to identify it as the Settlement layer from Bárðarbunga-Veiðivötn system. The plots on the right side contain comparison data from Hvítárvatn (Thorvaldur Thordarson, unpublished data 2018).

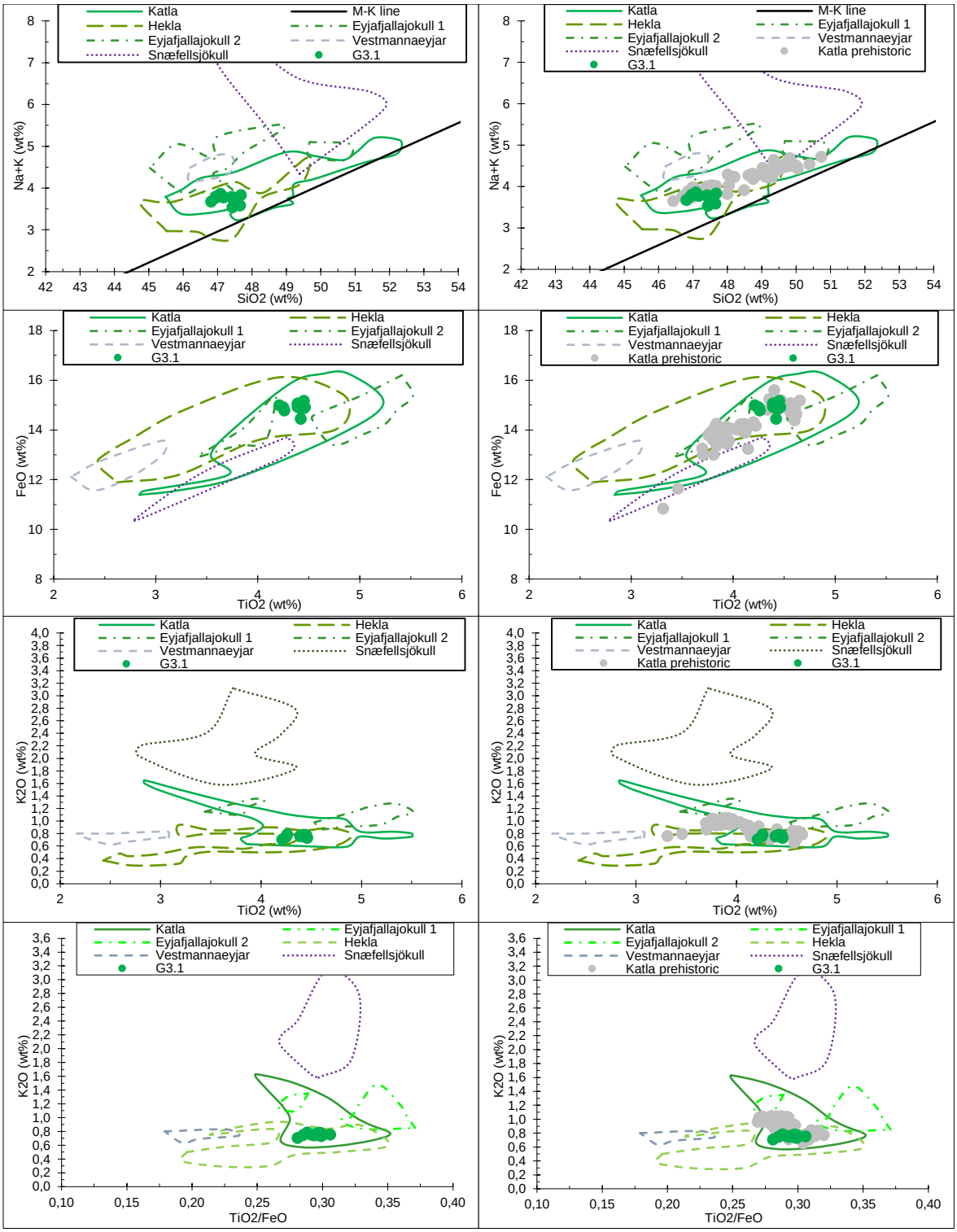

Figure 67. Alkalic basalt sample G3.1 which was identified as Katla prehistoric. Comparison data from Hvítárvatn used to help with the identification is shown on the plots to the right (Thorvaldur Thordarson, unpublished data 2018).

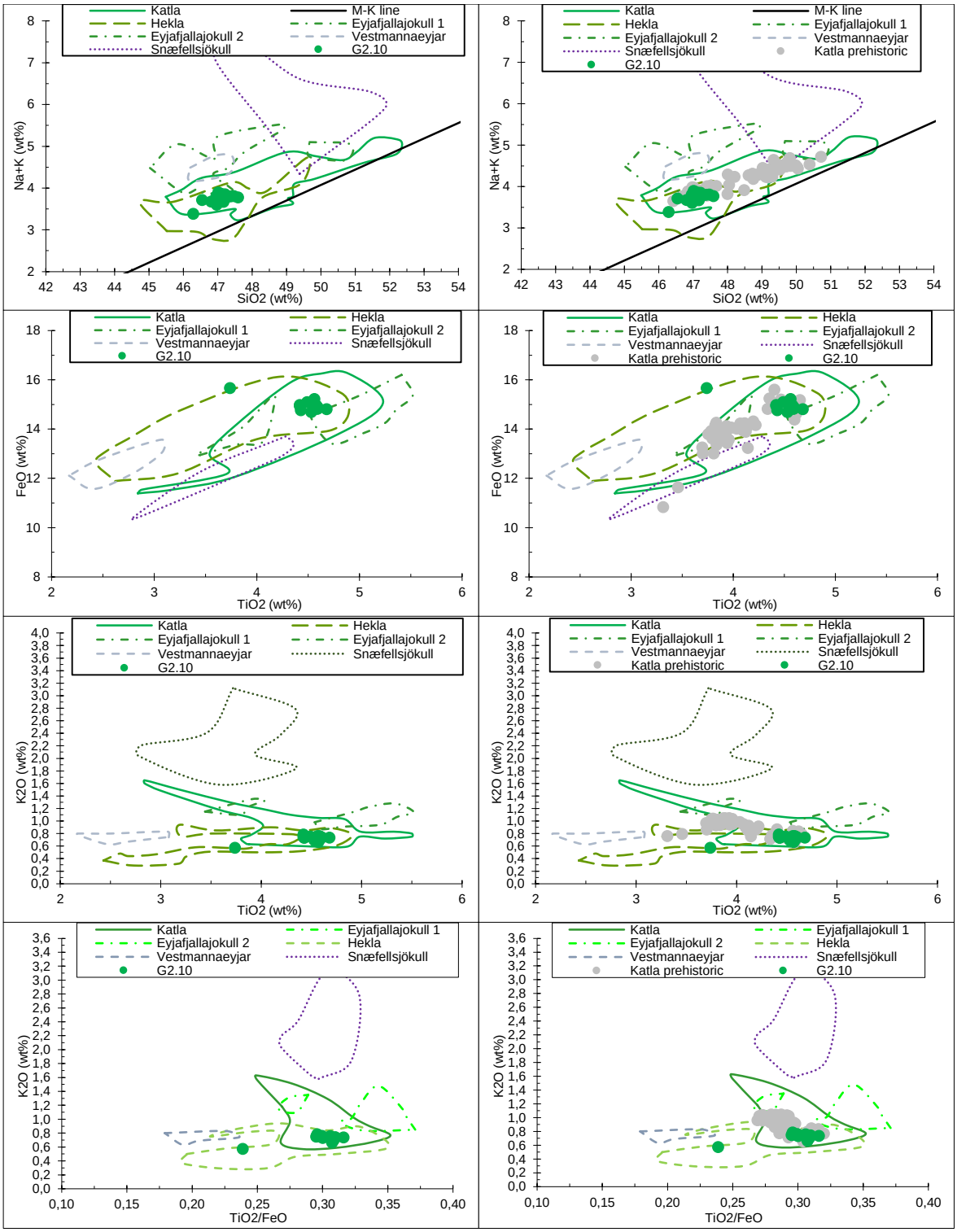

Figure 68. Sample G2.10 was identified as Katla prehistoric by using comparison data from Hvítárvatn (Thorvaldur Thordarson, unpublsihed data 2018), displayed in the graphs on the right side.

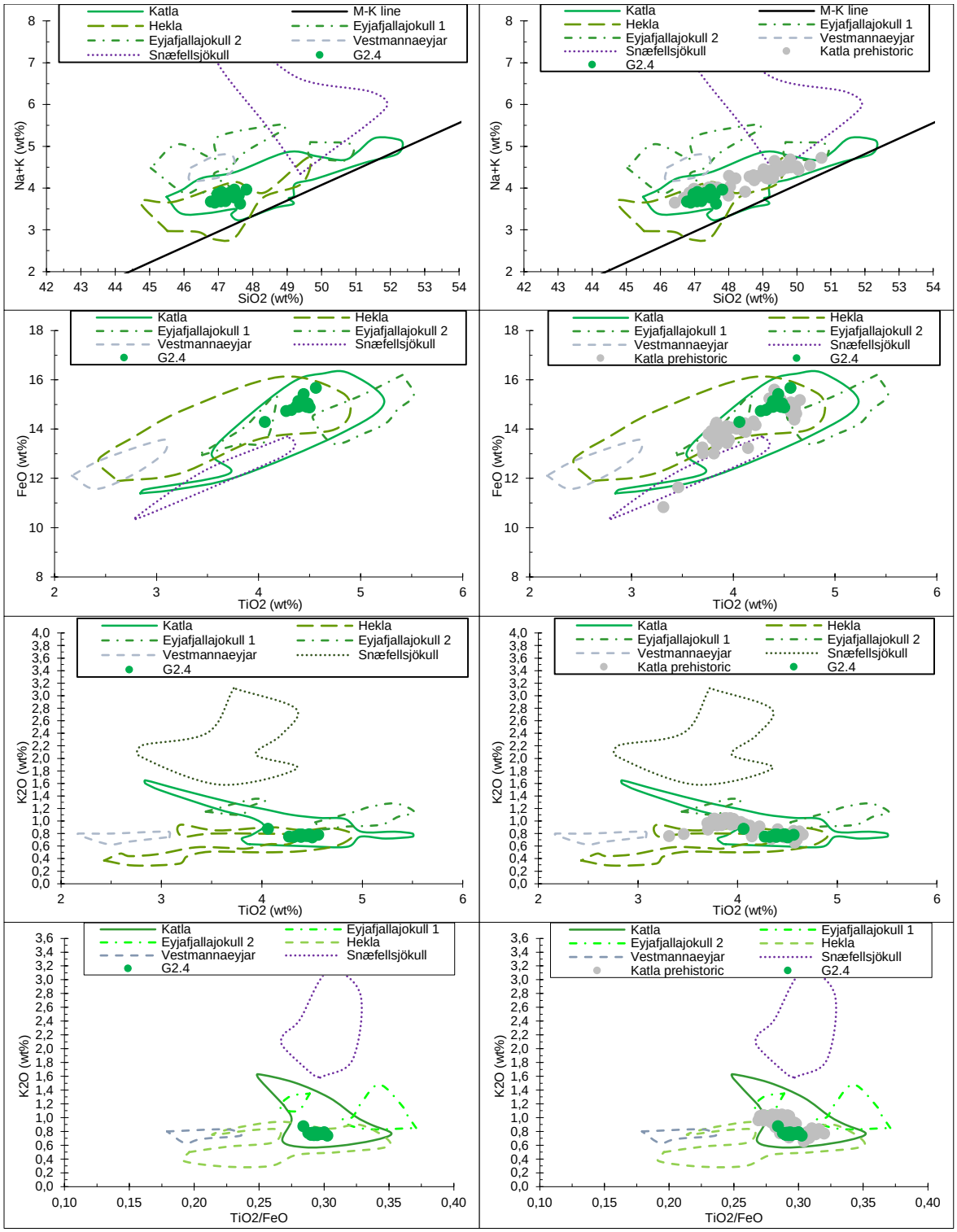

Figure 69. Geochemical discrimination plots used to identify sample G2.4 as Katla prehistoric. Comparison data from Hvítárvatn (Thorvaldur Thordarson, unpublished data 2018) helped to reach the conclusion.

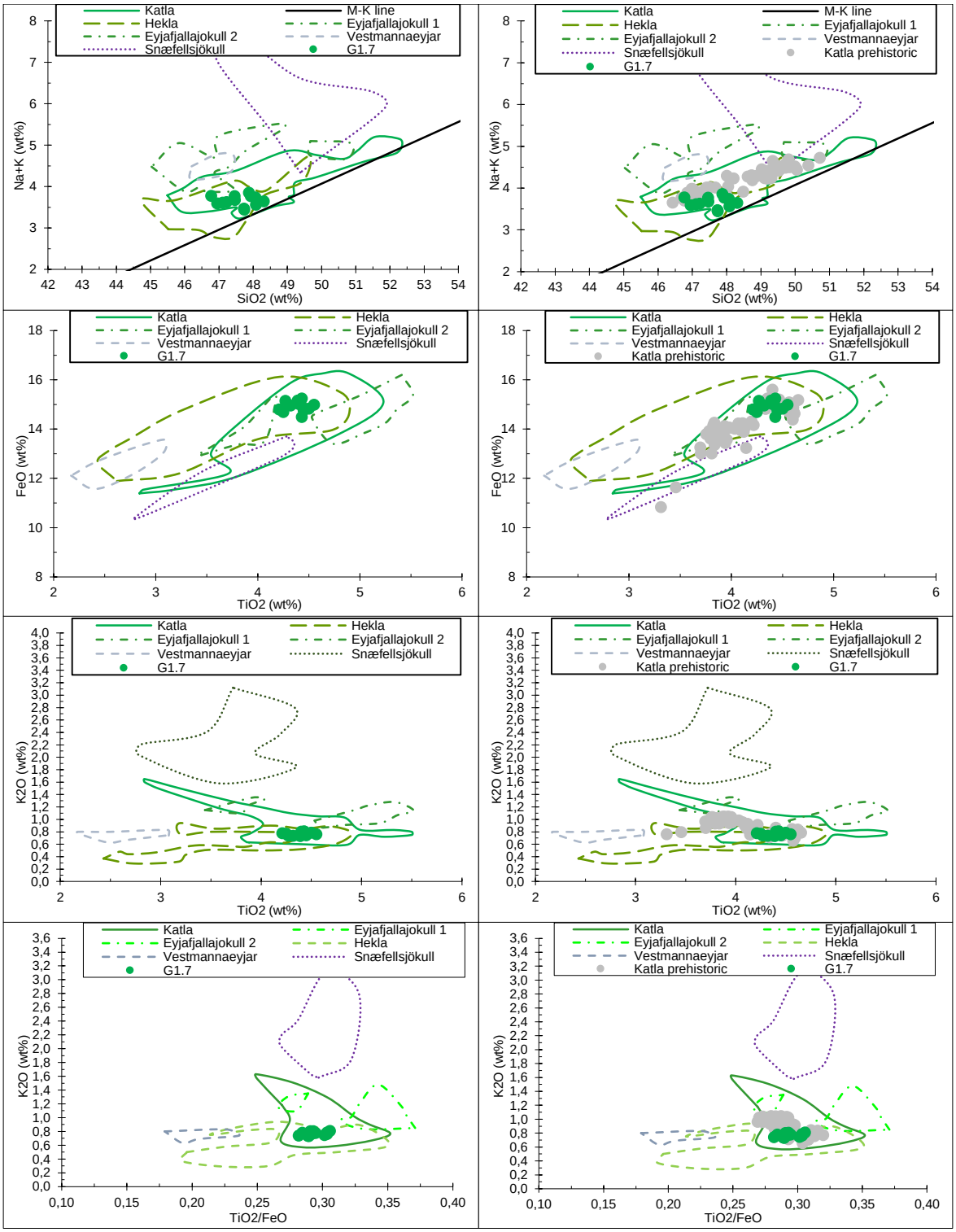

Figure 70. Alkalic basalt sample G1.7 which was identified as Katla prehistoric by comparing to geochemical data from Hvítárvatn (Thorvaldur Thordarson, unpublished data 2018), displayed in the plots on the right side.

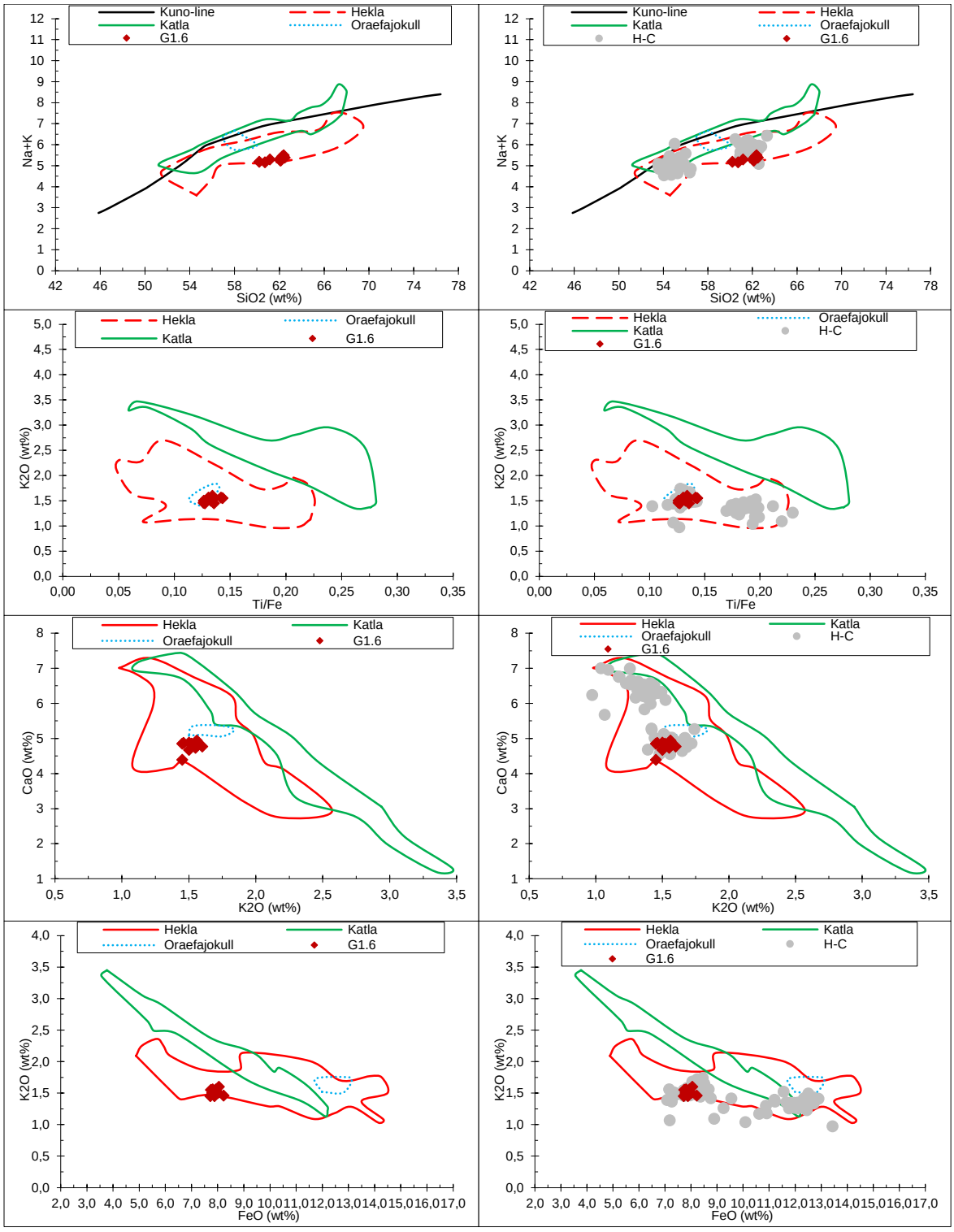

Figure 71. Sample G1.6 and the geochemical discrimination plots used to idendify it. By using comparison data from Hvítárvatn (Thorvaldur Thordarson, unpublished data 2018) the tephra was identified as Hekla-C.

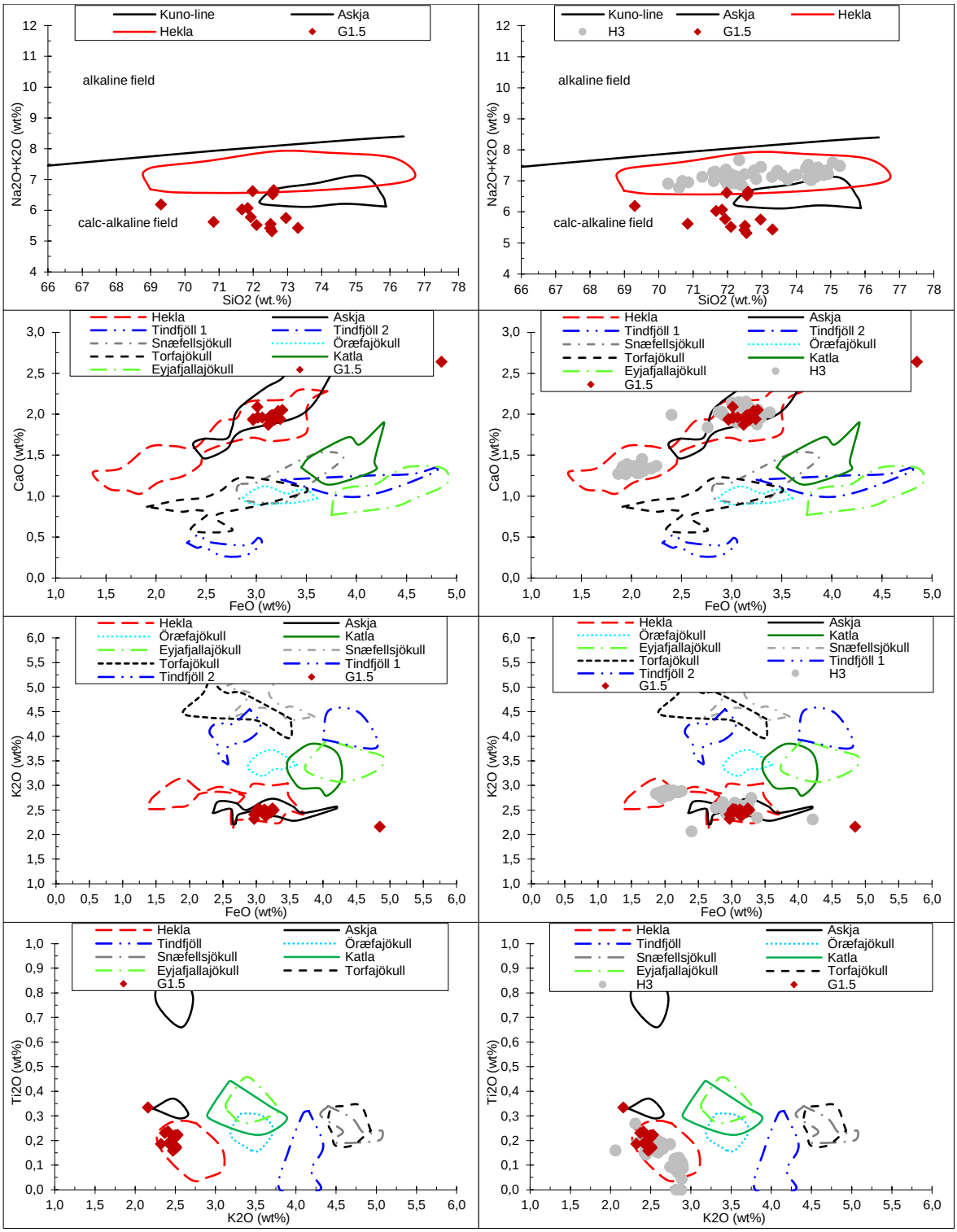

Figure 72. Geochemical discrimination plots used for rhyolite sample G1.5. By using comparison data from Hvítárvatn this tephra was identified as H3 (Thorvaldur Thordarson, unpublished data 2018).

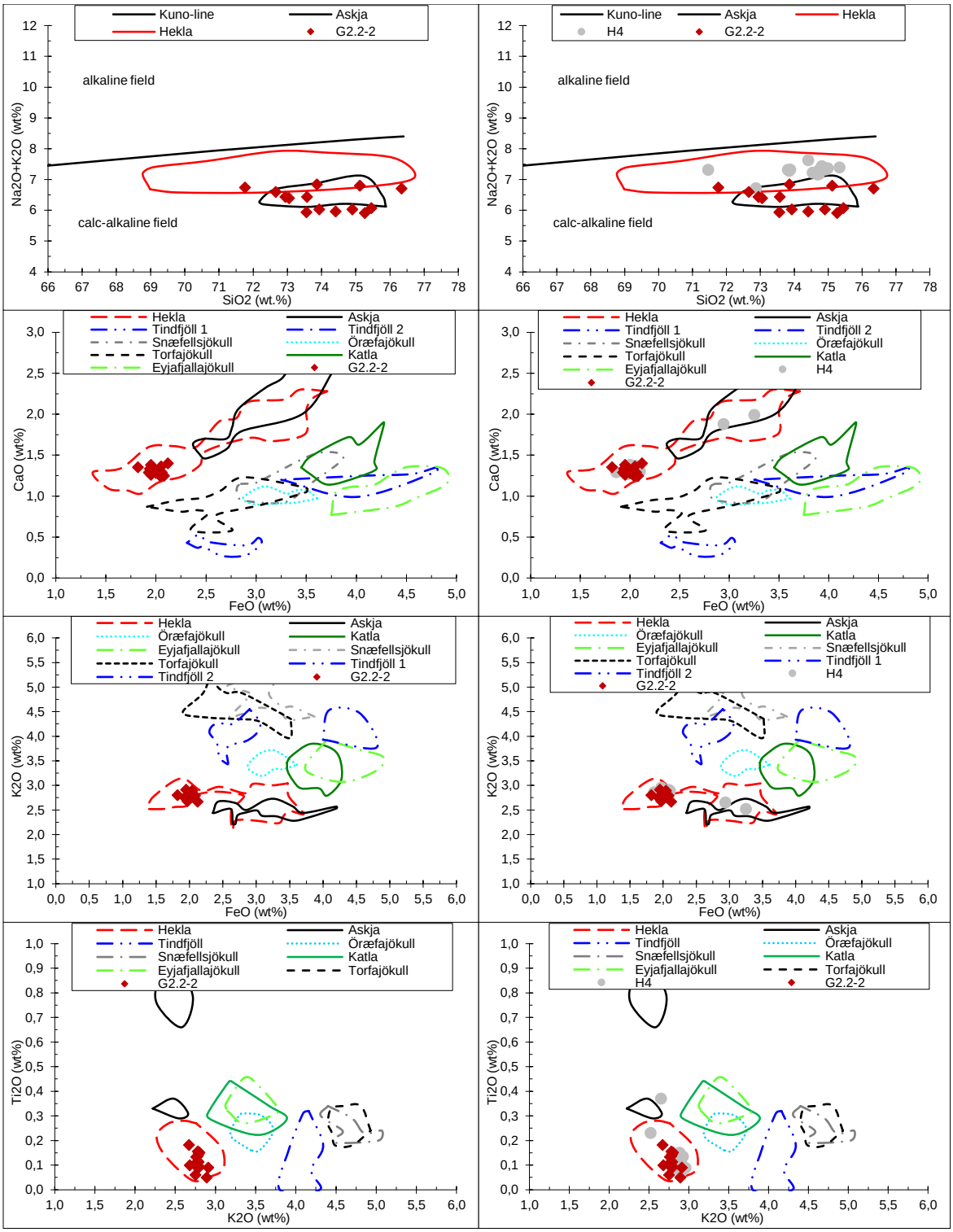

Figure 73. Rhyolite sample G2.2-2 displayed in geochemical discrimination plots. On the right side are plots with comparison data from Hvítárvatn which helped to identify the tephra as H4 (Thorvaldur Thordarson, unpublished data 2018).

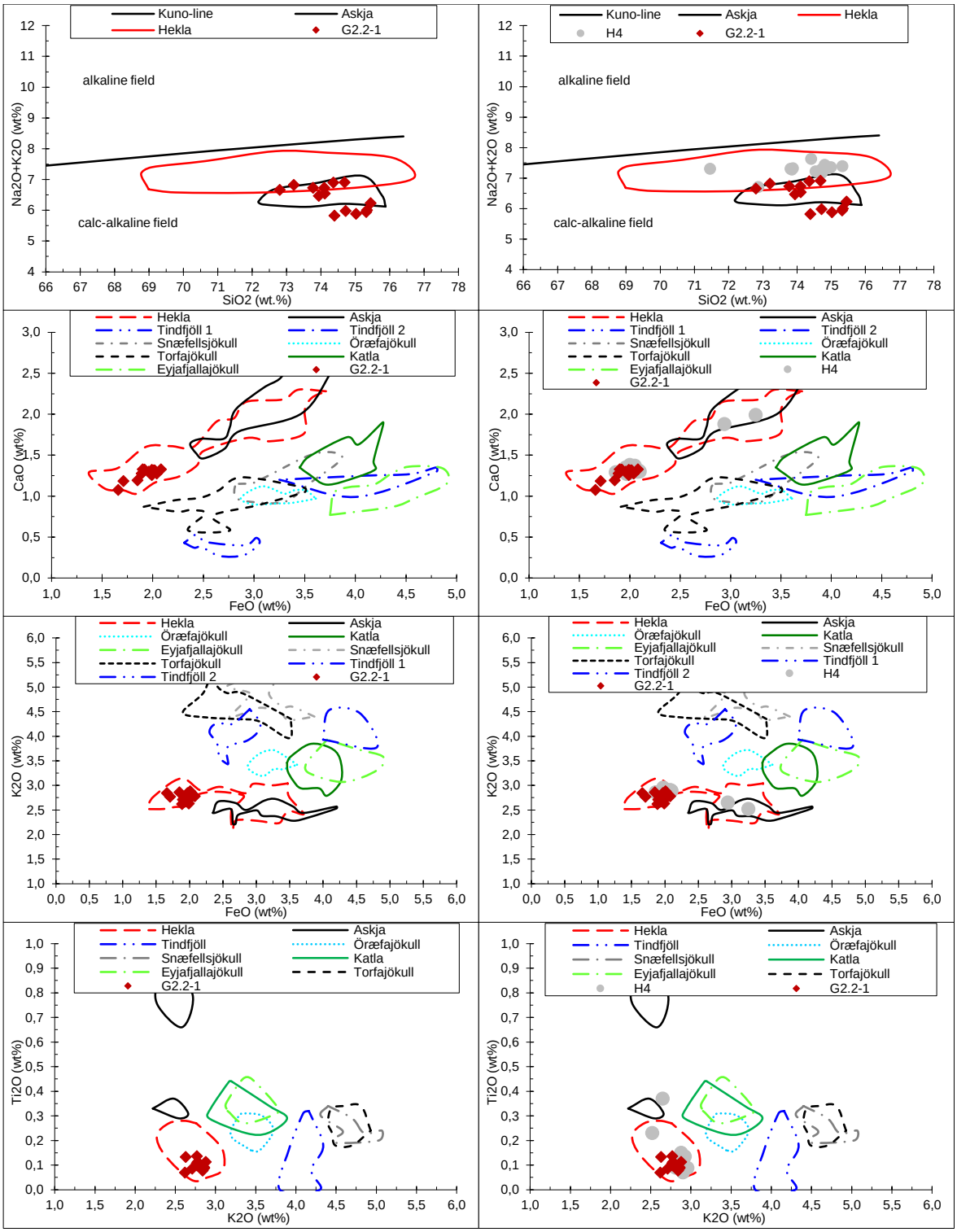

Figure 74. Geochemical discrimination plots for rhyolite sample G2.2-1. This sample was identified as H4 by using geochemical data from Hvítárvatn, shown in the plots on the right side (Thorvaldur Thordarson, unpublished data 2018).

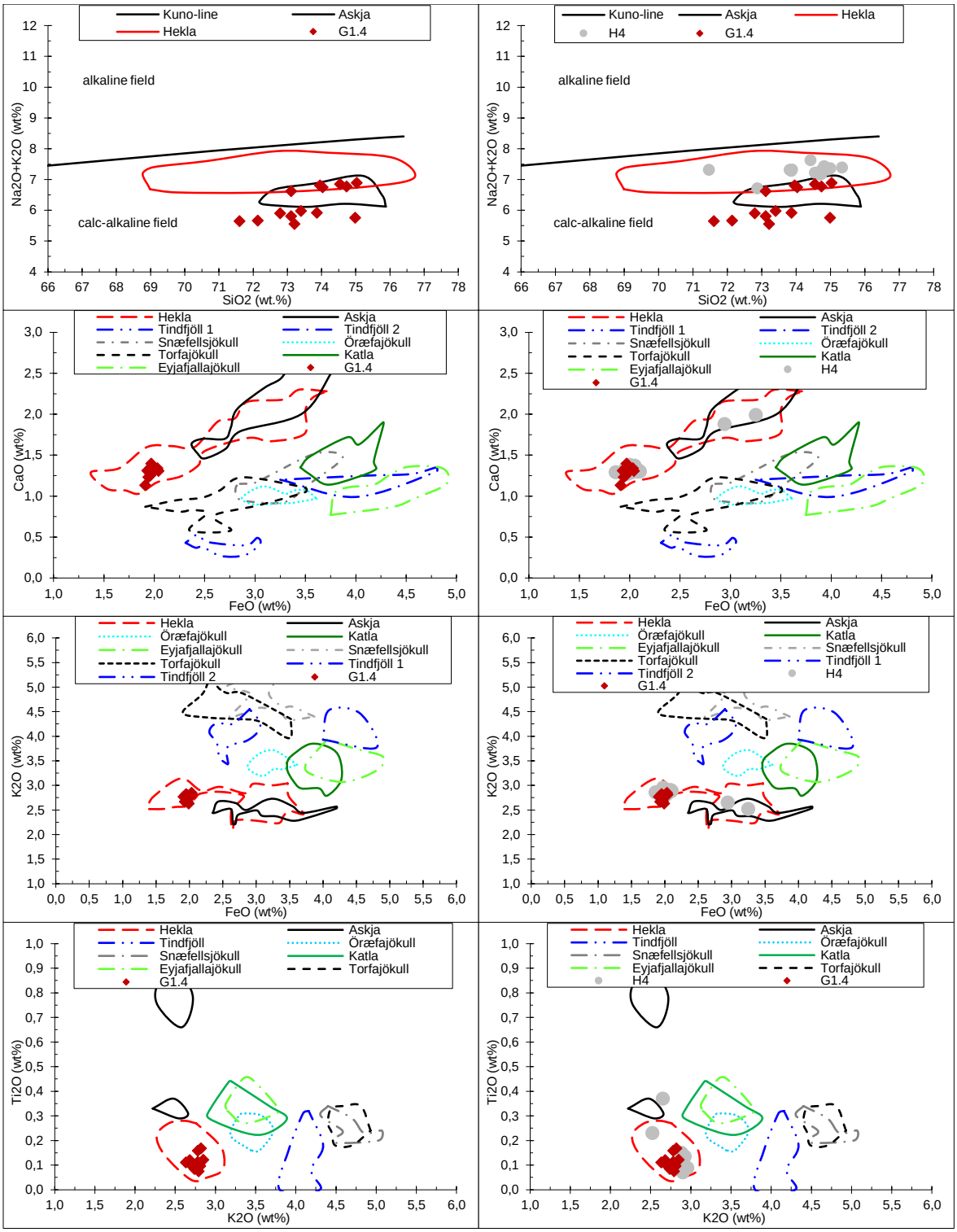

Figure 75. Rhyolite tephra sample G1.4 which was determined to be H4 by using these plots and comparison data from Hvítárvatn (Thorvaldur Thordarson, unpublished data 2018).

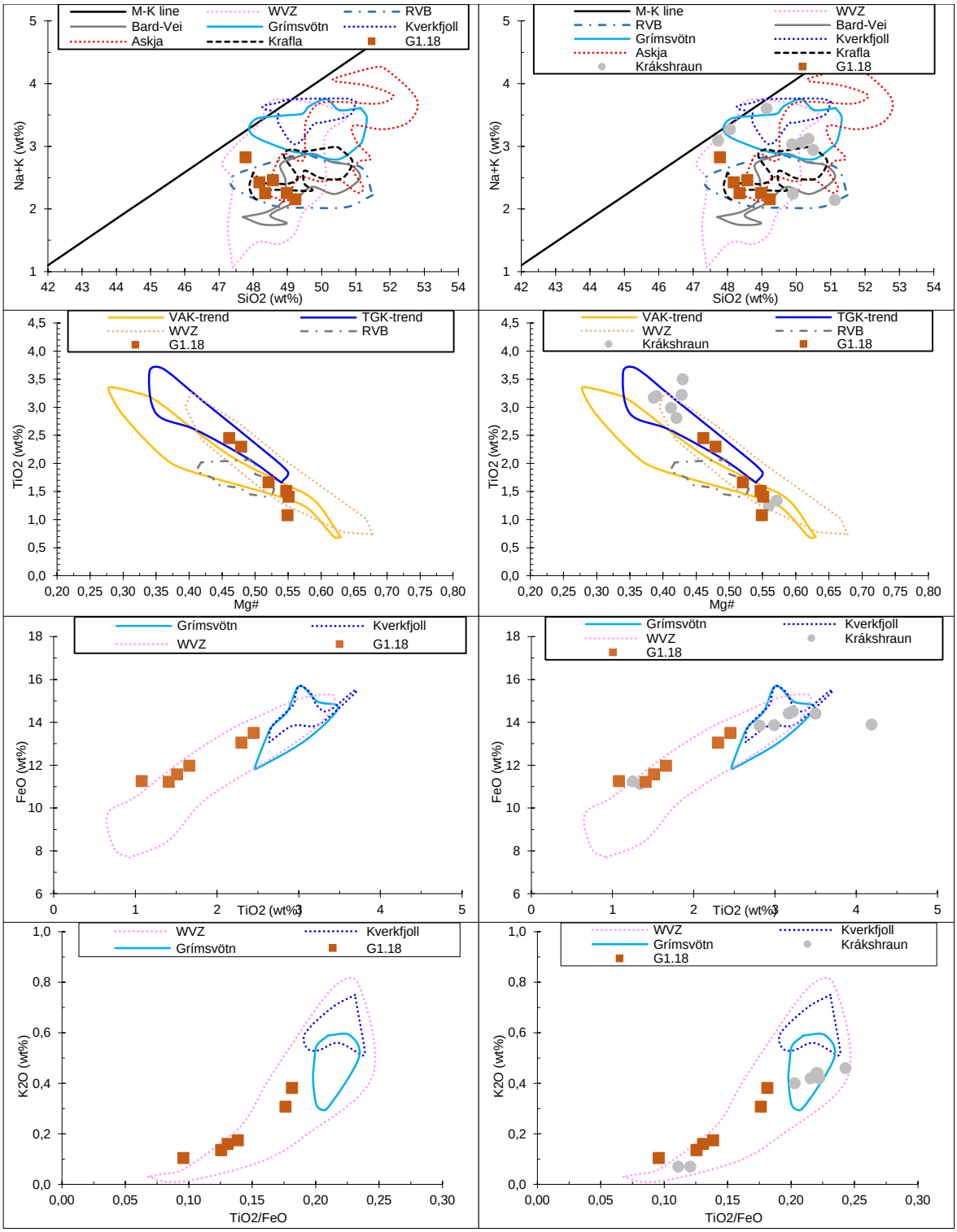

Figure 76. Geochemical discrimination plots for sample G1.18, which is tholeiitic basalt identified as Krákshraun 4500 from the WVZ (Sinton et al., 2005).

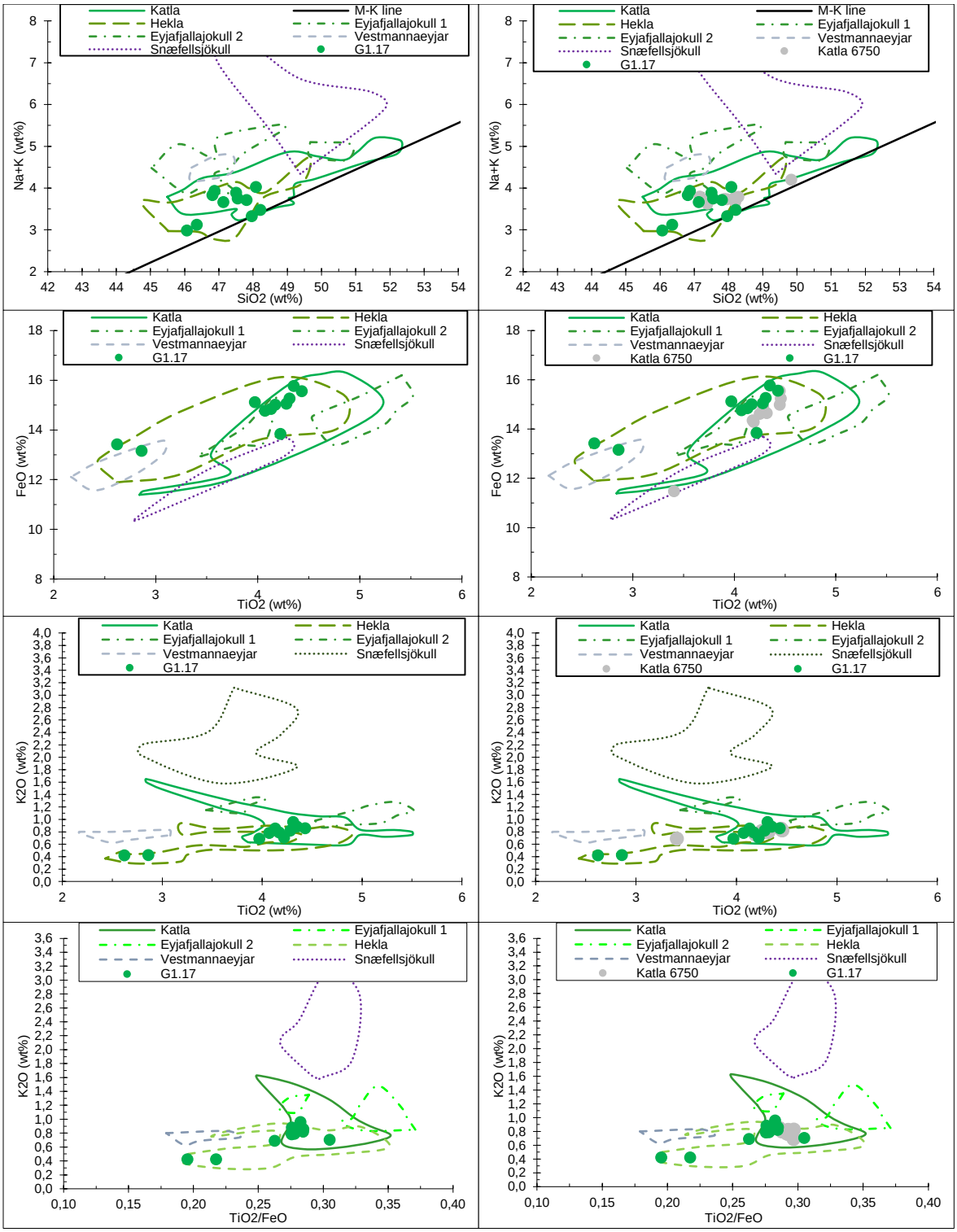

Figure 77. Alkalic basalt sample G1.17 shown in geochemical discrimination plots. This sample was identified as Katla 6750 by using comparison data from Hvítárvatn (Thorvaldur Thordarson, unpublished data 2018).

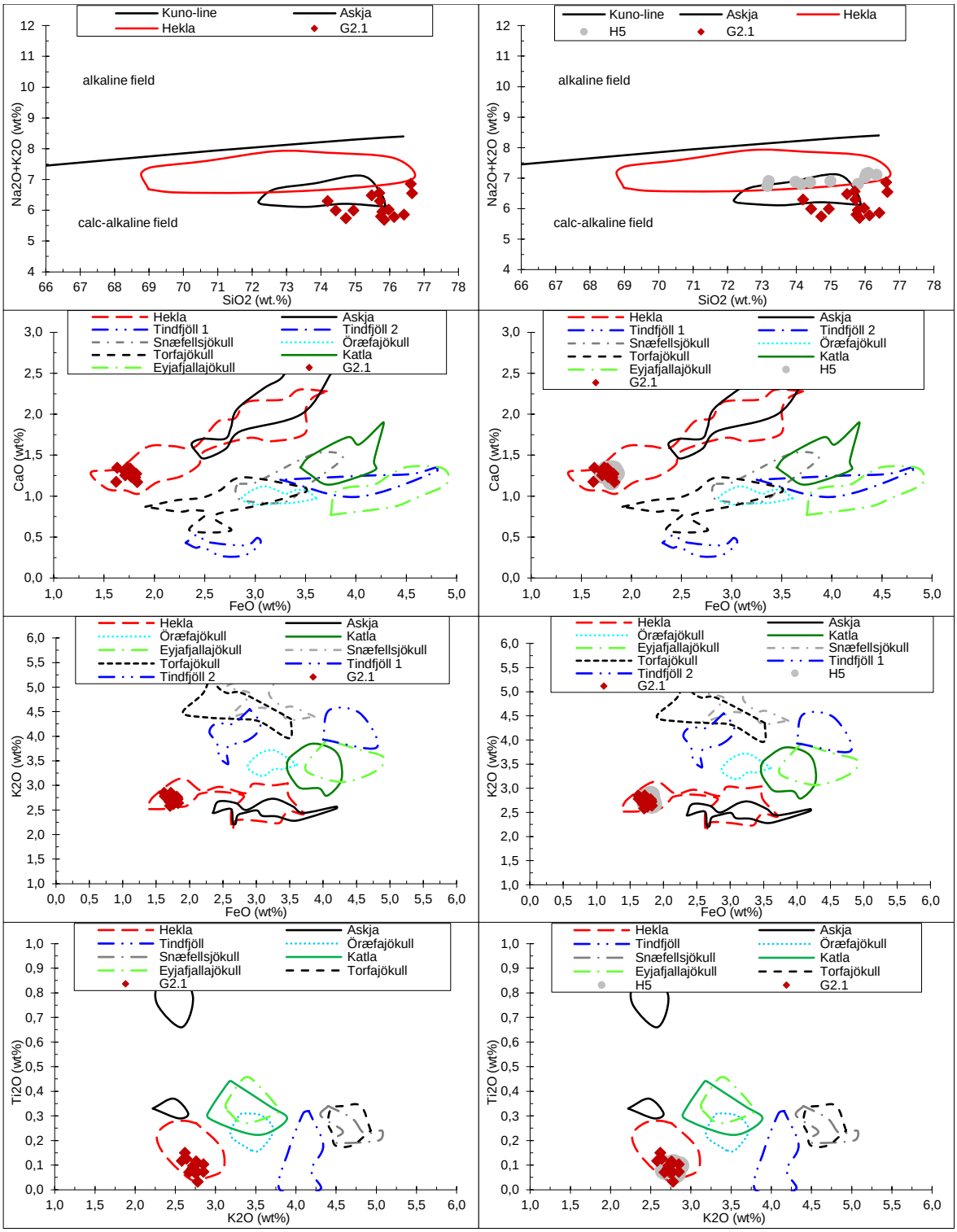

Figure 78. Sample G2.1 and the geochemical discrimination plots used to identify the tephra. This rhyolite sample was compared to geochemical data from Hvítárvatn as shown on the plots on the right side (Thorvaldur Thordarson, unpublished data 2018), the sample was determined to be H5.

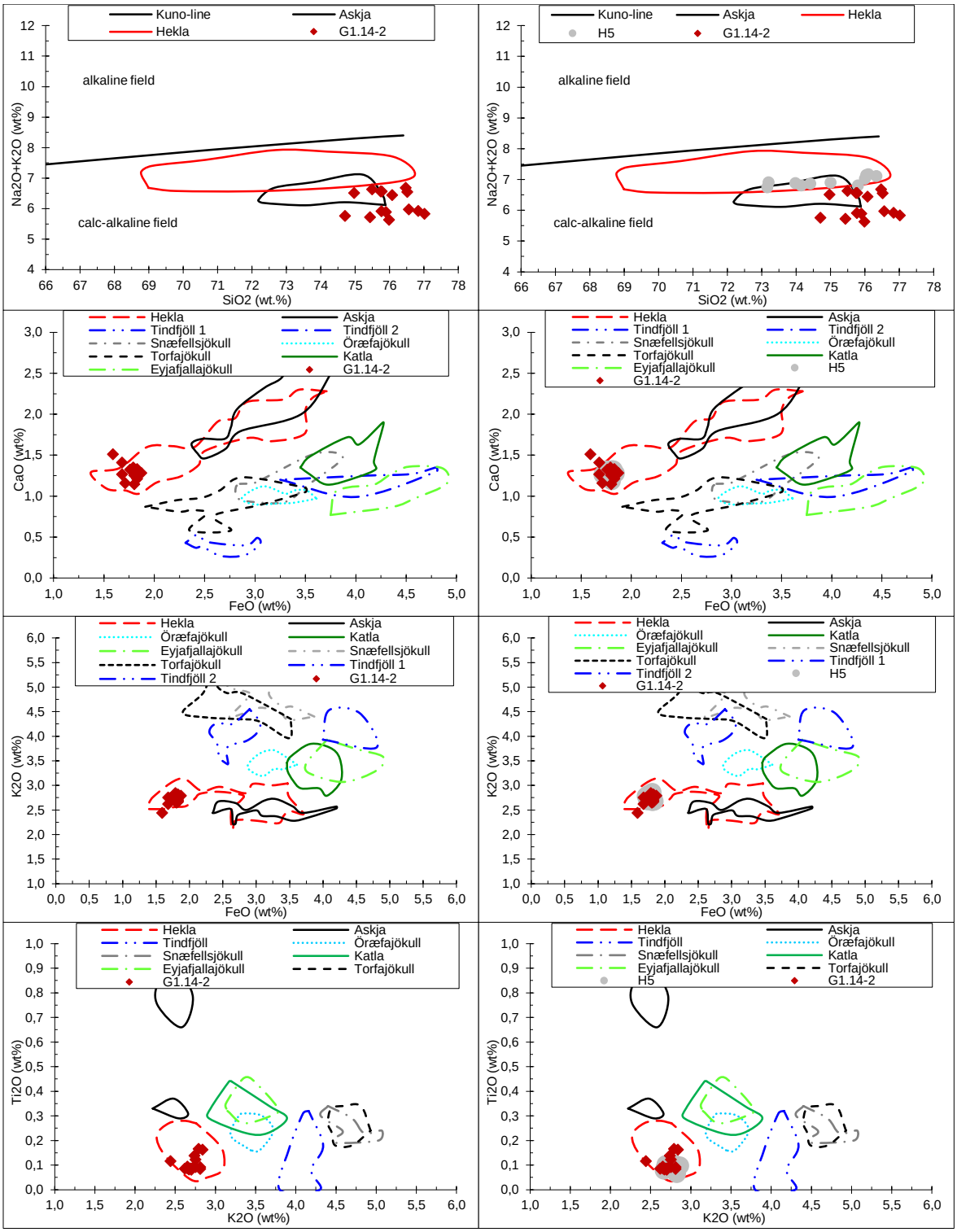

Figure 79. Geochemical discrimination plots used to determine the origin of the rhyolithe sample G1.14-2. The right side plots contain comparison data from Hvítárvatn that identified the tephra as H5 (Thorvaldur Thordarson, unplublished data 2018).

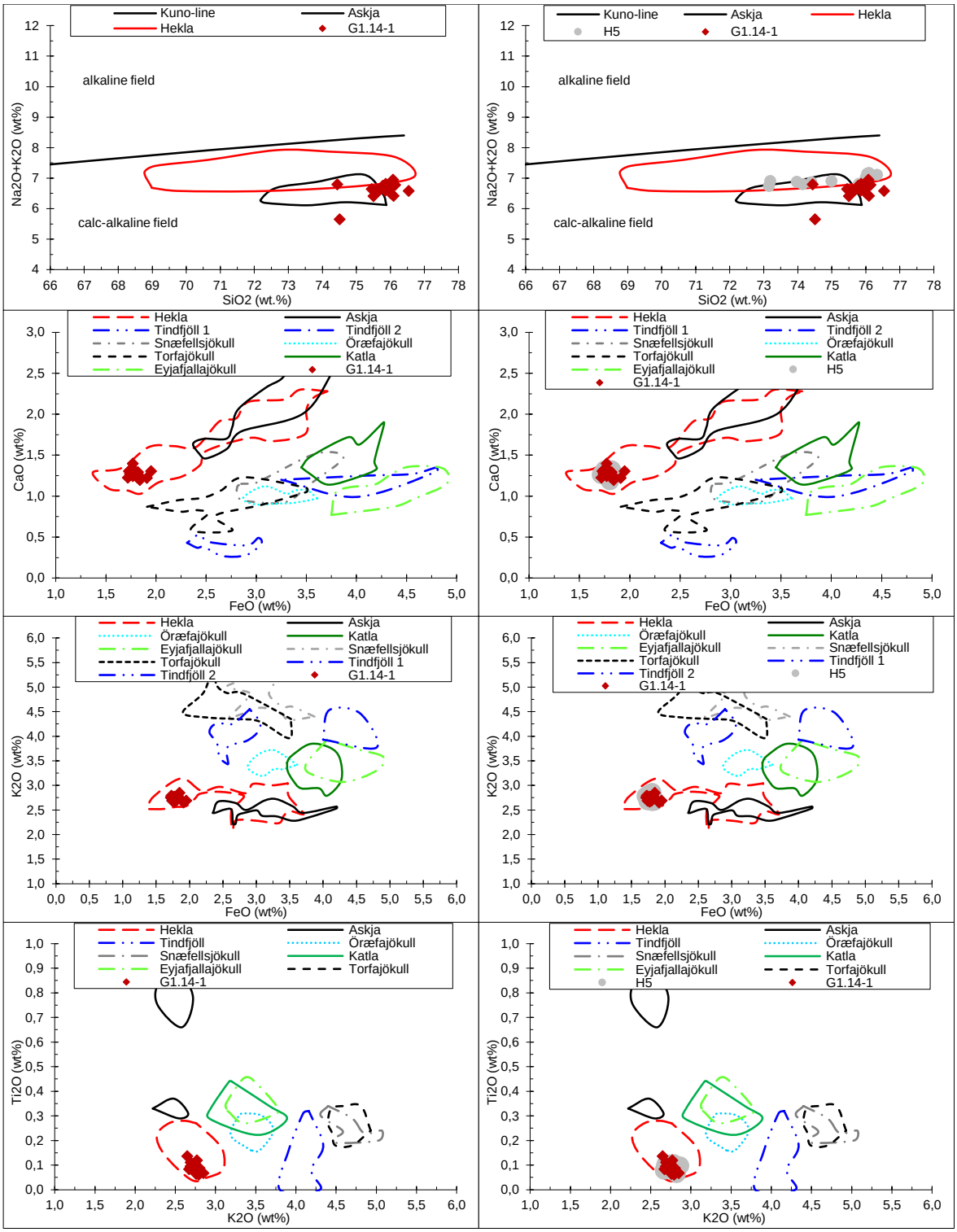

Figure 80. Rhyolite tephra sample G1.14-1 displayed in geochemical discrimination plots. By using comparison data from Hvítárvatn, shown in plots on the right side, this tephra was identified as H5 (Thorvaldur Thordarson, unpublished data 2018).

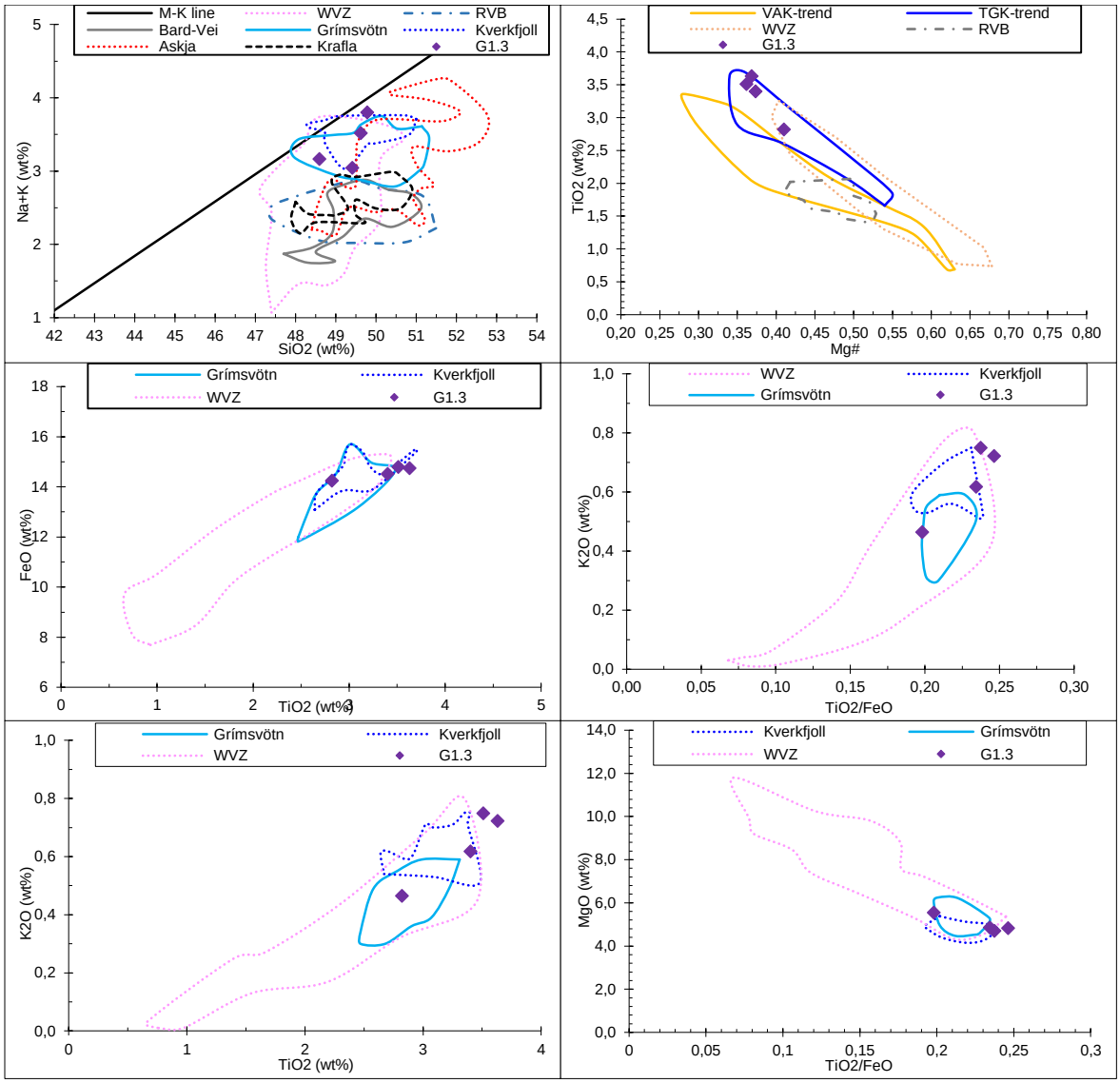

Figure 81. Sample G1.3 which was quite hard in identification. By using the geochemical discrimination plots (Thorvaldur Thordarson, unpublished data) the tephra was identifyed to originate from Kverkfjöll, but no geochemical data was available to compare with. By calculating SAR age and correlating with Óladóttir et al. (2011) the tephra got an estimated age of 6.890 years BP.

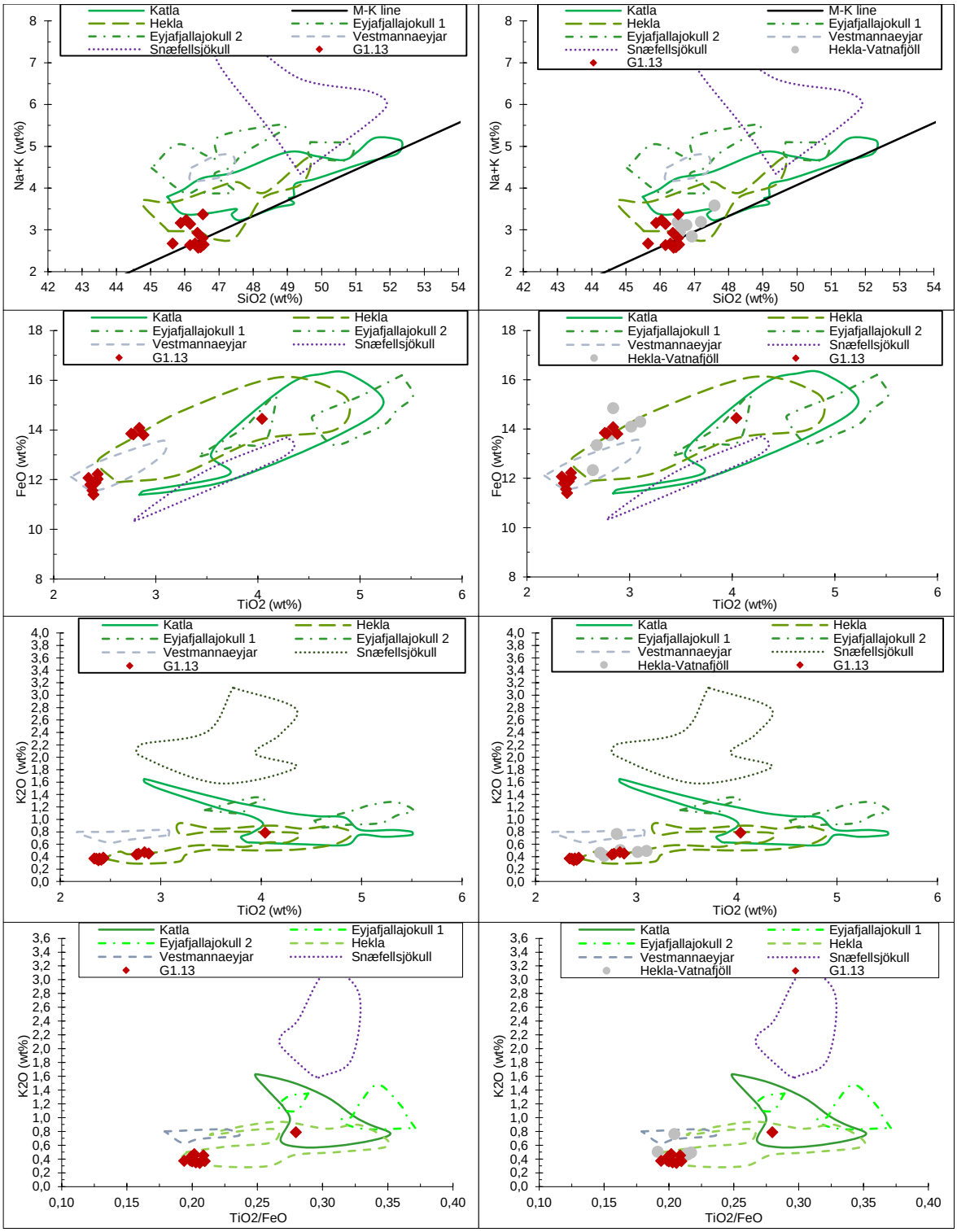

Figure 82. Alkalic basalt sample G1.13 and the geochemical discrimination plots used to identify it. The comparison data is shown in the graphs on the right side and helped to identify this tephra as Hekla-Vatnafjöll with an age of 9.100 (Thorvaldur Thordarson, unpublished data 2018).

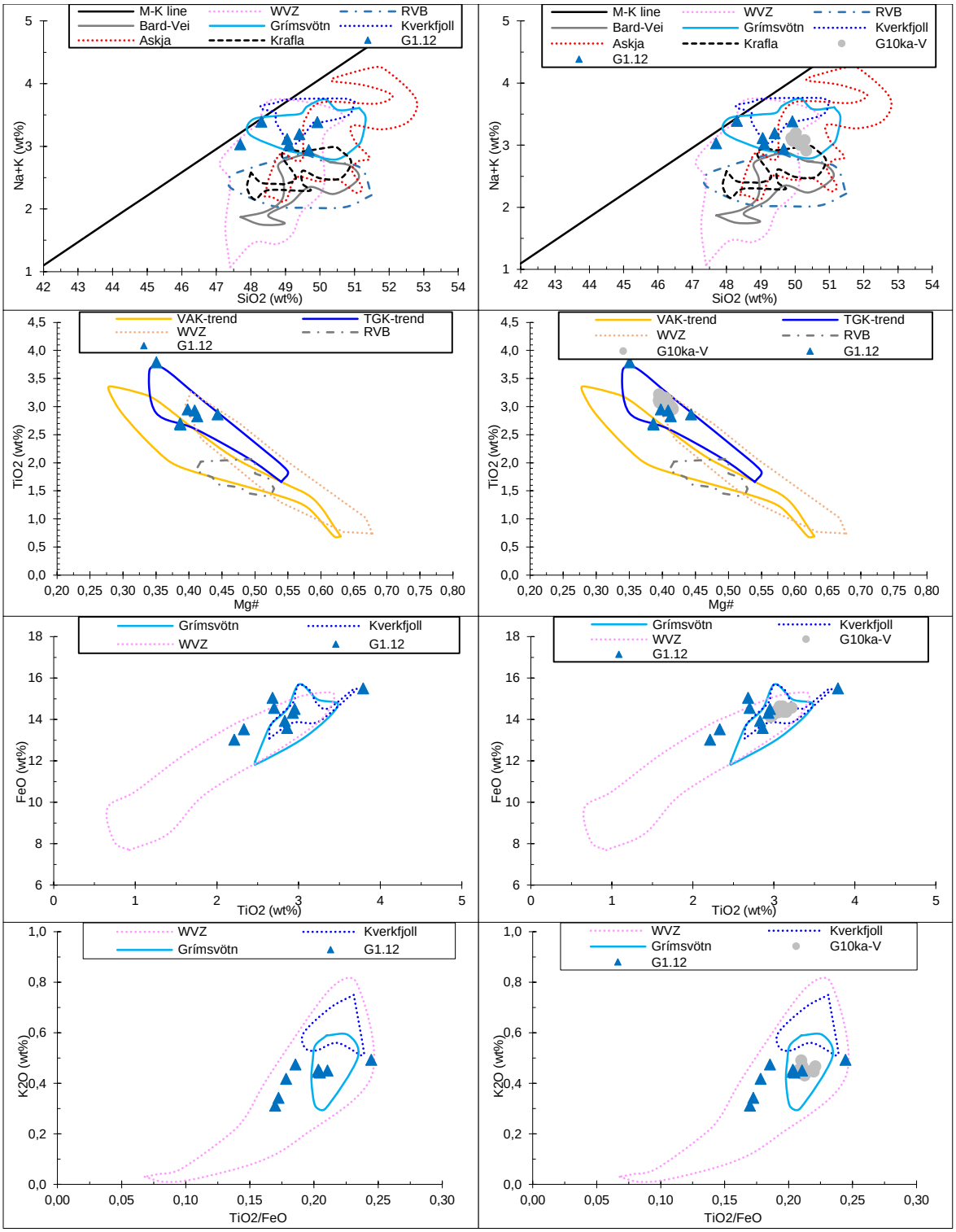

Figure 83. Tholeiitic basalt sample G1.12 and the geochemical discrimination plots used to identify the tephra as being from Grímsvötn. By using comparison data from Hvítárvatn (Thorvaldur Thordarson, unpublished data 2018) the sample was identified as one of the tephras from the 10 ka Grímsvötn series, with an estimated age of 10.000 years BP.

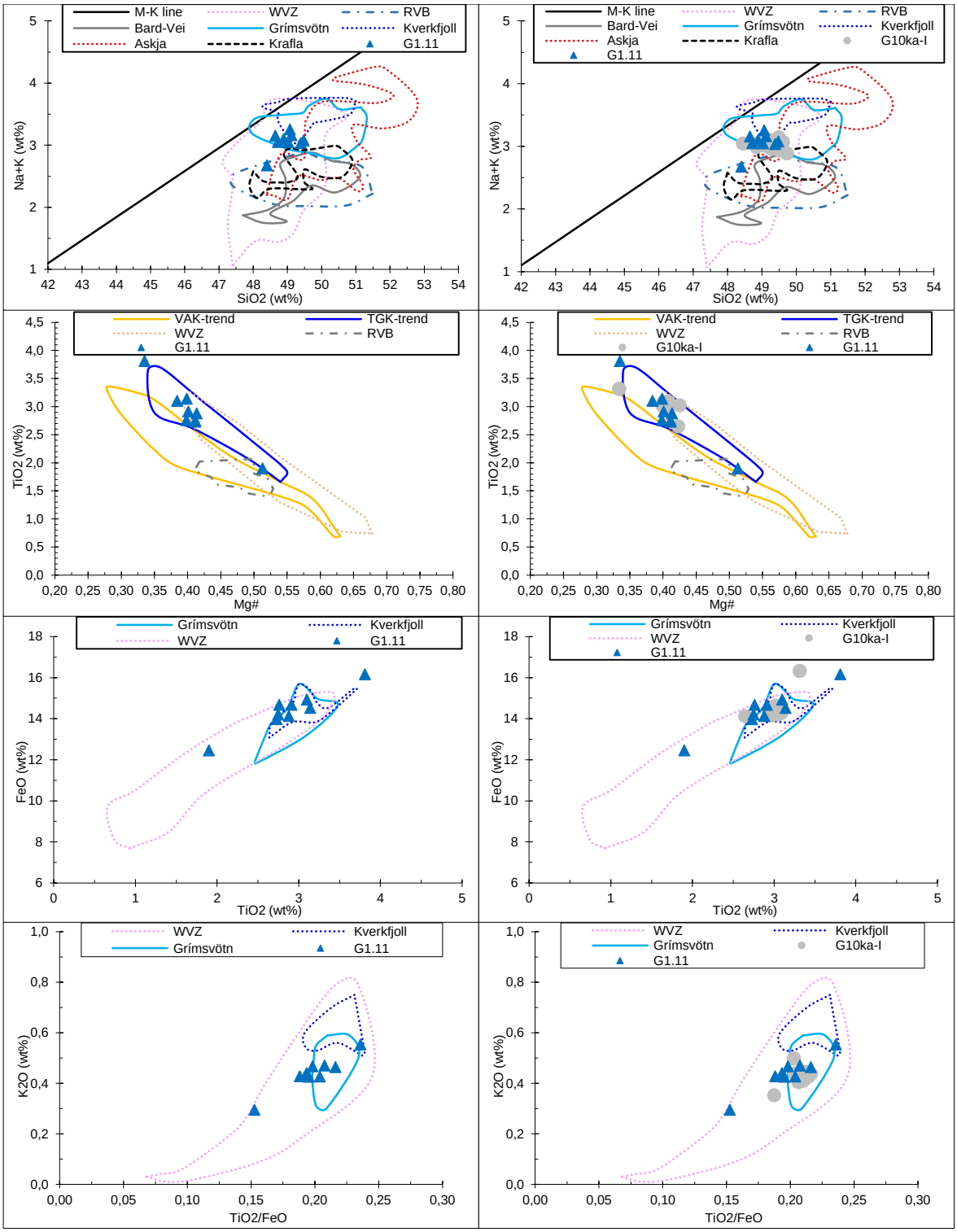

Figure 84. Sample G1.11 was identified by using these plots and comarison data from Hvítárvatn (Thorvaldur Thordarson, unpublished data 2018). The tephra was identified to by from the 10 ka Grímsvötn series with an age of 10.400 years BP.

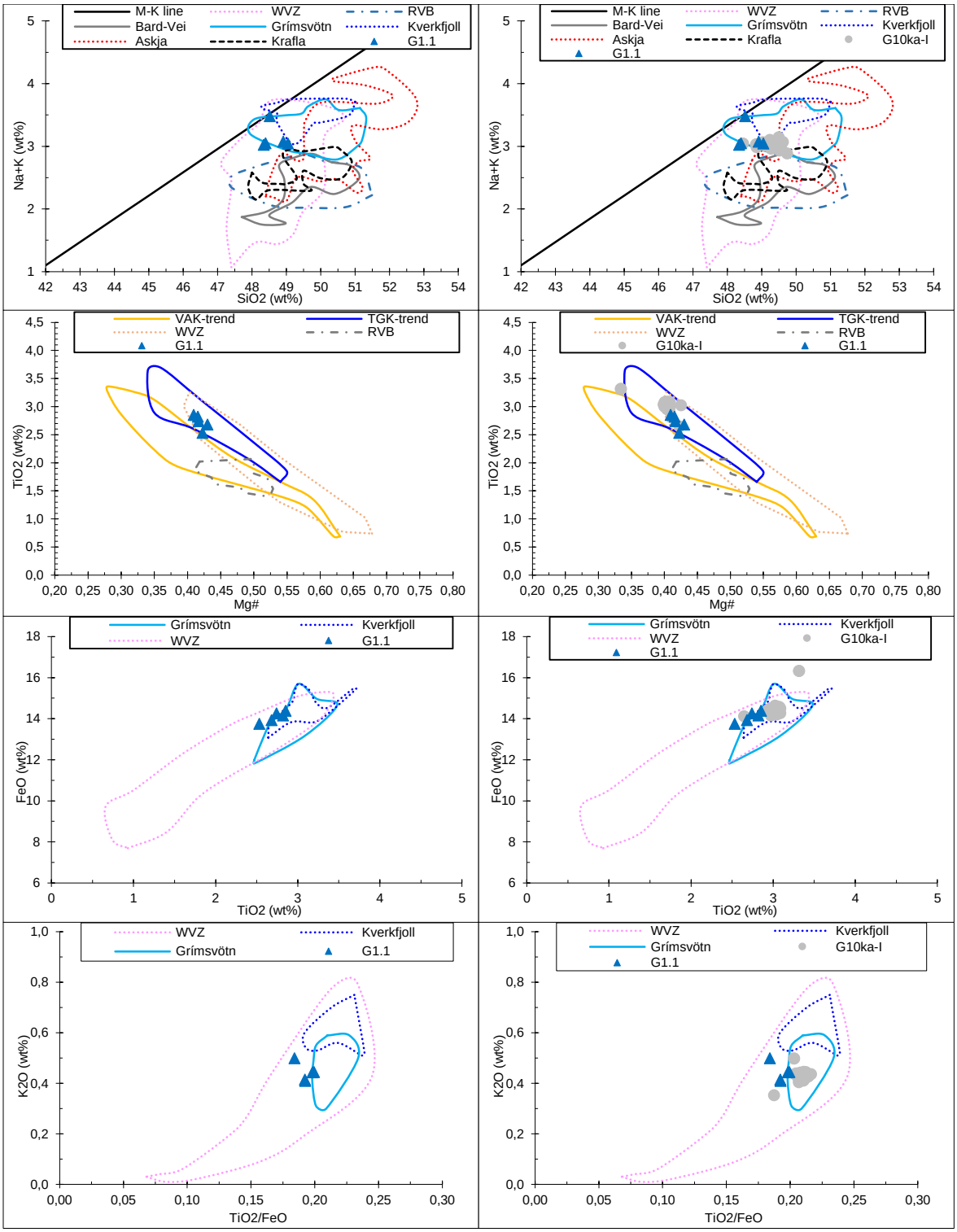

Figure 85. The tholeiitic basalt part of sample G1.1. This was identified to be a part of the 10 ka Grímsvötn series with an age of 10.400 yeasr BP, based on the plots and comparison data from Hvítárvatn (Throvaldur Thordarson, unpublished data 2018).

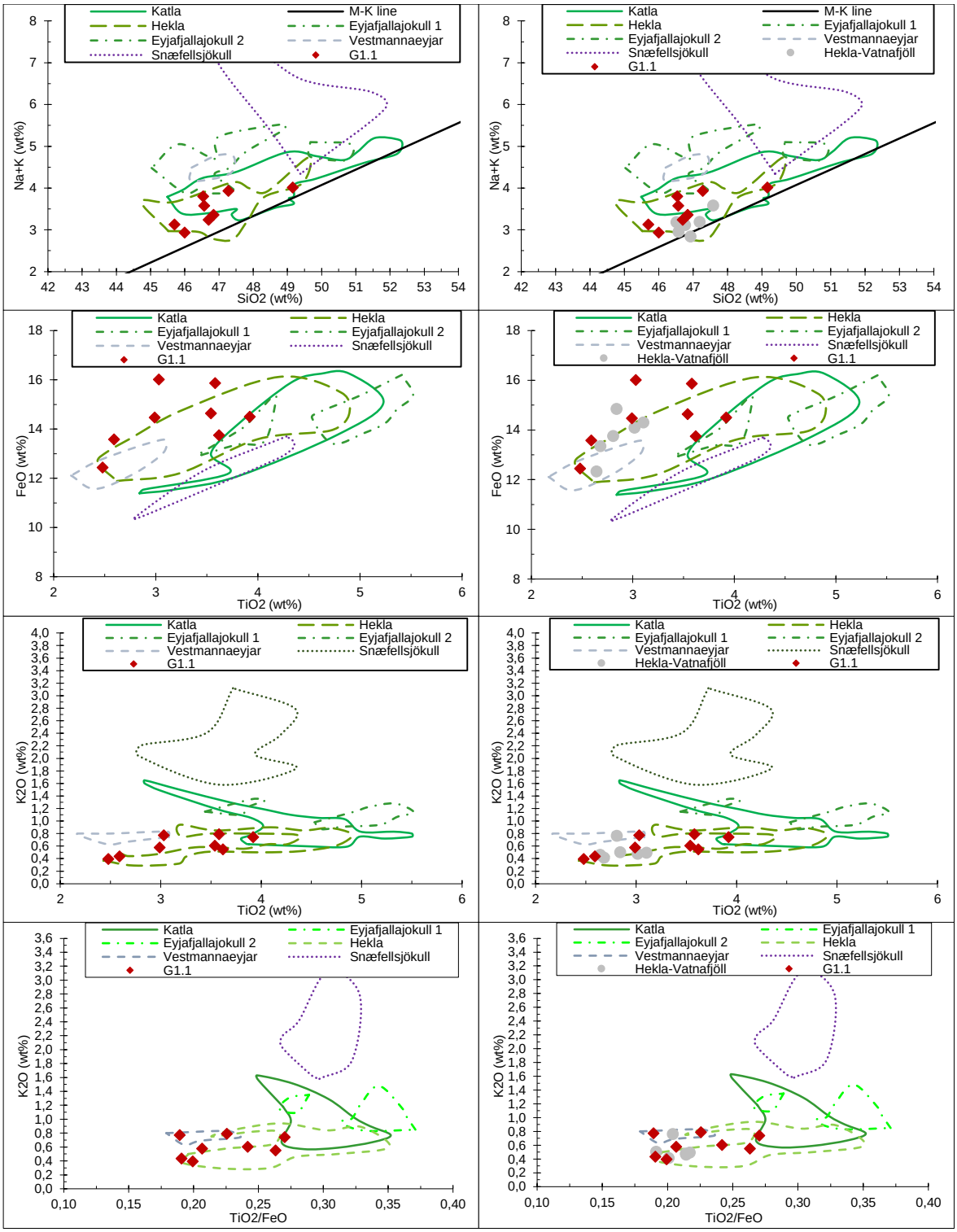

Figure 86. Alkalic basalt part of sample G1.1 and the geochemical discrimination plots used to identify it. By using comparison data from Hvítárvatn (Thorvaldur Thordarson, unpublished data 2018) the sample was identified as Hekla-Vatnafjöll with an age of 9.100 years BP.

Table 3. Geochemistry for all the tephra layers found in the soil sections. The major chemical components are displayed in weight percentage (wt%).

Volcanic source	**Sample name**	**Section**	**Age BP**	**SiO_2**	**TiO_2**	**Al_2O_3**	**FeO**	**MnO**	**MgO**	**CaO**	**Na_2O**	**K_2O**	**P_2O_5**	**Total**
Katla 1918	G3.14	3	32	46,49	3,86	13,10	14,59	0,21	5,54	10,59	2,87	0,59	0,43	98,27
				46,74	3,62	14,01	13,80	0,22	5,90	10,97	2,75	0,54	0,40	98,95
				47,61	4,37	13,32	14,70	0,22	4,91	9,59	2,95	0,76	0,53	98,96
				47,63	4,40	12,51	14,21	0,25	5,78	10,48	2,71	0,75	0,44	99,15
				48,14	4,21	13,07	14,51	0,24	4,74	9,28	3,04	0,80	0,50	98,54
				48,90	3,83	13,32	14,05	0,22	4,53	8,98	3,18	0,95	0,47	98,43
Katla 1918	G1.10	1.2	32	46,84	4,55	12,70	14,99	0,24	4,72	9,55	2,98	0,71	0,71	98,00
				46,98	3,94	13,21	14,58	0,21	5,08	9,75	3,00	0,75	0,48	97,98
				47,04	4,44	13,07	15,09	0,24	4,86	9,44	2,95	0,73	0,58	98,43
				47,15	4,53	12,98	15,11	0,22	4,95	9,71	3,09	0,75	0,74	99,23
				47,34	4,65	13,08	15,44	0,25	5,08	9,64	3,09	0,76	0,62	99,96
				47,48	3,96	13,29	14,75	0,22	5,13	9,57	2,95	0,73	0,47	98,55
				47,49	4,54	12,83	15,25	0,24	4,94	9,69	3,00	0,68	0,66	99,33
Hekla 1845	G3.13	3	105											
Alkalic basalt				46,40	3,51	13,82	13,83	0,23	5,90	11,17	2,89	0,54	0,37	98,66
				47,33	4,38	13,05	14,77	0,24	4,98	9,63	2,96	0,75	0,50	98,59
				47,71	4,37	13,30	14,65	0,23	4,79	9,64	2,66	0,78	0,52	98,64
				47,72	4,42	13,17	14,57	0,21	4,69	9,44	3,00	0,82	0,58	98,61
Tholeiitic				54,94	2,08	13,84	12,23	0,33	3,03	6,56	2,56	1,30	1,18	98,04
andesite				62,22	0,87	15,48	9,74	0,30	1,16	4,72	2,79	1,52	0,36	99,16
				63,04	1,06	15,87	7,93	0,21	1,52	4,70	2,89	1,58	0,41	99,20
Dacite				65,89	0,54	15,31	6,64	0,22	0,56	3,58	2,72	1,93	0,12	97,51
				66,57	0,48	15,52	6,52	0,18	0,54	3,65	2,48	1,92	0,10	97,97

Volcanic source	Sample name	Section	Age BP	SiO_2	TiO_2	Al_2O_3	FeO	MnO	MgO	CaO	Na_2O	K_2O	P_2O_5	Total
				66,98	0,46	14,69	6,97	0,23	0,44	3,24	2,52	2,30	0,14	97,96
				69,97	0,34	15,21	5,07	0,18	0,30	3,00	2,37	2,11	0,05	98,60
Hekla 1845	G1.9	1.2	105											
Alkalic basalt				46,03	4,92	11,10	17,83	0,28	3,81	12,37	2,40	0,78	0,47	100,00
				46,30	2,44	16,11	12,76	0,18	7,10	10,88	2,63	0,44	0,26	99,10
				46,95	3,83	14,03	14,32	0,20	5,80	11,30	2,79	0,56	0,39	100,16
				47,03	2,55	16,14	13,23	0,20	7,23	11,10	2,78	0,18	0,25	100,70
Tholeiitic				52,80	0,16	29,90	1,19	0,03	0,20	13,12	3,86	0,15	0,00	101,41
andesite				60,14	0,35	23,56	3,55	0,08	0,27	7,99	4,90	0,77	0,15	101,76
				60,28	1,28	13,59	10,41	0,29	1,62	4,43	3,37	2,03	0,57	97,87
				61,04	1,01	15,17	9,03	0,23	1,40	4,63	3,04	1,67	0,42	97,65
Dacite				65,24	1,08	13,67	8,29	0,28	0,93	3,95	2,82	2,20	0,65	99,11
				66,65	0,05	19,39	1,75	0,06	0,13	4,50	4,55	2,78	0,01	99,87
Hekla 1766	G3.11	3	184	58,65	1,42	15,56	9,86	0,24	1,97	5,54	2,89	1,43	0,61	98,17
				60,64	1,21	15,68	9,49	0,25	1,66	4,96	2,60	1,54	0,49	98,53
				59,10	1,37	15,52	9,94	0,28	2,00	5,61	3,01	1,31	0,61	98,76
				61,82	1,10	15,60	8,85	0,25	1,40	4,88	2,59	1,68	0,42	98,58
				58,75	1,37	15,60	10,05	0,25	2,03	5,64	3,01	1,54	0,72	98,96
				62,05	1,01	15,83	8,67	0,28	1,40	4,95	3,08	1,70	0,39	99,36
				61,13	1,12	15,72	9,45	0,24	1,57	5,22	2,92	1,58	0,43	99,38
				58,22	1,43	15,64	9,95	0,26	2,03	5,79	3,02	1,36	0,63	98,33
				58,60	1,45	15,70	10,04	0,25	2,14	5,54	2,87	1,41	0,64	98,63
				59,11	1,42	15,60	9,78	0,22	2,04	5,23	3,09	1,54	0,60	98,63
				59,42	1,38	15,63	9,63	0,28	1,89	5,49	2,97	1,44	0,62	98,75
				60,98	1,23	15,61	9,41	0,26	1,53	5,12	2,94	1,59	0,46	99,12

Volcanic source	Sample name	Section	Age BP	SiO_2	TiO_2	Al_2O_3	FeO	MnO	MgO	CaO	Na_2O	K_2O	P_2O_5	Total
				60,66	1,11	15,69	9,38	0,26	1,52	5,01	2,71	1,60	0,51	98,44
Hekla 1766	G2.13	2.2	184	57,04	1,61	15,44	10,48	0,27	2,53	6,09	3,65	1,26	0,80	99,17
				60,64	0,93	15,20	9,87	0,28	1,34	4,89	2,64	1,53	0,43	97,75
				60,71	1,33	14,47	10,50	0,31	1,85	5,16	2,74	1,61	0,62	99,30
				62,67	1,03	15,80	8,31	0,21	1,56	4,78	3,05	1,57	0,40	99,39
				59,06	1,36	15,50	10,13	0,26	2,14	5,70	3,05	1,46	0,59	99,25
				63,31	0,75	14,90	8,53	0,29	1,04	4,63	2,44	1,75	0,41	98,05
				60,41	1,18	15,44	9,62	0,30	1,70	5,30	3,08	1,60	0,44	99,07
				68,09	0,42	15,33	6,01	0,21	0,44	3,23	2,50	2,01	0,10	98,34
				67,32	0,43	15,04	5,91	0,19	0,42	3,36	2,53	2,03	0,09	97,32
				69,46	0,36	15,15	5,46	0,19	0,35	2,96	2,42	2,10	0,08	98,54
Katla 1721	G3.8	3	229	46,95	4,58	12,82	14,87	0,27	4,85	9,53	2,97	0,75	0,66	98,24
				47,48	4,61	12,87	14,94	0,27	4,99	9,72	3,05	0,73	0,65	99,31
				46,54	4,08	13,18	14,78	0,22	5,05	9,82	2,92	0,76	0,51	97,86
				47,38	3,95	13,20	14,26	0,24	4,96	9,76	2,92	0,80	0,44	97,91
				47,11	4,53	12,97	14,64	0,24	5,02	9,52	3,06	0,74	0,66	98,49
				47,45	3,58	13,48	14,64	0,25	5,09	9,58	3,13	0,71	0,49	98,39
				47,14	4,55	12,80	15,01	0,25	4,90	9,60	2,92	0,65	0,62	98,44
				47,34	4,40	12,98	14,47	0,23	4,93	9,65	2,94	0,77	0,57	98,28
				46,89	4,37	12,90	14,55	0,22	4,95	9,47	3,09	0,73	0,68	97,84
				46,83	4,52	12,80	14,91	0,24	4,89	9,42	2,98	0,74	0,65	97,98
				46,57	4,44	12,70	14,75	0,22	4,87	9,45	3,10	0,75	0,71	97,56
				46,52	3,66	13,38	14,03	0,21	5,86	10,97	2,86	0,55	0,37	98,41
				46,96	4,54	12,84	14,85	0,24	4,84	9,52	2,91	0,74	0,74	98,18
				47,39	4,25	12,94	15,09	0,25	4,95	9,39	2,88	0,74	0,67	98,56

Volcanic source	Sample name	Section	Age BP	SiO_2	TiO_2	Al_2O_3	FeO	MnO	MgO	CaO	Na_2O	K_2O	P_2O_5	Total
				47,27	4,46	12,90	14,88	0,23	4,97	9,62	3,08	0,74	0,70	98,85
Katla 1721	G2.9	2.1	229	44,82	4,41	12,31	13,90	0,21	4,81	9,32	3,03	0,72	0,61	94,14
				46,94	4,54	12,86	14,65	0,23	4,99	9,70	3,07	0,72	0,63	98,33
				46,66	4,56	12,74	14,89	0,25	5,07	9,44	3,03	0,69	0,61	97,95
				47,39	4,67	12,80	14,89	0,24	4,93	9,66	2,97	0,70	0,61	98,85
				47,62	4,56	12,78	15,29	0,23	5,03	9,53	2,48	0,74	0,64	98,90
				47,04	4,52	12,75	14,99	0,24	4,99	9,52	2,73	0,73	0,62	98,13
				47,40	4,49	12,85	14,75	0,23	4,91	9,34	3,03	0,75	0,67	98,42
				47,16	4,68	12,84	15,11	0,25	5,06	9,82	2,90	0,67	0,73	99,23
				47,12	4,52	12,83	14,96	0,22	4,83	9,62	2,92	0,70	0,67	98,39
				47,72	4,29	12,74	15,08	0,24	5,22	9,58	2,90	0,71	0,66	99,14
				48,40	4,66	12,83	14,79	0,23	4,84	9,66	3,07	0,72	0,71	99,91
				47,20	4,42	12,79	14,68	0,24	5,08	9,40	2,98	0,72	0,63	98,13
Bárðarbunga 1477	G2.8	2.1	473	49,32	1,71	13,76	12,43	0,22	6,83	11,66	2,29	0,22	0,15	98,58
				49,37	1,73	14,19	12,66	0,22	7,01	11,52	2,38	0,17	0,20	99,45
				49,61	1,91	13,71	12,83	0,19	6,56	10,97	2,42	0,22	0,17	98,59
				49,63	1,67	14,07	12,59	0,22	6,79	11,69	2,41	0,20	0,16	99,44
				49,66	1,83	13,85	12,78	0,22	6,45	11,17	2,49	0,25	0,16	98,86
				49,69	1,79	13,64	12,93	0,21	6,40	11,26	2,35	0,24	0,18	98,69
Grímsvötn 1335?			*615*	49,09	2,87	13,39	14,27	0,22	5,61	9,78	2,57	0,43	0,34	98,57
				49,14	2,55	13,45	13,84	0,22	5,76	10,44	2,54	0,37	0,31	98,63
				49,21	2,49	13,60	13,61	0,25	6,33	10,58	2,42	0,35	0,28	99,13
				49,44	2,74	12,70	15,41	0,24	5,02	9,70	2,76	0,42	0,29	98,72
				49,57	3,05	12,57	15,29	0,25	4,82	8,95	2,92	0,46	0,35	98,23
Hekla 1300	G3.4	3	650	62,83	1,33	13,72	9,86	0,24	1,41	4,36	4,06	1,85	0,60	100,27

Volcanic source	Sample name	Section	Age BP	SiO_2	TiO_2	Al_2O_3	FeO	MnO	MgO	CaO	Na_2O	K_2O	P_2O_5	Total
				61,69	1,38	13,89	9,78	0,23	1,14	4,32	3,31	2,02	0,64	98,41
				65,54	1,07	13,26	8,66	0,26	0,91	3,54	2,65	2,27	0,41	98,58
				67,07	0,52	15,48	6,58	0,23	0,54	3,71	2,63	1,94	0,14	98,84
				62,26	1,32	13,95	10,08	0,30	1,38	4,40	2,93	1,94	0,55	99,10
				62,05	1,40	13,68	10,52	0,28	1,34	4,40	3,32	1,98	0,66	99,63
				63,52	1,30	13,95	9,65	0,25	1,12	4,22	3,03	2,03	0,58	99,65
				67,03	1,00	13,61	7,63	0,24	0,73	3,33	3,08	2,43	0,42	99,50
Hekla 1300	G2.12	2.2	650	58,43	1,38	15,58	9,79	0,29	2,11	5,68	3,59	1,47	0,66	98,97
				60,24	1,25	15,34	9,72	0,24	1,57	4,99	3,48	1,63	0,40	98,87
				60,45	1,12	15,35	9,23	0,24	1,47	4,80	3,66	1,59	0,41	98,32
				59,94	1,46	15,48	9,86	0,27	2,05	5,50	3,00	1,48	0,61	99,66
				59,65	1,49	15,38	10,11	0,26	2,07	5,40	3,04	1,75	0,64	99,79
				59,13	1,39	15,27	10,18	0,27	2,20	5,76	3,07	1,42	0,67	99,36
				58,99	1,43	15,51	10,15	0,28	2,16	5,58	3,05	1,47	0,64	99,26
				58,73	1,50	15,22	10,65	0,28	2,25	5,77	3,09	1,49	0,64	99,61
				61,63	1,12	15,75	9,40	0,27	1,54	5,07	3,13	1,63	0,47	100,01
				60,57	1,18	15,60	9,43	0,30	1,66	5,19	2,98	1,57	0,40	98,87
				58,80	1,45	15,38	10,08	0,24	2,16	5,78	3,17	1,47	0,59	99,12
				59,03	1,47	15,62	10,26	0,26	2,14	5,72	2,97	1,45	0,66	99,57
				59,39	1,49	15,52	10,08	0,27	2,13	5,77	2,96	1,46	0,66	99,72
				61,32	1,12	15,79	9,36	0,24	1,54	5,17	2,87	1,65	0,44	99,49
				58,83	1,45	15,49	10,38	0,31	2,14	5,72	2,90	1,40	0,62	99,25
Hekla 1104	G2.6	2.1	846	72,16	0,21	14,55	3,30	0,13	0,12	1,94	4,41	2,70	0,03	99,54
				72,19	0,18	14,01	3,28	0,12	0,12	1,93	3,08	2,61	0,03	97,55
				72,56	0,23	13,65	3,32	0,12	0,10	1,76	3,47	2,68	0,02	97,90

Volcanic source	Sample name	Section	Age BP	SiO_2	TiO_2	Al_2O_3	FeO	MnO	MgO	CaO	Na_2O	K_2O	P_2O_5	Total
				72,86	0,22	14,16	3,30	0,12	0,11	1,90	2,90	2,72	0,02	98,31
				72,59	0,27	14,38	3,25	0,11	0,10	1,95	4,02	2,65	0,12	99,45
				72,27	0,18	14,35	3,20	0,11	0,10	1,94	2,89	2,72	0,00	97,77
				72,21	0,22	14,09	3,33	0,10	0,13	2,02	3,28	2,70	0,02	98,09
				72,07	0,20	14,16	3,40	0,12	0,10	1,89	4,25	2,66	0,02	98,87
				71,73	0,18	14,39	3,29	0,11	0,11	1,99	3,12	2,65	0,03	97,60
				72,32	0,19	14,51	3,15	0,13	0,10	1,99	3,70	2,47	0,02	98,58
				72,87	0,21	14,27	3,27	0,10	0,11	1,94	3,06	2,64	0,00	98,47
				72,27	0,21	14,29	3,24	0,08	0,09	1,92	3,93	2,68	0,00	98,71
				71,85	0,23	14,38	3,26	0,09	0,13	1,82	3,11	2,65	0,04	97,56
				71,85	0,23	14,43	3,23	0,08	0,13	1,89	3,09	2,66	0,00	97,59
				72,41	0,30	14,27	3,09	0,12	0,12	1,84	3,13	2,69	0,03	98,00
Bárðarbunga-Veiðivötn Settlement	G3.2-2	3	1079	49,52	1,77	13,97	13,05	0,22	6,42	11,03	2,38	0,23	0,18	98,76
				49,64	1,60	13,78	12,81	0,24	6,40	11,31	2,45	0,24	0,13	98,59
				49,65	1,79	13,80	12,92	0,23	6,38	11,21	2,37	0,21	0,15	98,72
				49,69	1,81	13,98	12,97	0,22	6,54	11,37	2,34	0,22	0,15	99,29
				49,70	1,74	13,74	13,03	0,23	6,58	11,74	2,33	0,20	0,19	99,49
				49,73	1,84	14,06	12,52	0,20	6,53	11,41	2,36	0,22	0,15	99,02
				49,75	1,75	13,68	12,41	0,21	6,43	11,12	2,35	0,22	0,10	98,02
				49,79	1,79	13,74	12,71	0,23	6,57	11,27	2,35	0,22	0,13	98,81
				49,86	1,79	13,93	12,95	0,24	6,48	10,97	2,28	0,21	0,17	98,88
				49,89	1,83	13,86	12,79	0,22	6,50	10,99	2,41	0,22	0,16	98,87
				49,96	1,75	13,91	12,66	0,24	6,08	11,38	2,33	0,22	0,15	98,68
Bárðarbunga-Veiðivötn	G3.2-1	3	1079	49,21	1,77	13,82	12,69	0,25	6,51	11,46	2,35	0,21	0,17	98,45
				49,60	1,79	13,85	12,77	0,21	6,39	11,42	2,30	0,23	0,18	98,74

Volcanic source	Sample name	Section	Age BP	SiO_2	TiO_2	Al_2O_3	FeO	MnO	MgO	CaO	Na_2O	K_2O	P_2O_5	Total
Settlement				50,09	1,77	13,87	12,66	0,22	6,47	11,14	2,35	0,22	0,14	98,93
				49,58	1,75	14,01	12,89	0,24	6,44	11,40	2,28	0,22	0,20	99,01
				49,85	1,68	14,06	12,73	0,21	6,37	11,51	2,32	0,23	0,16	99,12
				49,80	1,81	13,89	12,89	0,23	6,32	11,15	2,29	0,22	0,16	98,77
				49,45	1,65	13,78	12,82	0,24	6,43	11,45	2,36	0,23	0,17	98,58
				49,96	1,86	13,91	12,80	0,21	6,45	11,44	2,49	0,22	0,18	99,52
				50,02	1,76	13,70	13,34	0,25	6,17	11,26	2,15	0,23	0,17	99,05
				49,58	1,91	13,68	12,99	0,22	6,32	11,22	2,43	0,24	0,19	98,78
				50,35	1,86	14,06	13,05	0,23	6,30	11,32	2,47	0,24	0,15	100,03
				50,02	1,85	13,94	13,17	0,27	6,28	11,16	2,39	0,23	0,17	99,48
				49,85	1,86	13,86	13,00	0,25	6,31	11,38	2,37	0,23	0,16	99,27
				49,84	1,88	13,81	13,36	0,24	6,19	11,04	2,50	0,25	0,19	99,30
				49,75	1,78	13,82	12,91	0,23	6,29	11,26	2,32	0,23	0,16	98,75
Bárðarbunga-Veiðivötn Settlement	G2.5	2.1	1079	49,95	1,77	14,11	12,59	0,23	6,59	11,76	2,29	0,21	0,13	99,63
				49,75	1,69	13,82	12,58	0,25	6,69	11,68	2,29	0,22	0,16	99,13
				49,56	1,81	13,91	12,94	0,24	6,50	11,48	2,45	0,22	0,15	99,26
				49,55	1,65	14,09	12,54	0,22	6,73	11,61	2,30	0,21	0,17	99,08
				49,59	1,88	13,87	13,24	0,21	6,41	11,02	2,37	0,22	0,14	98,96
				49,58	1,84	13,95	13,02	0,23	6,47	11,53	2,32	0,21	0,20	99,35
				49,24	1,85	13,85	13,26	0,24	6,57	11,35	2,43	0,22	0,17	99,17
				49,31	1,85	13,59	13,11	0,20	6,42	11,11	2,46	0,22	0,17	98,43
				49,69	1,78	13,88	12,84	0,23	6,43	11,35	2,41	0,22	0,18	99,01
				49,99	1,85	13,79	13,20	0,21	6,54	11,37	2,41	0,22	0,16	99,74
				49,65	1,78	13,89	12,42	0,23	6,73	11,92	2,32	0,21	0,17	99,32
				49,41	1,69	13,99	12,48	0,24	6,76	11,62	2,35	0,21	0,17	98,92

Volcanic source	Sample name	Section	Age BP	SiO_2	TiO_2	Al_2O_3	FeO	MnO	MgO	CaO	Na_2O	K_2O	P_2O_5	Total
				49,46	1,68	13,93	13,12	0,19	6,48	11,17	2,41	0,22	0,18	98,84
				49,69	1,90	13,46	13,41	0,25	6,32	11,32	2,46	0,22	0,18	99,22
				49,77	1,85	13,78	12,73	0,23	6,43	11,45	2,30	0,22	0,16	98,92
Bárðarbunga-Veiðivötn Settlement	G1.8	1.2	1079	49,88	1,78	14,01	13,04	0,24	6,25	11,14	2,38	0,23	0,14	99,09
				50,16	1,82	14,13	12,55	0,24	6,57	11,46	2,40	0,22	0,17	99,73
				49,55	1,86	13,97	13,07	0,24	6,35	11,23	2,39	0,22	0,20	99,09
				49,62	1,72	13,71	12,46	0,21	6,76	11,20	2,33	0,22	0,18	98,40
				49,94	1,80	13,71	13,15	0,23	6,43	11,25	2,48	0,23	0,17	99,39
				49,43	1,82	13,59	13,21	0,19	6,66	11,16	2,44	0,21	0,14	98,85
				49,96	1,83	13,90	12,78	0,22	6,41	11,46	2,45	0,22	0,16	99,39
				49,53	1,87	14,17	12,90	0,24	6,48	11,48	2,41	0,22	0,17	99,46
				49,56	1,77	14,02	12,81	0,23	6,27	11,05	2,28	0,22	0,17	98,38
				49,79	1,83	14,03	13,11	0,21	6,46	11,39	2,39	0,23	0,18	99,62
				50,22	1,65	13,99	12,33	0,21	6,62	11,64	2,36	0,23	0,18	99,43
				49,43	1,78	13,82	12,86	0,22	6,45	11,41	2,34	0,22	0,18	98,70
				49,56	1,78	13,79	13,48	0,22	6,37	11,33	2,43	0,22	0,17	99,35
				49,15	1,90	13,86	13,05	0,22	6,44	11,17	2,37	0,23	0,15	98,54
				49,87	1,78	14,08	13,02	0,22	6,55	11,57	2,42	0,23	0,16	99,91
Katla prehistoric	G3.1	3	1150	46,81	4,42	13,03	14,45	0,24	4,99	9,50	2,92	0,75	0,55	97,66
				46,93	4,46	13,04	14,91	0,25	4,84	9,63	3,03	0,73	0,57	98,39
				46,96	4,39	13,05	14,93	0,24	4,93	9,74	3,04	0,76	0,47	98,51
				47,08	4,42	12,94	14,87	0,22	4,87	9,44	3,08	0,78	0,54	98,25
				47,10	4,45	13,01	14,88	0,25	4,80	9,46	3,06	0,77	0,57	98,35
				47,12	4,44	13,15	14,97	0,24	4,93	9,51	3,06	0,75	0,58	98,74
				47,14	4,42	13,12	14,87	0,24	5,01	9,56	3,03	0,76	0,49	98,64

Volcanic source	Sample name	Section	Age BP	SiO_2	TiO_2	Al_2O_3	FeO	MnO	MgO	CaO	Na_2O	K_2O	P_2O_5	Total
				47,17	4,21	12,99	14,99	0,25	5,04	9,49	3,07	0,71	0,56	98,47
				47,41	4,39	12,96	15,07	0,23	4,90	9,66	3,03	0,76	0,51	98,92
				47,41	4,45	13,14	14,93	0,27	4,99	9,63	3,00	0,78	0,52	99,12
				47,43	4,25	13,25	14,91	0,24	4,98	9,50	2,79	0,75	0,54	98,63
				47,65	4,45	13,40	15,17	0,24	4,94	9,67	2,84	0,74	0,57	99,67
				47,67	4,26	13,13	14,78	0,26	4,80	9,41	3,05	0,78	0,51	98,65
Katla prehistoric	G2.10	2.2	1150	46,55	4,43	12,67	14,76	0,25	5,04	9,57	2,98	0,73	0,68	97,66
				46,81	4,53	12,77	14,69	0,24	4,99	9,65	2,98	0,69	0,62	97,98
				46,96	4,42	12,80	14,98	0,24	5,04	9,59	3,06	0,75	0,59	98,43
				46,97	4,59	12,82	14,90	0,21	5,04	9,49	2,89	0,71	0,66	98,29
				47,02	4,49	12,80	15,09	0,24	5,00	9,56	3,14	0,75	0,70	98,79
				47,10	4,57	12,78	14,87	0,23	4,93	9,48	3,20	0,66	0,62	98,45
				47,17	4,60	12,89	14,85	0,22	4,88	9,54	2,93	0,74	0,60	98,43
				47,21	4,56	12,89	15,22	0,24	4,94	9,32	3,09	0,76	0,63	98,86
				47,28	4,68	12,98	14,81	0,24	5,04	9,70	3,05	0,74	0,71	99,22
				47,37	4,59	12,69	14,82	0,30	5,06	9,55	3,07	0,73	0,66	98,83
				47,47	4,58	12,82	14,97	0,20	4,83	9,58	3,05	0,76	0,69	98,95
				47,59	4,42	12,70	14,94	0,23	4,71	9,49	2,99	0,78	0,63	98,48
Katla prehistoric	G2.4	2.1	1150	47,20	4,32	13,05	14,78	0,23	4,97	9,61	2,94	0,75	0,55	98,40
				47,31	4,27	12,79	14,73	0,25	4,80	9,57	3,13	0,75	0,51	98,10
				47,81	4,06	13,41	14,29	0,22	4,60	9,06	3,09	0,87	0,50	97,91
				47,46	4,56	13,10	15,67	0,25	4,88	9,65	3,18	0,78	0,54	100,07
				47,07	4,50	12,98	14,88	0,23	4,94	9,64	2,94	0,74	0,57	98,49
				46,78	4,48	12,90	15,04	0,24	4,86	9,64	2,90	0,78	0,61	98,23
				47,26	4,39	13,06	15,14	0,24	4,90	9,51	3,00	0,78	0,52	98,80

Volcanic source	Sample name	Section	Age BP	SiO_2	TiO_2	Al_2O_3	FeO	MnO	MgO	CaO	Na_2O	K_2O	P_2O_5	Total
				46,97	4,39	12,87	14,90	0,23	4,89	9,47	3,11	0,75	0,55	98,13
				46,93	4,44	12,87	14,95	0,21	4,87	9,46	2,97	0,76	0,50	97,97
				47,07	4,44	13,26	15,06	0,21	4,97	9,69	3,06	0,76	0,52	99,04
				47,46	4,40	12,95	14,97	0,23	4,90	9,62	2,99	0,78	0,56	98,86
				46,89	4,47	13,00	14,95	0,22	4,86	9,52	2,89	0,76	0,56	98,12
				47,59	4,37	13,05	14,92	0,24	4,96	9,47	3,04	0,78	0,56	98,98
				47,09	4,47	12,86	14,90	0,24	4,77	9,52	3,12	0,79	0,54	98,30
				47,63	4,44	13,14	15,42	0,23	4,95	9,66	2,85	0,78	0,55	99,65
Katla prehistoric	G1.7	1.2	1150	46,77	4,50	13,03	14,83	0,21	4,87	9,61	2,99	0,78	0,51	98,11
				46,95	4,27	13,00	15,15	0,24	4,95	9,58	2,85	0,74	0,54	98,27
				47,11	4,45	13,13	14,76	0,25	4,93	9,52	2,87	0,75	0,60	98,37
				47,22	4,32	13,18	14,96	0,22	4,93	9,65	2,89	0,74	0,53	98,63
				47,46	4,42	12,89	15,00	0,21	4,90	9,68	2,99	0,78	0,54	98,87
				47,47	4,40	13,14	15,07	0,23	4,95	9,29	2,91	0,77	0,51	98,74
				47,73	4,43	13,20	14,49	0,24	4,95	9,83	2,66	0,81	0,59	98,92
				47,74	4,43	13,39	15,24	0,27	4,95	9,76	2,64	0,80	0,53	99,76
				47,88	4,40	12,98	15,02	0,24	4,78	9,55	3,05	0,80	0,63	99,34
				47,93	4,25	13,11	14,69	0,22	4,85	9,45	3,00	0,77	0,57	98,83
				48,07	4,21	13,12	14,80	0,22	4,90	9,49	2,96	0,78	0,56	99,11
				48,08	4,39	13,08	15,16	0,26	5,01	9,63	2,83	0,73	0,56	99,73
				48,31	4,55	13,24	14,99	0,26	4,94	9,48	2,88	0,76	0,47	99,88
Hekla H-C	G1.6	1.2	2869	61,14	1,04	15,40	8,22	0,22	1,62	4,87	3,84	1,46	0,44	98,24
				62,48	1,04	15,65	7,94	0,22	1,52	4,78	3,82	1,56	0,40	99,41
				60,70	1,00	15,46	7,88	0,20	1,51	4,39	3,71	1,45	0,33	96,63
				62,37	1,05	15,55	7,85	0,17	1,52	4,85	3,97	1,52	0,38	99,24

Volcanic source	Sample name	Section	Age BP	SiO_2	TiO_2	Al_2O_3	FeO	MnO	MgO	CaO	Na_2O	K_2O	P_2O_5	Total
				62,26	1,08	15,83	8,05	0,22	1,48	4,77	3,85	1,60	0,37	99,51
				62,13	1,06	15,51	8,01	0,20	1,55	4,67	3,86	1,50	0,36	98,85
				62,09	0,98	15,92	7,79	0,18	1,55	4,88	3,74	1,50	0,34	98,98
				62,12	1,11	16,08	7,81	0,20	1,58	4,94	3,77	1,56	0,39	99,55
				60,19	1,05	15,47	7,72	0,21	1,57	4,85	3,74	1,45	0,44	96,69
				62,12	1,11	15,88	7,74	0,20	1,59	4,73	3,69	1,55	0,38	98,99
Hekla H3	G1.5	1.2	3000	70,84	0,19	14,28	2,97	0,10	0,11	1,94	3,30	2,32	0,01	96,06
				71,67	0,17	14,31	3,06	0,12	0,12	1,96	3,52	2,51	0,00	97,44
				71,93	0,18	14,49	3,01	0,09	0,11	1,96	3,33	2,44	0,03	97,57
				72,60	0,22	14,53	3,24	0,07	0,13	1,94	4,12	2,53	0,01	99,39
				73,31	0,23	14,57	3,14	0,10	0,12	1,98	3,06	2,37	0,00	98,88
				72,49	0,19	14,38	3,18	0,08	0,12	1,93	2,99	2,43	0,02	97,81
				69,30	0,33	14,97	4,85	0,15	0,23	2,64	4,03	2,16	0,06	98,72
				72,96	0,19	14,10	3,22	0,09	0,14	2,04	3,30	2,45	0,03	98,52
				72,51	0,22	14,43	3,02	0,09	0,12	1,96	3,03	2,52	0,00	97,90
				72,10	0,24	14,17	2,97	0,11	0,12	1,93	3,11	2,41	0,03	97,19
				71,98	0,21	14,40	3,01	0,07	0,14	2,09	4,12	2,50	0,00	98,52
				71,84	0,22	14,32	3,13	0,08	0,12	1,94	3,58	2,49	0,01	97,73
				72,57	0,22	14,54	3,26	0,11	0,10	2,05	4,02	2,50	0,01	99,38
				72,58	0,17	14,62	3,12	0,09	0,09	1,87	4,09	2,51	0,03	99,16
				72,55	0,16	14,41	3,16	0,08	0,13	1,99	2,85	2,47	0,00	97,81
Hekla H4	G2.2-2	2.1	4260	71,76	0,13	12,66	1,95	0,08	0,02	1,26	3,98	2,76	0,01	94,61
				72,94	0,10	12,97	1,97	0,08	0,02	1,34	3,75	2,68	0,03	95,87
				74,41	0,10	13,34	2,00	0,07	0,01	1,28	3,18	2,78	0,02	97,19
				75,26	0,09	13,45	1,95	0,13	0,03	1,38	3,00	2,91	0,00	98,20

Volcanic source	Sample name	Section	Age BP	SiO_2	TiO_2	Al_2O_3	FeO	MnO	MgO	CaO	Na_2O	K_2O	P_2O_5	Total
				74,90	0,11	13,32	2,08	0,06	0,01	1,25	3,24	2,79	0,00	97,77
				73,93	0,05	13,16	2,04	0,10	0,02	1,25	3,14	2,89	0,02	96,59
				75,45	0,14	13,63	2,05	0,06	0,01	1,36	3,28	2,79	0,00	98,78
				76,34	0,09	13,31	1,82	0,10	0,04	1,35	3,90	2,80	0,02	99,77
				75,12	0,16	13,27	1,98	0,10	0,01	1,30	4,02	2,78	0,00	98,74
				73,56	0,10	13,23	1,94	0,10	0,01	1,33	3,19	2,74	0,00	96,21
				73,57	0,06	13,23	1,93	0,07	0,02	1,29	3,68	2,75	0,00	96,60
				73,05	0,14	12,95	2,06	0,08	0,05	1,29	3,61	2,78	0,02	96,02
				73,86	0,15	13,30	1,99	0,07	0,02	1,30	4,04	2,80	0,00	97,53
				72,66	0,18	12,97	2,12	0,07	0,07	1,40	3,92	2,67	0,05	96,11
Hekla H4	G2.2-1	2.1	4260	73,77	0,13	13,21	1,99	0,10	0,01	1,26	4,10	2,63	0,00	97,20
				74,72	0,09	13,28	1,85	0,09	0,02	1,19	3,12	2,86	0,00	97,21
				72,80	0,10	13,16	1,92	0,08	0,02	1,32	3,89	2,77	0,00	96,07
				74,39	0,10	13,46	2,04	0,09	0,03	1,28	3,04	2,78	0,00	97,20
				73,94	0,11	12,88	1,71	0,12	0,01	1,18	3,70	2,77	0,00	96,42
				75,34	0,09	13,31	2,02	0,07	0,02	1,31	3,14	2,86	0,00	98,17
				75,32	0,08	13,34	1,97	0,09	0,02	1,28	3,10	2,84	0,00	98,04
				74,69	0,14	13,44	1,96	0,07	0,02	1,30	4,14	2,77	0,01	98,53
				75,02	0,11	13,40	2,08	0,06	0,03	1,33	3,10	2,78	0,00	97,91
				74,36	0,11	13,02	2,01	0,10	0,03	1,31	4,02	2,88	0,00	97,85
				75,45	0,09	13,43	1,99	0,05	0,02	1,32	3,41	2,82	0,00	98,58
				74,10	0,07	13,29	1,89	0,09	0,03	1,28	4,11	2,62	0,00	97,48
				73,21	0,09	12,90	1,90	0,08	0,02	1,33	4,11	2,71	0,01	96,34
				74,11	0,08	12,75	1,66	0,08	0,03	1,08	3,70	2,84	0,00	96,32
Hekla H4	G1.4	1.1	4260	73,11	0,08	13,40	1,96	0,06	0,00	1,32	3,88	2,74	0,00	96,55

Volcanic source	Sample name	Section	Age BP	SiO_2	TiO_2	Al_2O_3	FeO	MnO	MgO	CaO	Na_2O	K_2O	P_2O_5	Total
				73,40	0,09	12,87	1,91	0,06	0,01	1,13	3,21	2,77	0,00	95,46
				74,73	0,09	13,24	1,96	0,06	0,01	1,32	4,03	2,74	0,06	98,25
				73,95	0,07	13,14	1,96	0,12	0,00	1,35	4,02	2,79	0,01	97,41
				73,11	0,10	12,66	1,96	0,05	0,00	1,27	3,05	2,76	0,00	94,96
				72,79	0,11	13,21	1,93	0,07	0,01	1,31	3,23	2,67	0,00	95,33
				72,13	0,16	12,78	1,96	0,10	0,01	1,25	2,88	2,78	0,00	94,05
				73,21	0,12	13,10	1,97	0,10	0,01	1,29	2,87	2,68	0,00	95,35
				74,98	0,11	13,07	1,94	0,09	0,03	1,23	2,98	2,78	0,01	97,23
				71,60	0,11	12,86	1,99	0,08	0,01	1,34	3,02	2,63	0,00	93,64
				74,03	0,10	13,14	1,97	0,09	0,03	1,40	3,95	2,80	0,05	97,56
				75,03	0,10	13,14	2,04	0,10	0,02	1,31	4,08	2,81	0,02	98,65
				74,54	0,17	13,45	1,95	0,06	0,01	1,33	4,03	2,82	0,00	98,35
				73,86	0,12	13,33	2,03	0,10	0,02	1,34	3,07	2,85	0,05	96,77
WVZ	G1.18	1.2	*4500*	49,23	1,08	14,51	11,26	0,18	7,69	13,13	2,05	0,10	0,09	99,32
				48,35	1,51	15,11	11,57	0,21	7,84	12,05	2,09	0,16	0,11	99,00
				48,98	1,41	14,97	11,22	0,20	7,72	12,41	2,12	0,13	0,12	99,29
				48,18	1,66	14,84	11,97	0,20	7,29	12,06	2,25	0,17	0,10	98,73
				48,58	2,30	13,98	13,05	0,20	6,73	11,46	2,15	0,31	0,23	98,99
				47,78	2,45	13,66	13,50	0,23	6,47	11,19	2,44	0,38	0,27	98,37
Hekla?				47,61	2,66	13,89	14,52	0,26	5,56	10,70	2,77	0,51	0,25	98,73
				49,03	3,18	12,90	16,14	0,28	4,76	9,42	2,64	0,66	0,50	99,51
				46,17	3,83	13,08	14,93	0,19	5,21	10,86	3,06	0,61	0,39	98,33
				52,13	3,10	12,59	14,98	0,30	3,32	7,64	3,04	0,79	0,73	98,62
				47,13	4,10	13,58	13,96	0,25	4,81	9,36	3,11	0,80	0,71	97,81
				48,65	3,03	13,15	15,39	0,28	4,57	9,26	3,21	0,72	0,39	98,65

Volcanic source	Sample name	Section	Age BP	SiO_2	TiO_2	Al_2O_3	FeO	MnO	MgO	CaO	Na_2O	K_2O	P_2O_5	Total
Katla	G1.17	1.2	6750	46,35	2,62	15,61	13,42	0,21	7,12	10,57	2,70	0,42	0,21	99,23
				46,81	3,97	12,95	15,12	0,24	5,15	9,64	3,14	0,69	0,48	98,18
				46,06	2,86	15,22	13,16	0,19	6,69	10,67	2,56	0,42	0,27	98,10
				47,50	4,17	13,29	15,01	0,22	4,80	9,76	3,10	0,79	0,45	99,09
				47,55	4,28	13,16	15,05	0,26	4,65	9,82	2,93	0,82	0,45	98,97
				46,87	4,35	12,80	15,77	0,24	4,64	9,59	3,05	0,88	0,52	98,71
				47,96	4,43	13,16	15,56	0,24	4,76	9,81	2,47	0,86	0,53	99,78
				48,21	4,31	13,38	15,26	0,22	4,80	9,93	2,52	0,96	0,42	100,01
				48,08	4,13	13,07	14,85	0,24	4,87	9,76	3,17	0,85	0,46	99,48
				47,13	4,22	13,29	13,84	0,24	4,96	9,83	2,96	0,71	0,50	97,68
				47,81	4,07	13,41	14,77	0,24	4,84	9,80	2,93	0,78	0,41	99,07
Hekla H5	G2.1	2.1	7000	75,72	0,07	13,10	1,70	0,04	0,03	1,31	3,63	2,67	0,00	98,27
				75,48	0,10	13,20	1,82	0,04	0,04	1,27	3,76	2,72	0,05	98,47
				76,42	0,07	12,95	1,62	0,06	0,03	1,17	3,01	2,85	0,03	98,23
				74,43	0,15	13,11	1,76	0,04	0,03	1,33	3,37	2,62	0,02	96,86
				74,95	0,10	12,87	1,81	0,07	0,04	1,27	3,24	2,75	0,01	97,11
				74,20	0,12	12,80	1,71	0,06	0,03	1,25	3,72	2,58	0,00	96,48
				75,84	0,10	12,65	1,72	0,05	0,03	1,30	2,84	2,85	0,05	97,43
				75,70	0,09	13,06	1,78	0,10	0,04	1,29	3,85	2,71	0,00	98,61
				74,73	0,13	12,64	1,83	0,07	0,03	1,17	3,10	2,64	0,03	96,36
				75,75	0,12	12,75	1,73	0,08	0,03	1,35	3,04	2,76	0,00	97,60
				76,13	0,07	12,87	1,80	0,09	0,03	1,27	3,04	2,74	0,00	98,05
				76,65	0,07	12,98	1,81	0,06	0,03	1,23	3,78	2,77	0,01	99,38
				75,79	0,07	12,96	1,77	0,05	0,03	1,23	3,18	2,77	0,01	97,87
				76,61	0,03	12,85	1,63	0,08	0,03	1,35	4,08	2,78	0,00	99,44

Volcanic source	Sample name	Section	Age BP	SiO_2	TiO_2	Al_2O_3	FeO	MnO	MgO	CaO	Na_2O	K_2O	P_2O_5	Total
				75,97	0,07	13,00	1,81	0,09	0,04	1,26	3,26	2,76	0,01	98,28
Hekla H5	G1.14-2	1.2	7000	75,89	0,09	13,08	1,83	0,09	0,04	1,29	3,08	2,81	0,00	98,20
				75,77	0,14	13,00	1,71	0,05	0,01	1,16	3,82	2,74	0,00	98,40
				75,98	0,08	13,04	1,83	0,08	0,04	1,30	2,96	2,67	0,04	98,03
				76,47	0,09	13,35	1,76	0,09	0,03	1,32	3,93	2,75	0,02	99,81
				76,56	0,08	12,98	1,83	0,03	0,05	1,21	3,16	2,81	0,00	98,72
				74,97	0,12	13,77	1,59	0,07	0,04	1,51	4,07	2,44	0,00	98,57
				76,07	0,09	13,17	1,68	0,04	0,03	1,41	3,82	2,62	0,03	98,94
				74,70	0,09	12,86	1,79	0,10	0,05	1,31	3,07	2,69	0,04	96,69
				75,49	0,09	13,15	1,81	0,09	0,03	1,26	3,98	2,65	0,03	98,56
				75,74	0,12	13,13	1,68	0,02	0,03	1,27	3,81	2,75	0,02	98,58
				75,43	0,09	13,01	1,80	0,06	0,04	1,25	3,07	2,65	0,02	97,42
				76,51	0,17	13,12	1,87	0,09	0,04	1,28	3,76	2,79	0,01	99,64
				77,01	0,16	13,09	1,79	0,09	0,02	1,35	2,99	2,84	0,00	99,35
				76,83	0,08	13,37	1,83	0,07	0,04	1,33	3,22	2,70	0,00	99,47
				75,76	0,09	13,12	1,80	0,08	0,04	1,15	3,18	2,73	0,03	97,98
Hekla H5	G1.14-1	1.2	7000	75,85	0,11	12,85	1,77	0,04	0,02	1,40	3,85	2,74	0,00	98,63
				76,09	0,14	12,95	1,91	0,10	0,03	1,22	3,77	2,65	0,00	98,86
				76,08	0,06	12,93	1,81	0,08	0,06	1,23	4,19	2,76	0,02	99,23
				75,45	0,09	12,96	1,95	0,08	0,05	1,31	3,95	2,69	0,00	98,53
				75,60	0,06	13,00	1,73	0,07	0,03	1,30	3,83	2,79	0,00	98,42
				76,04	0,08	13,11	1,77	0,08	0,05	1,33	4,03	2,67	0,00	99,17
				75,68	0,08	12,86	1,84	0,03	0,04	1,20	3,86	2,75	0,01	98,36
				75,86	0,11	13,02	1,80	0,06	0,04	1,27	4,12	2,69	0,01	98,97
				74,51	0,09	12,44	1,80	0,05	0,04	1,28	2,96	2,69	0,00	95,86

Volcanic source	Sample name	Section	Age BP	SiO_2	TiO_2	Al_2O_3	FeO	MnO	MgO	CaO	Na_2O	K_2O	P_2O_5	Total
				76,54	0,09	13,14	1,74	0,04	0,02	1,27	3,81	2,77	0,01	99,44
				76,01	0,07	12,95	1,85	0,10	0,03	1,23	3,65	2,85	0,00	98,74
				75,50	0,09	13,13	1,72	0,05	0,01	1,22	3,66	2,75	0,00	98,14
				76,14	0,09	12,83	1,74	0,08	0,04	1,31	4,09	2,69	0,00	99,01
				75,78	0,09	13,08	1,82	0,09	0,05	1,29	3,95	2,80	0,02	98,97
				74,44	0,12	12,72	1,77	0,06	0,03	1,24	4,02	2,77	0,04	97,21
Kverkfjöll	G1.3	1.1	*6890*	48,59	2,82	13,24	14,24	0,26	5,55	9,81	2,70	0,46	0,33	98,01
				49,41	3,63	13,41	14,74	0,27	4,82	9,04	2,32	0,72	0,52	98,88
				49,62	3,40	12,74	14,51	0,22	4,85	9,03	2,90	0,62	0,46	98,35
				49,78	3,51	12,83	14,79	0,27	4,70	8,81	3,05	0,75	0,54	99,03
Hekla-Vatnafjöll	G1.13	1.2	9100	45,65	2,43	15,24	12,03	0,21	7,32	11,76	2,29	0,38	0,24	97,55
				45,88	2,76	15,27	13,85	0,21	6,63	10,33	2,73	0,43	0,29	98,38
				46,04	2,88	15,33	13,80	0,18	6,44	10,34	2,78	0,45	0,33	98,57
				46,16	2,43	15,48	12,23	0,19	7,38	11,30	2,26	0,38	0,24	98,05
				46,16	2,78	15,24	13,82	0,20	6,51	10,33	2,69	0,45	0,25	98,42
				46,30	2,41	14,86	11,88	0,18	7,90	12,06	2,32	0,35	0,24	98,50
				46,37	4,04	13,55	14,45	0,22	5,25	10,56	2,14	0,79	0,40	97,76
				46,39	2,39	14,89	11,40	0,19	7,90	11,91	2,20	0,37	0,22	97,87
				46,46	2,38	15,09	11,56	0,17	7,61	12,50	2,24	0,34	0,21	98,57
				46,52	2,34	14,75	12,07	0,19	7,95	12,06	2,43	0,37	0,19	98,87
				46,53	2,84	14,95	14,08	0,21	6,29	10,40	2,90	0,47	0,32	98,98
				46,55	2,36	15,83	11,80	0,20	7,74	11,69	2,28	0,37	0,22	99,03
10 ka Grímsvötn series	G1.12	1.2	10.000	47,69	2,86	14,38	13,59	0,21	6,07	10,24	2,58	0,45	0,33	98,40
				49,05	2,95	13,06	14,51	0,26	5,38	9,56	2,66	0,45	0,31	98,20
				49,10	2,93	13,10	14,32	0,24	5,55	9,85	2,58	0,44	0,28	98,40

Volcanic source	Sample name	Section	Age BP	SiO_2	TiO_2	Al_2O_3	FeO	MnO	MgO	CaO	Na_2O	K_2O	P_2O_5	Total
				49,40	2,83	13,37	13,93	0,24	5,49	9,73	2,75	0,44	0,30	98,48
				49,67	2,68	12,83	15,04	0,26	5,32	9,94	2,52	0,42	0,36	99,04
				49,92	2,70	13,04	14,56	0,25	5,14	9,41	2,91	0,47	0,26	98,66
				48,30	3,79	12,33	15,50	0,28	4,69	9,00	2,90	0,49	0,41	97,69
10 ka Grímsvötn series	G1.11	1.2	10.400	48,40	1,90	14,80	12,45	0,22	7,35	11,38	2,38	0,29	0,20	99,38
				48,65	3,81	12,37	16,16	0,25	4,57	9,20	2,60	0,55	0,44	98,61
				48,72	2,75	13,06	14,21	0,25	5,58	9,79	2,61	0,44	0,32	97,73
				48,89	2,91	13,04	14,68	0,25	5,51	9,60	2,63	0,47	0,35	98,33
				49,03	2,88	13,18	14,13	0,23	5,59	9,88	2,62	0,43	0,30	98,27
				49,07	3,14	13,21	14,52	0,25	5,40	9,67	2,79	0,46	0,34	98,86
				49,12	3,10	12,88	14,93	0,26	5,22	9,6	2,69	0,47	0,32	98,61
				49,39	2,73	13,32	13,98	0,26	5,48	9,67	2,61	0,43	0,31	98,18
				49,48	2,76	12,80	14,67	0,25	5,45	10,01	2,65	0,43	0,36	98,85
10 ka Grímsvötn series	G1.1	1.1	10.400	48,34	2,82	13,27	14,15	0,25	5,64	10,02	2,58	0,44	0,33	97,84
				48,39	2,68	13,28	13,93	0,23	5,89	10,11	2,64	0,41	0,25	97,81
				48,51	2,53	13,50	13,75	0,24	5,64	10,26	2,98	0,50	0,27	98,18
				48,91	2,85	13,25	14,39	0,25	5,59	9,81	2,63	0,44	0,33	98,46
				49,04	2,74	13,27	14,26	0,22	5,71	9,80	2,63	0,41	0,34	98,42
Hekla-Vatnafjöll			9100	45,70	2,59	15,60	13,58	0,20	7,11	10,40	2,69	0,43	0,26	98,56
				46,00	2,48	15,86	12,44	0,18	7,38	10,90	2,54	0,39	0,24	98,42
				46,54	3,92	13,19	14,50	0,19	5,16	10,01	3,06	0,74	0,56	97,87
				46,57	3,54	13,34	14,64	0,22	5,51	10,67	2,97	0,60	0,37	98,43
				46,70	3,62	13,78	13,75	0,20	5,95	11,04	2,69	0,55	0,37	98,65
				46,84	2,99	13,04	14,47	0,25	5,67	10,86	2,78	0,58	0,37	97,85
				49,16	3,03	12,73	16,01	0,29	4,34	8,76	3,24	0,77	0,65	98,99

	47,28	3,58	12,43	15,86	0,32	4,36	9,11	3,14	0,79	1,06	97,93

A.3 brGDGT

Table 4. Data used to put together the brGDGT temperature graph with estimated MAT based on calibration from De Jonge et al. (2014).

Sample	**Depth (cm)**	**Clam age (BP)**	**MAT (°C)**
J1.35	19	151	6,397
J1.34	27	431	5,430
J1.33	31	614	9,439
J1.31	58	1628	10,792
J1.28	76	2375	10,287
J1.25	97	3043	11,855
J1.24	116	3715	13,742
J1.22	126	4065	14,914
J1.4	179	8103	10,339
J1.3	182	8222	8,454
J1.2	185	8341	8,335
J1.1	196	8800	13,259
G-J	208	9358	14,146

A.4 Loss on Ignition

Table 5. Results from burning soil samples for LOI measurements.

Sample	Depth (cm)	Clam age (BP)	Initial dry weight (g)	Dry weight after 50°C (g)	Dry weight after 105°C (g)	Dry weight after 550°C (g)	Organic carbon (%)
J1.36	15	72	2,985	2,887	2,796	2,378	14,950
S1.12	33	706	1,868	1,742	1,695	1,500	11,504
S1.11	45	1151	4,323	3,905	3,788	3,364	11,193
S1.10	51	1356	4,986	4,508	4,403	4,055	7,904
S1.9	58	1628	3,463	2,824	2,736	2,451	10,417
S1.8	69	2088	4,614	3,424	3,271	2,840	13,176
S1.7	75	2335	5,113	3,818	3,650	3,221	11,753
S1.6	81	2564	3,684	2,744	2,627	2,309	12,105
S1.5	87	2763	3,557	3,019	2,926	2,693	7,963
S1.4	91	2878	4,949	3,504	3,345	2,972	11,151
S1.3	98	3072	2,713	2,034	1,961	1,780	9,230
S1.2	115	3677	3,212	2,043	1,925	1,592	17,299
S1.1	118	3791	4,655	3,196	3,028	2,632	13,078
J1.60	150	4358	4,141	3,931	3,799	3,603	5,159
J1.58	163	4364	3,569	3,418	3,319	3,190	3,887
J1.55	177	4386	4,700	4,422	4,260	4,048	4,977
J1.54	182	4389	4,319	3,919	3,732	3,463	7,208
J1.52	191	4518	2,921	2,543	2,398	2,107	12,135
J1.51	199	4738	3,419	2,632	2,503	2,187	12,625

Sample	Depth (cm)	Clam age (BP)	Initial dry weight (g)	Dry weight after 50°C (g)	Dry weight after 105°C (g)	Dry weight after 550°C (g)	Organic carbon (%)
J1.50	208	5096	3,313	2,745	2,602	2,265	12,952
J1.49	216	5484	3,781	3,217	3,057	2,822	7,687
J1.48	224	5907	3,567	3,073	2,925	2,698	7,761
J1.46	241	6794	3,219	2,587	2,412	2,116	12,272
J1.45	256	7417	3,233	2,746	2,630	2,416	8,137
J1.43	272	7956	4,165	3,768	3,619	3,423	5,416
J1.42	287	8475	4,127	3,579	3,417	3,186	6,760
J1.41	303	9185	3,391	2,742	2,609	2,375	8,969
J1.40	310	9578	4,331	3,994	3,872	3,709	4,210
J1.39	319	10137	4,241	3,393	3,250	3,047	6,246